MIS 5e relative sea level indicators: new methodologies to sustain the quantitative estimate of past sea level changes

Dissertation

zur Erlangung des Doktorgrades

der Naturwissenschaften

(Dr. rer. nat.)

am Fachbereich Geowissenschaften

der Universität Bremen

Vorgelegt von

Thomas Lorscheid

Bremen, September 2017

... and the anchor has been found on the summit of the hills.

Sir Charles Lyell in 'Principles of Geology'

Gutachter / Reviewer:
Dr. Alessio Rovere
PD Dr. Gösta Hoffmann

Prüfungskommission / Examination Board:
Dr. Alessio Rovere
PD Dr. Gösta Hoffmann
Prof. Dr. Hildegard Westphal
Dr. Jürgen Pätzold
Dr. Thomas Felis
Jan Drechsel

Tag der Verteidigung / Day of Defense:
13. November 2017

Versicherung an Eides Statt

gem. § 5 Abs. 5 der Promotionsordnung vom 15.07.2015

Ich, Thomas Lorscheid, Suhrfeldstr. 66, 28207 Bremen, Matr.-Nr.: 3013583

versichere an Eides Statt durch meine Unterschrift, dass ich die vorliegende Dissertation selbständig und ohne fremde Hilfe angefertigt und alle Stellen, die ich wörtlich dem Sinne nach aus Veröffentlichungen entnommen habe, als solche kenntlich gemacht habe, mich auch keiner anderen als der angegebenen Literatur oder sonstiger Hilfsmittel bedient habe und die zu Prüfungszwecken beigelegte elektronische Version (PDF) der Dissertation mit der abgegebenen gedruckten Version identisch ist.

Ich versichere an Eides Statt, dass ich die vorgenannten Angaben nach bestem Wissen und Gewissen gemacht habe und dass die Angaben der Wahrheit entsprechen und ich nichts verschwiegen habe.

Die Strafbarkeit einer falschen eidesstattlichen Versicherung ist mir bekannt, namentlich die Strafandrohung gemäß § 156 StGB bis zu drei Jahren Freiheitsstrafe oder Geldstrafe bei vorsätzlicher Begehung der Tat bzw. gemäß § 161 Abs. 1 StGB bis zu einem Jahr Freiheitsstrafe oder Geldstrafe bei fahrlässiger Begehung.

_____ _____

Ort, Datum Unterschrift

I. Abstract

The elevation of sea level is not a constant level and changes over time. Since the last glacial maximum sea level is generally rising, although with different rates. The industrial revolution and the related global warming, accelerated the rate of sea-level rise. Precise predictions of future sea-level rise are therefore essential for developing shoreline protection strategies. These predictions are calibrated to the sea-level highstand in past warmer climates and need consequently accurate estimates of the paleo sea levels. Besides the Holocene, the most studied past period in sea level studies is the last major interglacial, the Marine Isotopic Stage (MIS) 5e between ca. 128 and 116 ka. During this period the global sea level was 6-9 m higher than today with probably one or two rapid sea-level rises. The only direct observations of sea level in this time, can be made by the investigation of paleo relative sea-level (RSL) indicators. Any geological feature with a quantifiable relation to the sea level during the time of its formation can be used as RSL indicators. This relationship is called the indicative meaning and is quantified with two values: the distance between the feature and sea level (i.e. the reference water level) and the possible, vertical variability (i.e. the indicative range). Studies of the MIS 5e sea level have explored a large number of locations to assess the paleo sea-level elevation, but is currently facing five fundamental problems: (i) the measurement of RSL indicator elevations needs to be done always with the highest precision and referred to a defined tidal or geodetic datum; (ii) the indicative meaning needs to be utilized as standard procedure in all MIS 5e studies, as it is done for Holocene sea-level studies; (iii) the age attribution outside areas with fossil corals is often difficult and needs more research; (iv) the effects of post-depositional movements have to be attributed to all studies of RSL indicators; (v) in contrast to Holocene sea-level studies, MIS 5e studies are often lacking a standardized structure to report their results.

In this thesis, some of the problems around the determination of the indicative meaning, precise elevation measurements and structured reporting of databases are addressed. In the first chapter, I will show how sea-level indicators can be categorized from a geomorphological perspective. In the second and third chapter, I will show the possibility of using morpho- and hydrodynamic models to derive the limits of the indicative meaning and to assess changes in paleo tidal ranges. In a final chapter, I will use these methodologies, describe how they can help deriving the paleo RSL without site-specific data and attribute the results to the global MIS 5e sea-level database.

The interpretation of RSL indicators and the attribution of the indicative meaning is a key points in assessing MIS 5e eustatic sea levels. Therefore, I propose a way to classify the vast majority of reported RSL indicators by using 10 geomorphological categories. For each category, the limits describing the indicative meaning of the RSL indicator can be defined by using relevant wave- and tide-related datums. This categorization can help to establish a standardized database structure for MIS 5e studies, as it is common practice in Holocene sea-level studies.

Although the categorization of RSL indicators can be done in a standardized way, the limits of their indicative meaning are often hard to quantify. In the best case, this quantification should be done together with the measurement of RSL indicators with a site-by-site approach. If this is not possible, I

show a method in determining the indicative range for beach deposits by using a morphodynamic model. For the island of Mallorca, several storm events three different areas were modeled. From the results the average values of the respective indicative meaning were extracted. This approach could help in establishing new insights on the MIS 5e sea-level history of Mallorca.

The quantification of the indicative meaning by observing modern processes, relies on the assumption that the indicator-shaping processes are today similar to those in the past. This usually solid assumption needs always to be carefully assessed. As example tidal ranges are known to change their amplitudes in very shallow areas already with small changes in water depth. In order to evaluate these tidal changes, I employed for the southern Caribbean Sea two simulations of a hydrodynamic model, which predicts the tidal range. With a first simulation, using present-day inputs, the modern conditions were reconstructed and evaluated against real-time measurements. Then a second simulation with the same model setup, but using a paleo bathymetry, could reconstruct the paleo tidal ranges. These simulations confirm that tidal ranges change strongly in areas with a very shallow continental shelf, but are consistent in areas with steeper shelf. This simple model approach can help in estimating the tidal ranges between the past and today, which have to be added to the paleo RSL estimate.

The global database of MIS 5e RSL indicators consists out of several thousand measurements. Nevertheless, this data is not compiled in a standardized way and lacks in large parts the attribution of the indicative meaning. By using the categorization of RSL indicators, different morpho- and hydrodynamic equations and global wave and tide datasets, this database can be attributed with the indicative meaning in a standardized way. By recalculating the paleo RSL for each site, including the indicative meaning, a global average RSL of + 4.5 m at passive margins can be determined. This estimate is not corrected for post-depositional movements and does therefore not represent the eustatic sea level during MIS 5e. Nevertheless, using these simple equations is a valid method to establish the indicative meaning for global datasets or if no site-specific data is available.

II. Zusammenfassung

Die Höhe des Meeresspiegels ist nicht konstant und ändert sich im Laufe der Zeit. Seit dem letzteiszeitlichen Maximum steigt der Meeresspiegel grundsätzlich an, wenn auch mit unterschiedlichen Raten. Die industrielle Revolution und die damit verbundene globale Erwärmung sorgen für einen beschleunigten Anstieg des Meeresspiegels. Präzise Vorhersagen über den zukünftigen Meeresspiegelanstieg sind daher essentiell um Anpassungsstrategien für Küstenregionen zu erstellen. Diese Vorhersagen werden anhand der Meeresspiegelhöchststände in früheren Warmzeiten kalibriert und benötigen daher auch akkurate Abschätzungen dieser Paläomeeresspiegel. Neben dem Holozän, ist die am stärksten untersuchte Zeitspanne in der Meeresspiegelforschung das letzte große Interglazial, der Marine Isotope Stage (MIS) 5e zwischen etwa 128 und 116 ka. Während dieser Zeit war der globale Meeresspiegel etwa 6-9 m höher als heute, möglicherweise mit einem oder zwei schnellen Anstiegen. Die einzige direkte Möglichkeit zur Beobachtung des Meeresspiegels in dieser Zeit, ist die Untersuchung von Anzeigern des relativen Meeresspiegels (RSL, „relative sea level“). Jedes geologisches Merkmal, mit einer quantifizierbaren Verbindung zum Meeresspiegel zur Zeit seiner Entstehung, kann als RSL Anzeiger genutzt werden. Diese Beziehung wird als anzeigende Bedeutung („indicative meaning“) bezeichnet und besteht aus zwei Werten: die Distanz zwischen Merkmal und Meeresspiegel (Referenzwasserstand; „relative water level“) und der möglichen, vertikalen Variabilität (Anzeigebereich; „indicative range“). Studien über die Erforschung des Meeresspiegels in MIS 5e haben eine große Anzahl an Lokalitäten untersucht um die Paläomeeresspiegelhöhe zu bestimmen, allerdings existieren dabei zur Zeit noch fünf grundlegende Probleme: (i) die Messung der RSL Anzeiger muss immer mit höchster Präzision erfolgen und sich auf ein bekanntes geodätisches oder Gezeitendatum beziehen; (ii) die anzeigende Bedeutung sollte als Standard in allen MIS 5e Studien verwendet werden, wie es für Studien des holozänen Meeresspiegels bereits üblich ist; (iii) die Altersbestimmung außerhalb Regionen mit fossilen Korallen ist oft schwierig und benötigt weitergehende Erforschung; (iv) die Auswirkungen von Bewegungen nach der Ablagerung dieser Anzeiger müssen berücksichtigt und berichtet werden; (v) im Gegensatz zu holozänen Meeresspiegelstudien fehlt es Studien des Meeresspiegels in MIS 5e oft an einer strukturierten Wiedergabe der Ergebnisse.

In der vorliegenden Arbeit werden einige Probleme rund um die Bestimmung der anzeigenden Bedeutung, präziser Höhenmessungen und strukturierter Wiedergabe der Ergebnisse behandelt. Im ersten Kapitel werde ich zeigen wie Meeresspiegelanzeiger aus einer geomorphologischen Sicht kategorisiert werden können. Im zweiten und dritten Kapitel werde ich zeigen wie morpho- und hydrodynamische Modelle genutzt werden können um die Abgrenzungen der anzeigenden Bedeutung zu bestimmen und um Veränderungen des Tidenhubs zu bestimmen. In einem abschließenden Kapitel werde ich diese Methoden nutzen um zu beschreiben, wie der relative Paläomeeresspiegel ohne ortspezifische Daten bestimmt und wie die Ergebnisse für die globale Datenbank des MIS 5e Meeresspiegels genutzt werden können.

Die Interpretation von RSL Anzeigern und der Bestimmung der anzeigenden Bedeutung ist ein Schlüsselpunkt um den eustatischen Meeresspiegel in MIS 5e bestimmen zu können. Dafür schlage ich eine

Möglichkeit vor, die große Mehrheit der berichteten Meeresspiegelanzeiger anhand von 10 geomorphologischen Kategorien zu klassifizieren. Für jede Kategorie, können die Grenzen der anzeigenden Bedeutung der RSL Anzeiger durch relevante Wellen- und Gezeitenlevel definiert werden. Diese Kategorisierung kann dabei helfen eine standardisierte Datenbankstruktur für MIS 5e Studien zu erschaffen, wie es bereits für Studien des Holozäns übliche Praxis ist.

Obwohl die Kategorisierung von RSL Indikatoren standardisiert erfolgen kann, ist es oft schwer die Grenzen der anzeigenden Bedeutung zu quantifizieren. Im besten Fall sollte dies zusammen mit der Vermessung der Meeresspiegelanzeiger, durch einen ortspezifischen Ansatz, erfolgen. Ist dies nicht möglich, zeige ich eine Methode um den Anzeigebereich für Strandablagerungen durch ein morphodynamisches Modell zu bestimmen. Für die Insel Mallorca wurden diverse Sturmereignisse in drei Regionen modelliert. Aus den Resultaten wurden die Mittelwerte der jeweiligen anzeigenden Bedeutung berechnet. Dieser Ansatz konnte helfen neue Erkenntnisse über die Meeresspiegelentwicklung in MIS 5e auf Mallorca zu gewinnen.

Die Quantifizierung der anzeigenden Bedeutung durch die Beobachtung heutiger Prozesse beruht auf der Annahme, dass die heutigen Prozesse, die zur Bildung der RSL Anzeiger führen, vergleichbar zu denen in der Vergangenheit sind. Diese, üblicherweise zuverlässige, Annahme muss allerdings immer sorgsam überprüft werden. Als Beispiel ist bekannt, dass sich die Höhe des Tidenhubs in sehr flachen Bereichen schon mit kleinen Veränderungen der Wassertiefe ändern. Um die Veränderungen des Tidenhubs zu beurteilen, habe ich im südlichen Karibischen Meer zwei Simulationen eines hydrodynamischen Modells genutzt, welches den Tidenhub prognostizieren kann. Bei der ersten Simulation wurden die gegenwärtigen Bedingungen durch die Nutzung moderner Eingabedaten rekonstruiert und mit Echtzeitbeobachtungen verglichen. In einer zweiten Simulation wurde dieselbe Konfiguration des Modells, aber mit einer Paläobathymetrie, genutzt, sodass der Paläotidenhub rekonstruiert werden konnte. Diese Simulationen zeigen, dass sich der Tidenhub in Gegenden mit flachem Kontinentalhang ändert, aber bei steileren Kontinentalhängen ähnlich bleibt. Dieses einfache Modell kann dabei helfen die Veränderungen des Tidenhubs über die Zeit zu bestimmen.

Die globale Datenbank der MIS 5e RSL Indikatoren besteht aus mehreren tausend Messungen. Dennoch sind die Daten nicht in einem standardisierten Weg erstellt und ihnen fehlt meist die Angabe über die anzeigende Bedeutung. Durch die Nutzung der Kategorisierung der RSL Indikatoren, verschiedener morpho- und hydrodynamischer Gleichungen und globalen Wellen- und Gezeitendatensätzen kann die anzeigenden Bedeutung standardisiert dieser Datenbank zugeordnet werden. Durch Neuberechnung des relativen Paläomeeresspiegels für jede Lokation, einschließlich der anzeigenden Bedeutung, konnte ein globaler Mittelwert von +4.5 m an passiven Kontinentalrändern bestimmt werden. Diese Berechnung ist nicht für Bewegungen nach der Ablagerung korrigiert und repräsentiert daher nicht den eustatischen Meeresspiegel in MIS 5e. Trotzdem kann die Nutzung dieser einfachen Gleichungen eine zuverlässige Methode sein, die anzeigende Bedeutung für globale Datenbestände oder bei nicht verfügbaren ortspezifischen Daten zu bestimmen.

III. Acknowledgements

In the last three years I had the chance to learn a lot about paleo sea level research. This was only possible through the support of many people, I could meet along the way. First and most important, I would like to thank my supervisor Alessio Rovere for his guidance and help throughout all parts of my project. I am very grateful for his believe in me and his inputs for shaping this project according to my possibilities and interests. Molto grazie per tutto.

Further, I would like to thank my second reviewer, Gösta Hoffmann and my GLOMAR thesis panel, Maureen Raymo, Jürgen Pätzold, Paolo Stocchi and Matteo Vacchi for some very interesting and helpful meetings and their help throughout this project.

The University of Bremen, the Center for Environmental Marine Science – MARUM and the Leibniz-Centre for Tropical Marine Research – ZMT I would like to thank for their combined effort in providing the generous funding of my PhD position. Further, I would like to thank the Bremen International Graduate School for Marine Science (GLOMAR) for providing helpful courses and especially Dana Pittauer for organizing the monthly research seminars.

Further, I would like to thank Daniel Gray, Julia Haberkern, Lennart van Maldegem, Benjamin Halstenberg, Diana Martínez-Alacón and Charlotte Breitkreuz for an interesting and nice time as part of the PhD-reps team.

My colleagues of the Sea Level and Coastal Changes working group, in order of appearance Daniel Harris, Elisa Casella, Alexander Janßen, Jan Drechsel and Maren Bender, I would like to thank for their support, their company in the different offices and their friendship.

Also the members of my ‘second’ working group, Hildegard Westphal, Sebastian Flotow, Claire Raymond, Gita Narayan, André Wizemann, Thomas Mann, Peter Müller, Natalia Herrán Navarro, Kim Vane, Marleen Stuhr and Sebastian Höpker, I would like to thank for many interesting group meetings and especially for all the lunch and coffee breaks.

Auch meinen ‘Bonner’ Freunden möchte ich für ihre Unterstützung und all die schönen Aktionen über die Jahre danken. Ein ganz spezielles Dankschön geht zudem an Jana, Steffi, Kathrin und Barbara, dass ihr immer für mich da seid und mich auch in schweren Zeiten in der Spur haltet.

Zum Schluss möchte ich mich ganz besonders bei meinen Eltern und meiner ganzen Familie, für all ihre Unterstützung und ihr Vertrauen bedanken, ohne die diese Arbeit nicht möglich gewesen wäre.

IV. Table of contents

V. List of figures

VI. List of Tables

1. From paleo sea level variability to future rise

At present, 2.7 billion people live less than 100 km from the shoreline (Kummu et al., 2016). Among these, ca. 14% have settled less than 5 m above present sea level. Since the industrial revolution (1880 AD), global temperatures rose around 0.85 °C (IPCC, 2014). This increase in global temperatures forced polar ice sheets to start melting and triggered sea level to rise. The sea level constantly fluctuated over geological timescales (Fig. 1.1) and it has been rising with high rates (Lambeck et al., 2014) from the last glacial maximum to ca. 6 ka ago. After this, the sea-level rise in the Common Era was 0.1-0.3 mm/a until 1800 AD, with a period between 1000 AD and 1400 AD of a 0.2 mm/a sea-level fall (Kopp et al., 2016). Then, in the 18th century, direct observations on the sea-level elevation started with the installation of tide gauges. Their record show a rising sea level with an increased rate of 1.1-1.2 mm/a since 1900 AD (Hay et al., 2015; Dangendorf et al., 2017). Since 1993 AD (TOPEX/Poseidon missions), also satellite altimetry gives an independent estimate on the rising sea level. These satellite measurements indicate a higher rate of global average sea level that is rising by 3.0-3.3 mm/a (Beckley et al., 2010; Hay et al., 2015). Until the end of this century, global temperatures are expected to increase by another 1 °C and polar temperatures by 3-6 °C (Kattsov et al., 2005). Hence, sea level is predicted to rise, under high greenhouse gas emission scenarios, up to 1 m by the end of the century and up to 13 m until 2500 AD (DeConto and Pollard, 2016).

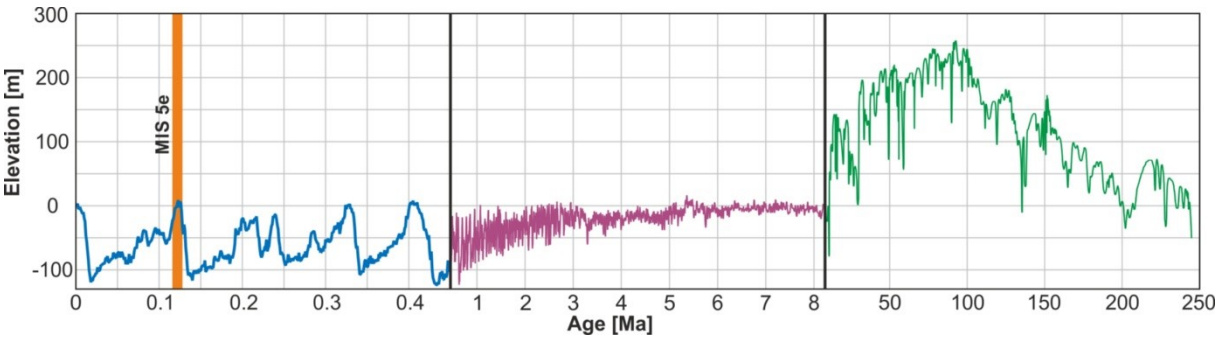

Fig. 1.1: Sea-level variability on different geological timescales. Orange bar represents the MIS 5e interglacial. The sea-level curve until 8.2 Ma is extracted from Haq et al. (1987), data from 8.2 Ma to present are taken from Miller (2005).

Changes in sea level are the result of the complex interplay of factors related to eustatic (e.g. ice melting or thermal expansion) and relative (e.g. Glacial Isostatic Adjustment (GIA) or tectonics) factors. In order to estimate how high the sea level will rise in the future due to polar ice melting, it is essential to disentangle these different factors. While the current rate of sea-level rise can be calculated using observational constraints provided by tide gauges and satellite altimetry and correcting them for relative factors (Rovere et al., 2016b), the study of past changes in sea level provides a window into worlds that were warmer than the modern and can be used as process-analogs for future warm climates. Under this rationale, periods of similar or warmer temperatures than today are interesting, as they can give us an understanding of the maximum elevation attained by sea level, and on possible patterns of rapid sea-level rise.

Besides the Holocene, the most investigated past period is the last major interglacial, the Marine Isotope Stage (MIS) 5e, that occurred between ca. 128 and 116 ka (Stirling et al., 1998). This timespan was characterized by greenhouse gas concentrations similar or slightly higher than pre-industrial levels (Petit et al., 1999; Otto-Bliesner et al., 2013). This resulted in global mean temperatures of 1.5 °C (Turney and Jones, 2010; Lunt et al., 2013) to 2 °C (Hoffman et al., 2017) higher than today. Polar temperatures during MIS 5e rose up to 3-5 °C above modern (Otto-Bliesner et al., 2006). In this time period, higher temperatures resulted in smaller ice sheets and therefore in higher sea levels. The eustatic sea level (ESL), representing the global mean sea level, reached a maximum of 6-9 meters above its present equivalent (Hearty et al., 2007; Kopp et al., 2009; Dutton and Lambeck, 2012; O'Leary et al., 2013; Dutton et al., 2015a). While there is general consensus about the 6-9 meters MIS 5e ESL, the rates and timing of sea level changes within MIS 5e are still the focus of ongoing research. The classical view of a MIS 5e sea-level curve (e.g. Lambeck and Nakada, 1992) assumes the melting of both hemispheres ice sheets simultaneous at the beginning of the interglacial and then regrowing at the end of this period. Recent studies suggest more variability in the sea-level behavior with one or two rapid sea level rises during the interglacial (Hearty et al., 2007; Kopp et al., 2009). For example, data from the Seychelles suggest an early (ca. 125 ka) maximum sea level elevation by up to 7.6 m (Dutton et al., 2015b), whereas a study in Western Australia (O'Leary et al., 2013) shows a maximum ESL at 9.5 m happening after a sudden sea level jump in the later interglacial (ca. 118 ka). In contrast, some near-field areas, e.g. Northern Europe (Long et al., 2015), do not show any clear evidence of abrupt changes of sea level within the interglacial.

The MIS 5e sea level can be estimated in different ways. Stable oxygen isotopes are incorporated in the skeleton of planktonic foraminifera according to the composition of the ocean waters during their lifetime (Rohling et al., 2008). The distribution of oxygen isotope ($\delta^{18}O$) in the ocean is dependent on the quantity of land-based ice (Chappell and Shackleton, 1986). Using this relationship past sea levels can be reconstructed by measuring the changes in the oxygen isotope signature. Nevertheless, as they show the amount of continental ice, oxygen isotopes are an indirect proxy for the sea level elevation. Therefore, the observation of relative sea-level (RSL) indicators represents the only possibility to assess directly paleo sea levels. The term 'relative' sea level indicates that the elevation derived by this approach is per definition not corrected for post-depositional movements. These displacements, e.g. tectonic uplift or GIA, need to be taken into account to achieve reliable estimates on the ESL (Rovere et al., 2016b).

Many landforms, deposits or biological structures can serve as RSL indicator, if (i) their elevation above/below present sea level is measured, (ii) an age of formation can be determined and (iii) the relation to the sea level at the time of formation, known as the indicative meaning, can be quantified (Van De Plassche, 1986; Shennan, 2015). The indicative meaning of a RSL indicator can be calculated using a modern analog, i.e. the same feature developing in the modern environment. For example, the indicative meaning of a fossil coral reef terrace can be derived from the depth distribution of a modern coral reef. Once a modern analog is measured, it is possible to calculate the distance between the modern feature and sea level (the Reference Water Level, RWL) and the related, possible variability

(Indicative Range, IR). A detailed description of this approach and possible landforms are described in chapter 4.

1.1. State of the art and general research gaps

Paleo shorelines and their importance for studies of former sea levels were already described in 'The Principles of Geology' by Charles Lyell (1837), and since the late 1920s studies started to focus on the Pleistocene and the Last Interglacial (Antevs, 1929; Cooke, 1930). Today, more than 980 papers report RSL indicators globally, and new reports or measurements of classic sections are being published every year. A recent compilation (Pedoja et al., 2011a) shows that MIS 5e sea levels left their imprint at nearly one thousand sites worldwide. Despite this long history of research and the large body of literature on this subject, there are still several aspects in the investigation of these shorelines that need to be addressed:

1. The elevation of a RSL indicator is a fundamental property that is measured in the field. Errors or reference to incorrect sea level datums may have a large influence on the calculated paleo sea level. In general, it is recommended that RSL indicators are surveyed with high-precision GPS or levelling (Woodroffe and Barlow, 2015). Until very recently, elevation measurements of MIS 5e RSL indicators were done with metered rods or less precise levelling tools and reported above the sea level at the time of measure, seldom referring to tidal datums. This means the necessary precision could not be achieved, or worst, the elevation errors were not properly estimated or reported. While examples of reporting the elevation of MIS 5e RSL indicators with high-precision survey techniques are starting to flourish (e.g. Meco et al., 2007; Muhs et al., 2011; O'Leary et al., 2013; Dutton et al., 2015b; Sivan et al., 2016), the MIS 5e sea level research community is still far from using standard techniques to measure and report elevations of RSL indicators.
2. The elevation of a RSL indicator does not represent the elevation of the paleo RSL when the indicator was formed. This is due to a simple reason: most indicators do not form precisely at sea level, but are correlated to it with some quantifiable relationship. The definition of the indicative meaning (Van De Plassche, 1986; Shennan, 2015) is important in order to tie the elevation of a RSL indicator with the elevation of paleo RSL. This method origins in the study of Holocene sea level, where it is also widely used as a standard procedure (Shennan and Horton, 2002; Engelhart and Horton, 2012; Woodroffe et al., 2012; Mann et al., 2016). In the analysis of older sea levels, especially MIS 5e, standard quantifications of the indicative meaning were only considered recently (Hibbert et al., 2016; Rovere et al., 2016a; Lorscheid et al., 2017), and need to be applied to both newly collected and reanalyzed data. Only once the indicative meaning has been taken into account, one can calculate the elevation of a paleo RSL.
3. The age attribution of many RSL indicators is difficult and several dating methods have been applied. For constructive and depositional indicators an age attribution is usually possible, although with different precisions. For erosive indicators it is much harder to establish an age, and indirect methods or associated features have to be dated. Best results are usually derived from fossil corals, measured with U/Th-methods (Broecker and Thurber, 1965; Stirling et al., 1995; Obert et al., 2016). Nevertheless, the age attribution is essential in order to decipher the timing of sea-level

changes and variability within the interglacial and should be done with the highest accuracy for new data (Obert et al., 2016) and needs to be carefully recalculated in published data (Hibbert et al., 2016).

4. Even when the elevation of a RSL indicator and its age are known with high accuracy, to calculate paleo ESL, post-depositional movements should be estimated or modeled. The influences of GIA (Peltier, 2001; Milne and Mitrovica, 2008; de Boer et al., 2014b) and Dynamic Topography (DT, Moucha et al., 2008; Austermann et al., 2017) can add up to several meters, and may be bounded by large uncertainties. Even more problematic is the fact that these effects, while well-studied and always accounted for in Holocene and more recent sea-level studies (Lambeck et al., 2004; Engelhart et al., 2011; Khan et al., 2015; Mann et al., 2016; Vacchi et al., 2016), are sometimes considered negligible or not considered at all in reconstructing MIS 5e studies. Recent global compilations (Kopp et al., 2009; Dutton and Lambeck, 2012) reanalyzed former literature accounting for GIA, but DT is still considered negligible, while recent studies pointed out that it may have a large effect in displacing MIS 5e shorelines at passive margins. At active margins, tectonic displacements are often calculated using the MIS 5e shoreline as benchmark, though it is not possible to use these tectonic movement rates to correct for tectonic displacements.
5. Many studies report paleo shorelines from the MIS 5e on a local or regional scale, often building compilations of high regional importance (Koike and Machida, 2001; Ferranti et al., 2008; Muhs et al., 2011; O'Leary et al., 2013). However, in contrast to Holocene sea level studies, data on MIS 5e RSL indicators is usually not reported in a structured way or in a standardized format (Düsterhus et al., 2016). In order to produce databases that can be used to produce more reliable estimates of global sea levels in MIS 5e, there is the need for reporting data in a structured way. Besides new data, which should follow some standard reporting pattern (e.g. Düsterhus et al., 2016), published data has to be reevaluated and new research has to be undertaken to fill geographical gaps.

1.2. Motivation and research questions

As mentioned in the previous sections, the study of MIS 5e paleo sea levels is relevant to predict the evolution of ice sheets in future warmer climates. An example of how MIS 5e ESL estimates can be used to improve our understanding of ice melting (and hence sea-level changes) in warmer climatic statuses is provided by a recent study by DeConto and Pollard (2016). In this study, the authors are using the ESL estimates for the mid-Pliocene and MIS 5e to calibrate a model, reconstructing the Antarctic ice-sheet stability since these times until today. Then they use the same model set-up to predict the future ice-sheet stability and hence the potential sea-level rise due to Antarctic ice sheet melting. Therefore, the estimate of paleo sea-level elevations has a direct influence on the prediction of future sea-level rise and needs further refinement. Given the five research gaps presented above, I focused my thesis on the information that can be extracted from RSL indicators, and on the real uncertainties, which we must face when using them to reconstruct paleo RSL histories. I focused on four main research questions that are the object of four manuscripts I am presenting in this dissertation.

1. How can RSL indicators be described from a geomorphological perspective?
2. Is it possible to use modern morphodynamic models to determine the indicative meaning of beach deposits?
3. Can particular RSL indicators give an insights on further environmental information, e.g. changes in the tidal range?
4. How could the indicative meaning be derived without site-specific data and reanalyze a global database in a more standardized way?

2. Methods

To address the research questions proposed in this thesis, I used a range of field and laboratory methods. Here, I summarize the employed methods hereafter. For detailed descriptions of each method, the reader is referred to the relevant chapters in the thesis.

2.1. GPS

Chapter 4, 5, 6

For positioning and elevation measurements, I used a differential GPS (Global Positioning System). The device is composed of a receiver (Trimble ProXRT), an antenna (Trimble Tornado) and a handheld datalogger (Trimble Juno 5). For remote measurements, a laser pointer device (Trimble LaserAce) could be connected to the datalogger. For recording data the software TerraSync was used. The receiver is equipped with the OmniSTAR G2 real-time corrections, allowing to get a precision down to 0.1 m in the field under best survey conditions. In some cases, like bad satellite reception, a post-processing using the program GPS Pathfinder Office was necessary. The GPS data was then referred following the method of Foster (2015) to a defined global or local geoid (EGM08 (Pavlis et al., 2012) or EGM08_REDNAP (IGN, 2009), respectively) in order to make the data comparable to other studies.

2.2. Water level sensors

Chapter 6

In the absence of tide gauges, water level sensors can help in measuring the water levels, from which tidal datums can be extracted. In Bonaire, an INW PT2X water level sensor was attached under water for the time of fieldwork and used to record the water levels. Data extraction and processing was done using the software Aqua4Plus.

2.3. Thin sections

Chapter 5

In order to determine the depositional conditions of lithified beach deposits, especially if the deposition took place subaerial or intertidal, several outcrops in Mallorca were sampled and thin sections have been prepared. These sections have been prepared with a thickness of 35 µm and analyzed with a polarizing microscope.

2.4. ^{230}Th/U-dating

Chapter 6

The age determination of a coral head below a paleo tidal notch in Bonaire was done by using the ^{230}Th/U method. A piece of a *Montastraea* sp. colony was sampled and split in two subsamples. Both subsamples were probed with a diamond-coated micro-cutting disc. After bleaching with weak HNO_3, the U and Th isotopes were separated and analyzed with a MC-ICP-MS at the Max Planck Institute for Chemistry in Mainz, following the methods described in (Obert et al., 2016).

2.5. Glacial Isostatic Adjustment model

Chapter 4, 5, 6

In order to evaluate the influences of GIA to the study site in Mallorca and for assessing a paleo bathymetry for the Southern Caribbean Sea, the coupled ice-earth model ANICE-SELEN was used (de Boer et al., 2014b). The ice-sheet-shelf-model ANICE (Bintanja and van de Wal, 2008; de Boer et al., 2013; de Boer et al., 2014a) couples dynamically the major ice-sheets and covers a history of 410 ka. The global solid earth model SELEN (Stocchi and Spada, 2009) calculates the solid earth changes including changes of the geoid and RSL. In this coupled version, the two independent models communicate in 1 ka steps and exchanging their results. Different ice-melting scenarios and mantle viscosities have been used for the predictions.

2.6. Morphodynamic modelling

Chapter 5

The limits of the indicative meaning for beach deposits in Mallorca were done by using the nearshore, morphodynamic model CSHORE (Kobayashi, 1999, 2009). This 1D model is freely available (*https://sites.google.com/site/cshorecode/, last accessed 2nd September 2017*) and predicts the changes in a beach profile and the wave runup by using an initial, bathymetric profile and wave conditions as inputs. For Mallorca, the bathymetric input was extracted from GPS surveys during field work and from beach surveying campaigns of the Balearic Island Coastal Observing and Forecasting System (SOCIB). As wave data input data from the SIMAR dataset (provided by Puertos del Estados, *http://calipso.puertos.es/BD/informes/INT_8.pdf, last accessed 2nd September 2017*) was used.

2.7. Tidal modelling

Chapter 6, 7

Two model simulations for predicting the tidal range in the Southern Caribbean Sea were established by using the model Delft3D-FLOW. Simulation setup was done with the software Delft Dashboard v2.01. The main input to this model is the bathymetric grid, which was obtained from the GEBCO_2014 terrain model (GEBCO_2014_Grid, 2014). For a second simulation this grid was altered by a prediction of the ANICE-SELEN model, as described above, in order to get a bathymetry representing the paleo environment. A second input are the global tidal inverse solutions TPXO7.2 (Egbert et al., 1994; Egbert and Erofeeva, 2002), which are used as boundary conditions.

Another tidal model, the OSU Tidal Prediction Software (OTPS, Egbert and Erofeeva, 2002) has been used for calculating tidal ranges on the basis of modern tidal harmonic constituents. These tidal ranges were used for comparing the results of the Delft3D-FLOW results and for a global analysis of tidal ranges for all locations representing RSL indicators. As input the TPXO8-atlas dataset was employed (available at: *http://volkov.oce.orst.edu/tides/tpxo8_atlas.html, last accessed 2nd September 2017*). For model setup and running, the Tidal Model Driver (TMD, available from *https://www.esr.org/research/polar-tide-models/tmd-software/, last accessed 2nd September 2017*) was utilized.

2.8. Other processing software

Chapter 4, 5, 6, 7

Several spatial tasks (mainly spatial interpolation, map creation and digitizing) have been done using the software ESRI ArcGIS 10.2/10.4 and QGIS 2.16.

For different statistical calculations (including calculation of probability density functions and averaging long-term datasets of global wave and tide conditions) as well as data processing and visualization the software MathWorks MATLAB 2015a was used.

3. Outline of manuscripts

The cumulative thesis is compiled from four manuscripts, which represent the main chapters. Here, a short summary with list of authors, publication status and overview of the main objectives of each paper is presented. In addition, a short overview of the authors and my own contributions to each chapters is given.

3.1. Manuscript 1 – The analysis of Last Interglacial (MIS 5e) relative sea-level indicators: Reconstructing sea-level in a warmer world

A. Rovere, M.E. Raymo, M. Vacchi, T. Lorscheid, P. Stocchi, L. Gómez-Pujol, D.L. Harris, E. Casella, M.J. O'Leary & P.J. Hearty

Published in Earth-Science Reviews (2016) ***159****, p. 404–427*

Research highlights:

- Definition of standardized procedures for new and reanalyzing MIS 5e sea-level studies and their implementation in sea-level databases.
- Categorization of the 10 most common sea-level indicators and definition of upper and lower limit in their modern formation.
- Discussion of the impacts of using these procedures in the reconstruction of paleo sea level in MIS 5e

Author contributions: A.R. and M.E.R. developed original research idea. M.V. translated concepts of Holocene studies to MIS 5e. T.L. conducted literature research, organized and performed fieldwork to define the working example together with A.R., L.G.P., D.L.H. and E.C. M.J.O. and P.J.H. contributed field examples. A.R. and M.E.R. wrote the initial manuscript and all authors contributed to the text and discussions.

Detailed own contributions: For this manuscript I collected literature examples for the datasets underlying Fig. 4.6 and Fig. 4.11, and I collaborated with the first author to define the different landforms and deposits. I participated to the survey of the modern analog shown in chapter 4.6.1. Finally, as this review paper is also addressed to young geologists starting to work on MIS 5e sea levels, I critically commented the first draft of the manuscript from the perspective of a PhD student in order to clarify the manuscript objectives. I helped the first author in the compilation of the supplementary database structure annexed to the publication.

3.2. Manuscript 2 – Paleo sea-level changes and relative sea-level indicators: Precise measurements, indicative meaning and glacial isostatic adjustment perspectives from Mallorca (Western Mediterranean)

T. Lorscheid, P. Stocchi, E. Casella, L. Gómez-Pujol, M. Vacchi, T. Mann & A. Rovere

Published in Palaeogeography, Palaeoclimatology, Palaeoecology (2017) ***473****, p. 94–107*

Research highlights:

- Presentation of results from fieldwork on Mallorca island (GPS measurement, thin section analysis and detailed outcrop description)
- Determination of the indicative range of beach deposits by using a morphodynamic model (CSHORE) with modern wave and morphological conditions.
- Presentation of a set of new GIA model results for the Western Mediterranean for MIS 5e and discussion of their implications to the paleo RSL

Author contributions: T.L. and A.R. developed research idea. T.L. organized and led the fieldwork, co-ordinating the contributions of E.C., L.G.P., T.M. and A.R. P.S. contributed the GIA predictions. T.L. and E.C. performed morphodynamic modelling. L.G.P. contributed bathymetric data and field surveys. T.L. and M.V. analyzed thin sections. T.L. and A.R. wrote initial manuscript and all author contributed to the text.

Detailed own contributions: I organized two field trips in Mallorca. During two field trips, I collected elevation data of RSL indicators, created a detailed description and post-processed the field data. The morphodynamic model-ling with CSHORE was done by me. The description of the thin section was conducted by myself under the supervision of Matteo Vacchi. I analyzed the field data, attributed the indicative meaning from the modelling results and calculated the paleo RSL as well as the probability density function. I wrote the initial manuscript with supervision by Alessio Rovere and comments of all other co-authors.

3.3. Manuscript 3 – Tide gauges in past warmer worlds: the use of tidal notches for the validation of tidal modelling

T. Lorscheid, T. Felis, P. Stocchi, J.C. Obert, D. Scholz & A. Rovere

Pending revisions, Scientific Reports

*(*Published on 24th November 2017 in *Scientific Reports, **7**, 16241.)*

Research highlights:

- Survey of the paleo and tidal notch geometry and their elevation on the island of Bonaire (Southern Caribbean Sea)
- Hydrodynamic modelling of tides with paleo and modern bathymetry
- Discussion of advantages in using tidal notches and tidal modelling for paleo sea-level studies

Author contributions: T.L., T.F. and A.R. developed research idea, participated in the field work and interpreted the field evidence. T.L. and A.R. performed tidal modelling. P.S. performed GIA modelling. J.C.O. and D.S. performed ^{230}Th/U-dating. T.L. and A.R. wrote the initial manuscript and all authors revised the text.

Detailed own contributions: I organized the fieldwork in Bonaire. Field data (elevations measurement and notch geometry) for this manuscript was collected by myself with the help from Alessio Rovere and Thomas Felis. The post procession of the GPS data was done by me as well as the analysis of the geometric data. I learned how to set up and performed the model DELFT 3D, and I tested several model set-ups and performed the two simulations for tidal modelling. Analysis of the modelling data as well as processing was also done by myself. I wrote the initial manuscript with revisions by Alessio Rovere and comments of all other co-authors.

3.4. Manuscript 4 – Quantification of the indicative meaning for paleo sea-level studies

T. Lorscheid & A. Rovere

In preparation for submission to Quaternary Science Reviews

Research highlights:

- Concatenation of previous published databases of MIS 5e RSL indicators around the world
- Usage of modern hydro- and morphodynamic equations for quantifying the indicative meaning for each location from global tide and wave datasets
- Procedure for standardized application and database storage

Author contributions: T.L. and A.R. developed research idea and wrote the manuscript. T.L. conducted tidal modelling and analyzed data.

Detailed own contributions: The preparing and combination of published databases of RSL indicators was done by myself. Also downloading and analysis of wave datasets and modelling of tidal ranges for all locations was per-formed by myself. I performed literature research of suitable hydrodynamic equations and calculated the indicative meaning and paleo RSL for all sites. Discussion of the results and writing of the manuscript was done under the supervision of Alessio Rovere.

4. The analysis of Last Interglacial (MIS 5e) relative sea-level indicators: Reconstructing sea-level in a warmer world

A. Rovere, M.E. Raymo, M. Vacchi, T. Lorscheid, P. Stocchi, L. Gómez-Pujol, D.L. Harris, E. Casella, M.J. O'Leary, P.J. Hearty

Originally published in *Earth-Science Reviews* (2016) 159, p. 404–427

4.1. Abstract

The Last Interglacial (MIS 5e, 128–116 ka) is among the most studied past periods in Earth's history. The climate at that time was warmer than today, primarily due to different orbital conditions, with smaller ice sheets and higher sea-level. Field evidence for MIS 5e sea-level was reported from thousands of sites, but often paleo shorelines were measured with low-accuracy techniques and, in some cases, there are contrasting interpretations about paleo sea-level reconstructions. For this reason, large uncertainties still surround both the maximum sea-level attained as well as the pattern of sea-level change throughout MIS 5e. Such uncertainties are exacerbated by the lack of a uniform approach to measuring and interpreting the geological evidence of paleo sea-levels. In this review, we discuss the characteristics of MIS 5e field observations, and we set the basis for a standardized approach to MIS 5e paleo sea-level reconstructions, that is already successfully applied in Holocene sea-level research. Application of the standard definitions and methodologies described in this paper will enhance our ability to compare data from different research groups and different areas, in order to gain deeper insights into MIS 5e sea-level changes. Improving estimates of Last Interglacial sea-level is, in turn, a key to understanding the behavior of ice sheets in a warmer world.

4.2. Introduction

Past interglacials are of interest to the scientific community as they can be used to study the behavior of the climate system during times as warm as or slightly warmer than today. Of particular interest is the degree to which relatively small perturbations to climate forcing variables such as atmospheric or sea surface temperature, insolation, or CO_2 can lead to polar ice volume and sea-level changes. For instance, during marine isotope stage (MIS) 5e, the Last Interglacial (LIG, ~128 to 116 ka, Stirling et al., 1998), ice core evidence suggests that greenhouse gas concentrations were slightly higher than pre-industrial levels (Petit et al., 1999) and summer insolation at high latitudes was also higher by ~ 10%. These small changes in climate forcing were apparently sufficient to warm polar temperatures (> 66° latitude) in both hemispheres by about 3-5 °C relative to today (Otto-Bliesner et al., 2006) and global mean temperature by an estimated 1.5 °C (Turney and Jones, 2010; Lunt et al., 2013). By comparison, global mean temperature has increased by about half this, or by ~0.85 °C, since 1880 (IPCC, 2014) and an additional global warming of 1 °C, that could be expected to raise polar temperatures by 3–6 °C (Kattsov et al., 2005), is likely to occur by the end of this century. Indeed, the Antarctic Peninsula has been warming by an average of 0.5 °C per decade over the last 60 years (Mulvaney et al., 2012).

There is increasing evidence suggesting that the MIS 5e climatic conditions resulted in smaller ice sheets and, therefore, higher than present sea-levels (e.g. Kopp et al., 2009). The study of sea-level indicators dating from the Last Interglacial, therefore, is fundamental to unravel potential patterns of future sea-level rise caused by global warming (IPCC, 2014). The only direct observations that allow reconstruction of MIS 5e sea-levels are features associated with paleo sea-levels such as, for example, fossil coral reef terraces (Murray-Wallace and Woodroffe, 2012). However, reconstructing MIS 5e sea-level from such observations carries uncertainties related to age attribution and to how sea-level indicators are measured and interpreted by field geologists.

Two main issues are related to, i) the methods used to establish the elevation of a sea-level indicator, ii) how precisely those measurements are referred to modern mean sea-level. Standard topographic techniques (e.g. differential GPS, with vertical accuracy down to a few centimeters) have been employed in Pleistocene and Pliocene field studies only recently and therefore measurement errors reported by older studies need to be re-assessed. A fundamental issue relates to how paleo sea-level is calculated from the elevation of an indicator. Indeed, most MIS 5e (and older) markers cannot be correlated precisely to a tidal datum as happens, for example, with particular foraminifera assemblages in Holocene salt marshes (Shennan and Horton, 2002) or with coral microatolls (Woodroffe et al., 2012; Mann et al., 2016). Most MIS 5e sea-level indicators carry with them large sea-level uncertainties that are often not reported or properly defined.

The overall aim of this paper is to give a complete account of the best field practices that should be adopted when surveying MIS 5e and older sea-level indicators. In this study we aim to:

i) Present a set of definitions and standardizations that should be adopted in MIS 5e sea-level studies. Adopting such definitions both in studies reporting new sea-level indicators as well as in literature reviews will ensure that the results will be easily integrated in sea-level databases (Düsterhus et al., 2016).
ii) Describe the most common landforms and deposits used as MIS 5e sea-level indicators, together with their upper and lower limits of formation under modern conditions.
iii) Present an example of how the standard methodology described in this paper can be applied to a real study case.
iv) Discuss the implications for paleoclimate reconstructions of adopting correct procedures in the measurement and reporting of MIS 5e datasets.

4.3. Definitions

Today, processes acting near modern mean sea-level (MSL) are shaping a set of landforms on both rocky and sedimentary coasts. These features include, for example, shore platforms or cobble beaches. When these features are found in the geologic record, disconnected from their environment of formation (for instance, a shore platform observed several meters above present-day sea-level), we infer that a Relative Sea-Level (RSL) change has occurred. Any elevation difference between the original and the present-day elevation of similar features is called RSL change. RSL changes may be caused by factors such as ice volume changes, isostatic crustal adjustments, tectonics or compaction-related subsidence. Any stratigraphic horizon, landform, or paleobiologic indicator of past sea-level is called an RSL indicator (or RSL marker). An RSL indicator must have at least three properties:

i) Its elevation needs to be referred to a known height datum, and its position (latitude and longitude) needs to be referred to a known geographic system;
ii) Its offset (relative or absolute) from a former sea-level needs to be known;
iii) The age (relative or absolute) of the RSL indicator needs to be established with radiometric methods (such as ^{230}Th/U dating) or through chronostratigraphic correlation with other dated features.

Note that a RSL indicator is a more general form of 'sea-level index point', a concept used in Holocene sea-level studies (Shennan and Horton, 2002; Engelhart et al., 2009; Hijma et al., 2015). If the first two properties listed above are known, it is possible to calculate the paleo RSL (and its uncertainties) from the elevation of the RSL indicator (Table 4.1, Eq. 4.1-4.4). This paleo RSL is still uncorrected for post-depositional land movements (PD) or glacial isostatic adjustment effects (GIA). To correct for these processes, or obtain one of them from the RSL record, one must also know the age of the RSL indicator (see Section 4.5) and apply a workflow that includes Eq. 4.5-4.8 (see applied example in Section 4.6). Post-depositional land movements include all the vertical displacements that have happened since the RSL indicator was deposited or shaped. These may include local or regional tectonic effects, sediment compaction, isostatic response to sediment loading or unloading (Dalca et al., 2013) and dynamic topography (Moucha et al., 2008; Rowley et al., 2013; Rovere et al., 2015b).

Table 4.1: Relevant equations in MIS 5e paleo sea level studies, with definitions. For a calculator containing the equations in this table, see the spreadsheet in the supplementary material S4.1.

	Equation	Definitions
Eq. 4.1	$RWL = \left[\frac{U_l + L_l}{2}\right]$	RWL = Reference Water Level IR = Indicative Range Ul = Upper limit of landform in the modern analog Ll = Lower limit of landform in the modern analog RSL = paleo Relative Sea Level E = elevation of sea-level indicator(measured in the field) Ee = Error in elevation measurement (standard deviation) δRSL = uncertainty of RSL (standard deviation) PD = Post-depositional displacement uplift/subsidence PDr = Post-depositional displacement uplift/subsidence rate δPDr = uncertainty of PDr (standard deviation) GIA = Glacio-hydro-isostatic Adjustment contribution ESL = Paleo Eustatic Sea Level T = age of the paleo RSL indicator δGIA = uncertainty of GIA (standard deviation) δESL = uncertainty of ESL (standard deviation) δT = uncertainty of T (standard deviation)
Eq. 4.2	$IR = (U_l - L_l)$	
Eq. 4.3	$RSL = (E - RWL)$	
Eq. 4.4	$\delta_{RSL} = \sqrt{E_e^2 + \left(\frac{IR}{2}\right)^2}$	
Eq. 4.5a	$PD = [RSL - (GIA + ESL)]$	
Eq. 4.5b	$ESL = [RSL - (GIA + PD)]$	
Eq. 4.6	$PDr = \left[\frac{RSL - (GIA + ESL)}{T}\right]$	
Eq. 4.7a	$\delta_{PD} = \sqrt{(\delta_{RSL}^2 + \delta_{GIA}^2 + \delta_{ESL}^2)}$	
Eq. 4.7b	$\delta_{ESL} = \sqrt{(\delta_{RSL}^2 + \delta_{GIA}^2 + \delta_{PD}^2)}$	
Eq. 4.8	$\delta_{PD} = \sqrt{\left(\frac{\delta_{PD}^2}{T^2}\right) + \left[\left(\frac{PD}{T^2}\right)^2 * \delta T^2\right]}$	

Any geological study on MIS 5e shorelines should aim to obtain the most accurate estimate of paleo RSL and its associated uncertainties. In the next section we describe how this can be achieved using field procedures and a standardized approach to the calculation of uncertainties.

4.3.1. Measuring the elevation of Last Interglacial RSL indicators

The elevation of an RSL indicator is the vertical distance between the marker and modern mean sea-level, while the elevation error represents the accuracy of the measurement itself. Every measurement needs to be referred to a vertical datum (i.e. a 'zero' reference frame, representing modern MSL). In literature, the survey instruments used to establish elevation, their accuracy, and the vertical datum used are seldom reported.

Several instruments can be used to measure the elevation of a RSL indicator - they vary in accuracy and in the ease with which they can be precisely related to a vertical datum (Table 4.2). The best measurement technique is represented by differential global positioning systems (DGPS) that can determine elevations either in real time or via post-processing (Muhs et al., 2011; O'Leary et al., 2013; Muhs et al., 2014; Rovere et al., 2014b; Rovere et al., 2015b). DGPS elevation measurements can be referred to either a global geoid model (currently, EGM2008, Pavlis et al., 2012) or, where available, a local geoid model typically calculated by national geodetic institutes (*http://www.isgeoid.polimi.it/*). If a local geoid model is not available, one should calibrate the GPS measurements against a known tidal datum using the procedure described in Foster (2015; Handbook of Sea-level Research, Chapter 10.4.2,

page 166–167, Fig. 10.1). Errors in elevation measurements with DGPS typically range between 0.02 and 0.08 m depending on the differential positioning technique used as well as other factors such as the spatial distribution of satellites at the time of measurement or the presence of obstacles masking the satellite view (e.g. trees, buildings).

Table 4.2: Description of the vertical accuracy and error of techniques used to measure elevations in the field.

Measurement technique	**Description**	**Typical vertical error under optimal conditions**
Differential GPS	Positions are acquired in the field and are corrected, either in real time or during post-processing, with respect to the known position of a base station or a geostationary satellite system (e.g. Omnistar). Accuracy depends on satellite signal strength, distance from base station, and number of static positions acquired at the same location.	± 0.02/±0.08 m
Total station	Total stations or levels measure slope distances from the instrument to a particular point and triangulate relative to the XYZ coordinates of the base station. The accuracy of this process depends on how well defined the reference point and on the distance of the surveyed point from the base station. Thus, it is necessary to benchmark the reference station with a nearby tidal datum, or use a precisely (DGPS) known geodetic point. The accuracy of the elevation measurement is also inversely proportional to the distance between the instrument and the point being measured.	± 0.1/±0.2 m
Auto or hand level		± 0.2/±0.4 m
Metered tape or rod	The end of a tape or rod is placed at a known coordinate or elevation point, and the elevation of the unknown point is calculated using the metered scale and, if necessary, clinometers to calculate angles. The accuracy of this method decreases considerably with elevation offsets > 10 m between the known and unknown points.	Up to ± 10% of elevation measurement
Barometric altimeter	Difference in barometric pressure between a point of known elevation (often sea level) and a point of unknown elevation. Not accurate and used only rarely (e.g. Pedoja et al., 2011b)	Up to ± 20% of elevation measurement
Topographic map and digital elevation models	Elevation derived from the contour lines on topographic maps. Most often used for large-scale landforms (i.e. marine terraces). Several meters of error are possible, depending on the scale of the map or the resolution of the DEM (Rovere et al., 2015b).	Variable with scale of map and technique used to derive DEM.

Other common survey instruments used to measure paleo shorelines (Table 4.2) are Total stations (Dutton et al., 2015b), metered tapes or rods (Antonioli et al., 2006, their Fig. 5b), hand or auto levels (often combined with other more precise techniques such as DGPS, O'Leary et al., 2008; Dutton et al., 2015b), and barometric altimeters (Pedoja et al., 2011b). With each of these methods, an estimate of the vertical error can be obtained through replication of the measurement, followed by calculation of the mean and standard deviation of the measured elevations. This practice is not often followed. Furthermore, these techniques do not provide elevations that are directly referenced to a global or local

geoid, but rather provide a measurement relative to a local starting point - a point that must then be benchmarked against a tidal datum (see Dutton et al., 2015b for an example).

To measure the elevation of large-scale landforms (such as marine terraces extending hundreds of meters to kilometers) one can employ topographic maps and Digital Elevation Models (DEMs). Depending on the scale of the map or the grid size of the DEM, errors can range up to several meters. However, these techniques are particularly useful in tracking landforms at landscape scale, in order to identify possible warping or differential uplift due to tectonics or other post-depositional movements (Muhs et al., 1992; Rovere et al., 2015b). Airborne LIDAR datasets can be used for a similar purpose, with the advantage of a higher vertical accuracy (± a few centimeters, dependent on the specific laser sensor employed, GPS positioning and Inertial Measurement Unit). Recent developments in DEMs obtained from satellite imagery are providing elevations with a vertical accuracy < 1.5 m and 1 m grid spacing (e.g., DEMs derived from tri-stereo Pleiades satellite imagery).

4.3.2. Determining indicative meaning of a sea-level indicator according to the modern analog

After accurate elevation measurements of paleo RSL features are made, one must then evaluate where, relative to sea-level, those features formed (e.g., was the feature forming exactly at sea-level, above, or below it?). While the elevation measurement (and associated error) of any RSL indicator is an objective measure, the estimation of paleo RSL from a RSL indicator can be more subjective, commonly reported in sea-level studies as the 'geologic interpretation' of the data and thus more likely to give rise to controversy.

It is then important to introduce here the concept of indicative meaning. This is the most fundamental elevation attribute in RSL reconstructions and describes where, with respect to tide levels, the sea-level indicator formed (Shennan, 1982; Van De Plassche, 1986; Hijma et al., 2015). The indicative meaning consists of two parameters: the indicative range (IR) and reference water level (RWL). IR and RWL are concepts that are already widely applied in Holocene sea-level studies (Shennan and Horton, 2002; Engelhart and Horton, 2012; Vacchi et al., 2016) and are beginning to be employed in sea-level studies focused on older periods (Kopp et al., 2009; Rovere et al., 2015b). These terms can be defined as follows (Hijma et al., 2015):

The IR is the elevation range over which an indicator forms and the RWL is the mid-point of this range, expressed relative to the same datum as the elevation of the sampled indicator (geodetic datum or tide level). The greater the indicative range, the greater the uncertainty in the final paleo RSL reconstruction.

The indicative meaning for a given type of feature is determined by measuring its relationship with a specific contemporary tidal level (usually the mean sea-level, MSL) along the modern shorelines (i.e. the modern analog). The application of the concept of modern analog to Holocene sea-level studies has allowed the development of transfer function techniques, which have significantly improved our ability to assess, in a quantitative and standardized way, Holocene RSL changes (Juggins and Birks, 2012; Kemp and Telford, 2015).

As an example, we assume in Fig. 4.1 that a Last Interglacial exposed beach deposit (yellow unit in Fig. 4.1) contains corals that were sampled and dated (e.g. with ^{230}Th/U) to MIS 5e. The beach deposit is found in close proximity to the inner margin of a marine terrace (red dot), which is used as RSL indicator. The measured elevation of the inner margin is +2.12 ± 0.13 m. In the modern shoreline adjacent to the paleo RSL indicator, the inner margin of a terrace mantled by a shallow submerged beach deposit is defined as the modern analog. We observe that the modern inner margin is located between -0.9 and -1.8 m below MSL depending upon where along the coast we are. In the lower left corner of Fig. 4.1 we show how we can use the upper and lower limits for the RSL indicator to calculate RWL and IR using Eq. 4.1 and Eq. 4.2 (Table 4.1). Once IR and RWL are determined, it is possible to calculate the Paleo RSL index point and its associated uncertainty using Eq. 4.3 and 4.4 in Table 4.1 (i.e., an index point is a point that estimates relative sea-level at a specified time and place, cf. Gehrels and Long, 2007; Hijma et al., 2015).

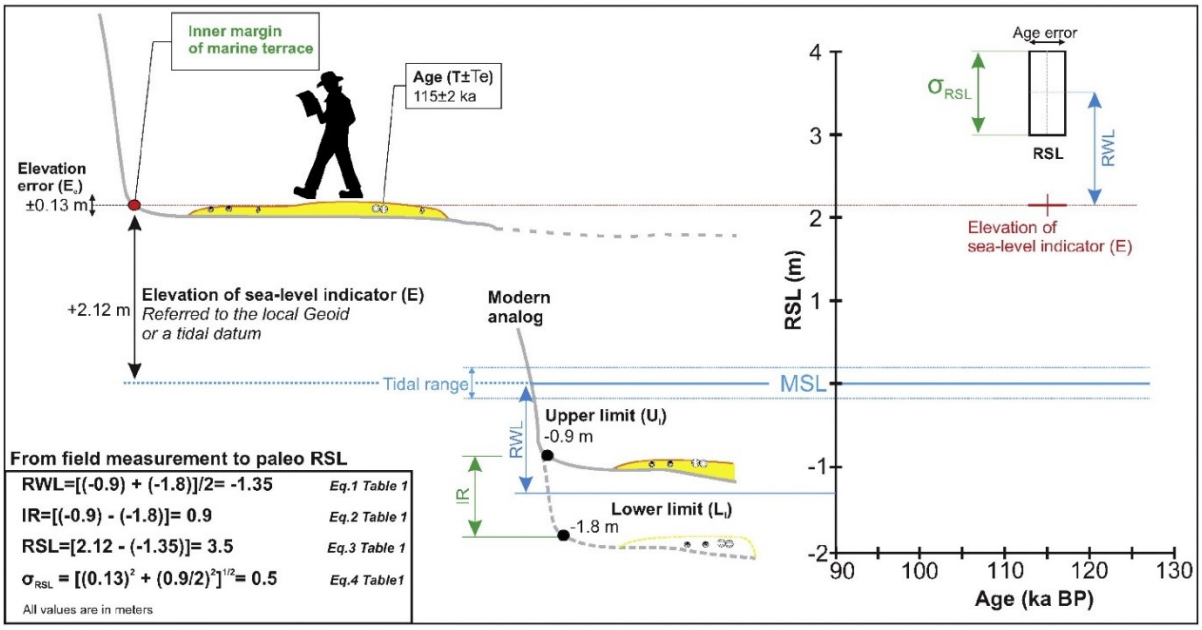

Fig. 4.1: Example of calculation of RWL, IR, RSL and RSL error from a paleo RSL indicator (marine terrace) and a modern analog.

In this example, we calculate the paleo RSL index point, and associated error, using Eq. 4.1-4.4 in Table 4.1, resulting in a paleo RSL elevation of +3.5 ± 0.5 m (e.g. 2.12 m - (-1.35) = 3.5). It is worth noting that the final paleo RSL is 1.35 m higher than the initial measurement of marker elevation, obviously taking into account that the inner margin of a marine terrace forms on average at -1.35 m in the modern local setting. In terms of ice sheet melting, this difference is significant, equal to roughly half of the proposed Greenland contribution to MIS 5e sea-level (Rybak and Huybrechts, 2013). A second aspect worth highlighting regards the number of significant digits with which we can approximate paleo RSL. While in the measured elevation, IR and RWL can be indicated with centimetric precision (i.e. 2.12 m) if derived from high-accuracy instruments (e.g. DGPS), we suggest that the calculated paleo RSL should be indicated with decimetric precision, as it is unlikely that the calculations from Eq. 4.1-4.4 can yield, for MIS 5e, values that are accurate at centimeter level.

Application of the indicative meaning approach to the interpretation of past sea-level requires the assumption that the local conditions responsible for the shaping of the landform, such as tidal or wave regime, have not changed significantly between the two times. It is possible that in some cases this assumption is not true, for example if higher sea-level during the Last Interglacial resulted in major changes in the paleogeography of the study area and therefore changes in how wave action or different tidal ranges may have influenced the formation of a marker. In this case, corrective factors with respect to the modern analog would need to be adopted (and of course described).

In order to calculate both IR and RWL, it is necessary to couple site-specific research on paleo sea-levels with that on modern shoreline processes, existing landforms and/or biological zonation of living organisms. Such information can be obtained by performing surveys on the modern shoreline, identifying, if present, the same facies and organisms encountered in the paleo record and measuring their modern elevation range. This approach was used, for example, by O'Leary et al. (2013), who measured the elevation (relative to MSL) of modern biological communities and geomorphic features in Western Australia, and then used these observed offsets to estimate the position of paleo RSL as indicated by the same facies in the fossil record (see Fig. 2 of O'Leary et al., 2013 for details).

Another site-specific approach involves the use of data available in literature to establish the boundaries of specific landforms. As an example, Rovere et al. (2015b) inferred the indicative meaning for the mid-Pliocene shoreline scarp on the US Atlantic Coastal Plain referring to studies of modern beach profile variations at different places along the modern shoreline in the same region. On the modern shoreface, a major break in slope is observed at 3-7 m depth (Hallermeier, 1980; Larson and Kraus, 1994; Lee et al., 1998) that corresponds to the maximum water depth for nearshore erosion caused by average wave conditions. Using -3 and -7 m as upper and lower limits of the IR, they calculated paleo RSL and associated uncertainties using Eq. 4.1-4.4 in Table 4.1.

It is worth noting that paleo RSL indicators exclude those landforms that cannot be directly related to sea-level. As an example, a dune deposit will always be located above sea-level, but it is not possible to quantify with any useful accuracy where the dune was forming relative to the MSL. Such indicators are defined as terrestrial limiting points. Similarly, a marine deposit with in situ fauna with no stratigraphic or sedimentologic information that would allow one to tie it closely to sea-level must be considered as a marine limiting point. The only information that can be derived from terrestrial and marine limiting points is that, at the time of their formation, sea-level was respectively above or below the elevation of such indicators (Fig. 4.2).

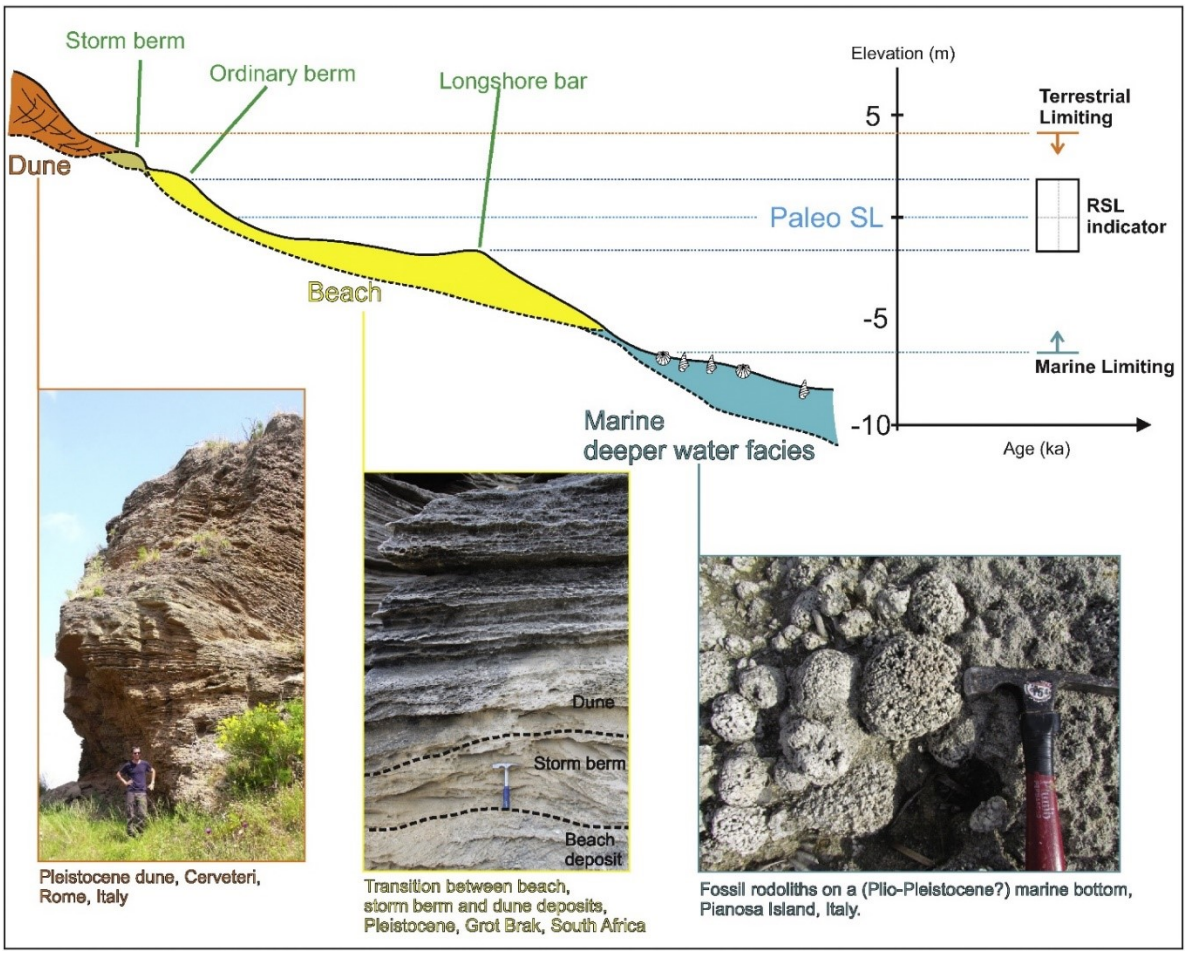

Fig. 4.2: Difference between RSL, terrestrial and marine limiting points. The Pleistocene dune of Cerveteri is described in Nisi et al. (2003) and references therein. The deposits at Grot Brak are described in Carr et al. (2010). The Plio-Pleistocene marine facies in Pianosa Island are described in Graciotti et al. (2002).

4.4. Last Interglacial RSL indicators

Scientific observations of late Quaternary, and particularly MIS 5e, shorelines higher than present date back almost two centuries (Lyell, 1837; Darwin, 1846; Hutton, 1885). Since then, numerous papers have addressed Last Interglacial relative sea-levels. Pedoja et al. (2014) compiled the most extensive review of paleo sea-level studies to date, identifying 987 studies that reported at least the elevation of an MIS 5e site. It is worth noting that the number of such studies increased dramatically in the decade 1970–1980, and has been growing steadily since (Fig. 4.3c). Analyzing the Pedoja et al. (2014) database in a spatial context, we can identify the areas where the most MIS 5e sites are concentrated (Fig. 4.3a). These include the west coast of the US (Muhs et al., 2003), the western Mediterranean Sea (Zazo et al., 2003; Ferranti et al., 2006) and the Japanese coasts (Ota and Omura, 1991). Relevant compilations of shoreline data at a regional scale include Ferranti et al. (2006); Hearty et al. (2007); Muhs et al. (2003); Murray-Wallace and Belperio (1991); O'Leary et al. (2013), while more recent reviews are centered mostly on the timing of MIS 5e sea-level changes (e.g. Dutton and Lambeck, 2012; Medina-Elizalde, 2013).

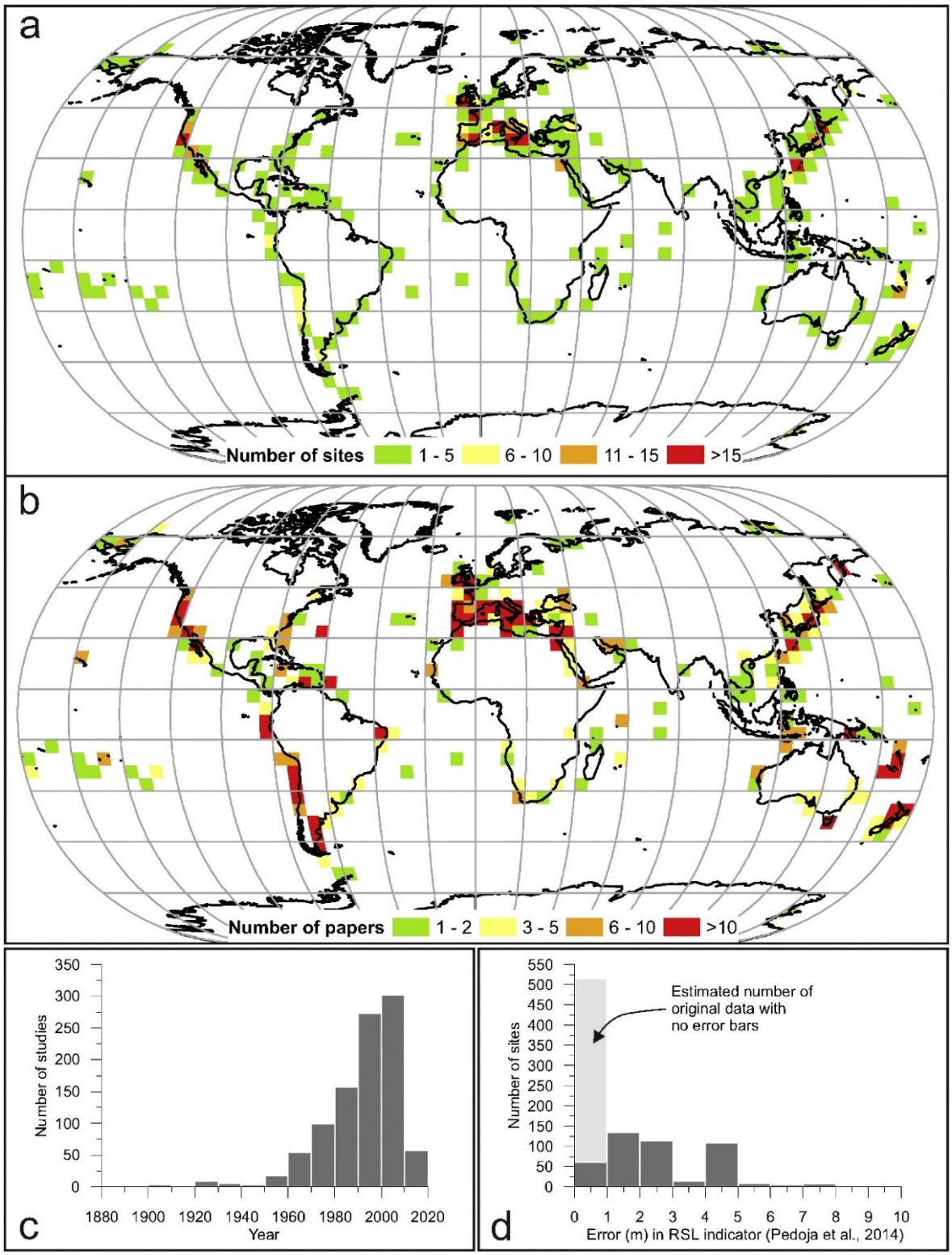

Fig. 4.3: Number of a) sites and b) papers published within land parcels of 500 km2; c) number of studies reporting MIS 5e shorelines per year; d) error bars on MIS 5e sea-level. Based on data from Pedoja et al. (2014).

Several problems are encountered when comparing MIS 5e data from different compilations. The main issue is that each MIS 5e database uses a different table structure as well as varying definitions of landforms and of their indicative meaning. Often, no distinction is given between measurement of the

RSL indicator and the interpretation (e.g. the IR and RWL), although some observations that might inform the determination of indicative meaning are sometimes included in the description of the landforms (e.g. see Supplementary Data in Pedoja et al. (2011a); Pedoja et al. (2014), or main paper in Ferranti et al. (2006)). In addition, the measurement methods adopted by authors and the vertical datum to which they reference their field elevation measurements are seldom described in detail, thus it is very difficult to assess measurement error in published studies.

Very few studies published prior to 2010 used high-precision techniques (e.g. differential GPS) to measure the elevation of RSL indicators or reported uncertainties associated with elevation measurements. Pedoja et al. (2014, their Suppl. Data) highlight that, in their sea-level database, they 'systematically attributed a minimum error range of one meter to the measurements on elevation published without any margin of error'. Among the sites they reviewed, almost half (456 over 943) have error bars equal to ±0.5 m (Fig. 4.3d). In another large MIS 5e database, Kopp et al. (2009) included only sites where published information was detailed enough to derive a measurement error, IR and RWL. As a result, the number of sites in their database is much lower than in Pedoja's (78 data points vs 943), however, they presumably are much more accurate.

Major research need is to re-evaluate the measurement error of published data and perform new topographic measurements (e.g. with differential GPS, or a total station benchmarked to tidal gauges) in order to minimize the uncertainties in paleo sea level estimates related to measurement error. Differential GPS instruments are becoming more accessible both in terms of usability by non-experts as well as cost (Takasu and Yasuda, 2009; Stempfhuber and Buchholz, 2011).

A common denominator of MIS 5e studies and databases is the relatively low number of landforms and deposits that have been used as RSL indicators (Fig. 4.4, Table 4.3). For each one of these indicators, it is possible, in theory, to define their IRs relative to modern sea-level by studying modern analogs. This information can then be used to calculate paleo RSL with more rigorously determined uncertainties. In the next sections, we describe the most common RSL indicators that have been used in MIS 5e studies and we address, for each one, how upper and lower bounds of their indicative range can be calculated or estimated.

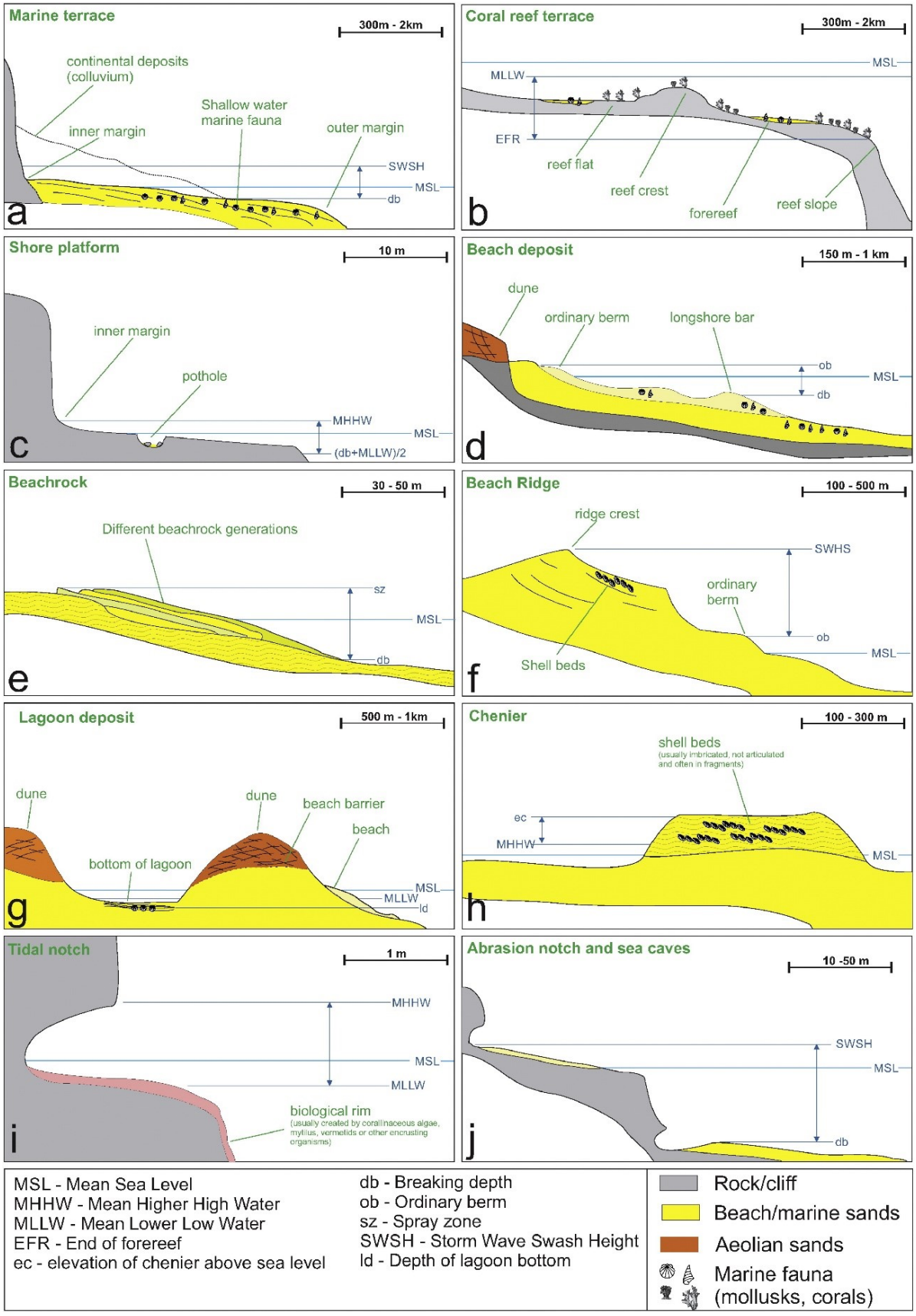

Fig. 4.4: Landforms commonly used as RSL indicators for MIS 5e with the upper and lower limits of the Indicative Range shown by the thin dark blue lines (see Table 4.3 for more details and definitions).

Table 4.3: Summary of landforms most commonly used in Last Interglacial sea level studies, including upper and lower limits of indicative range as described in the text and elements within the landform that might help inform the indicative range. In the last column, each parameter used in the table and in the text is described.

Landform	Upper limit	Lower limit	Elements improving RSL estimate
Marine terraces	Storm wave swash height (SWSH)	Breaking depth (db)	Presence of fixed biological indicators or sedimentary features in the deposits covering the terrace.
Coral reef terraces	Mean lower low water (MLLW)	End of forereef (EFR)	Living ranges of different species, or particular growth forms (e.g. microatolls).
Shore platforms	Mean higher high water (MHHW)	Between Mean Lower Low Water and breaking depth (db + MLLW)/2	Presence of biological indicators.
Beach deposits	Ordinary berm (ob)	Breaking depth (db)	Biofacies, orientation and integrity of shells, sedimentary structures.
Beach rock	Spray zone (sz)	Breaking depth (db)	Sedimentary structures, types of cement.
Beach ridges	Storm wave swash height (SWSH)	Ordinary berm (ob)	Sedimentary structures
Lagoon deposits	Mean lower low water (MLLW)	Depth of lagoon bottom (ld)	Sedimentary structures, presence of biological indicators or species with limited depth ranges or upper limits in their depth range (i.e. MLLW).
Cheniers	Elevation of chenier above sea level (ec)	Mean higher high water (MHHW)	Biological indicators or sedimentary structures.
Tidal notches	Mean higher high water (MHHW)	Mean lower low water (MLLW)	Fixed biological indicators
Abrasion notches and sea caves	Storm wave swash height (SWSH)	Breaking depth (db)	Fixed biological indicators, despite difficult to find due to abrasion.

MHHW: mean higher high water, the average of the higher high water height of each tidal day observed over a Tidal Datum Epoch (NOAA).
MLLW: mean lower low water, the average of the lower low water height of each tidal day observed over a Tidal Datum Epoch (NOAA).
SWSH: storm wave swash height, it is the maximum elevation reached by extreme storms on the beach (Otvos, 2005).
db: breaking depth. Horizontal water particle velocities reach their maximum values at the breaking depth, so that the sea floor beneath the breaker zone is where the coarsest sediments are trained or brought into suspension. This zone is function of the wave climate and can be empirically calculated knowing average annual wave period and wave height, wave approach angle, and coefficients depending on the slope and type of coast. In absence of site-dependent data, db can be calculated using the dimensionless parameter H/d. This parameter is used for the relative height of the wave compared to the water depth, and is often used to determine wave breaking criteria. For a smooth, flat slope, the maximum ratio of H/db = 0.78 (therefore db = H/0.78) is commonly used for wave breaking criteria, and increases as the bottom slope increases (US Army Corps Of Engineers, 1984).
EFR: end of forereef, the break in slope marking the transition between the quasi-horizontal surface shaped by waves and the reef slope.
ob: ordinary berm. Berms are depositional features formed by the wave-induced accumulation of sand on the beach (Schwartz, 2005). The ordinary berm is the one produced by average or more typical waves. The elevation of the berm depends on wave climate and sediment size, and it can be assumed that it is function of ordinary

wave runup. The berm can be either measured at the modern analog or deduced from the wave runup calculated using models. In absence of site-dependent data, to estimate runup once can adopt the empirical formula R/Hs = α (Mayer and Kriebel, 1994) where R is the wave runup and α depends on wave properties and beach slope. Usually, α is estimated empirically between 0.1 < α < 0.3 for regular waves acting on uniform, smooth, and impermeable laboratory beaches with slopes typical of many natural beach slopes. Once can ideally set α as the average of the two values, i.e. 0.2, and add to R the value of MHHW, as an high tide would be responsible for shifting upwards the runup height. Therefore ob = R + MHHW = (Hs*0.2) + MHHW.
sz: spray zone, above the MHHW and regularly splashed but not submerged by ocean water. It is very difficult to define the elevation range of the spray zone without observations of a modern analog. As an approximation, one can adopt as a sz value twice the elevation of the ordinary berm calculated as described above.
ld: the depth of the lagoon bottom, usually very shallow.ec: elevation of chenier, up to few meters above sea level.

4.4.1. Marine terraces

Any relatively flat surface of marine origin can be defined a marine terrace (Pirazzoli, 2005, Fig. 4.4a). Marine terraces can be shaped by marine erosion (wave-cut terraces) or can consist of shallow water to slightly emerged accumulations of materials redistributed by shore erosional and depositional processes (i.e., marine-built terraces Pirazzoli, 2005). Marine terraces range in width from few hundreds of meters to up to 1-2 km, are often mantled by subtidal, intertidal or slightly supratidal deposits, and can stretch along many kilometers of coastline. They are widely used in sea-level studies, especially those addressing coastal uplift (Ku and Kern, 1974; Kern, 1977; Muhs and Szabo, 1982; Muhs et al., 1992; Zazo et al., 1999; Schellmann and Radtke, 2000; Zazo et al., 2007; Gaki-Papanastassiou et al., 2009).

The feature of a marine terrace that is most commonly used as the paleo RSL indicator is the inner margin (Fig. 4.5a), specifically the knickpoint between the sub-horizontal surface of the terrace and the vertical or sub-vertical landward cliff. If a relict inner margin is covered by colluvium deposits after its formation, the precision of the sea-level reconstruction necessarily decreases (see the example of the reconstruction of mid-Pliocene sea-level from the inner margin of the Orangeburg scarp, a Pliocene marine surface on the Atlantic Coastal Plain of the US, Rovere et al. (2015b)). In such cases, the thickness of the colluvium can be estimated independently, or it can be surveyed with indirect techniques such as ground penetrating radar (e.g. O'Neal and Dunn, 2003).

Fig. 4.5: a) Example of an MIS 5e marine terrace on Santa María Island, Azores (see Ávila et al., 2015 for details); b) modern inner margin of marine terrace located in the swash zone, being actively shaped by beach erosion processes (Portugal, Algarve); c) modern inner margin located near the breaking depth of waves at around 4–5 m depth (NW Italy, Capo Noli, (Rovere et al., 2011; Rovere et al., 2014a)). The gray line in each figure represents the location of the inner margin.

Along modern shorelines, it is possible to observe the inner margin of marine terraces in two settings. The first is above sea-level, usually bounded by a beach (Fig. 4.5b). The inner margin can also be found below sea-level in the zone where marine abrasion is still active (Fig. 4.5c; Ferranti et al., 2006). Therefore, the upper limit of the indicative range for the inner margin of a marine terrace can be set to the storm wave swash height (SWSH), while the lower limit can be set to the breaking depth of significant waves that form the terrace (db , i.e. the depth at which waves start breaking; (Smith, 2003; Vacchi et al., 2014)). The sea-level information may be more precise if other features, such as in situ biological indicators, are found in proximity to the inner margin or knickpoint.

4.4.2. Coral reef terraces

Coral reef terraces can be considered a particular type of marine terrace (Fig. 4.4b) as they are formed by the interplay of erosive processes (wave abrasion, bioerosion) and bioconstructional processes (coral reef growth, Anthony, 2008), while marine terraces are mostly related to wave erosion processes and sedimentary deposition. In general, reef terraces are discussed within the framework of keep-up/catch-up/give-up (Macintyre, 1967; Neumann and Macintyre, 1985) and backstepping processes (Murray-Wallace and Woodroffe, 2012), and they usually range from few hundred meters to 1-2 km in width (Fig. 4.7a). The possibility to date corals preserved on the terrace surface using U-series (^{230Th}/U) methods (e.g. Muhs et al., 1994; Stirling et al., 1998) has resulted in the widespread use of coral reef terraces as sea-level indicators, especially in uplifting areas (such as Barbados or Papua New Guinea, Bard et al., 1990; Chappell et al., 1996; Schellmann and Radtke, 2004; Schellmann et al., 2004) where coralline stair-stepped landscapes are preserved (Kelsey, 2015).

In general, paleo RSL is determined from the average elevation of the terrace or, if present, from the elevation of the highest in situ corals which are usually found on the paleo reef crest. Merging stratigraphic and geologic information with considerations on the water-depth range of different coral species, or the occurrence of particular benthic assemblages or growth forms with a limited living range (e.g., such as microatolls which are constrained to the intertidal zone, Woodroffe et al., 2012) can further improve paleo RSL estimates. It is worth noting that considering only the palaeo ecology of single coral genuses on a former reef terrace does not allow to obtain precise sea level information (Hibbert et al., 2016), as the living depth of one genus can span several tens of meters. A relevant information that can be used in paleo sea level reconstructions is that a reef flat typically extends up to the mean lower low water (MLLW, Fig. 4.6a), which represents the general upper limit of the living range of corals. The depth of the coral reef terrace is dependent on the hydrodynamic conditions it is exposed to. A modern reef flat is rarely observed deeper than 3 m (Blanchon, 2011).

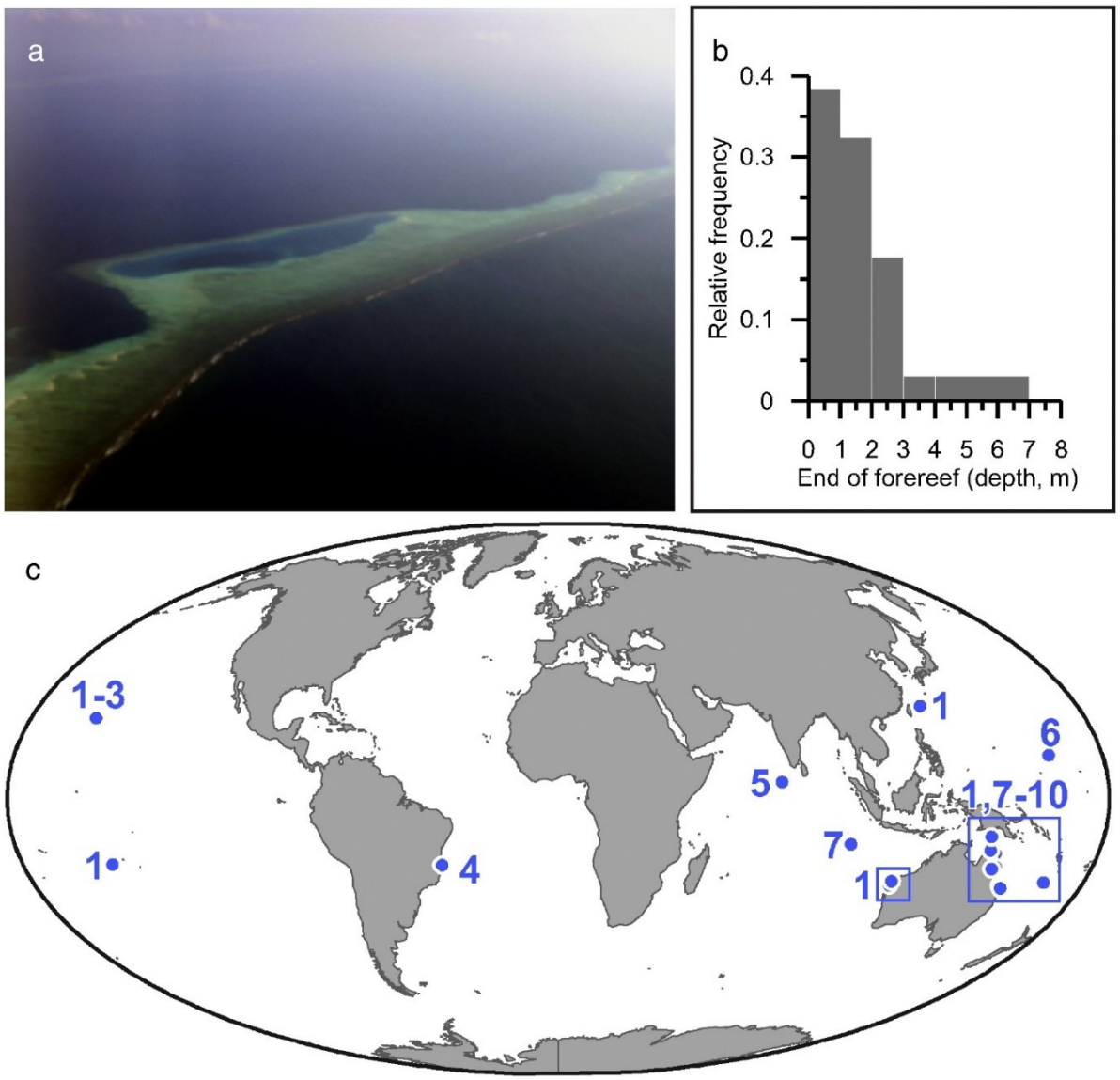

Fig. 4.6: a) Reef flat in Malé Atoll, Maldives; b) frequency distribution of the maximum reef flat depth of 34 reefs worldwide (see supplementary material S4.1 for details); c) the location of these reefs. References: 1. Falter et al. (2013); 2. Jokiel et al. (2014); 3. Storlazzi et al. (2003); 4. Mariath et al. (2013); 5. Lasagna et al. (2010); 6. Buddemeier et al. (1975); 7. Kench and Brander (2006); 8. Goatley and Bellwood (2012); 9. Dean et al. (2015); 10. Mongin and Baird (2014); Other datasets: Blanchon (2011); Montaggioni (2005).

4.4.3. Shore platforms

Shore platforms (Fig. 4.4c and 4.7a,b) are sub-horizontal rocky surfaces that interrupt vertical or sub-vertical cliffs near sea-level (Kennedy, 2015). Shore platforms have been classically divided in two categories: those sloping gently between about 1° and 5°, and those which are horizontal (Trenhaile, 1987; Sunamura, 1992). To these two types, Bird (2008) added structural shore platforms, which are found where waves have exposed the surface of a flat or gently dipping resistant rock formation, usually a bedding plane. Shore platforms can be characterized by a number of smaller scale features such as wave ramps, potholes and other abrasion forms created by wave action, bioerosion, and/or chemical erosion (Fig. 4.7f). Although the terms ‘shore platform’ and ‘marine terrace’ have been often used

as synonyms, we highlight that they indicate different landforms. One of the main differences resides in the width scale: few tens of meters for shore platforms, few hundreds of meters to kilometers for marine terraces (see scale bars in Fig. 4.4a,c). Another important difference is that, often, a shore platform represents an exposed rock surface, while a marine terrace is often covered by coastal or marine deposits.

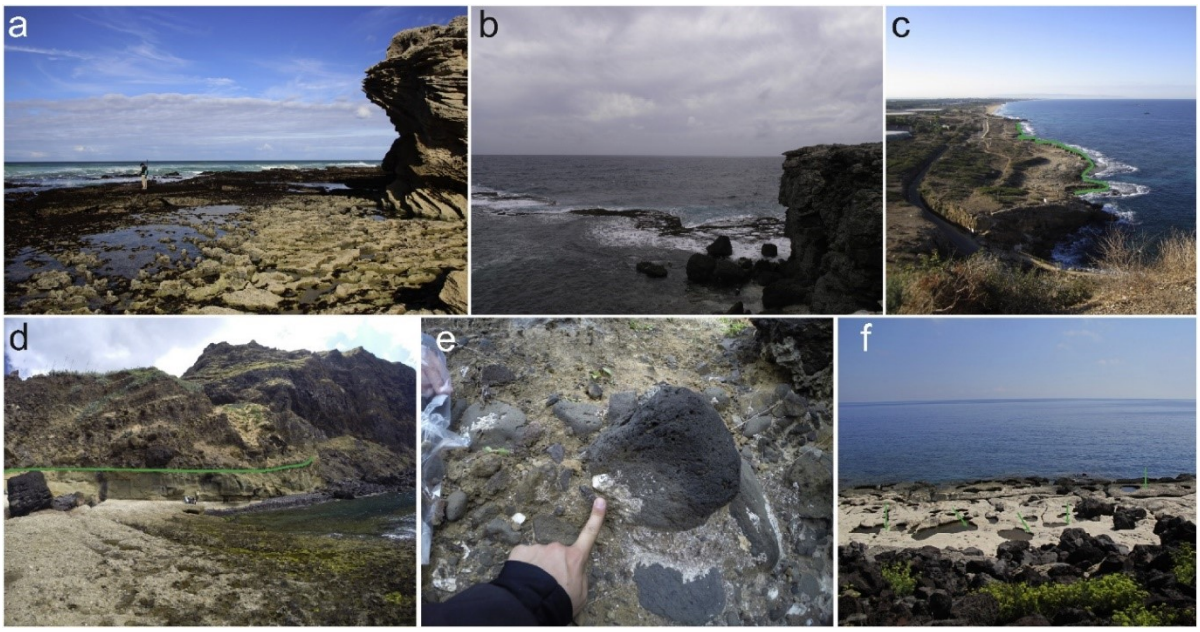

Fig. 4.7: Modern shore platforms in a) South Africa, De Hoop Nature Reserve and b) Guadeloupe, French Caribbean; c) modern shore platform in Galilee, Israel. The green line separates the modern platform from an upper platform shaped during MIS 5e (Sivan et al., 1999); d) MIS 5e shore platform (green line) on Santa Maria Island, Azores ("Pedra que Pica" outcrop, for details see Ávila et al., 2015); e) deposits still preserved on the Santa Maria platform include rounded boulders of volcanic origin with fossil limpets (Patella sp.) still attached in living position. Such observations can be used to better constrain the indicative range of this deposit as the preferred habitat of Patella is generally ranges between the supra-littoral zone and the spray zone (Rovere et al., 2015a); f) Potholes (green arrows) on a shore platform in Biddiriscottai, Sardinia, NW Italy, that are shaped during winter storms.

The contact point between the horizontal bedrock and the vertical rocky cliff (i.e. the inner margin) is usually considered a good paleo RSL indicator, and shore platforms have been used as RSL indicators in a number of settings (Fig. 4.7c–e). Nevertheless, disagreement exists as to whether marine or subaerial processes play the major role in shaping shore platforms (Stephenson, 2000; Stephenson and Kirk, 2000; Trenhaile and Kanyaya, 2007; Trenhaile and Porter, 2007; Trenhaile, 2008; Gomez-Pujol et al., 2014). The amplitude of the tidal range is considered to be significant as it determines the height of wave attack as well as the kind of waves reaching the platform, factors which can influence both weathering and biological activities (Kanyaya and Trenhaile, 2005). To be more exact, the initiation and evolution of a shore platform depends on a balance between the geological properties of the bedrock and the coastal environmental forcing (Gómez-Pujol et al., 2006; Kennedy and Dickson, 2006; Naylor and Stephenson, 2010). Wave energy appears to play a significant role, with sloping platforms formed in environments characterized by higher wave energy than horizontal platforms.

Following the above, the use of shore platforms as sea-level indicators must be informed by an understanding of the processes active in their development (Pirazzoli, 1996). In fact, while some platforms are carved above sea-level, others are initiated in intertidal to slightly subtidal zones. According to Kennedy (2015) 'the seaward edge of a shore platform is defined as: the point where active erosion of the bedrock ceases'. In general, the limits of the indicative range associated with shore platforms vary from mean higher high water (MHHW) to a point that, according to the above definition of Kennedy (2015), lies between the mean lower low water (MLLW) and the breaking depth of significant waves. A first-order estimate of the lower limit of a shore platform can be the midpoint between these two depths (Fig. 4.4c).

4.4.4. Beach deposits and beach rocks

Beaches are loose accumulations of sand, gravel or pebbles that characterize many coasts worldwide (Anthony, 2005). The upper limit of a beach is on land while its lower limit is typically found in the upper subtidal zone (Fig. 4.4d). Cemented beach deposits have been used as RSL indicators in a number of MIS 5e studies (see sup. Mat. in Pedoja et al., 2014), but very few of these studies consider their vertical range of formation in the calculation of the paleo RSL (see example for the cemented beach deposit in Cala Millor, Fig. 4.15).

There are several potential ways to define the upper and lower limits of a beach (Short, 1999; Chrzastowski, 2005). As an example, the beach can range from the wave base (often located at -10 to -30 m depth) to the toe of the dune (several meters above sea-level). Here we consider that a beach is limited offshore by the longshore bar (located at the breaking depth, d_b), and onshore by the ordinary berm (o_b). These two features can be up to 1 km apart. More exact sea-level information might be derived from sedimentary structures that are related to particular zones within the beach (Fig. 4.8). For example, keystone vugs or beach fenestrae (Dunham, 1970) are formed as air bubbles are trapped in fine sand when inundated by sheets of water (Hearty et al., 1998), and thus typically indicate an environment between mean sea-level and the mean higher high tide (MHHW). On the other hand, the contact between subtidal and intertidal beach beds characterizes an environment close to the mean lower low tide (MLLW). A detailed account of beach structures that might be used for paleo sea-level studies is contained in Tamura (2012, their Fig. 6).

While fossil beach deposits may be composed of loose sediments sometimes slightly cemented, beachrocks are lithified coastal deposits (Fig. 4.4e and 4.9a,b) that are organized in sequences of slabs with seaward inclination generally between 5° and 15° (Desruelles et al., 2009; Vacchi et al., 2012). Lithification is 'a function of CO_3^{2-}ion concentration in seawater, microbial activity and degassing of CO_2 from seaward flowing groundwater' (Mauz et al., 2015). In other words, beachrock forms in a mixing zone at the interface between seawater and meteoric water (see Mauz et al., 2015, their Fig. 2).

Fig. 4.8: a) Last Interglacial beach deposit in Grape Bay, Bermuda (Hearty et al., 1992; Hearty, 2002). The observed sedimentary structures suggest a sequence where water depth is shoaling upwards. The paleo RSL is best placed at the top of the foreshore beds; b) last interglacial beach deposit in Campo de Tiro, Mallorca, Spain (Hearty, 1987) where no diagnostic sedimentary structures have been preserved. In c) a detail of the same deposit shows that it contains fragments of shells and small pebbles. The indicative range of this deposit cannot be constrained to better than the general range shown in Fig. 4.4d; d) contact (white line) between planar laminations and beach berm horizons on a modern beach near Keta, Ghana.

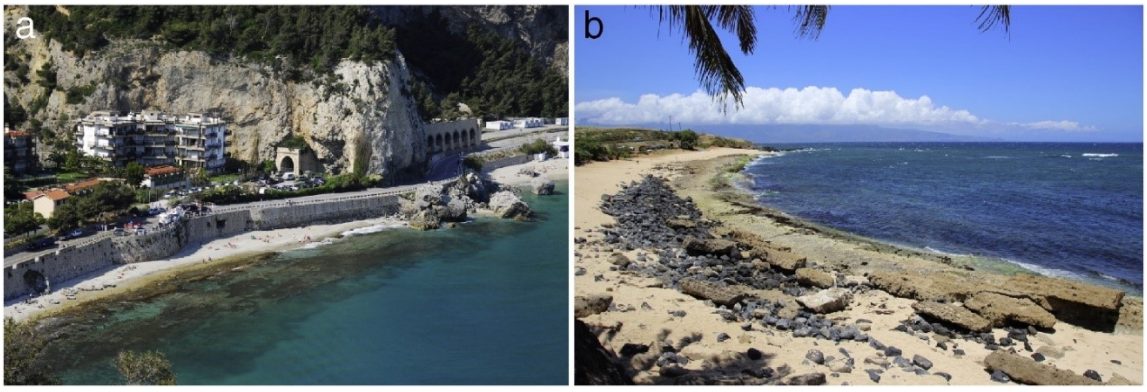

Fig. 4.9: Late Holocene beachrock in a) Liguria, NW Italy (Rovere et al., 2014a); and b) Maui, Hookipa Park, Hawaii (Meyers, 1987).

Although the utility of beachrock as a sea-level indicator has been debated (Kelletat, 2007; Knight, 2007), beachrocks have often been used as indicators for Last Interglacial sea-level (e.g. Sherman et al., 1993; Ramsay and Cooper, 2002; O'Leary et al., 2008). In general, beachrock forms in a coastal environment between the upper shoreface, also defined as the surf zone, and the spray zone (Mauz et al., 2015). The upper shoreface (or surf zone) can be defined as the portion of the seafloor that is shallow enough to be agitated by everyday wave action, and usually corresponds to the breaking depth

(db) of the significant wave height in the studied area over the longest possible recording period. In coastal engineering, the significant wave height (often indicated as SWH or Hs) is the mean wave height of the highest third of the waves over a defined period.

The sea-level information from beachrock deposits can be improved if information on cement fabric, mineralogy, and sediment bedding structures are reported (Mauz et al., 2015). As an example, irregularly distributed needles of aragonite, isopachous fibers of aragonite, or isopachous aragonitic rims (bladed or fibrous) as well as micritic high-magnesium-calcite cement or small-scaled trough cross stratification can all constrain the indicative range to the lower intertidal zone (see Mauz et al., 2015, their Table 5 and Fig. 2).

4.4.5. Beach ridges

The broadest definition of beach ridges is the one given by Otvos (2005), who defined them as 'stabilized, relict intertidal and supratidal, eolian and wave-built shore ridges that may consist of either siliciclastic or calcareous clastic matter of a wide range of clasts dimensions from fine sand to cobbles and boulders'. Although eolian beach ridges may be used to reconstruct paleoenvironments (Hesp, 1984) and can define the terrestrial limits to sea-level (Mauz et al., 2013), wave-built beach ridges (Fig. 4.4f and 4.10a, b) can be used as last interglacial RSL indicators (e.g. Nichol, 2002; Schellmann and Radtke, 2010).

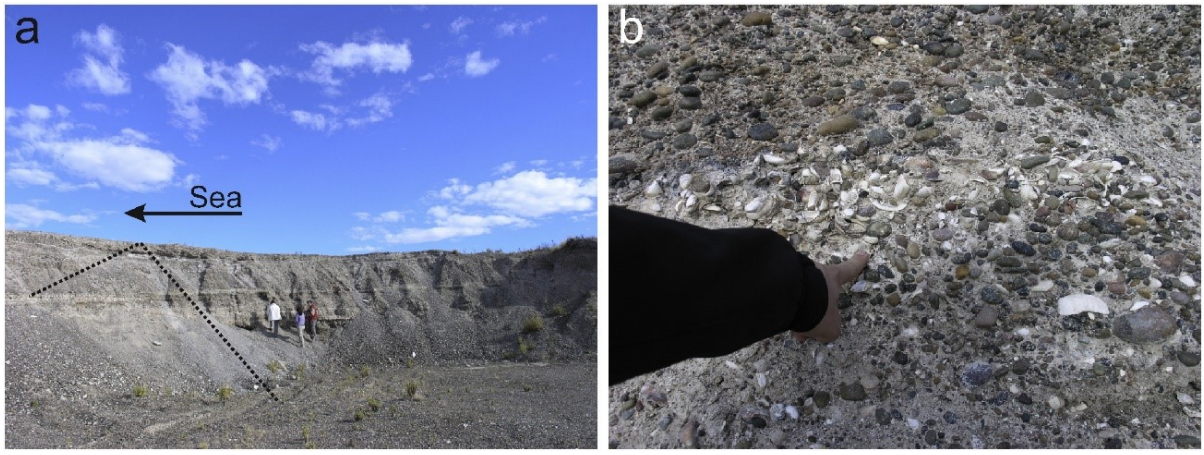

Fig. 4.10: A) Back of a Last Interglacial beach ridge in Camarones, Argentina, cut by roadworks (see Fig. 6 in Schellmann and Radtke, 2000); b) detail of the same beach ridge, showing a layer of pebbles and imbricated shells near the top of the ridge.

Wave-built ridges are created by accumulation of sediments on the upper part of the shoreline, and indicate sea-level with a broad indicative range, one that is limited in the seaward direction by the base of the ordinary berm (o_b) and in the landward direction by the maximum ingression of storm waves (storm wave swash height, SWSH, (Tamura, 2012; Kelsey, 2015)). More precise sea-level reconstruction can be obtained from specific sedimentary structures or biological indicators within the beach ridge, but usually beach ridges can be regarded as low-quality sea-level indicators. Nevertheless, in some regions (e.g. Patagonia, Schellmann and Radtke, 2010), beach ridges are the only MIS 5e sea-level indicators available (Ribolini et al., 2011). Tamura (2012) observes that it is particularly important

to analyze the modern counterparts of relict beach ridges, in order to identify their characteristic elevation range and apply this range to paleo sea-level reconstructions in the same region.

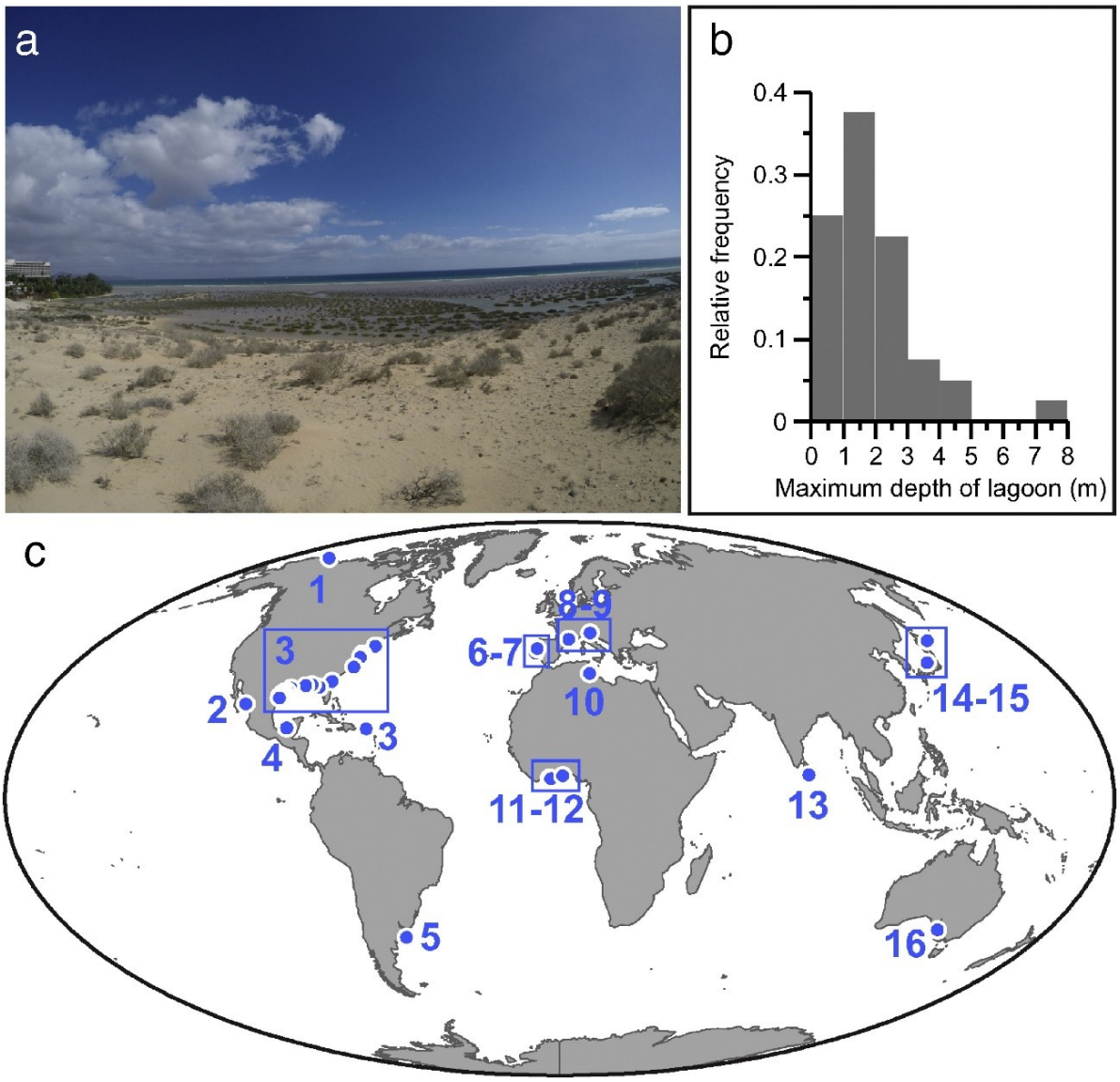

Fig. 4.11: A) Coastal lagoon near Jandia, Fuerteventura, Spain. The maximum depth of the lagoon is –1.5 m. It is separated from the open ocean by a sand bar; b) frequency distribution of the maximum depth of lagoons worldwide based on 42 locations (see supplementary material S4.1 for details); c) the location of these lagoons. References: 1. Hanna et al. (2014); 2. Serrano et al. (2013); 3. Nichols (1989); 4. Contreras Ruiz Esparza et al. (2014); 5. De Francesco and Isla (2003); 6. Bruneau et al. (2011); 7. Dias et al. (2001); 8. Bellucci et al. (2002); 9. Bonnet et al. (2012); 10. Kharroubi et al. (2012); 11. Lamptey et al. (2013); 12. Seu-Anoï et al. (2011); 13. Chandana et al. (2008); 14. Nagasaka and Takano (2014); 15. Suga and Montani (2012); 16. Tulipani et al. (2014).

4.4.6. Lagoon deposits

Lagoons are inland water bodies with continuous or intermittent connection to the open sea (Kjerfve, 1994). Lagoonal deposits typically consist of silty and clayey sediments, frequently characterized by the presence of brackish or marine water fauna (Fig. 4.4g). Usually, lagoon sediments are horizontally

laminated (Zecchin et al., 2004) and may be interrupted by one or more sandy layers (possibly with fragments of marine shells) that represent the transport, into the lagoon, of storm deposits.

Normally the indicative range of a coastal lagoon is constrained between the mean lower low tide (MLLW) and the depth of the lagoon (ld) (Fig. 4.11a). In Fig. 4.11b,c we show that the depth of several lagoons worldwide (see supplementary material S4.1) averages at 2 ± 1.5 m, although some lagoons can reach down to -8 m depth (Fig. 4.11b, c). The stratigraphic context and living range of fossil fauna can further inform sea-level information from lagoonal sequences.

In general, the sea-level information yielded by paleo lagoon deposits is improved when they contain fossil in situ fauna, such as articulated bivalves or remnants of reefs built by bioconstructors. Several species of serpulids are known as primary builders that form reef-like structures with calcareous tubes that grow vertically on the substrate. Often these structures form in clumps and become cemented to each other (Ten Hove, 1979). Large serpulid reefs are today found in quiet, enclosed embayments and/or in brackish estuaries and lagoons (Ten Hove and Weerdenburg, 1978; Bianchi et al., 1995; Fornós et al., 1997; Schwindt et al., 2004). In addition, lagoonal facies are often characterized by foraminiferal and ostracod assemblages dominated by marine or brackish taxa (Debenay et al., 2000). All these biological features, if found in the fossil record, may serve to narrow the indicative range (Murray-Wallace et al., 1999).

4.4.7. Cheniers

Chenier ridges (cheniers, Fig. 4.4g) can be defined as ‘sandy or shelly ridges, differentiated from other sand or shell beach ridges by the fact that they are perched on and separated laterally from other cheniers on a chenier plain, by fine-grained, muddy (or sometimes marshy) sediments’ (The ‘Encyclopedia of Coastal Science’, (Schwartz, 2005)). More simply, cheniers are land strips separating different sections of a coastal lagoon (Fig. 4.12b). Coarser sediments can accumulate on cheniers from overwashing of storm waves. With regards their dimensions, cheniers can be up to 6 m high (Fig. 4.12a, b), tens of kilometers in length and hundreds of meters wide (Schwartz, 2005).

As they develop in near shore environments, cheniers can be used as sea-level indicators (Carlston, 1950; Trowbridge, 1954), but their precision is low unless additional stratigraphic information is present. In general, the indicative range of a chenier is from the mean higher high water (MHHW) to the top elevation of the feature, above MHHW. In general, the best guideline to the relationship between a paleo chenier and paleo RSL is given by observations of the distribution of modern cheniers in a region.

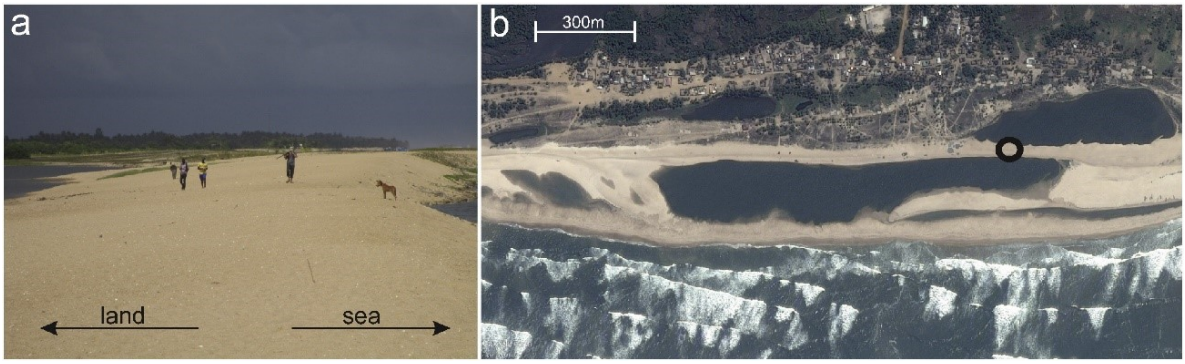

Fig. 4.12: A) Modern chenier ridge at the estuary of the Volta River, Ghana; b) aerial view with indication of the location where the photo in a) has been taken. The maximum elevation of this chenier above sea-level is 2.3 m.

4.4.8. Tidal notches

Tidal notches (Fig. 4.4i) are indentations or undercuttings (Fig. 4.13a, b), a few centimeters to several meters deep, cut into rocky coasts by processes acting in the tidal zone (such as tidal wetting and drying cycles, bioerosion, or mechanical action). Tidal notches are shaped by the interplay of bioerosion, wave action and tidal wetting and drying cycles on limestone coasts (Pirazzoli, 1996; Antonioli et al., 2015; Carobene, 2015). The shape and preservation of tidal notches depend on the duration of the high-stand: as a notch can be formed in few hundreds of years, a prolonged highstand might result in cliff retreat and the undercutting of ever new surfaces.

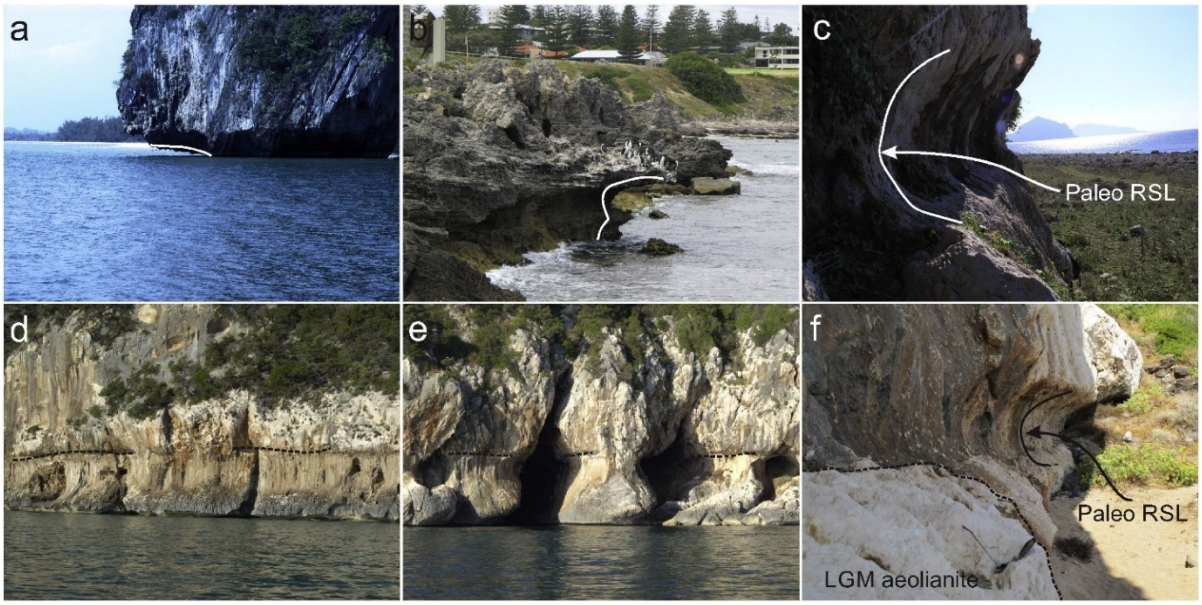

Fig. 4.13: Modern tidal notches in a) Krabi, Thailand, and b) Cottesloe Beach, Perth, Western Australia; Last Interglacial tidal notches in c) Capo S. Vito, Sicily; and d) and e) preserved on vertical cliffs in the Orosei Gulf, Sardinia, Italy (Antonioli et al., 2006; Carobene, 2015). The notch is indicated by the black dashed line; f) a tidal notch in Biddiriscottai, Dorgali, Sardinia, partially covered by aeolianites of last glacial maximum age (Antonioli et al., 2015).

Tidal notches are shaped near Mean Sea-level (MSL) on calcareous cliffs and their highest elevation is constrained by local tides, while their depth (i.e. how deep they are cut into the rocky cliff) is related

to intensity of local waves, bioerosion agents and presence of waters undersaturated of calcium carbonates (e.g. freshwater springs, Antonioli et al., 2015). MSL usually corresponds to the point of maximum concavity of the notch (Fig. 4.13c, f). The height of the notch is always less than extreme tide values, and instead typically falls between mean higher high water (MHHW) and mean lower low water (MLLW).

Tidal notches formed during the Last Interglacial have been used as RSL indicators in several locations (Antonioli et al., 2006; Hearty et al., 2007; Carobene, 2015). They are especially effective sea-level indicators in regions with a low tidal range (such as the Mediterranean Sea), where they can indicate sea-level with a precision of few decimeters (Fig. 4.13d,e). The sea-level information can be even more precise if biological indicators, such as traces left by bioerosional organisms near MLLW (Laborel and Laborel-Deguen, 1996; Rovere et al., 2015a) have been preserved in the notch. While such bioerosional remains can be used to date Holocene notches, MIS 5e biological assemblages associated with tidal notches are very rare. The main limitation on the use of tidal notches as MIS 5e RSL indicators is therefore that they can be hardly dated directly – their age can only be derived from chronostratigraphic correlations with other RSL indicators, such as beach or lagoonal deposits found in proximity to the notch.

4.4.9. Abrasion notches and sea caves

Abrasion processes are active where sand, gravel or pebbles are thrown against the rock by incoming waves resulting in erosion of a rocky shore face. This process creates abrasion notches (Fig. 4.14a, b) that usually span a larger vertical distance than tidal notches. They also occur in all lithologies (while tidal notches occur only on carbonate rocks). As the formation of abrasion notches occurs where sediments can be mobilized by waves, abrasion notches have a large indicative range reaching from the storm swash wave height to the breaking depth of significant waves.

Coastal caves can be classified according to whether they are submerged or subaerial (Ferranti, 1998). Submerged caves originally formed in continental environments above sea-level and were later drowned by a relative sea-level rise. The largest submerged caves are formed by karst dissolution of the landscape. Other caves of continental origin include, for example, volcanic caves (Cicogna et al., 2003). One of the most widely recognized examples of submerged (karst) caves are blue holes on carbonate banks (Mylroie et al., 1995). Other examples of submerged karst caves can be found along the coastlines of central and southern Italy (Ferranti, 1998) or Croatia (Surić et al., 2009; Surić et al., 2010). In his review of underwater cave systems in carbonate rocks, Ferranti (1998) argues that, in the absence of further paleo RSL indicators, karst caves are an imprecise sea-level indicator.

Subaerial coastal caves, on the other hand, form near sea-level by mechanical abrasion processes (Colantoni, 1976). In general, this kind of cave displays an elongated shape, narrowing towards the interior, resulting in a short, wedge-shaped section orthogonal to the shore and a triangle or trapezium-shaped section parallel to the coastline (Ferranti, 1998). Coastal caves usually form along structural weaknesses in the bedrock (faults, joints, strata) and bioerosion and chemical dissolution are important processes in carving the cave, especially along carbonate coastlines. While good sea-level

indicators such as tidal notches or fixed biological indicators can be preserved in these caves (Carobene, 2015), typically it is the levelled floor at the entrance of the cave, often associated with abrasion notches, that provides a marker for RSL. This level represents the minimum level of constant wave action, and its precision in indicating sea-level is comparable to that of abrasion notches, described above.

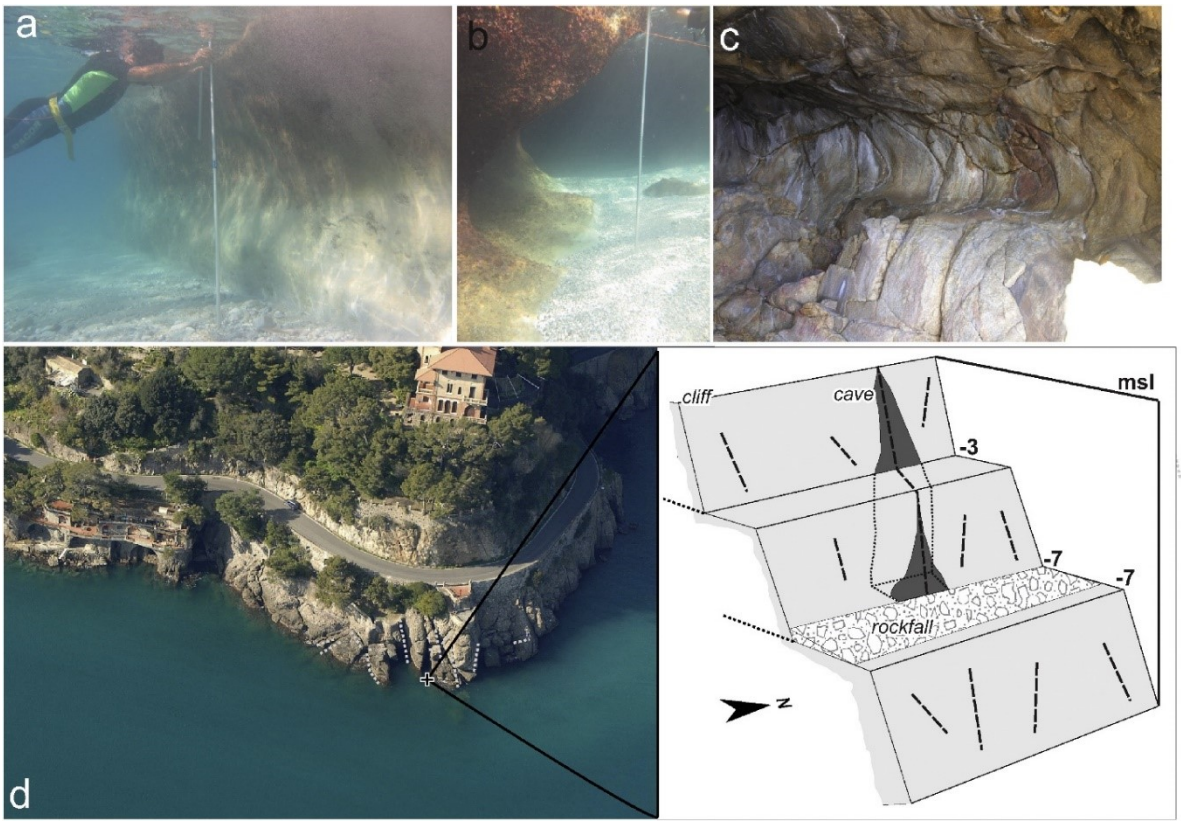

Fig. 4.14: A), b) Abrasion notches at Capo Noli, Italy, NW Mediterranean Sea. The length of the stick is 1.5 m; c) abrasion notch formed inside a coastal cave, Cap D'Agde, southern France; d) and e) perspective photo and scheme of a coastal cave formed by abrasion in highly fractured conglomerates in Portofino, NW Italy. The cave formed along a major fault in the bedrock and is still actively being modified by abrasion. The abrasion occurs by pebbles mobilized by wave action. The cave is few meters wide and deepens with a trapezoidal shape. Perspective photo in d) by Regione Liguria.

Finally, the use of deposits found inside marine caves is widespread in sea-level studies. Caves can effectively preserve deposits from marine erosion including beach deposits (Hearty et al., 1999) and archeological indicators (e.g. in the Cosquer Cave, near Marseille, France, described by Lambeck and Bard, 2000). In addition, speleothems (Vesica et al., 2000; Bard et al., 2002) containing alternations of continental and marine layers have been used to reconstruct Pleistocene sea-level history (Antonioli and Oliverio, 1996; Vesica et al., 2000; Antonioli et al., 2001; Antonioli et al., 2004; Dutton et al., 2009a; Dutton et al., 2009b).

4.5. Dating methods

Together with the measurement and interpretation of the elevation of MIS 5e RSL indicators, it is essential to establish their age as precisely as possible with absolute or relative dating methods. Among

the absolute dating techniques most often used in Last Interglacial studies, only ^{230Th}/U dating of corals can resolve timing of deposition within the interglacial (Dutton and Lambeck, 2012; O'Leary et al., 2013). Other techniques, such as electron spin resonance (ESR), optically stimulated and thermos luminescence (OSL and TL), can be used mostly to distinguish if the RSL indicators, or associated fossil remnants, were formed within MIS 5e, as opposed to other time frames (e.g. MIS 5a, MIS 5c) leaving the establishment of the relative timing of deposition within MIS 5e to other stratigraphic considerations (e.g. Grün, 1989; Hearty and Kaufman, 2000). A recent review of luminescence dating (Lamothe, 2016) highlighted that, while luminescence dating is more widely applicable than U-series, this technique is too imprecise to draw conclusions about sedimentary processes at the century or multi-century scale.

The most widely used relative dating technique in MIS 5e studies is probably amino acid racemization (AAR). Other relative methods, such as biostratigraphy and chronostratigraphic correlations are also widely used in MIS 5e studies. In the absence of absolute chronological constraints, these age attributions can usually help to distinguish between different interglacials, but they cannot be used to give a precise age. Although a complete review of dating methods applied to MIS 5e shorelines is beyond the scope of this paper, Table 4.4 lists the absolute and relative methods used in MIS 5e studies with the typical uncertainty in the final age attribution.

Table 4.4: Most common dating methods used in Last Interglacial studies.

Method	Typical uncertainty in ka (1-sigma)	Examples
Absolute dating methods		
U-Series	0.5-4 ka	Stirling and Andersen (2009), Dutton and Lambeck (2012) and Obert et al. (2016)
Optically stimulated luminescence	3-7 ka	Mauz et al. (2015) and Carr et al. (2010)
Electro spin resonance	14-20 ka	Pirazzoli et al. (1991) and Schellmann et al. (2008)
Thermo luminescence	15–20 ka or limiting ages (e.g. deposit older than 60 ka)	Woodroffe et al. (1995) and Mauz and Hassler (2000)
Relative dating methods		
Amino acid racemization	Usually relative dating methods help to discern between different interglacials.	Hearty and Kaufman (2000) and Wehmiller (2013)
Biostratigraphy		Ávila et al. (2015)
Chronostratigraphic correlation		Choi et al. (2008)

4.6. Last Interglacial shorelines: an applied example

4.6.1. From field measurement to paleo RSL

As described in the previous sections, the most accurate way to calculate the paleo RSL associated with a MIS 5e deposit is to study its modern analog. An example of how studies and datasets on modern coastal dynamics can be used to derive the indicative meaning of a MIS 5e beach deposit is presented in Fig. 4.15. The example is that of Cala Millor, Mallorca Island, Spain. Cala Millor is an ~1.7 km-wide sandy beach (Fig. 4.15a). The beach profile is bounded on its low end by the presence of a longshore

bar (Fig. 4.15a), which has been shown to be persistent throughout the year (Tintoré et al., 2009; Gómez-Pujol et al., 2011; Tintoré et al., 2013). On the upper part of the beach (above MSL), beach berms can form according to the wave conditions in the study area (Fig. 4.15c). Depending on the season or on the intensity of storm events in a given period, the berms are found higher (usually in winter) or lower (usually in summer) on the shoreline, with their location being a function of the maximum wave runup.

In the southern part of the beach of Cala Millor (white dot in Fig. 4.15a,b) we surveyed a fossil beach deposit containing the fossil *Strombus latus* (ex. *S. bubonius*). This fossil is widespread in Mediterranean MIS 5e deposits, and it is often used as a biostratigraphic age indicator (Ferranti et al., 2006). We measured the upper and lower elevation of the deposit with a DGPS equipped with Omnistar real-time differential corrections. The deposit respectively 1.47 ± 0.02 m and 0.97 ± 0.03 m above the EGM08-REDNAP geoid model, which closely approximates sea-level in Spain. The average of these two measurements represents the mean elevation of the paleo RSL indicator (1.22 m). The elevation error (Ee in Table 4.1) can be calculated as the sum of half of the range between the two values (0.25 m) and the two measurement errors (0.02 and 0.03 m). This results in an elevation for the RSL indicator of 1.22 ± 0.30 m, Fig. 4.15b).

From bathymetric data, we determine that the longshore bar in Cala Millor can be found at an average depth of -1.9 m (Fig. 4.15e). We adopt this value as the lower limit of the indicative range. For the upper limit, we need to establish the average elevation where beach berms are formed in Cala Millor. On the 19th of February 2015, we measured wave heights (Fig. 4.15c) using pressure sensors in the surf zone (Harris et al., 2015) and beach topography (Fig. 4.15b) using structure-from-motion techniques from drone (Casella et al., 2014; Casella et al., 2016). From these data, we determined that an onshore wave height averaging 0.6 m created a beach berm at +0.8 m (height of the maximum run-up shown on Fig. 4.15c,d). As the swell we measured is roughly representative of the average swells in the area (Gómez-Pujol et al., 2011), we adopt as an upper limit of our IR the measured value the measured elevation of the berm.

Using the depth of the longshore bar (-1.9 m) and the calculated elevation of the ordinary berm (+0.8 m) as respectively lower and upper limits of the indicative range, we can apply Eq. 4.1-4.4 (Table 4.1) to calculate the paleo RSL for Cala Millor. The calculated paleo RSL is 1.8 ± 1.4 m (Fig. 4.15e). The large uncertainty comes from the fact that, despite using precise measuring techniques, the beach deposit has a large indicative range and is therefore a relatively poor sea-level indicator. The indicative range might be reduced, for example, by investigating patterns in the cement of the lithified beach. It is worth highlighting that the paleo RSL calculated in this example matches, although with large uncertainties, the more precise elevation of MIS 5e paleo RSL inferred by measuring and dating phreatic overgrowths on speleothems inside Cova des Serral (Vesica et al., 2000), located few kilometers from this study site. The speleothem represents in fact a paleo RSL at +1.5 m (no uncertainties reported) dated with ^{230}Th/U at 121.3 ± 5.6 ka (see blue band Fig. 4.15e). Other nearby speleothems dated by the same author to MIS 5e do not grow above +2.5m.

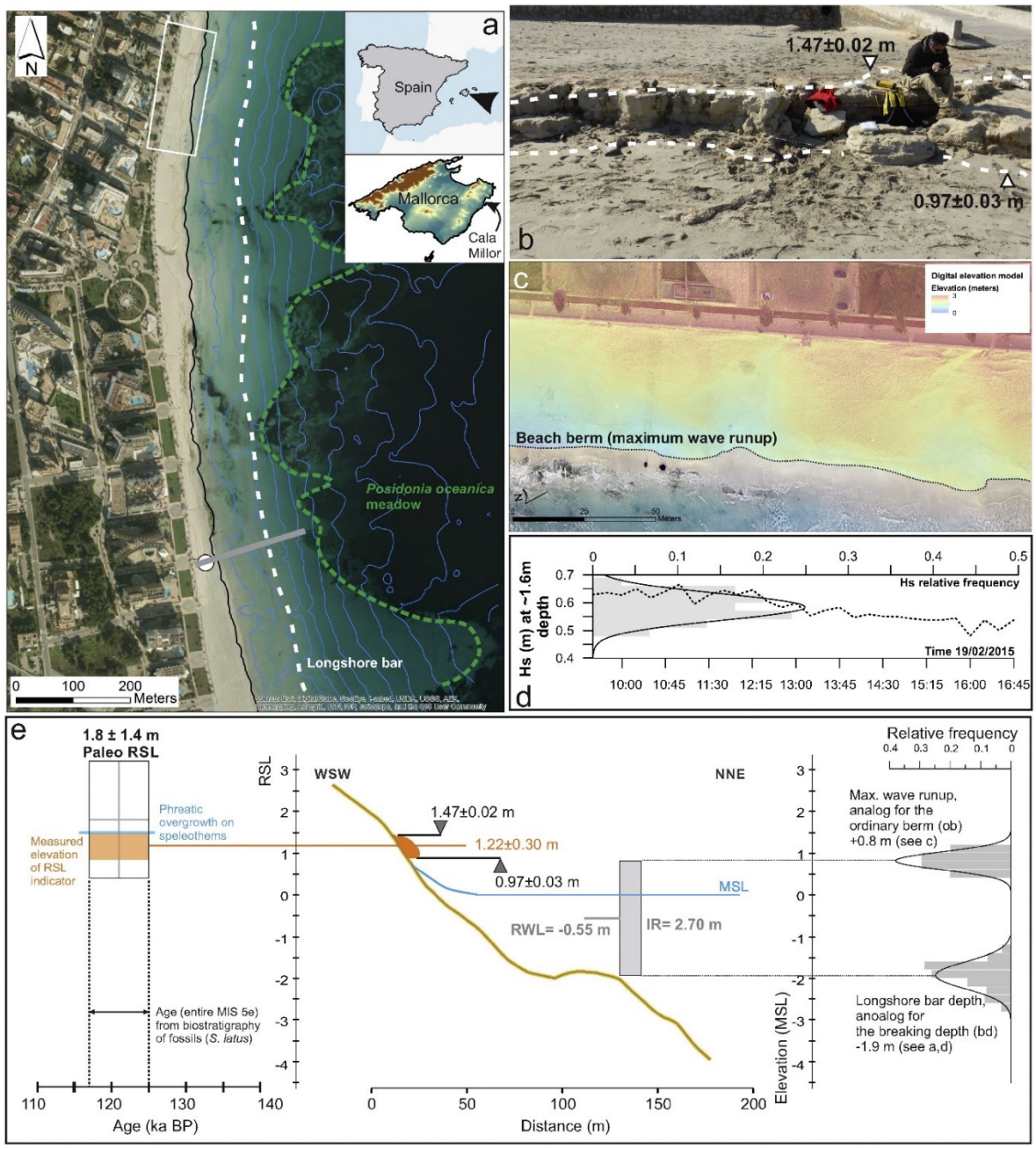

Fig. 4.15: a) Cala Millor, on the Island of Mallorca, Spain. The bathymetry and topography are derived from single beam and GPS surveys (10/07/2012). The gray transect line shows the location of Fig. 4.15e and the white rectangle shows the area where Unmanned Aerial Vehicle (UAV) surveys were performed, as detailed in c); b) the site where the MIS 5e beach deposit outcrops with measurements of the upper and lower elevations of the outcrop; c) Orthophoto and digital elevation model obtained from UAV surveys and structure from motion techniques (Casella et al., 2014; Casella et al., 2016). The beach berm has been identified in the DEM at an average elevation of + 0.8 m (see also histograms in e); d) data obtained from a pressure sensor located at − 1.6 m depth in the study area, from which we calculate significant wave height in 15 min bins (Hs, lower x axis) and the relative frequency of wave heights (upper x axis, dashed line); e) right side: histograms and Gaussian showing the depth of the longshore bar derived from bathymetric data in a) and the elevation of the maximum wave runup (proxy for the beach berm) derived from topographic data in c,d); center: topography of the beach, with measured elevations and position of RWL and IR; left: Age/elevation plot showing position of calculated paleo RSL, compared with that obtained in a nearby cave by Vesica et al. (2000).

Coupling research on paleo sea-levels with that on modern coastal dynamics is not always straightforward. Taking the above example of a beach deposit, the upper and lower limits of the indicative range depend strongly on the wave regime in the area of interest, a regime that can evolve over time. For instance, in the Bahamas, the Last Interglacial may have been characterized by storms of higher intensity than modern ones (Hearty et al., 1998; Tormey and Neumann, 2007; Hansen et al., 2016). If true, then a beach deposit in the Bahamas should be characterized by a broader indicative range than a modern one.

4.6.2. From paleo RSL to long-term tectonics

The elevation of the Last Interglacial shoreline is often used as a benchmark for long-term tectonics (e.g. Guillaume et al., 2013), which is in turn used, for example, to plan coastal infrastructures or evaluate coastal risks. In most literature attempting to calculate long-term tectonics from sea-level data, if the MIS 5e shoreline is between 3 and 7 m above present, it is assumed that a coastal region is tectonically stable in the long-term, especially if it is located on a passive margin. This view arises from the assumption that the elevation of MIS 5e eustatic sea-level was ~5 m above present and that there is no GIA disequilibrium between the past interglacial and present one. However, Creveling et al. (2015), showed that when calculating long-term tectonics from MIS 5e shorelines, one must take into account the departures from eustasy due to GIA in response to glacial-interglacial cycles as well as excess polar ice-sheet melt relative to present day values.

Therefore, to calculate the tectonic displacement of a MIS 5e shoreline it is necessary to know the elevation of the paleo RSL (as calculated for Cala Millor in the section above), together with the elevation of eustatic sea-level (ESL) and the amount of glacio-hydro-isostatic (GIA) disequilibrium since the marker was deposited. Hereafter, we follow-up on the example given in the previous section and show how the influence of tectonics can be evaluated using the Eq. 4.5a, 4.6 and 4.8 (Table 4.1).

First, we calculate two different ESL scenarios for MIS 5e using a 410 kyr-long global ice-sheet model (ANICE, a 3D thermo-mechanical ice-sheet model, de Boer et al., 2014b). The first represents a two-step highstand with Greenland contributing 2.0 m of ESL equivalent between 127 and 116 ka, while Antarctica contributes 5.0 m but only after 120 ka (Fig. 4.16a). This is in line with the scenario proposed by O'Leary et al. (2013). The second scenario reflects a more classical view of MIS 5e sea-level history, with melting of both Greenland (2.0 m) and Antarctica (5.0 m) happening early in the interglacial and ESL not changing until insolation in both hemispheres decreases and glacial conditions emerge (Fig. 4.16b). These represent only two possible MIS 5e sea-level histories (compare with Kopp et al., 2009, Fig. 4.16e). For each of these ESL scenarios, we calculate the MIS 5e GIA and RSL history at Cala Millor, Mallorca (Fig. 4.16c,d). This is done by coupling the ANICE model with SELEN, a GIA model (Spada and Stocchi, 2007). In order to explore the uncertainties of GIA predictions due to the mantle viscosity profile, we use three different viscosity models (see box in Fig. 4.16 for details). The average of all GIA-ESL scenarios for the time frame 125-117 ka is 4.1 ± 3.7 m.

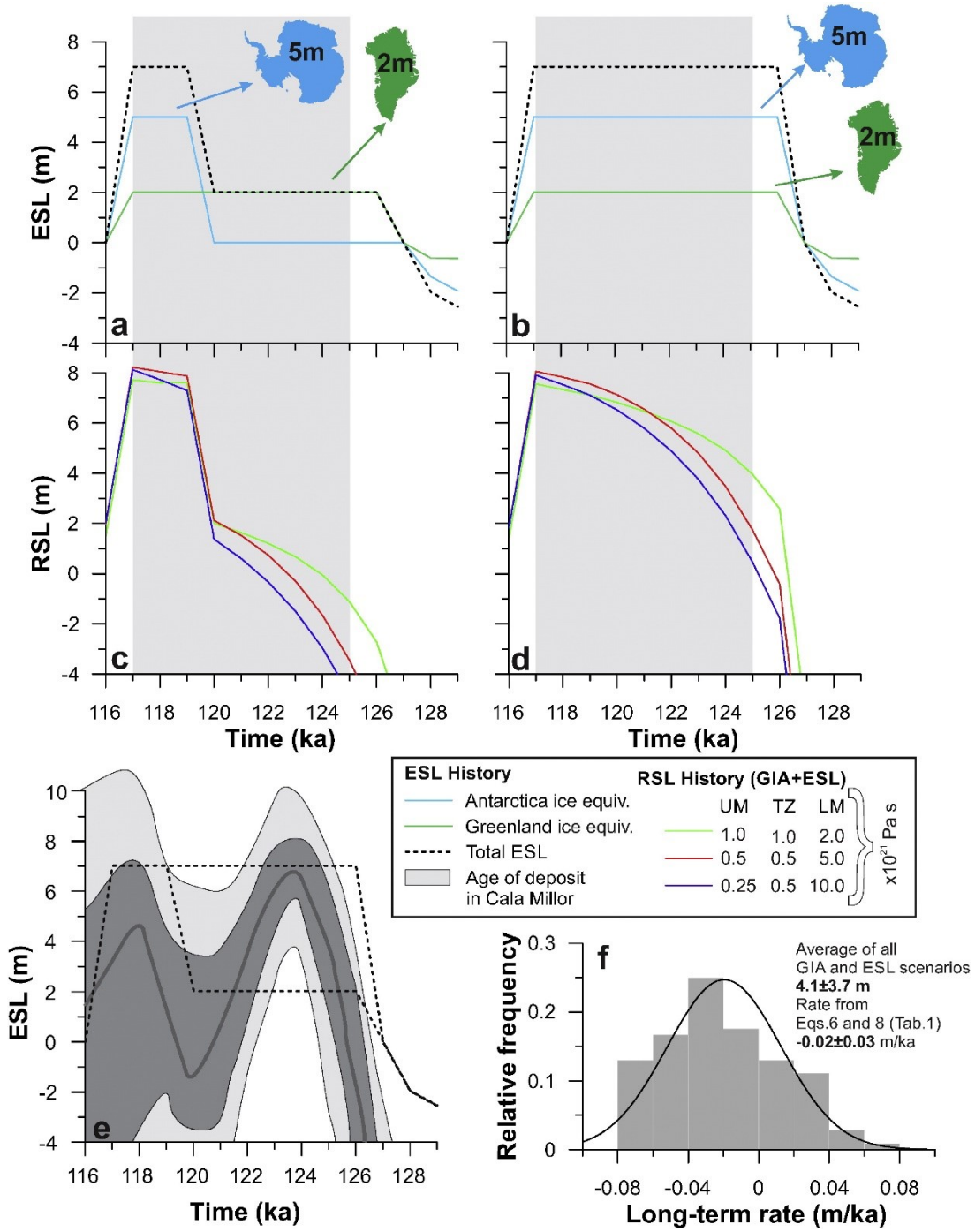

Fig. 4.16: a) and b) Sea-level scenarios for MIS 5e obtained from ANICE, a global ice-sheet model (de Boer et al., 2014b). c) and d) Show the GIA predictions calculated in Cala Millor, Mallorca, for each of the two sea-level scenarios. The predictions obtained using three mantle viscosities are shown in different line colors (see box: UM = Upper Mantle, TZ = Transition Zone, LM = Lower Mantle); e) sea-level scenarios used in this study (dashed lines) compared with the Last Interglacial sea-level history obtained by Kopp et al., 2009. The solid gray line indicates the median projection of Kopp et al., the light gray bands the 16th and 84th percentiles and the dark grey band the 2.5th and 97.5th percentiles (redrawn from Kopp et al., 2009); f) relative frequency of long-term rates of post-depositional displacement calculated in time steps of 1 ka using data in panels a–d and a paleo RSL of 1.8 ± 1.4 m.

Next, we use the model results described above and the RSL for Cala Millor (= 1.8 ± 1.4 m) as inputs to Eq. 4.6 and 4.8 (Table 4.1) to calculate the rate of post-depositional displacement since MIS 5e in Cala

Millor. As the age of the deposit has been constrained only by biostratigraphy, we assume that it could have been formed at any time during the MIS 5e highstand, therefore T in Eq. 4.6 and 4.8 spans from 125 to 117 ka, the time frame for which GIA and ESL models predict the highstand (see also Fig. 4.15e). We determine that possible tectonic rates in this area are constrained between -0.02 ± 0.03 m/ka (Fig. 4.16f).

While Mallorca is usually considered to have been tectonically stable since MIS 5e (e.g. Dorale et al., 2010), our results show that stability, mild subsidence or mild uplift are all possible influences given uncertainty in GIA models, ESL scenarios and RSL observations. It is worth highlighting that this example shows only a small range among the possible ESL scenarios (Kopp et al., 2009, Fig. 4.16e), GIA predictions (e.g. compare the three mantle viscosities shown here with the 36 different mid-Pliocene earth models with varying mantle viscosities shown in Rovere et al., 2015b) and duration of the MIS 5e highstand. As more eustatic scenarios and Earth models are considered, the tectonic rate range shown in Fig. 4.16f is likely to change. In general, we conclude that the assumption that Mallorca is tectonically stable in the long term is supported by the MIS 5e shoreline record, but with considerable uncertainty. This has direct implications for Holocene studies - if we assume that the rates calculated here (-0.02 ± 0.03 m/ka) are constant trough time, a mid-Holocene RSL marker deposited at 5 ka in Mallorca could already have been displaced by -25 to + 6 cm. This 31 cm range, albeit small, should be added to the uncertainties on the Holocene sea-level index points in this area. It is worth noting, in fact, that some Holocene sea-level indicators can have accuracies down to few decimeters (Vacchi et al., 2016) and therefore a variation in the range of 3 decimeters is not negligible.

4.7. Discussion

How did the polar ice sheets, and hence sea-level, respond to MIS 5e warm conditions? Last Interglacial RSL indicators are often used to infer paleo RSL at one location. In turn, observations at many sites can contribute to a global understanding how polar ice sheets responded to moderate climate warming. Despite the long tradition of MIS 5e studies, often the methods used to measure the markers are not sufficiently described, are of low accuracy, or are not referred to a known tidal datum. Additionally, in many cases the measurement and interpretation are not clearly disentangled, making it virtually impossible to understand how the paleo RSL was derived, and assumptions of post-depositional vertical movements are often circular, not taking into account the effect of GIA disequilibrium since the LIG (Fig. 4.16).

All of these factors contribute to discrepancies in MIS 5e sea-level reconstructions despite the fact that these sea-level indicators have been studied at hundreds of sites worldwide (Kopp et al., 2009; Pedoja et al., 2011a; Dutton and Lambeck, 2012; Pedoja et al., 2014). Early studies concluded that sea-level during MIS 5e was 3-6 m higher than today (Stearns, 1976; Harmon et al., 1981; Neumann and Hearty, 1996; Stirling et al., 1998) but none of these studies factored in the subsequent displacement of the field sites caused by glacial isostatic adjustment (GIA) which is now recognized as an important post-depositional process capable of biasing sea-level reconstructions (Lambeck and Nakada, 1992; Potter and Lambeck, 2004; Milne and Mitrovica, 2008). Recent studies by Kopp et al. (2009) and Dutton and

Lambeck (2012) analyzed global datasets of MIS 5e sea-level indicators and, after accounting for tectonics and GIA, concluded that the maximum eustatic (i.e., globally averaged) sea-level (ESL) was higher than previously thought, between +5 and +9.4 m above modern sea-level.

Uncertainty also surrounds the question of whether rapid century to millennial-scale oscillations in ESL occurred within MIS 5e. Field evidence from Bahamas (Chen et al., 1991; Hearty and Neumann, 2001; Hearty et al., 2007; Thompson et al., 2011), Yucatan (Blanchon et al., 2009), Western Australia (Eisenhauer et al., 1996; O'Leary et al., 2013), and the Aldabara Atoll (Braithwaite et al., 1973) suggest that sea-level may not have been uniform throughout MIS 5e and that a rapid sea-level rise happened at the end of the interglacial. These studies support the hypothesis that, after a period when sea-level remained relatively stable at ~+3–4 m from the beginning of the interglacial, a sudden melting occurred at ~120 ka coinciding with maximum spring-summer insolation in the Southern Hemisphere (> 60°S). This inferred melting caused the sea-level to rise up to ~9 m. The results of Kopp et al. (2013) do not exclude the possibility of ESL oscillations during MIS 5e (Fig. 4.16e), while Dutton and Lambeck (2012) invoke GIA overprinting as the reason for an apparent late MIS 5e sea-level rise at some of the sites mentioned above, especially those in the Caribbean region. In the Seychelles, where GIA effects are considered minimal, Dutton et al. (2015b) show that between 125 and 130 ka the eustatic sea-level reached its maximum elevation at ~+7 m, early in the interglacial.

The controversy that exists over the shape of the MIS 5e sea-level curve stems from discrepancies in field data and is in part caused by the fact that MIS 5e sea-level markers often have a wide indicative range. This undermines our ability to understand sea-level variability in a slightly warmer world, with obvious implications for the future. If a late, rapid ESL rise occurred during MIS 5e, then we might surmise that the dual climatic effects of a) ~8 ka of interglacial warmth penetrating the surface layers of the ocean, and b) local southern hemisphere summer insolation intensity approaching a maximum, could have been instrumental in leading to the rapid collapse of a significant additional fraction of the Antarctic polar ice sheets (as much as 6 m sea-level equivalent), possibly including sectors of the East Antarctic Ice Sheet. This possibility eerily mirrors recent reports by Joughin et al. (2014) and Rignot et al. (2014) suggesting that a runaway collapse of the West Antarctic Ice Sheet may already be underway, ~8 ka into the Holocene interglacial interval and at a time of near maximum southern hemisphere summer insolation.

4.8. Conclusions

Although MIS 5e is the most studied period of the Earth's past, at least in terms of paleo sea-level, much research still need to be directed towards obtaining better paleo RSL elevations from field data. In this review we addressed all the relevant observations that are needed when studying MIS 5e RSL markers. Most of the concepts reviewed here can also be applied to other interglacials. In conclusion, we highlight the following points:

- **Measurement.** The measured elevation of a RSL indicator should be surveyed with the maximum possible accuracy and referred to a known sea-level datum. An elevation measurement must always carry an uncertainty, as well as a description of how the uncertainty was calculated. The measured elevation can be updated (for instance, if better measurement techniques become available) but it represents the most fundamental sea-level information, therefore its longevity must be ensured. The location on the landform where the measurement was taken should also be precisely described.
- **Interpretation.** For any RSL indicator surveyed in the field a correct indicative meaning, composed of an Indicative Range (IR) and a Reference Water Level (RWL), must be given. These values allow the reconstruction of the paleo RSL, which is the only observation that can be used to constrain GIA, other land movements, or ESL. As estimates of IR and RWL might be improved as new techniques or more detailed analyses are carried out, it is necessary that these parameters are reported separately from the measured elevation of the RSL indicator.
- **Modern analog.** In order to estimate the indicative meaning correctly, ancillary research on modern analogs should always be reported alongside the research on paleo landforms. At the same time, consideration must be given to the possible differences in environmental conditions between the time of formation of RSL indicators and the present. If surveys of the modern analog are not possible, it is necessary to estimate IR and RWL using available literature data, or by inferring the general upper and lower bounds of similar landforms in the modern setting. Recent works (Hibbert et al., 2016) show that basing the modern analogs only on the ecology of corals results in large indicative ranges: it is necessary that modern analogs are defined, whenever possible, on the basis of integrated ecological, geologic and stratigraphic considerations.
- **Age.** The information on RSL indicators (elevation, IR, RWL) should be always accompanied by information on how the age has been determined. If radiometric ages are available, it is necessary to indicate not only the final age, but all the analytical measurements that were used to define it. Each sample within the same site should carry its own positioning information (latitude, longitude and elevation with uncertainty). It is important also to disentangle the concept of sample for dating from that of RSL indicator: in Fig. 4.1, we show an example where dating is derived from corals, but the RSL indication is obtained from the nearby terrace inner margin.
- **Tectonics.** Different possible ESL histories, glacial isostatic adjustment effects, uncertainty in age, and uncertainties in the paleo RSL reconstruction should always be included in tectonic calculations. In MIs 5e studies, the tectonic stability of an area should be evaluated on the basis of data that are independent from the MIS 5e sea-level marker.
- **Other vertical movements.** Together with crustal tectonics, it is necessary to consider all the other forces that can cause uplift or subsidence of a MIS 5e shoreline. Among these, sediment isostasy (Dalca et al., 2013) and earth dynamic topography (Moucha et al., 2008; Müller et al., 2008) are often overlooked, but are potentially relevant also along passive margins, that are usually considered ‘stable’ for which concerns MIS 5e histories. As an example, for the Atlantic Coast of the US,

Rovere et al. (2014b) estimated that dynamic topography can contribute to the uplift or subsidence of a MIS 5e shoreline from -0.25 to 3 m, depending on where the shoreline is located along a North-South transect from North Carolina to Georgia. We remark that the amount of such displacements is equal to the sea-level equivalent of a large part of the Antarctic Ice Sheet.

Following these six points in the collection, analysis and reporting of field data will ensure their longevity and allow for their use in global compilations. In the supplementary material S4.1 of this paper we propose the spreadsheet structure for building compilations of MIS 5e (and older) sea-level data, updating a formerly proposed one (Rovere et al., 2012). A similar approach applied to Holocene and Common Era sea-level reconstructions (Khan et al., 2015) has ensured that data collected by different research units are consistent and appropriate for use in global analyses of recent sea-level trends (Kopp et al., 2016).

4.9. Acknowledgments

AR, DH and TL's research is supported by the Institutional Strategy of the University of Bremen, funded by the German Excellence Initiative (ABPZuK-03/2014) and by ZMT, the Center for Tropical Marine Ecology. The authors acknowledge NSF grant OCE-1202632 'PLIOMAX' for support, as well as MEDFLOOD - Modelling Paleo Processes (INQUA CMP projects 1203P and 1603P) and PALSEA (PAGES/INQUA/WUN) working groups for useful discussions. MV contributes to the Labex OT-Med (ANR-11-LABX-0061) and to the A*MIDEX project (n°ANR-11-IDEX-0001-02), funded by the «Investissements d'Avenir» program of the French National Research Agency (ANR). Data to build Fig. 4.15a were obtained from the Beach Monitoring Programme of the Balearic Islands Coastal Observing and Forecasting System, SOCIB (www.socib.es). The ideas in this review have been discussed with many colleagues, with whom separate papers have been published or are in preparation: M. Aguirre (University of La Plata, AR); F. Antonioli (ENEA Rome, IT); K. Appeaning Addo (University of Ghana, GH); S. Avila (University of the Azores, PT); C.N. Bianchi (University of Genoa, IT); I. Castellanos (University of La Plata, AR); G. Cornamusini (University of Siena, IT); A. Droxler (Rice University, US); L. Ferranti (University of Napoli, IT); L. Foresi (University of Siena, IT); J.J. Fornos (University of Balearic Islands, ES); M. Firpo (University of Genoa, IT); B.P. Horton (Rutgers University, US); P. Jayson-Quashigah (University of Ghana, GH); T. Mann (ZMT Bremen, DE); T. Mensah-Senoo (University of Ghana, GH); M. Pappalardo (University of Pisa, IT); R. Ramalho (Bristol University, UK); D. Roberts (Council for Geosciences, SA); D. Sivan (University of Haifa, IL); G. Wiafe (University of Ghana, GH); and E. Zilbermann (Israel Geological Service, IL). We thank I. Candy, C. Murray-Wallace and another anonymous reviewer for their insightful comments on a previous version of the MS.

4.10. Supplementary material

This manuscript is accompanied with supplementary data, which can be found with the corresponding paper online at *http://dx.doi.org/10.1016/j.earscirev.2016.06.006* and as part of a data collection of this thesis at *https://doi.pangaea.de/10.1594/PANGAEA.883825*.

This supplementary consists of:

- Supplementary Tables S4:
  - S4.1 - A calculator for calculating the paleo RSL
  - S4.2 - References for building Fig. 4.3
  - S4.3 - References and data for building Fig. 4.6
  - S4.4 - References and data for building Fig. 4.11
  - S4.5 - Template for compiling new data in a database format

5. Paleo sea-level changes and relative sea-level indicators: Precise measurements, indicative meaning and glacial isostatic adjustment perspectives from Mallorca (Western Mediterranean)

T. Lorscheid, P. Stocchi, E. Casella, L. Gómez-Pujol, M. Vacchi, T. Mann, A. Rovere

Originally published in *Palaeogeography, Palaeoclimatology, Palaeoecology* (2017) **473**, p. 94–107

5.1. Abstract

Paleo relative sea-level (RSL) indicators formed during the Marine Isotope Stage (MIS) 5e have been reported by a large number of studies worldwide. Despite this, three main aspects are seldom reported: (1) use of high-precision survey techniques applied to MIS 5e RSL indicators; (2) application of modern analogs to understand the indicative meaning of MIS 5e RSL indicators; (3) estimates of the effects of glacial isostatic adjustment (GIA) on the MIS 5e records. In this study, we show how the three points above have been addressed in a focused study on Last Interglacial outcrops on the island of Mallorca. We measured the elevation of several RSL indicators with high-accuracy differential GPS (vertical accuracies down to 0.1 m) and we established the relationship between each RSL indicator and the paleo sea level through calculation of the indicative meaning for each RSL indicator. In particular, we present a novel technique to calculate the indicative meaning of fossil beach deposits with a phase-averaged morphodynamic model (CSHORE). We show how this approach helps overcoming difficulties with the survey of the modern analogs for these indicators. Our results show that two paleo RSLs are imprinted in Mallorca at +2.9 ± 0.8 m and +11.3 ± 1.0 m. We then compare our field-based results with modelled paleo RSL, calculated from the predictions of the ice-earth coupled ANICE-SELEN model, using few different ice-sheet melting scenarios during MIS 5e. We conclude that indicative ranges can be derived from relatively simple morphodynamic models and that the comparison of field-derived and modelled RSL values is a good method to validate possible scenarios of MIS 5e sea-level variability, especially in absence of precise dating.

5.2. Introduction

The position of eustatic sea level during past interglacials has often been used to understand the sensitivity of polar ice sheets to warmer climates (Kopp et al., 2009; Dutton and Lambeck, 2012; Dutton et al., 2015a). More recently, paleo sea-level estimates have been used to constrain models predicting the future configuration of ice sheets (DeConto and Pollard, 2016). The Last Interglacial, and in particular MIS 5e (~130-116 ka) was characterized by average global temperatures 1-2 °C higher than today and CO_2 concentrations similar to the pre-industrial levels (Otto-Bliesner et al., 2013). During this warmer period, polar ice sheets were smaller and sea levels were several meters higher than today (Dutton et al., 2015a).

While there is general consensus that, during MIS 5e, eustatic sea level (ESL) rose up to 6-9 m above present (Hearty et al., 2007; Kopp et al., 2009; Dutton and Lambeck, 2012), there is still uncertainty on how and when sea level attained its maximum position. For example, field evidence (corrected for GIA) from the Seychelles (Dutton et al., 2015b) show that ESL rose up to 7.6 m early in the interglacial (~125 ka), while in Western Australia (O'Leary et al., 2013) comparable evidence show that ESL reached 9.5 m only following a sudden meltwater pulse in the last part of the interglacial (~118 ka). A similar MIS 5e peak sea level was shown by Kopp et al. (2009) after the analysis of a large dataset of globally distributed sites through a Bayesian statistical approach. The same study highlighted that it cannot be excluded that MIS 5e sea level had a double-peaked highstand, with an early peak followed by a sea-level fall and a second rise leading to a second eustatic sea-level peak. On the other hand, data from the Northern hemisphere (Long et al., 2015) report the lack of clear evidence for abrupt sea-level changes during MIS 5e for near-field locations.

The estimate of global ESL during MIS 5e relies either on sea-level records based on the stable oxygen isotopes of planktonic foraminifera (e.g. Rohling et al., 2008) or on the measurement, interpretation and analysis of relative sea-level (RSL) indicators (e.g. beach sediments or fossil remains, see Rovere et al., 2016a for the description of different types of RSL indicators). The elevation of a RSL indicator, though, does not represent directly the elevation of the former RSL, but it can be reconnected to sea level through the calculation of its indicative meaning (Shennan, 2015). Moreover, the term 'relative' sea level indicates that any RSL indicator might have been subject to a series of post-depositional processes that might have changed its elevation through time, such as tectonics or sediment compaction (see Rovere et al., 2016b and references therein for a review of such processes). Even in tectonically stable areas, the elevation of a RSL indicator is different than the paleo ESL due to the net effects of glacial isostatic adjustment (GIA), which vary with both the distance from and the distribution of former ice sheets (Peltier, 2001; Milne and Mitrovica, 2008; de Boer et al., 2014b).

The study of MIS 5e shorelines dates back to at least one century ago (Antevs, 1929; Cooke, 1930), and RSL indicators formed during MIS 5e were reported at over one thousand sites worldwide (Pedoja et al., 2011a). Despite the large number of existing studies, there are still at least three aspects that need attention in the study of MIS 5e (and, in general, Pleistocene) sea levels:

i) Precise measurement (i.e. centimeter-level accuracy) of RSL indicators in the field is limited to few studies (e.g. Meco et al., 2007; Muhs et al., 2011; O'Leary et al., 2013; Sivan et al., 2016).
ii) Application of modern analogs to understand the indicative meaning of MIS 5e RSL indicators has been recently theorized (Hibbert et al., 2016; Rovere et al., 2016a), but is seldom applied in comparison with Holocene sea-level studies (e.g. Van De Plassche, 1986; Woodroffe and Horton, 2005; Engelhart and Horton, 2012; Shennan, 2015).
iii) The fact that GIA causes departures from eustasy of MIS 5e records is well-known (Dutton and Lambeck, 2012; Creveling et al., 2015) but still under-reported if compared to Holocene sea-level studies (Lambeck et al., 2004; Engelhart et al., 2011; Khan et al., 2015; Mann et al., 2016; Vacchi et al., 2016).

In this paper, we present how the three points above were addressed to study MIS 5e RSL indicators on the island of Mallorca (Western Mediterranean Sea). Those RSL indicators represent common, subtropical/temperate depositional paleo RSL proxies (Butzer and Cuerda, 1962; Butzer, 1975) and have been often referred to as a Quaternary benchmark for the Mediterranean Sea (Ginés et al., 2012). After measuring each deposit with high-accuracy GPS, we describe the indicative meaning for each RSL indicator using a combination of field surveys and 1D morphodynamic modelling of the modern coastal conditions. In contrast with other studies on Mallorcan MIS 5e RSL indicators, that either excluded (Dorale et al., 2010) or assumed minimal GIA effects (Muhs et al., 2015), we here present a set of GIA model results for the study area, and discuss the implications of GIA-driven RSL in light of the paleo RSL calculated from indicators observed in the field.

5.3. Study area

The island of Mallorca (Balearic Islands) is located in the Western Mediterranean, east of the Iberian Peninsula. The morphology of the island corresponds to a series of NE-SW orientated horst- and graben-structures. The horsts correspond to two subparallel mountain ridges of Oligo-Miocene age in the Northwest and Southeast (Serra de Tramuntana and Serra de Llevant, respectively). These are separated by the Palma-Inca-basin, a graben structure with the Bay of Palma and the Bay of Alcudía at its southern and northern ends respectively (Sàbat et al., 2011). These basins are filled by sediments from Miocene to Quaternary age. Only few minor tectonic events are reported for the island of Mallorca since the Pliocene and therefore the island is assumed to have been tectonically stable (or tilting with very mild rates) after the late Miocene (Butzer and Cuerda, 1962; Fornós et al., 2002; Sàbat et al., 2011). Countering this view, Zazo et al. (2003) argued that different MIS 5e deposits on the island have been tectonically up- or downlifted depending on their location within horsts or grabens. However, these findings are challenged by more precise MIS 5e sea-level data obtained from speleothems around the southern and eastern coast of the island (Dorale et al., 2010; Tuccimei et al., 2012), that do not record tectonically-driven variations as large as those identified by Zazo et al. (2003).

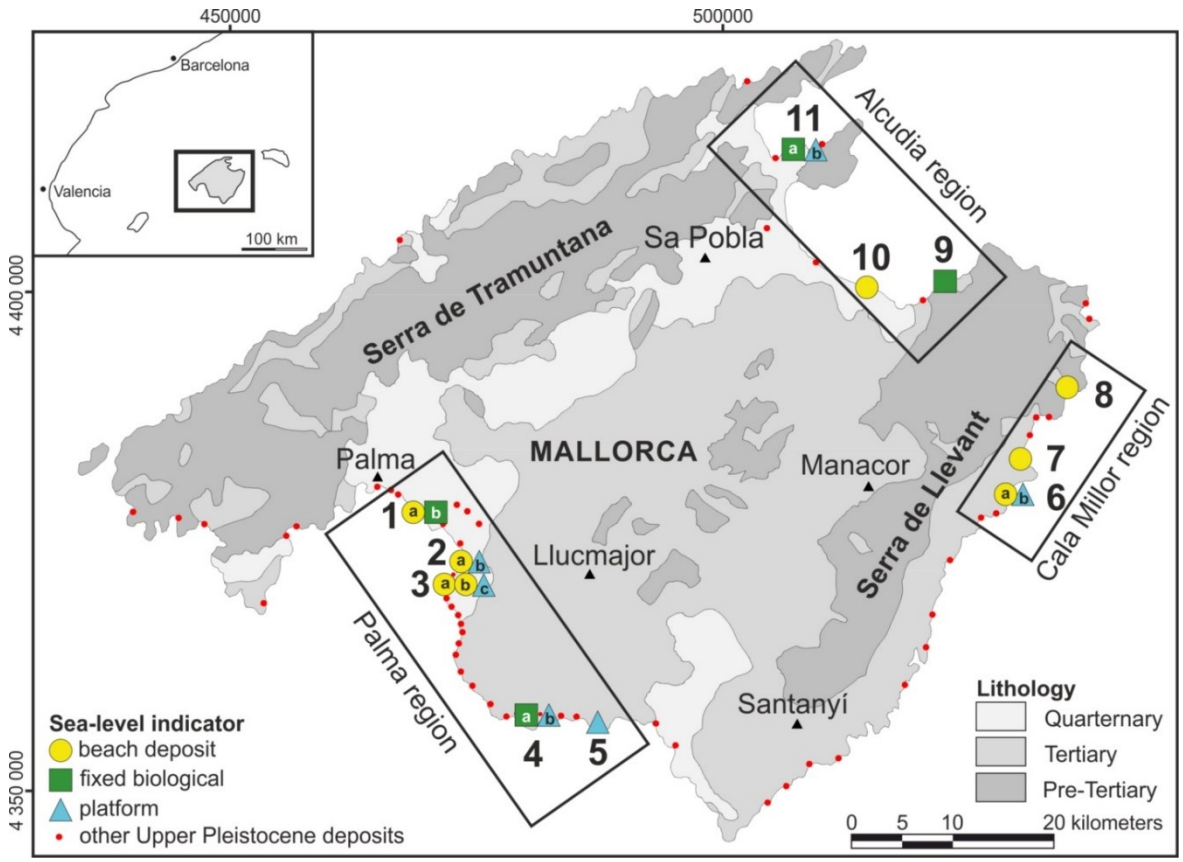

Fig. 5.1: Inset: location of the island of Mallorca within the Western Mediterranean Sea. Main map: the island of Mallorca, with outcrop location and survey regions and main geological units. Colors and shape of each point indicate the type of RSL indicator. See the section 5.4.2 for further details. Sites are as follows (a, b, c refer to different RSL indicators at the same location): 1 - Cala Pudent/Camp de Tir, 2 - Cova Baixa, 3 - Cala Blava, 4 - Cala Pi, 5 - S'Estalella, 6 - S'Illot, 7 - Cala Millor, 8 - Canyamel, 9 - Caló des Camps, 10 – Torrent de Son Real, 11 - Platja de Sant Joan. See Table 5.4 and 5.5 for elevation of RSL indicators measured in the field and relative paleo RSL calculation.

Studies on the Pleistocene geology of Mallorca date back to the early 1960's (Butzer and Cuerda, 1962; Cuerda, 1975) and describe in detail the sedimentology and paleontology of Pleistocene marine deposits on the island. These deposits are attributed mostly to MIS 5e (see red dots in Fig. 5.1), and are dated using both analytical (U-series, AAR, OSL) (Stearns and Thurber, 1965; Hearty et al., 1986; Hillaire-Marcel et al., 1996; Rose et al., 1999) and bio-/chronostratigraphic methods. Upper Pleistocene outcrops are mainly concentrated in the southwestern and northeastern coasts of Mallorca, where the low topography facilitated their deposition and preservation. The eastern coast is mostly characterized by cliffs and MIS 5e deposits are preserved only in some small, protected areas. Along the western margin, no major MIS 5e deposits are reported, probably because the preservation along this section of coast is low due to its erosive character and small accommodation space (Gelabert et al., 2003). The majority of the MIS 5e outcrops in Mallorca (Butzer and Cuerda, 1962; Hearty, 1987; Rose et al., 1999; Zazo et al., 2003; Bardají et al., 2009; Vicens et al., 2012) are reported at elevations between +1 m and +6 m above present sea level, except two higher deposits at around +10 m in Cala Blava and S'Estalella (no. 3 and 5 in Fig. 5.1). Two studies focusing on the littoral karst caves that developed along the eastern and southern coast of Mallorca (Tuccimei et al., 2007; Dorale et al., 2010)

investigated the phreatic overgrowth on speleothems (POS) as a RSL indicator. POS is a secondary feature, which forms as inorganic, carbonate encrustation on pre-existing structures (e.g. stalactites) at the top of brackish water lenses inside cave pools. As long as the hydraulic gradient between these lenses and sea water is negligible, these encrustations are interpreted as forming within the tidal range (Van Hengstum et al., 2015). For Mallorca, these indicators were measured with U-series to ages between 138.0 ± 1.9 and 109.9 ± 1.1 ka (Tuccimei et al., 2007; Dorale et al., 2010) and suggest a paleo RSL during MIS 5e in a range between +1.5 m and +3.0 m along the southern and eastern coast.

5.4. Methods

5.4.1. Fieldwork and elevation measurements

We remeasured the 11 most prominent MIS 5e outcrops in Mallorca (Fig. 5.1), including those reported by Hearty (1987) and Vicens et al. (2012). Elevation measurements were performed using a high-precision differential GPS system (Trimble ProXRT receiver and Trimble Tornado antenna) equipped to receive OmniSTAR G2 real-time corrections. These corrections, in optimal conditions, allow to establish the elevation of a point with an absolute accuracy of ~0.1-0.2 m, depending on the survey conditions (e.g. presence of trees or buildings affecting the GPS signal reception).

Elevation data were originally recorded in geographic WGS84 coordinates and in height above the ITRF2008 ellipsoid. Following the procedure described by Foster (2015) we calculated the elevation above mean sea level using the SOPAC GPS-station 'MALL' with the co-located permanent tide station at Palma de Mallorca (PSMSL ID 1892). The vertical datum of these calculated elevations is the EGM08 REDNAP geoid (IGN, 2009), which is a refined version of the global EGM08 geoid for Spain and is the best available approximation of mean sea level in this region. The GPS values of two sites (10 - Torrent de Son Real and 11 - Platja de Sant Joan), where the OmniSTAR signal was not available, have been postprocessed with the software Trimble GPS Pathfinder Office using base station data from the SOPAC GPS-station 'MALL'.

Three types of RSL indicators were identified and measured: beach deposits, fossil fixed biological indicators and the inner margin of shore platforms. Elevation measures for the first two types of indicators represent the highest point where the sediment layer or fossil can be identified as being in situ. For the measurement of the inner margin of shore platforms, we performed, whenever possible, several GPS profiles along the platform, in order to take into account the lateral variability of this RSL indicator. We interrupted each GPS profile at the inner margin or at the point where it was not possible to follow further the sub-horizontal platform surface. Therefore, the elevation measurements reported for shore platforms in this study corresponds to the average between the highest and lowest measured profile, and the measurement error corresponds to half the difference between these two values plus the GPS error. In two cases (3 - Cala Blava and 11 - Platja de Sant Joan) we performed only one transect and in one case (4 - Cala Pi) only one point measurement, therefore the measurement and its error correspond to the original GPS values obtained for these sites.

5.4.2. Relative sea-level indicators and the modern analog

The elevation of a relative sea-level (RSL) indicator measured in the field can be used to reconstruct the paleo RSL, that is the paleo sea level still uncorrected for non-eustatic effects, e.g. tectonics or GIA. The standard methods to calculate the paleo RSL from the elevation of a RSL indicator have been defined in the seminal works by Shennan (1982) and Van De Plassche (1986), and they proved effective in the reconstruction of Holocene sea-level histories (Milne et al., 2005; Engelhart and Horton, 2012; Shennan et al., 2012; Barlow et al., 2013; Barnett et al., 2015; Hijma et al., 2015; Khan et al., 2015; Shennan, 2015; Vacchi et al., 2016). A recent work by Rovere et al. (2016a) attempted to transfer these concepts to the Last Interglacial (and generally older than Holocene) shorelines.

The paleo RSL can be calculated from the elevation of an indicator if the relation between the RSL indicator and the paleo RSL (i.e. the 'indicative meaning') is defined. Such relation can be defined by understanding the upper and lower limits of the RSL indicator formation in the modern environment. From these limits, it is possible to calculate the indicative range (IR), which is defined as 'the vertical range over which the indicator occurs at present' (Shennan, 2015) and the reference water level (RWL), which is defined as 'the modern equivalent elevation at which the indicator occurs' (Shennan, 2015).

Table 5.1: Formulas from Rovere et al. (2016a) used for calculating the indicative meaning and the paleo RSL.

	Value	Equation
Eq. 5.1	Reference water level	$RWL = \frac{upper\ limit\ +\ lower\ limit}{2}$
Eq. 5.2	Indicative range	$IR = upper\ limit\ -\ lower\ limit$
Eq. 5.3	Paleo relative sea level	$Paleo\ RSL = dGPS\ measurement\ -\ RWL$
Eq. 5.4	Error of paleo relative sea level	$Paleo\ RSL\ error = \sqrt{\left(\frac{IR}{2}\right)^2 + \left(\frac{dGPS\ precision}{2}\right)^2}$

Table 5.2: Summary of Reference Water Level and Indicative Range values for each RSL indicator in this study.

Indicator type	Description (details see section 5.4.2.1 - 5.4.2.3)	Reference Water Level[a]	Indicative Range[a]
Beach deposit	Structureless, unsorted sandstone containing shell fragments or nearly entire specimens (e.g. *Strombus latus*) and some larger pebbles	$(O_b + d_b)/2$	$O_b - d_b$
Fossil fixed biological indicators	Fossil remains of Vermetids, Serpulids and *L. lithophaga* boreholes	(MLLW + LLR)/2	MLLW - LLR
Inner margin of shore platform	Highest preserved point of a platform, that was carved in the bedrock by wave action	$[(MLLW - d_b)/2 + MHHW]/2$	$(MLLW - d_b)/2 - MHHW$

[a] d_b - breaking depth; MLLW - mean lower low water; MHHW - mean higher high water; LLR - lower abundant living range; O_b - Ordinary berm

Rovere et al. (2016a) suggested that a set of simple equations can be used to calculate the paleo RSL and the associated uncertainty once the elevation of a MIS 5e RSL indicator is known. These formulas

are adapted to older RSL indicators from those largely used for Holocene sea-level studies (e.g. Engelhart and Horton, 2012; their Table 1) and foresee that, for each indicator, the upper and lower limits of the modern environment of formation (defining the IR) are known. The RWL is then simply the midpoint of the IR (see formulas in Table 5.1).

In this study, we surveyed three different types of RSL indicators: Beach deposits (Tamura, 2012), fossil fixed biological indicators (Rovere et al., 2015a) and shore platforms (Kennedy, 2015). Each RSL indicator is described hereafter and its indicative meaning is summarized in Table 5.2.

5.4.2.1. Beach deposits

A fossil beach deposit can be defined as a cemented sediment layer with variable grain size, containing fragments or fully preserved specimens of marine shells. Particular structures (e.g. subtidal cross-bedding or laminated lagoonal facies) can help in detailing the sea-level information carried by a beach deposit. In absence of these elements it is possible to constrain the indicative range of a beach deposit between the ordinary berm of a modern beach (O_b, upper limit) and the breaking depth (d_b, lower limit) of typical waves on the shoreline of interest (Rovere et al., 2016a).

In order to obtain these two values (d_b and O_b) for the three regions shown in Fig. 5.1 (Palma, Cala Millor and Alcudía) we used a nearshore 1D morphodynamic model (CSHORE, Kobayashi, 1999, 2009). The code is freely available at *https://sites.google.com/site/cshorecode/ (last accessed 12 December 2016)*. This model uses the initial beach topography and wave data as inputs and calculates the resulting beach profile after a swell event, including the wave runup. As model set-up we chose the one proposed by Casella et al. (2014), which was calibrated on a modern Mediterranean beach under different wave scenarios. The only variations we made with respect to the Casella et al. (2014) settings (their Table 1) is a different sediment grain size (d_{50}) of 0.27 mm (Gómez-Pujol et al., 2011) and the runup wire height was changed to 0.01 m in order to better represent the local sedimentary properties of Mallorcan beaches.

As initial beach topography, we used differential GPS beach profiles from either our GPS surveys (at Cala Pudent for the Palma region) or the SOCIB (Balearic Islands Coastal Observing and Forecasting System) beach monitoring campaigns (at Cala Millor for the Cala Millor region and at Can Picafort for the Alcudía region). As wave inputs, we extracted data from the SIMAR dataset (provided by Puertos del Estado, *http://calipso.puertos.es/BD/informes/INT_8.pdf, last accessed 12 December 2016*), that is a maintained and updated version of the HIPOCAS project (Ratsimandresy et al., 2008a; Ratsimandresy et al., 2008b). Thresholds for choosing the swells were a peak minimum significant wave height of 2.5 m (which represents an extreme swell in an enclosed basin such as the Mediterranean) and a general wave direction perpendicular to the beach.

In total, we modelled 8 swell events for the Alcudía region, 6 swell events for the Cala Millor region and 21 swell events for the Palma region (see results of example runs in Fig. 5.5a-c). The final output of each simulation is the maximum wave runup on the beach during the swell for different time steps, and the final beach profile after sediment was transported along the transect by waves. From each

swell simulation, we extracted the elevation range where the runup and the largest accumulation of sediment below mean sea level was recorded and averaged these values over all model runs for each region. We interpret these values as corresponding to, respectively, the ordinary berm (O_b) and the breaking depth (d_b), which we used as upper and lower limits of the indicative range (see supplementary material S5.3 for the model results of each swell).

In order to perform microstratigraphic analyses, we prepared thin sections (35 µm thickness) of the different beach deposits and analyzed them using a polarizing microscope. These observations allowed the characterization of the constituents, the presence of bioclasts as well as the type of the cementation pattern for each deposit (Vacchi et al., 2012). In particular, we investigated the possibility to differentiate between deposits that were formed within the intertidal zone (Desruelles et al., 2009; Vousdoukas et al., 2009; Mauz et al., 2015) from those forming slightly above the intertidal zone (e.g. storm deposits). Deposits formed in the intertidal zone typically show early intertidal cements characterized by a large proportion of high-magnesium calcite (HMC) or aragonite in their composition. Their formation is strongly controlled by the mixing between carbonate-saturated marine water and fresh groundwater (Neumeier, 1998; Mauz et al., 2015). Several typologies of early intertidal cements have been described in several Mediterranean Holocene beachrocks studies (Desruelles et al., 2009; Vousdoukas et al., 2009; Mauz et al., 2015; Ozturk et al., 2016). Conversely, there have been fewer investigations of cementation patterns of MIS 5e beach deposits, especially in the context of post-depositional processes (e.g. erosion of primary cements) that may have affected the perfect preservation of the cements in these beach deposits.

5.4.2.2. Fossil fixed biological indicators

Fossil fixed biological indicators (Rovere et al., 2015a) are the remains of organisms (Vermetids, Serpulids or *L. lithophaga*) that were living near the sea level. The upper limit of their living range corresponds to mean lower low water (MLLW), a value we extracted from tide stations at Palma de Mallorca (Palma region), Capdepera (Cala Millor region) and Alcudía (Alcudía region) from *http://www.tide-forecast.com (last accessed 13 August 2016)*. For which concerns the lower limit, it should be highlighted that some of the organisms that we used as fossil fixed biological indicator can live at great depths (Laborel and Laborel-Deguen, 1994), therefore the nominal lower limit of the indicative range would be several meters below sea level. Nevertheless, typical modern assemblages of these organisms in the Mediterranean have a clear peak in organism abundance at -1 to -2 m (Antonioli and Oliverio, 1996; Antonioli et al., 1999). Averaging this range, we set the lower limit to -1.5 m, with the remark that further studies on the modern distribution of such organisms at each site are needed to further improve this estimate.

5.4.2.3. Shore platforms

Shore platforms are sub-horizontal landforms that are carved by wave-interaction in existing bedrock on rocky shorelines (Kennedy, 2015). Typically, a long time period of quasi-stable sea level is needed to form these indicators, e.g. Stephenson and Kirk (1996) report a maximum erosion rate of 1.5 mm/a for modern shore platforms. Rovere et al. (2016a) suggest that the indicative range of shore platforms

can be defined as bounded by the mean higher high water (MHHW) upwards and by the midpoint between MLLW and the breaking depth (d_b) downwards. The values for d_b were derived from the CSHORE model output in each region (as described above), the values for MHHW and MLLW were extracted from the website *http://www.tide-forecast.com (last accessed 13 August 2016)*.

5.4.3. Glacial isostatic adjustment (GIA) model

As discussed in the introduction, observations of sea-level changes made through RSL indicators must be considered as 'relative' due to perturbations that cause the observation to depart from the global eustatic sea level (Rovere et al., 2016b). As highlighted in Section 5.3, the island of Mallorca is considered tectonically stable at least since the Pliocene. Therefore, one of the major causes of departure from eustasy of MIS 5e RSL indicators in this area should be related to GIA processes. In this study, these processes were modelled using the coupled ANICE-SELEN model, an ice-earth coupled GIA model (de Boer et al., 2014b).

The ANICE model (Bintanja and van de Wal, 2008; de Boer et al., 2013; de Boer et al., 2014a) is an ice-sheet-shelf-model, which dynamically couples the 3-dimensional influences of four different ice sheets (Antarctic (AIS), Greenland (GrIS), North American (NaIS) and European (EuIS) Ice Sheet) and covers the time from 410 ka to present. The SELEN model (Stocchi and Spada, 2009) is a global earth model calculating the changes in the geoid, solid earth and RSL. These two models are coupled with an interval of 1 ka and interact dynamically between the calculations for every time step. For each step, the ANICE model delivers the ice-load to SELEN, which is then calculating the RSL variations and the distribution of ice sheets that is then send back to ANICE for the next calculation step.

In Fig. 5.2a we show the eustatic curve of a full, 410 ka-long model run where the extent of ice sheets for the time between 126 and 117 ka was kept to their modern value and the resulting RSL. Taking just eustatic effects into account, this would result in a sea level during MIS 5e equal to the modern (blue curve), but including the deformation of the earth, GIA in Mallorca causes a RSL rise during interglacials (e.g. MIS 5e and MIS 9). We then calculated the GIA-driven RSL history of Mallorca from 410 ka (Fig. 5.2a) to present day, modulating the melting of GrIS and Western AIS in MIS 5e according to four different scenarios:

i) A scenario reflecting the most classical view of MIS 5e sea-level history (e.g. Lambeck and Nakada, 1992), with melting of both Greenland (2.0 m) and Antarctica (5.0 m) happening early in the interglacial (Fig. 5.2b), and not changing until insolation in both hemispheres decreases and glacial conditions start to resettle.
ii) A scenario contemplating a two-step highstand (Fig. 5.2c). Greenland ice sheet contributes with 2.0 m of ESL equivalent between 127 and 116 ka while Antarctica contributes with 5.0 m only after 120 ka.
iii) A scenario where Greenland and Antarctic ice sheets release, respectively, 2.5 and 1.0 m ESL equivalent at 126 ka (Fig. 5.2d). The Greenland ice sheet remains stationary until 117 ka, while Antarctic ice sheet releases another 4.5 m after 120 ka. The two-step retreat of Greenland and Antarctic ice sheets, therefore, results in a maximum eustatic peak of 8.0 m between 119 and 117

ka. Scenarios 2 and 3 are in line with the timing and magnitudes proposed by Hearty et al. (2007) and O'Leary et al. (2013).

iv) A scenario that is chronologically opposite to scenario 2 and 3 (Fig. 5.2e) and at odds with O'Leary et al. (2013). It implies that AIS and GrIS are melting early in the interglacial by 5.5 m and 2.5 m respectively, as hypothesized, for example, by Dutton et al. (2015b) from data in the Seychelles. The AIS, though, enters into glacial conditions before the GrIS does, generating an earlier, stepwise sea-level fall.

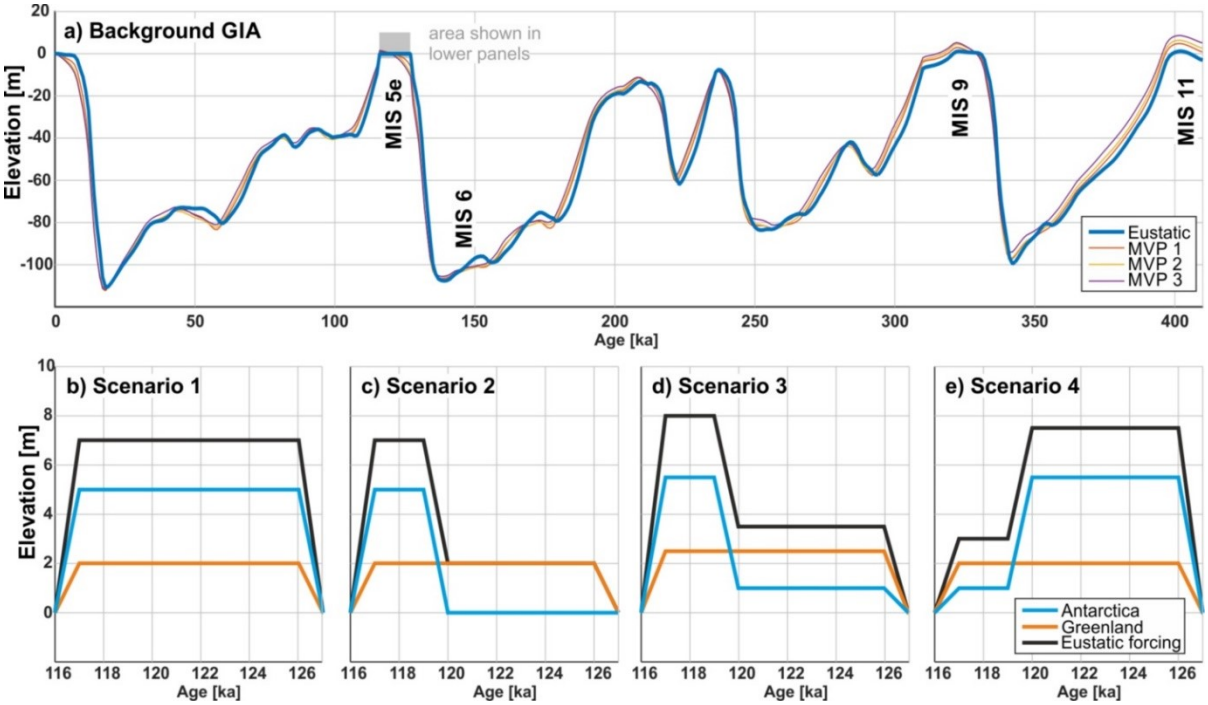

Fig. 5.2: a) Forcing of the GIA model (blue) and resulting sea-level predictions for different mantle viscosities. This complete ANICE-SELEN run shows that the model includes for every calculation the behavior during the previous glacial and interglacial time periods since 410 ka. The Eustatic scenario represented in the figure corresponds to the 'Background GIA' calculation, i.e. keeping all ice sheets during MIS 5e to the same extent than the modern value. b-e) The model was then run using the ESL scenarios for MIS 5e shown in the panels below, i.e. this additional meltwater has to be added to the eustatic signal in the grey box of the upper panel.

It is worth highlighting that these scenarios represent only some of the possible MIS 5e ice-melt scenarios, and must be regarded as an illustration of the different RSL curves produced by different sea-level histories within MIS 5e. These predictions could vary (also significantly) if either the length of the interglacial or the ice configuration at MIS 6 or during previous interglacials is varied. Nevertheless, with the GIA modelled as described above, it is possible to compare directly the elevation of a paleo RSL indicator observed in the field against the different RSL histories obtained by the model.

Another source of uncertainty in the GIA modelling is the composition of the solid earth. In this study, we employ a spherically symmetric, radially stratified, deformable but not compressible, self-gravitating and rotating Earth (de Boer et al., 2014b). The physical and rheological parameters depend on the radius only, which implies that the rheological model is 1D and accordingly, lateral heterogeneities are

not accounted. We assume a purely elastic lithosphere (outer shell) and keep its thickness fixed to 100 km. The mantle is discretized in three layers that are characterized by a linear Maxwell viscoelastic rheology respectively and that are called, from top to bottom, Upper Mantle, Transition Zone and Lower Mantle. We compare the performance of three different mantle viscosity profiles (Table 5.3), that represent the possible ranges of the most commonly used viscosities for MIS 5e GIA studies (Lambeck and Nakada, 1990; Peltier, 1996; Mitrovica and Forte, 1997).

Table 5.3: Mantle Viscosity used in the different GIA model runs.

	Upper mantle	**Transition Zone**	**Lower Mantle**
MVP 1	1.0 x 10^{21} Pa s	1.0 x 10^{21} Pa s	2.0 x 10^{21} Pa s
MVP 2	0.5 x 10^{21} Pa s	0.5 x 10^{21} Pa s	5.0 x 10^{21} Pa s
MVP 3	0.25 x 10^{21} Pa s	0.5 x 10^{21} Pa s	10.0 x 10^{21} Pa s

5.5. Results

5.5.1. Stratigraphy

A typical Mallorcan Last Interglacial coastal deposit is represented by a medium to very coarse sandstone that was deposited in a tide- and wave-influenced beach environment. The sandstones contain most often fragmented shells, some deposits contain integer specimens of large gastropods (such as *Strombus latus*, Fig. 5.3a), as well as larger pebbles. The grains are usually well-rounded and slightly sorted. The thickness of a Mallorcan MIS 5e beach deposit can reach a maximum of 1.8 m. The fossil content is dominated by a marine faunal assemblage, called 'Senegalese fauna' (Cuerda, 1979; Vicens et al., 2012), as well as fossil remains of *L. lithophaga*, Serpulids and Vermetids (Fig. 5.3b) that can be used as fossil fixed biological indicators.

Thin section analysis of samples from the beach deposits indicated that they are mainly composed of rounded and, in minor terms, angular clasts. Presence of several bioclasts was also recorded. The degree of cementation showed a significant variability among samples and the proper definition of the cementation patterns was sometimes difficult. The bounding materials observed between grains are early intertidal cements, micritic filling (including internal sediments) and low-magnesium calcite (LMC) meteoric cement (Fig. 5.3c and d). The latter is present in most of the analyzed deposits as final term of a general pattern characterized by multiple phases of cementation. Even if often reduced to a thin rim, we identified a first phase of early intertidal cements in most of the analyzed deposits. These are characterized by HMC cements with micritic texture forming isopachous fringes and a meniscus between the grains, by limpid crystal fringes (palissadic or blocky texture) or by fibrous aragonitic cements in stalactitic position. The observed micritic fillings are not diagenetic cements but were often described as result of infiltration in the pore space. Their formation may come from the percolation of fine particles originating from the water/sediment interface, both in the intertidal or in the supratidal zone. A detailed description (including profiles and thin section pictures) of all outcrops presented in Fig. 5.1 can be found in the supplementary material S5.1.

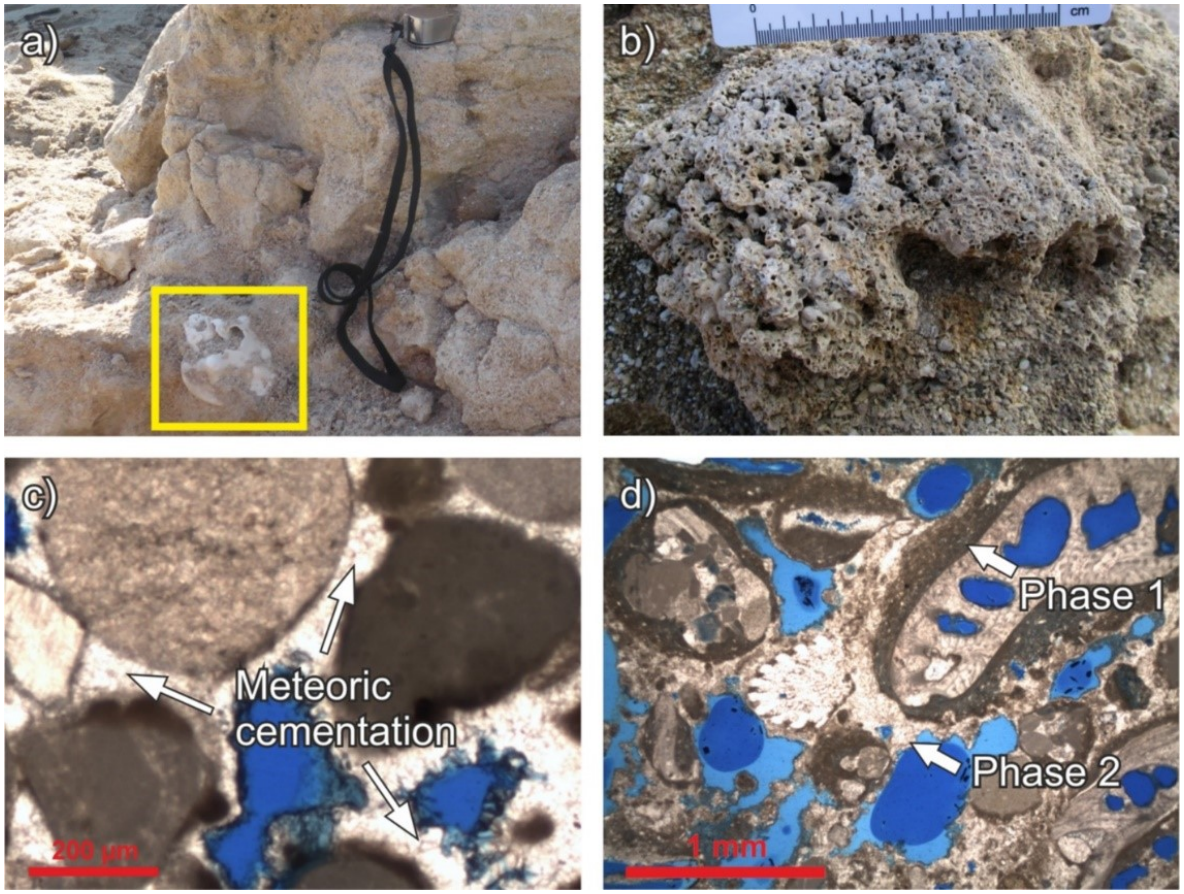

Fig. 5.3: a) Lower part of coarse sandstone layer in Cala Millor (7 in Fig. 5.1) including an example of *Strombus latus* (yellow box). b) Tubes from Vermetid worms on top of the Camp de Tir (1b) outcrop. c) Thin section picture from S'Illot (6a) showing the meteoric cementation d) Thin section picture from Cala Blava (3b) with large bioclasts and a first micritic and second meteoric cementation phase.

Three samples (Cala Blava, S'Estalella, and S'Illot) showed a peculiar cementation pattern. The higher deposit in Cala Blava (3b in Fig. 5.1, +6.72 ± 0.03 m), mostly composed of bioclasts (Fig. 5.3d), showed a first phase of micritic fillings followed by meteoric cement. In S'Estalella (5, +9.50 ± 1.50 m), we observed a very chaotic structure showing mixed rounded and angular clasts poorly cemented by micritic fillings. In S'Illot (6a, +5.54 ± 0.86 m), LMC meteoric cement is the predominant bounding material between grains (Fig. 5.3c). Evidence of a first phase of early intertidal cement is lacking in the observed thin section of this deposit. The different appearance of these three outcrops is also confirmed by the macroscopic occurrence that shows a patchy deposition and a very chaotic texture.

The radiometric determination of ages for the Pleistocene deposits in Mallorca was firstly carried out by Stearns and Thurber (1965). They applied U-series dating on mollusk shells, but achieved strongly diverging results (e.g. ages of 75 and 200 ka for a repeated measurement on the same sample). Kaufman et al. (1971) showed that marine mollusks do not behave as a closed system and therefore the application of U-series dating on mollusk shells is not a reliable method. Nevertheless, U-series dating on mollusk shells was often used in Mallorca (Hoang and Hearty, 1989; Hillaire-Marcel et al., 1996; Zazo et al., 2003), mainly because many outcrops are lacking other datable material. Despite showing large uncertainties, the results plot all within MIS 5. Until recently, there was only one dated

coral (*Cladocora caespitosa*) from Son Grauet/Cova Baixa (2a in Fig. 5.1) with an age of 129 ± 7 ka (Hearty et al., 1986). A recent study (Muhs et al., 2015) reports new dated corals from an outcrop previously interpreted as a MIS 5a deposit near Camp de Tir (1a and 1b in Fig. 5.1). Their results show ages between 125.7 and 117.8 ka using U-series dating on Cladocora caespitosa. This coral still lives in the Mediterranean, but the associated 'Senegalese fauna' (including *Strombus latus ex bubonius*) is today only found in the warmer water west of Africa. For this reason, this faunal assemblage is often used as a biostratigraphic marker in the Mediterranean (Torres et al., 2013). In Mallorca, the presence

Table 5.4: Location and elevation of outcrops reported in Fig. 5.1 (related RSL indicators can be found in Table 5.5).

Site	Site name	Lon[a]	Lat[a]	dGPS elevation[a]	Age attribution[b]
1a	Cala Pudent	2.700453	39.543536	2.33 ± 0.03	*Strombus latus* (1)
1b	Camp de Tir	2.702049	39.542175	1.31 ± 0.02	AAR (4); U-series on mollusks (5); U-series on corals (9)
2a	Cova Baixa	2.745646	39.497035	1.00 ± 0.16	AAR on mollusks (4); U-series on coral (3)
2b	Cova Baixa	2.742572	39.494798	11.72 ± 2.39*	-[c]
3a	Cala Blava	2.736524	39.488368	2.73 ± 0.03	U-series on mollusk (7)
3b	Cala Blava	2.736690	39.488375	6.72 ± 0.03	stratigraphic description (7)
3c	Cala Blava	2.736826	39.488354	12.02 ± 0.02	-[c]
4a	Cala Pi	2.835928	39.364069	3.16 ± 0.20	AAR on mollusks (4)
4b	Cala Pi	2.827559	39.356784	10.93 ± 0.09	-[c]
5	S'Estalella	2.901977	39.358766	9.50 ± 1.50*	AAR on mollusks (4)
6a	S'Illot	3.374083	39.559270	5.54 ± 0.86	AAR on mollusks (4)
6b	S'Illot	3.373875	39.559153	9.77 ± 1.85*	-[c]
7	Cala Millor	3.385249	39.590490	1.49 ± 0.02	*Strombus latus* (this study)
8	Canyamel	3.439101	39.653735	1.27 ± 0.25	AAR on mollusks (4)
9	Caló des Camps	3.299692	39.748067	1.30 ± 0.06	OSL on quartz grains (6)
10	Torrent de Son Real	3.209920	39.743077	0.87 ± 0.06	*Strombus latus* (8)
11a	Platja de Sant Joan	3.136148	39.865498	2.07 ± 0.05	*Strombus latus* (2)
11b	Platja de Sant Joan	3.136243	39.865622	2.95 ± 0.04	-[c]

[a] Geographic coordinates are presented in WGS 84 and elevations referred to the EGM08 REDNAP geoid.
[b] references for dating: 1 - Cuerda (1979), 2 - Cuerda et al. (1983), 3 - Hearty et al. (1986), 4 - Hearty (1987), 5 - Hillaire-Marcel et al. (1996), 6 - Rose et al. (1999), 7 - Zazo et al. (2003), 8 - Vicens (2010), 9 - Muhs et al. (2015). A list of all measurements including ages can be found in supplementary material S5.2.
[c] Platforms have no age attribution, but are assumed to be of an older age than MIS 5e (see section 5.5.2).
* For the sites of Cova Baixa, S'Estalella and S'Illot the errors on elevation measurements have been obtained by averaging the platform elevation across different profiles as shown in Fig. 5.4.

of the Senegalese fauna in a deposit is often used to assign a Last Interglacial age, especially for outcrops that have not been dated by analytical methods (Cuerda, 1979; Cuerda et al., 1983; Vicens, 2010; Vicens et al., 2012). Another relative dating method that confirmed a MIS 5e age for most deposits along the island of Mallorca is the Amino-Acid-Racemization (AAR, Hearty, 1987). A database with all published ages for each location can be found in supplementary material S5.2 and an overview is shown in Table 5.4. This database highlights that the Mallorcan deposits reported in this study are all of MIS 5e age.

Table 5.5: RSL indicators, upper and lower limits of the indicative range, reference water level, indicative range and paleo RSL for all outcrops reported in Fig. 5.1 and Table 5.4.

Site	Site name	Indicator[a]	dGPS elevation	LL	UL	RWL	IR	Paleo RSL
1a	Cala Pudent	beach	2.33 ± 0.03	-1.67	0.55	-0.56	2.22	2.89 ± 1.11
1b	Camp de Tir	verm	1.31 ± 0.02	-1.50	-0.09	-0.80	1.41	2.10 ± 0.71
2a	Cova Baixa	beach	1.00 ± 0.16	-1.67	0.55	-0.56	2.22	1.56 ± 1.12
2b	Cova Baixa	plat	11.72 ± 2.39*	-0.88	0.09	-0.40	0.97	12.12 ± 1.29
3a	Cala Blava	beach	2.73 ± 0.03	-1.67	0.55	-0.56	2.22	3.29 ± 1.11
3b	Cala Blava	beach	6.72 ± 0.03	terrestrial limiting				
3c	Cala Blava	plat	12.02 ± 0.02	-0.88	0.09	-0.40	0.97	12.42 ± 0.49
4a	Cala Pi	lith	3.15 ± 0.20	-1.50	-0.09	-0.80	1.41	3.95 ± 0.73
4b	Cala Pi	plat	10.93 ± 0.09	-0.88	0.09	-0.40	0.97	11.33 ± 0.49
5	S'Estalella	plat	9.50 ± 1.50*	-0.88	0.09	-0.40	0.97	9.90 ± 0.89
6a	S'Illot	beach	5.54 ± 0.86	terrestrial limiting				
6b	S'Illot	plat	9.77 ± 1.85*	-2.49	0.11	-1.19	2.60	10.96 ± 1.60
7	Cala Millor	beach	1.49 ± 0.02	-4.87	0.73	-2.07	5.60	3.56 ± 2.80
8	Canyamel	beach	1.27 ± 0.25	-4.87	0.73	-2.07	5.60	3.34 ± 2.81
9	Caló des Camps	serp/lith	1.30 ± 0.06	-1.50	-0.12	-0.81	1.38	2.11 ± 0.69
10	Torrent de Son Real	beach	0.87 ± 0.06	-3.59	0.94	-1.33	4.53	2.20 ± 2.27
11a	Platja de Sant Joan	serp	2.07 ± 0.05	-1.50	-0.12	-0.81	1.38	2.88 ± 0.69
11b	Platja de Sant Joan	plat	2.95 ± 0.04	-1.86	0.12	-0.87	1.98	3.82 ± 0.99

[a] RSL indicators: beach - top beach deposit, lith - top *L. Lithophaga* band, plat - elevated platform, serp - top Serpulids, verm - top Vermetids (more details on this data in supplementary material S5.2).
* For the sites of Cova Baixa, S'Estalella and S'Illot the errors on elevation measurements have been obtained by averaging the platform elevation across different profiles as shown in Fig. 5.4.

5.5.2. Paleo relative sea level

The modern elevations of the surveyed outcrops in Mallorca lie between +0.87 m and +12.02 m (Table 5.4). For the majority of the surveyed outcrops, the GPS vertical precision was below ± 0.5 m, mostly around ± 0.1 m. A larger direct GPS error (± 0.86 m) is only present in S'Illot, due to the location of the outcrop, where satellite reception is shadowed by a cliff. As described in Section 5.4.1, the elevations for shore platforms have been derived in three cases from several profiles (Fig. 5.4). This has the result

to increase the vertical uncertainty related to the measurement of these landforms up to ~1-2 m (cf. sites Cova Baixa, S'Estalella and S'Illot in Tables 5.4 and 5.5).

The results of our morphodynamic modelling (example runs in Fig. 5.5a-c) to establish the upper and lower levels of formation of beach deposits (Ordinary berm (O_b) and breaking depth (d_b) respectively) and the related indicative meaning are shown in Fig. 5.5d-i.

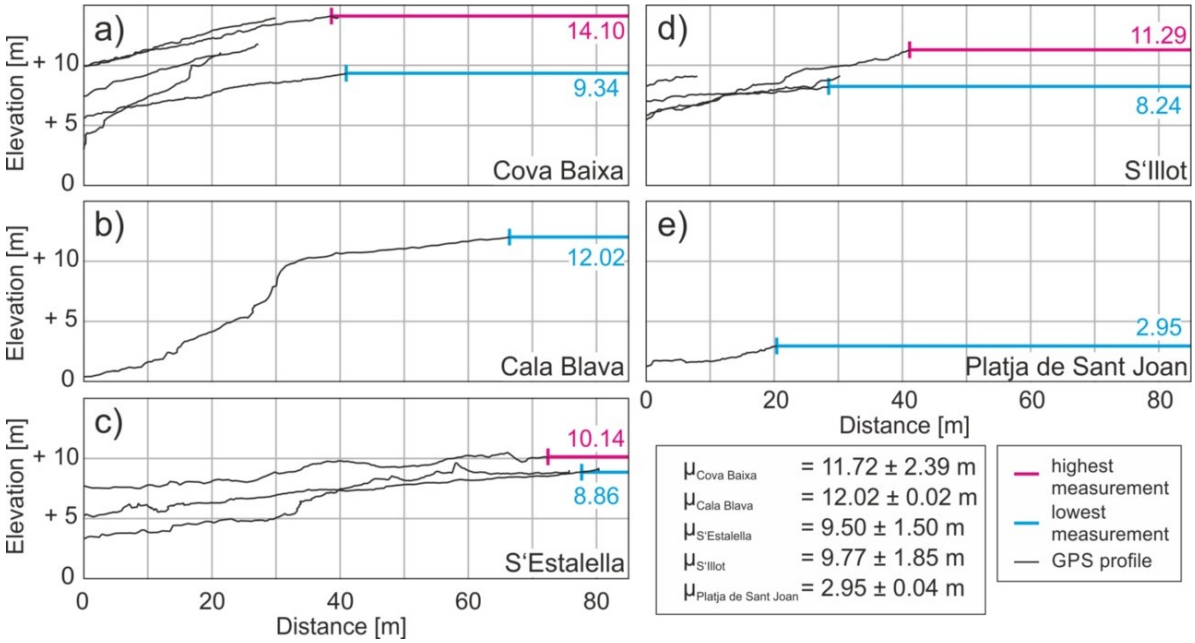

Fig. 5.4: GPS profiles showing the different lateral distribution of the elevated platform. Where possible, the mean value between the highest and lowest occurring limit was calculated. Together with the associated dGPS error, this was used as modern elevation value (μ) for the location.

The data used to perform paleo RSL calculations taking into account the indicative meanings of our indicators are shown in Table 5.5 and plotted in Fig. 5.6. Treating each paleo RSL and its associated uncertainty as a Gaussian distribution, and running a stacked probability density analysis (see MATLAB script in supplementary material S5.4) through our paleo RSL data, we obtained a curve representing the probability of an imprinted paleo RSL. The lower paleo RSL elevation of +2.9 ± 0.8 m (calculated by the mean of the related sites) include all locations with beach deposit and fossil fixed biological indicators. The sites Cala Blava (3b) and S'Illot (6a) that are interpreted as terrestrial limiting (i.e. they were deposited above sea level, and cannot be referred precisely to it), because of their microscopic and macroscopic occurrence (see Section 5.5.1). Although such interpretation gives some constraints on paleo sea levels (i.e., the sea level was not higher than these deposits), we do not include these two values in the sea-level probability density function of Fig. 5.6. The second paleo RSL elevation is at +11.3 ± 1.0 m and is represented by the shore platforms imprinted at higher elevations.

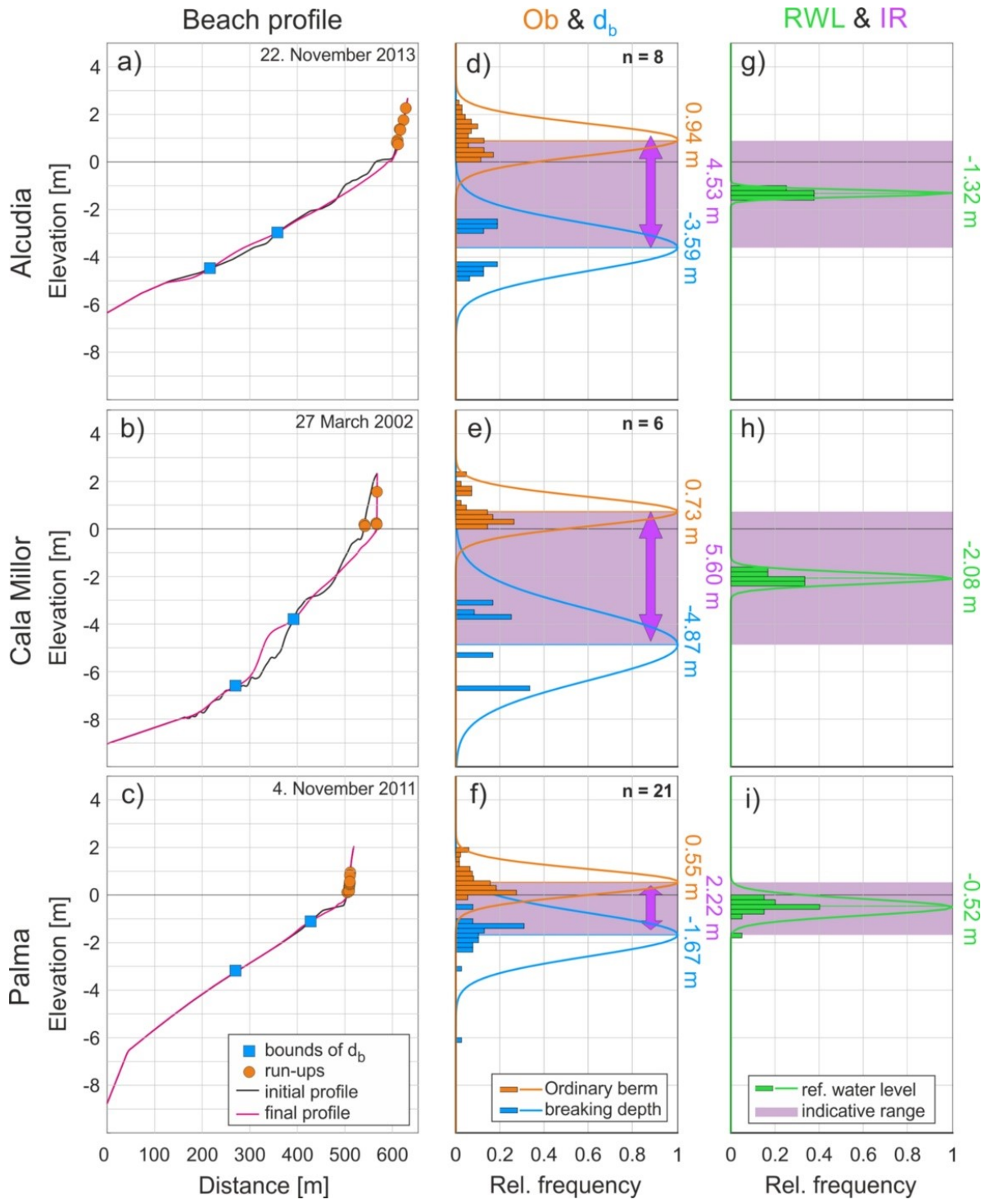

Fig. 5.5: Results of the CSHORE model runs. a)-c) Example of an initial and final beach profiles for a single event at Alcudía, Cala Millor and Palma including boundaries of the breaking depth (blue dots) and all runups heights for different time-steps during this swell (orange dots). d)-f) Histograms of the lower limits (blue) and upper limits (orange) calculated for all modelled swell event in each region. Lines show the normal distribution of the Ordinary berm (O_b) and the breaking depth (d_b). The range between O_b and d_b defines the IR (purple band). g)-i) Histogram and normal distribution for the RWL (green histograms, line representing the normal distribution) and the associated IR.

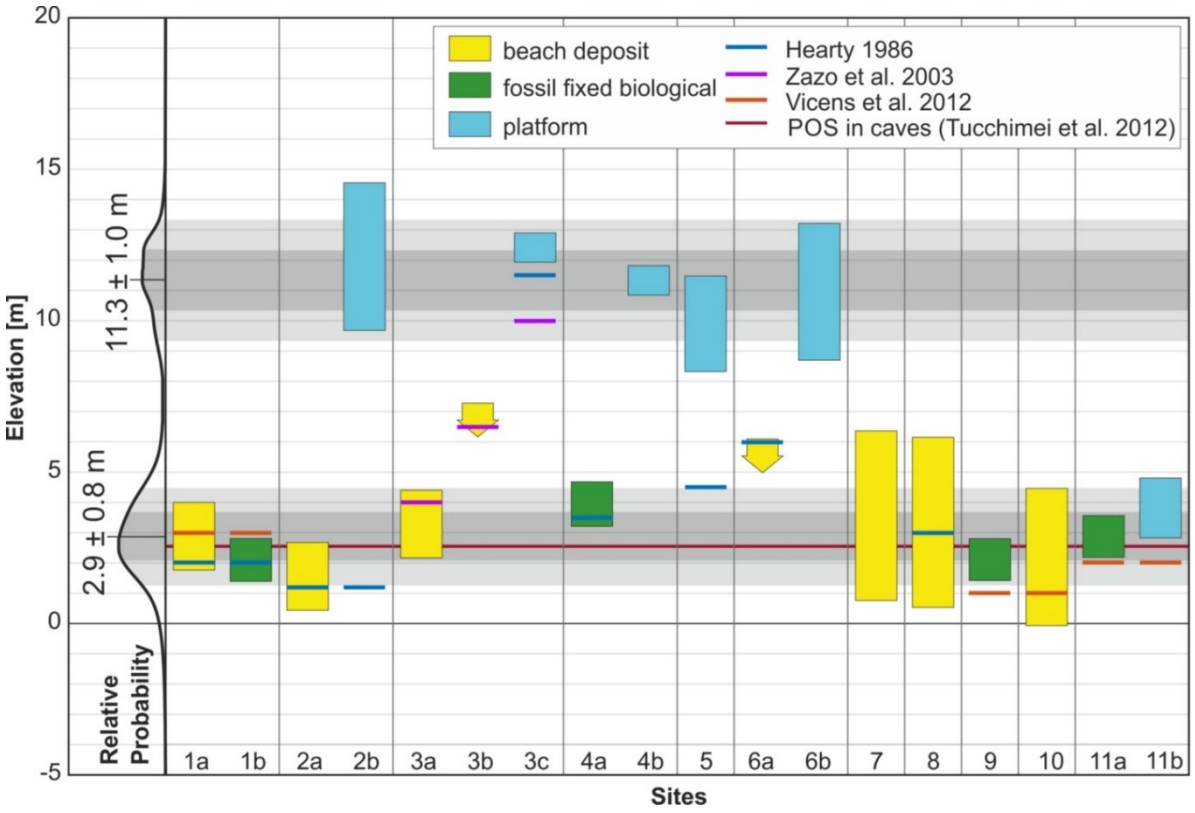

Fig. 5.6: Paleo RSL for all outcrops, including those showing a terrestrial limiting (3b & 6a). Bars represent total possible range, including the uncertainty. Also indicated are previously published elevations and the elevation of paleo sea level from the phreatic overgrowth on speleothems (POS) in the caves. On the left, a stacked probability density function curve for all locations and the mean elevations are shown. They represent two main elevations at +2.9 ± 0.8 m and +11.3 ± 1.0 m (grey bands show the 1-σ (darker) and 2-σ (lighter) uncertainty).

5.5.3. Glacial isostatic adjustment

As explained above, the paleo RSL elevation obtained from a RSL indicator does not represent the eustatic sea-level value. In part, this is due to the effects of glacial isostatic adjustment (GIA). In order to show the effect of GIA on the relative sea-level history of Mallorca, we performed GIA modelling as described in Section 5.4.3. Regardless of the modelled eustatic sea-level scenario, two different aspects stand out from our GIA model results, shown in Fig. 5.7.

First, the position of Mallorca near the forebulge of the former Eurasian Ice Sheet drives a GIA response, which causes a rise in relative sea level with rates between 0.6 and 1.2 m/ka, even in conditions of no global ESL change (cf. periods 125-120 ka in Fig. 5.7, when global sea level is kept stable for all panels). Second, the maximum elevations of GIA corrected sea level was between 8.0 and 9.1 m. Therefore, the lower paleo RSL identified in this study is intersected at some point in time by the RSL curves shown in Fig. 5.7. In contrast, the GIA curves do not cross the higher paleo RSL at any time.

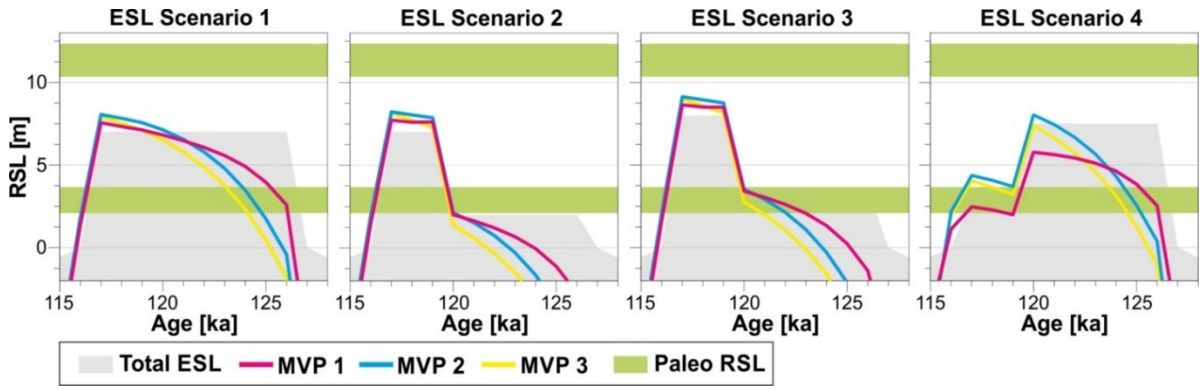

Fig. 5.7: Results of the GIA modeling. Shown are the results for all four eustatic sea-level scenarios (ESL, grey fillings represent melted ice, i.e. sea-level equivalent, see section 5.4.3 for description) with three different mantle viscosities (MVP; see Table 5.3) each. The green bands represent the paleo RSL elevations obtained from RSL indicators in Mallorca (Fig. 5.6).

5.6. Discussion

In the introduction, we highlighted that the study of MIS 5e sea levels needs more attention in (1) the precise measurement of MIS 5e RSL indicators in the field, (2) the application of modern analogs to understand the indicative meaning of MIS 5e RSL indicators and (3) accounting for the effects of GIA. We discuss how we addressed each of these points in our study area in the sections below, highlighting the 'lessons learned' from our study in the island of Mallorca.

5.6.1. Measurement

The starting point of this study was the precise measurement of paleo RSL indicators. Differential GPS measurements are regularly employed in Holocene sea-level studies (e.g. Bird et al., 2007; Hawkes et al., 2016), and are starting to be applied to the study of MIS 5e and older RSL indicators (e.g. Muhs et al., 2011; O'Leary et al., 2013; Rovere et al., 2015b). Precise GPS measurements allow obtaining low measurement errors (accuracies of few decimeters) that are then propagated into the paleo RSL calculations. In addition, they are always referenced to a known geodetic or tidal datum, which approximates MSL in the most precise way.

Our study shows that typical accuracies, obtainable with a differential GPS in the field are in the range of few decimeters in optimal survey conditions, although this is dependent on the real-time correction subscription, base station availability and post-processing. We used (except for two sites, where reception of differential corrections was not possible) a system receiving real-time satellite corrections that does not need the presence of a base station for GPS signal post-processing. Base stations can be set up by the surveyor or base station data can be provided by free or public services. This base station should be located within few kilometers from the surveyed site and accuracies can reach few millimeters. In the first case, the main limitation is the initialization time, which is usually few hours and reduces the number of sites that can be surveyed per day. The second case is often limited by the absence of free or public services in remote coastal areas.

In Mallorca, the inner margin of marine platforms represented a particular case that required a different approach to establish the elevation and its associated error. These marine platforms had a large

lateral variability or was not clearly visible (e.g. covered by younger deposits or constructions). In order to represent this variability in the elevation measurement, we averaged, where possible, several elevation profiles of the higher part of the terrace and calculated the error as a standard deviation of all the measurements, adding the instrumental measurement error obtained from the GPS. However, for places where the inner margin was covered, the reported elevation does not represent the maximum elevation.

It is worth highlighting that the elevation measurement of a RSL indicator must be regarded as an objective measure, that can be updated only if better measurement techniques or more accurate datums become available (Düsterhus et al., 2016). Unfortunately, the methods used to measure elevation of MIS 5e shorelines and the associated errors are not clearly reported in much of the literature available to date. This is the first factor that hinders the possibility to compare the relative sea-level histories at different sites or to build self-consistent databases of MIS 5e RSL indicators, as done for the Holocene (e.g. Khan et al., 2015).

5.6.2. Interpreting results: the indicative meaning

In conjunction with the measurement of elevation, the indicative meaning of a RSL indicator is the second fundamental property that should be always reported and used to calculate the elevation a paleo RSL and its associated uncertainty. Such calculation derives from the elevation measurement and the assessment of the relationship between the indicator and the past sea level that formed it. In literature, indicative meanings for MIS 5e and older RSL indicators are often obtained through analysis of literature datasets (Kopp et al., 2009; Rovere et al., 2015b; Hibbert et al., 2016), with the aim of obtaining the typical ranges for the deposition or formation of modern analogs.

We contextualized the general indicative meanings elaborated by Rovere et al. (2016a) for beach deposits, fossil fixed biological indicators and shore platforms to our study area. In particular, we adopted a novel approach (based on a 1D morphodynamic model) to calculate the indicative meaning of beach deposits, which represent the majority of the surveyed RSL indicators in Mallorca. It is worth highlighting that around 14% of the MIS 5e RSL indicators reported in a recent review (Pedoja et al., 2011a; Pedoja et al., 2014) are beach deposits, the most widespread RSL indicator after marine terraces and coral reefs. The objective interpretation of the paleo RSL from the elevation of beach deposits is therefore a central need in paleo sea-level science.

Our study shows that in a microtidal and relatively low energy environment, representative of a large basin such as the Mediterranean, the indicative range of modern beach deposits is up to 4 m. In other areas, such as the Atlantic or Pacific Ocean, this value might be greater due to higher wave heights during significant swells. One question that still remains open is how accurately the results of our models reflect the modern beach elevation ranges. A first, although not complete, answer can be given by comparing model results to field observations. A berm measured at Cala Pudent (Palma region) was at +0.7 m, while the modelled result for this region is +0.55 m. Another berm was reported by Rovere et al. (2016a) in Cala Millor at +0.8 m, whereas our modelled result for this region is +0.73 m. The same

authors report the breaking depth, extracted from bathymetric data, at this location at -1.9 m, whereas our modelled value is at -4.87 m.

This brief comparison shows that the modelling approach we adopted can be used to reconstruct the indicative meaning of beach deposits and helps overcoming the difficulties involved with site-specific surveying of modern analogs, as suggested by Rovere et al. (2016a). Nevertheless, it also suggests that better accuracies on paleo RSL estimates are obtained by on-site surveys of the modern analogs, although multiple surveys are needed in order to represent general values. It is worth noting indeed that, while the ordinary berm can be measured directly in the field, estimating the breaking depth is more difficult and requires an extended knowledge of the topography and the long-term wave regime of an area. The use of a simple morphodynamic model allows overcoming such difficulties, and allows gaining more objective numbers for the upper and lower depositional limit of these deposits. In order to use this methodology in calculating the indicative range, the assumption has to be made that the coastal morphology and wave conditions are similar to the modern environment.

We suggest that the methodology illustrated in this paper to define the indicative meaning of beach deposits can be used in every area where some information on the modern beach morphology and on the historical swells can be obtained. Wave data can be retrieved from satellite products, e.g. AVISO + (McGregor et al., 2012), or global wave models, e.g. WaveWatch III (Moon et al., 2003). This approach can prove particularly important in sites where beach deposits (and beachrocks) lack stratigraphic characteristics that can be used to detail sea-level information (Hearty, 1987; Tamura, 2012; Mauz et al., 2015).

5.6.3. Departure from eustasy

Every paleo RSL measured at any location around the world, even in absence of tectonics or other post-depositional deformations (see Rovere et al., 2016b for an overview), is not representative of the paleo eustatic sea level. The concept that GIA has a significant effect on MIS 5e (and older) shorelines, but has been implemented only recently in studies of past interglacials (Raymo et al., 2011; Dutton and Lambeck, 2012; Raymo and Mitrovica, 2012; Creveling et al., 2015; Sivan et al., 2016).

We show the results of a GIA model under four ice-sheet melting scenarios and three different mantle viscosity profiles, representative of typical ones used to model GIA in past interglacials (Lambeck and Nakada, 1990; Peltier, 1996; Mitrovica and Forte, 1997; Stocchi and Spada, 2009). We highlight that our GIA calculations represent only few of the many possible scenarios, and cannot be used for high-resolution studies. In fact, our ESL assumptions are limited to four scenarios, there is only one assumption on the MIS 6 ice volume configuration from the ANICE model (de Boer et al., 2013) and the maximum eustatic sea level during MIS 5e was limited to +8 m. Nevertheless, the GIA driven RSL change is interesting in light of the characteristics of the RSL indicators described in Mallorca.

Beach deposits such as those described in Mallorca are usually formed and better preserved in conditions of relatively slow sea-level changes (Fruergaard et al., 2015), especially if they are deposited along lithologically mixed coastlines. In this regard, the comparison between paleo RSL derived from field

data and that predicted from GIA models suggests that our data might be more consistent with scenarios characterized by a two-stepped RSL curve (scenarios 2, 3 and 4). Under scenario 4 the beach deposits would be formed late in the interglacial and then immediately abandoned by the following sea-level regression. In contrast, scenarios 2 and 3 support the beach deposits to be formed before 120 ka and then drowned by a rapid sea-level rise that followed Antarctica melting later in the interglacial (Hearty et al., 2007; O'Leary et al., 2013). Under a eustatic scenario with only one initial meltwater pulse (scenario 1), it is more difficult to interpret why the RSL indicators were not eroded by continuously rising seas after being deposited by a paleo RSL at +2.9 ± 0.8 m.

The second RSL peak identified in the field (+11.3 ± 1.0 m) does not cross the modelled RSL curve for two possible reasons: (1) Our eustatic sea-level scenarios and GIA modelling are underestimating the maximum sea-level peak by 2-3 m or (2) the higher platforms in the study area are not MIS 5e in age. In the first case, the platforms could represent the expression of the maximum MIS 5e sea level, corroborating the 'late meltwater pulse' hypothesis by Hearty et al. (2007) and O'Leary et al. (2013). Under any scenario, though, such wide platforms should have been formed in a short period of time (2-3 ka) towards the end of the interglacial (scenarios 1, 2 and 3) or in the mid part of it (scenario 4).

Given classical shore platform erosion rates of 0.6-1.5 mm/a (Stephenson and Kirk, 1996, 1998) or location-specific rates from Mallorca of 0.7-5.6 mm/a (Fornos et al., 2005), a 20-80 m wide platform (such as those shown Fig. 5.4) would need a significantly longer time span to form (up to more than hundred thousand of years in the most extreme cases). Such reasoning would point towards the second hypothesis that the higher platforms in Mallorca are probably of MIS 11 origin, as this interglacial represents the last longer time span when sea level was at this elevation. An independent constrain on MIS 11 RSL in Mallorca can be obtained from the Cava Bancals site, reported in Hearty (1987). Here, shells contained in a deposit at 14 m were dated with AAR to the Aminozone F-G, indicating a mid-Pleistocene (MIS 9-11) RSL at this level.

If the higher platforms do not represent the maximum sea level attained in Mallorca during MIS 5e, are there RSL indicators at 8-9 m that represent the second MIS 5e peak or the end of the transgression? The answer to this question relies into different considerations.

i) The rates of sea-level rise, even in times of constant eustatic sea level, according to the GIA predictions (~0.6–1.3 mm/a) are similar to the erosion rates for shore platforms and therefore a notch or similar morphological feature would have no time to fully form during the higher sea-level peak.
ii) Many areas, where the deposition of RSL indicators was possible, are used today by agriculture or for construction and therefore higher MIS 5e deposits could have been destroyed.
iii) The higher deposits of Cala Blava (3b) and S'Illot (6a) have been described as remnants of the maximum MIS 5e sea level by Hearty (1987). The evidences presented in this study do not support this interpretation and these deposits are interpreted here as a terrestrial limiting. Nevertheless, further investigations on these outcrops (aiming at the definition of their indicative ranges) and a

more thorough search of outcrops or landforms (such as tidal notches, Antonioli et al., 2015) at similar elevations, also along high cliffs that are hardly accessible, is essential in order to decline this theory.

iv) Although unlikely, given the independent constraints on tectonic stability of Mallorca, it is possible that the island has been subjected to tectonic forces or to other forces causing subsidence, e.g. earth dynamic topography (Moucha et al., 2008; Austermann and Mitrovica, 2015), since MIS 5e. In this case, the RSL indicators that today indicate a paleo RSL at +2.9 m were deposited by a maximum ESL around +8 m, and subsided since MIS 5e. Under this assumption, the +2.9 m sea level should be characterized by late MIS 5e ages. U-series ages from independent studies on POS in caves span from 138.0-109.9 ka (Tuccimei et al., 2006; Dorale et al., 2010; Tuccimei et al., 2012) and coral fragments associated to the beach deposits at Camp de Tir (1a and 1b in Fig. 5.1) were dated between 125.7 and 117.8 ka (Muhs et al., 2015). Therefore, standing the current status of dating of Mallorcan MIS 5e deposits, the hypothesis of subsidence cannot be either confirmed or entirely ruled out.

In any case, our results for which concerns the field data to GIA comparison suggest that GIA plays a fundamental role, not only to define the maximum elevation attained by MIS 5e at different sites, but also in determining the rates of RSL change and how they affected the formation, deposition and preservation of RSL indicators.

5.7. Conclusions

The island of Mallorca is one of the classical sites for MIS 5e sea-level studies in the Western Mediterranean. We measured the most important field sites showing RSL indicators with modern surveying techniques (differential GPS) and attributed values for the modern analog to each site. We then compared our results with the ANICE-SELEN ice-earth coupled GIA model. From our study, we draw three main conclusions:

i) The measurement of RSL indicators has to be done with the highest accuracy that is achievable with state-of-the-art equipment. Through using differential GPS, we could reach vertical measurement accuracies down to ± 0.05 m. This shows that the measurement can be done with a very high accuracy, but caution has to be taken for perturbing factors. Besides technique-related problems, e.g. bad satellite coverage, also the lateral variability of a RSL indicator, like shore platforms in this study, has to be taken into account and can affect the measurement uncertainty.

ii) Referring the measurements to a site-based modern analog is important in order to get useful paleo relative sea-level elevations. The survey of these analogs can be very difficult and become challenging if they are not accessible (e.g. the lower depositional limit of beaches). Besides using globally valid estimates, the modelling approach we propose here, allows to overcome some of these problems. Additionally, it is virtually applicable in any area where average wave conditions and a general beach topography are known.

iii) Finally, the comparison of field-derived and modelled RSL values is a good method to validate possible scenarios of MIS 5e sea-level variability. This is an important tool in absence of precise

dating (i.e. with error bars that are in the range of few centuries, such as U-series), which is the case for most MIS 5e data out of tropical regions, although these sites are essential in order to answer questions related to sea-level fingerprinting in past interglacials.

5.8. Acknowledgments

TL and AR's research is supported by the Institutional Strategy of the University of Bremen, funded by the German Excellence Initiative [ABPZuK-03/2014] and by ZMT, the Center for Tropical Marine Ecology. The authors acknowledge MEDFLOOD - Modelling Paleo Processes (INQUA CMP projects 1203P and 1603P). MV contributes to the Labex Archimede (ANR-11-LABX-0032-01). The authors thank S. Flotow (ZMT Bremen) for the thin section preparation and J. J. Fornós (Universitat de les Illes Balears) for useful insights on Mallorcan Quaternary outcrops. Data obtained from the Beach Monitoring Programme of the Balearic Islands Coastal Observing and Forecasting System, SOCIB (www.socib.es) was used to produce data in Fig. 5.5.

5.9. Supplementary Material

This manuscript is accompanied with supplementary data, which can be found with the corresponding paper online at *http://dx.doi.org/10.1016/j.palaeo.2017.02.028* and as part of a data collection of this thesis at *https://doi.pangaea.de/10.1594/PANGAEA.883825*.

This supplementary consists of:

- Supplementary Text S5.1
  - Detailed description of all outcrops investigated in this study
- Supplementary Tables S5
  - S5.2 - GPS & RSL database
  - S5.3 - Literature review for age attributions
  - S5.4 - Literature review for sea-level elevations
  - S5.5 - Results of the CSHORE runs
- Supplementary Material S5.6
  - MATLAB-script for calculating the probability density function of Fig. 5.6

6. Tides in the Last Interglacial: insights from notch geometry and palaeo tidal models in Bonaire, Netherland Antilles.

T. Lorscheid, T. Felis, P. Stocchi, J.C. Obert, D. Scholz, A. Rovere
In Preparation for resubmission to *Scientific Reports*
(Published on 24th November 2017 in *Scientific Reports, **7**, 16241.*)

6.1. Abstract

The study of past sea levels relies largely on the interpretation of sea-level indicators, i.e. landforms or deposits formed by past sea-level highstands. Palaeo tidal notches are considered as one of the most precise sea-level indicators as their formation is closely tied to the tidal range at one location. Here, we present geometric measurements of modern and palaeo (MIS 5e) tidal notches on Bonaire (southern Caribbean Sea) and results from two tidal simulations (forced by modern tidal constituents) that use as input the present-day bathymetry and a palaeo-bathymetry created adding to the present-day one, the output of a regional GIA model. We investigate changes in the tidal range since MIS 5e. Our models show that the tidal range changes most significantly in shallow areas, whereas both notch geometry and models results suggest that steeper continental shelfs such as the ones bordering the island of Bonaire are less affected to changes in tidal range in conditions of MIS 5e sea levels. We use our data and model results to discuss the importance of considering changes in tidal range while reconstructing MIS 5e sea level histories, and on the possibility of using hydrodynamic modelling and notch geometry as first-order proxies to assess whether, in a particular area, tidal range might have been different in MIS 5e with respect to today.

6.2. Introduction

Fossil landforms, deposits or bioconstructions can be used as indicators of the relative sea-level (RSL) position during past warm periods (Van De Plassche, 1986), under the assumption that the environment at the time of formation is known and its indicative meaning is quantifiable (Hibbert et al., 2016; Rovere et al., 2016a; Lorscheid et al., 2017). Once a RSL indicator has been measured in the field, its position with respect to the palaeo RSL needs to be quantified, ideally through comparison with modern analogue environments (Hibbert et al., 2016; Rovere et al., 2016a). Only after this quantification, and after the correction for tectonics, glacio-isostatic or other post-depositional effects (Dutton and Lambeck, 2012; Creveling et al., 2015; Rovere et al., 2016b) the elevation of the RSL indicator can be transformed into the local height of palaeo eustatic sea level, that is an essential information to assess past ice volumes and to constrain future ice-sheet and sea-level dynamics (Dutton et al., 2015a; Dutton et al., 2015b; DeConto and Pollard, 2016). Except for the Holocene (Khan et al., 2015), the only period of Earth's history for which a large number of RSL indicators was reported globally is the Last Interglacial and in particular, the Marine Isotope Stage (MIS) 5e (Pedoja et al., 2014).

MIS 5e RSL indicators can be divided into 10 general geomorphological types (Rovere et al., 2016a). Among the most commonly used MIS 5e RSL indicators, tidal notches are those that can be most tightly related to modern tidal datums. Tidal notches are undercuttings or indentations that are carved near sea level on limestone coasts (Pirazzoli, 1986). In general, the formation of a tidal notch is related to four main processes: bioerosion, wetting and drying tidal cycles, hyperkarst and mechanic abrasion (Antonioli et al., 2015). All these processes happen at or near sea level: the bioerosion affects mainly the lower, submerged part of the notch (Pirazzoli and Evelpidou, 2013), whereas the wetting and drying cycles as well as hyperkarst both have a stronger influence on the upper, subaerial part (Antonioli et al., 2015; Trenhaile, 2015). Mechanic abrasion acts where air and water alternate. Despite an ongoing debate (Evelpidou et al., 2012; Pirazzoli and Evelpidou, 2013; Antonioli et al., 2015; Antonioli et al., 2016) regarding the relative importance of these processes in shaping tidal notches, several studies (Trenhaile et al., 1998; Antonioli et al., 2015; Trenhaile, 2015; Rovere et al., 2016a) report that the width of a tidal notch (i.e., the vertical distance between the base and the roof) is correlated to the amplitude of the mean tidal range (Great Diurnal range, GT (Hill, 2016), defined as the distance between the Mean Lower Low Water, MLLW, and Mean Higher High Water, MHHW) (Antonioli et al., 2015). In contrast, the depth of a tidal notch (i.e., how deep the notch is carved into the cliff) is correlated to the rate, duration and intensity of biological and mechanical erosion (Trenhaile, 2014, 2015).

In general, the wider a tidal notch, the greater is the GT at the location where the notch is carved: Antonioli et al. (2015) show with geometric measurements from 73 modern tidal notches in the Mediterranean Sea that, in 'sheltered areas, the notch width is ~0.3-3.2 times the tidal range, a ratio that seems maintained in exposed sites (Fig. 8d,e,f), although with larger variability'. As the width of a notch is related to the tidal range of the location where it forms, the comparison of modern and palaeo tidal notches may give the opportunity to go beyond the simple reconstruction of palaeo RSL. In fact, under the assumption that notch formation was regulated in the past by the same processes as today, the

amplitude of palaeo tidal notches must also be related to the palaeo tidal range. Therefore, comparing the geometrical properties of a modern and a MIS 5e notch can give a first estimate on possible changes in the tidal range between today and MIS 5e.

Another possibility to quantify palaeo tidal ranges is the use of hydrodynamic models that simulate tidal water level change. Differences in tidal range over long time periods are, at least for the Quaternary, mostly related to changes in the topography of a coastal area under different sea-level conditions (Hill, 2016), thus it is necessary to either reconstruct or estimate a palaeo bathymetry to use as model input. Changes in tidal range are often taken into account when reconstructing Holocene sea-level histories (Gehrels et al., 1995; Hall et al., 2013; Kemp et al., 2015; Hawkes et al., 2016), but they have been considered very rarely at Pleistocene time scales (Tojo et al., 1999).

In this study, we take advantage of the geological record preserved on the island of Bonaire (Leeward Antilles) in the southern Caribbean Sea, where a palaeo and modern tidal notch are preserved at the same location, to investigate the potential of using tidal notches or tidal modelling to reconstruct MIS 5e tidal ranges. We first present the results of a survey of palaeo and modern tidal notches in this area, aiming at establishing their geometry and elevation. Then, we show the results from two simulations of a hydrodynamic model forced with modern satellite-derived tidal constituents (Egbert et al., 1994; Egbert and Erofeeva, 2002) and two different input bathymetries. We use our field data and model results to discuss the importance and implications of estimating past changes in tidal range.

6.3. Study Area

The island of Bonaire (Leeward Antilles) is situated ca. 100 km north of the Venezuelan coast, in the southern part of the Caribbean Sea. From the tectonic standpoint, the island is part of the Leeward Antilles Ridge and located between the Caribbean and the South American plates. This setting led to a range of compressional structures since the Pliocene and a general SE-directed tilting of the island (Hippolyte and Mann, 2011). The mild uplift rate of some parts of the island is described at 0.08 mm/a, whereas other parts are not considered to be uplifting in the Quaternary (Herweijer and Focke, 1977; Engel et al., 2014).

The southern part of the island is dominated by a very flat topography, whereas the northwestern and central parts of the island are dominated by a higher topography and large fossil reef terraces (Fig. 6.1a). The basement of the island is represented by the higher mountains in the North, that consists of Cretaceous-Eocene volcanites, conglomerates and intercalated limestones, followed by Mio-Pliocene limestones (Beets, 1977; Hippolyte and Mann, 2011). On these rocks, four levels of Pleistocene reef terraces developed during different interglacials (Kim and Lee, 1999). While these terraces are very wide at the northern and eastern coastline (up to 4 km, Fig. 6.1a), the northwestern coast is steeper, and the terraces are limited to a few hundred to tens of meters in width. The lowest of the Bonaire Pleistocene reef terraces has been speculated to have formed during MIS 5e based on chronostratigraphic correlations (Kim and Lee, 1999). This was recently confirmed by strictly reliable U-series ages obtained from corals sampled on the northeastern and eastern (windward) sides of the

island (Felis et al., 2015; Brocas et al., 2016; Obert et al., 2016). At the southern coastline of the north-western part of the island, steep limestone areas facilitated the formation and preservation of pronounced tidal notches.

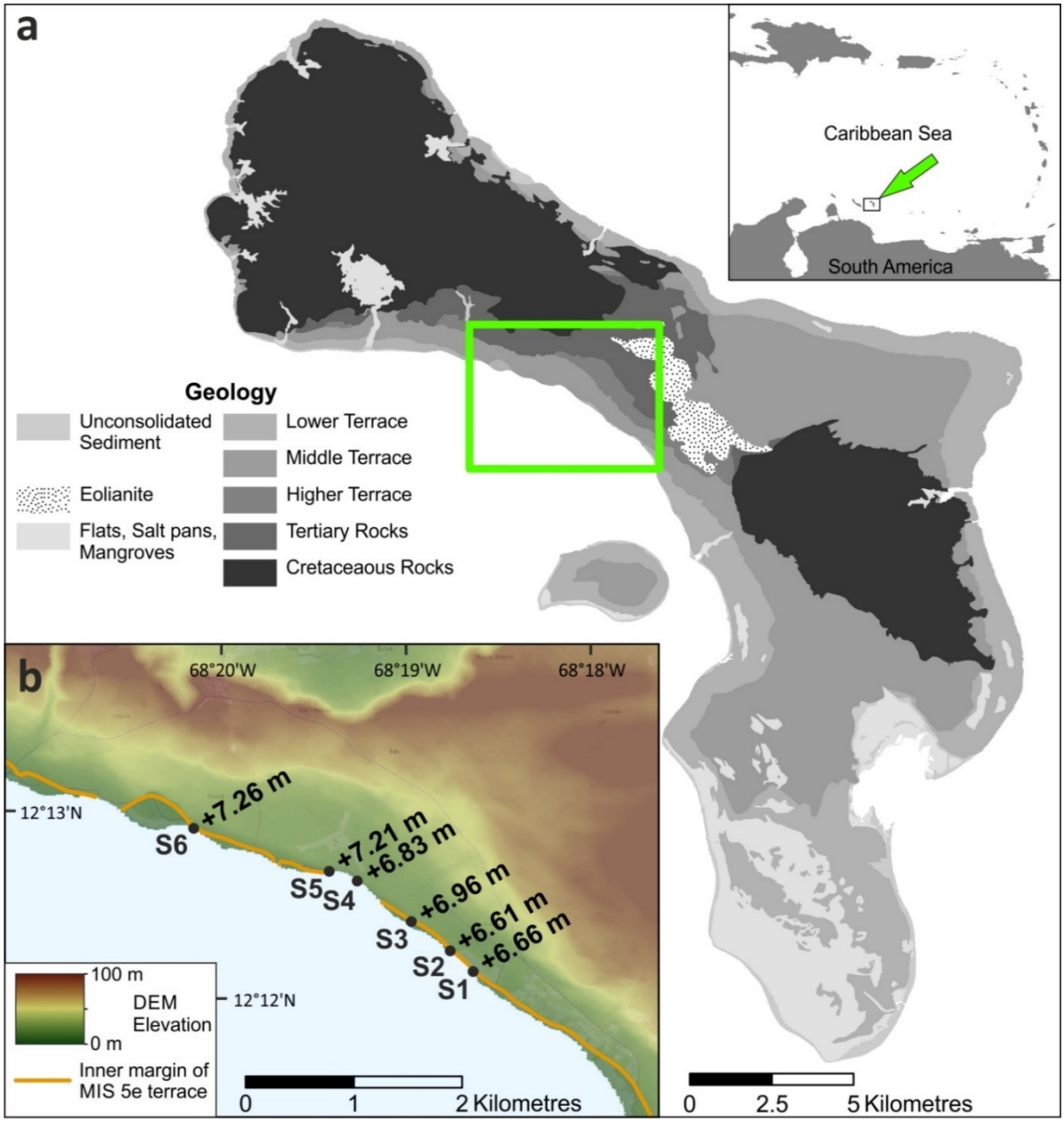

Fig. 6.1: Geology of Bonaire and location of study sites. a) Geological map of the island of Bonaire (modified from Koomen et al., 2012). b) Location of sites where modern and palaeo notches were measured (S1-S6). Elevations indicate the base of the palaeo notch (red point in Fig. 6.2a,b). The background map represents the high-resolution Digital Elevation Model (DEM, TanDEM-X © DLR 2017) for this area. The orange line indicates the inner margin of the MIS 5e terrace shown in the cross-section of Fig. 6.2a (The maps have been created with the software ESRI ArcMap 10.4.1 [http://www.arcgis.com], using data from the DCBD online database [http://www.dcbd.nl/document/geological-map-bonaire] and the TanDEM-X missions).

The target of this study is an area locally known as 'Tolo', and is located along the Queen's Highway, on the leeward side of Bonaire (Fig. 6.1a,b). The area is characterized by a relatively steep and narrow

coastline interrupted by a small fossil reef terrace (5-10 m wide), which forms the lowest fossil reef terrace along this part of the coast. About 2-3 meters above this terrace, a palaeo tidal notch is carved into older Pleistocene limestone (Fig. 6.2a). A modern tidal notch can be observed at sea level (Fig. 6.2a), and both modern and palaeo notches can be traced laterally for ca. 4 km (Fig. 6.1b). We measured both the modern and the palaeo notch at six sites, replicating our measurements three times per site (see Methods for details).

6.4. Results

6.4.1. Modern and palaeo tidal notches

Both the modern and palaeo tidal notches along the northwestern coast of Bonaire have a similar geometry, with an overhanging roof and a relatively narrow floor (Fig. 6.2g,h). The geometry of both tidal notches shows some variability within the different sites (supplementary material S6.1). We derived general geometric properties for modern and palaeo tidal notches by averaging all 18 measured notch profiles. We calculated that the average width of the palaeo tidal notch is 65 ± 19 cm (Fig. 6.2g), while that of the modern one is 81 ± 13 cm (Fig. 6.2h). Overall, the difference in width (i.e., the amplitude of the notch, Wr+Wf in Fig. 6.2b) between modern and palaeo tidal notch is 16 ± 26 cm, and therefore insignificant within the error. The depth of the notch (i.e., how deep into the rock the notch is carved, Df and Dr in Fig. 6.2b) is on average larger in the modern than in the palaeo notch (supplementary material S6.1). The elevations of the palaeo tidal notch were measured at the base of the notch and the respective Wf was added to calculate the palaeo RSL (Fig. 6.2a,b).

For the age attribution of the measured palaeo notches to MIS 5e, we consider that the corals on the fossil reef platform immediately below the notch (Fig. 6.2a) lived at the time when the notch was cut into older Pleistocene limestones. This is similar to what happens today, with corals living a few meters below sea level (below 3-4m depth, Fig. 6.2a,f) as the modern tidal notch is carved into older coral limestone (Fig. 6.2a,c-f). At site 4 (Fig. 6.1b), we sampled a fossil *Montastraea* sp. coral (BON-39-A; 12.2104°N, 68.3212°W) at +2.65 ± 0.36 m (Fig. 6.2a,d). Two subsamples of this coral yielded U-series ages of 139.8 ± 4.5 ka and 147.3 ± 3.6 ka (± 2σ) (supplementary material S6.1). According to the screening criteria applied in Obert et al. (2016) for 230Th/U-dating of other MIS 5e corals from Bonaire, the initial 234U/238U activity ratio of both subsamples of the fossil *Montastraea* sp. coral is higher than expected from the modern seawater value. In addition, the U content of both subsamples is relatively low, probably indicating post-depositional U loss.

6.4.2. Modern and palaeo tidal simulations

To calculate the modern and palaeo GT, we ran two tidal simulations (see Methods). The only difference between these simulations is the input topography. The Modern Tide Simulation (hereafter MTS) uses the GEBCO_2014 topography (GEBCO_2014_Grid, 2014). The Palaeo Tide Simulation (hereafter PTS) uses a palaeo terrain model obtained adding the maximum relative sea level predicted by the ANICE-SELEN GIA model (de Boer et al., 2014b) for the southern Caribbean Region (Fig. 6.3a,b) to the GEBCO_2014 topography.

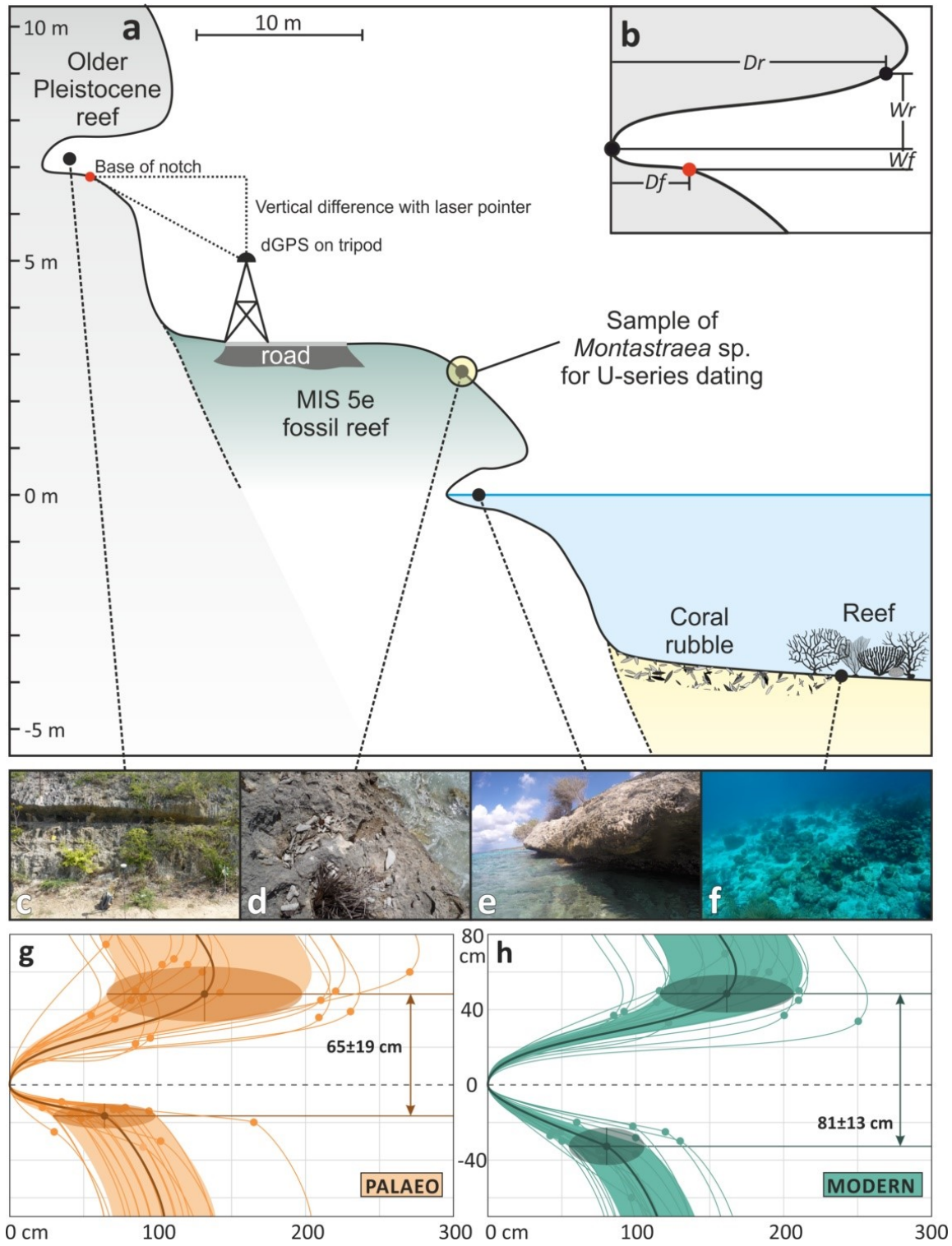

Fig. 6.2: Description of the geometric measurements and field observations. a) Cross-section representing the general morphology of the coastline and the shallow-water reef in the "Tolo" area; b) geometric measures of the notch Wr – upper notch width, Wf – lower notch width, Df – notch depth at foot, Dr – notch depth at roof, reported dGPS measurements represent the red point (base of notch); c) palaeo tidal notch (section S1 in Fig. 6.1b); d) MIS 5e fossil reef, from which the *Montastraea* sp. coral has been sampled; e) modern tidal notch (section S3 in Fig. 6.1b); f) shallow-water reef in the "Tolo" area (-3 to -4m below sea level). g-h) Geometry of palaeo (g) and modern (h) tidal notches. Dots represent the geometrical nodes represented in b, the bold line and ellipsoid show the mean value and the standard deviations, respectively, for all the measurements. Each line represents one notch measurement (see Methods).

The GT at most locations show only minor differences (0.1 cm or less) between the MTS and PTS calculations (Fig. 6.3c, supplementary material S6.1). The only exceptions are the Malecón and Amuay stations (located in close connection to the very large shelf of the Gulf of Venezuela, Fig. 6.3a). At these stations, the GT calculated by the PTS is 23.6 and 4.2 cm higher, respectively, than the tidal range calculated by the MTS. In percentage, with respect to the modern tidal range, this means that changes in palaeo tide at Malecón and Amuay are in the range of 15-28%. In Kralendijk (Bonaire), located five kilometres southeast of the surveyed notches, the MTS and PTS both predict a GT of 23.4 cm.

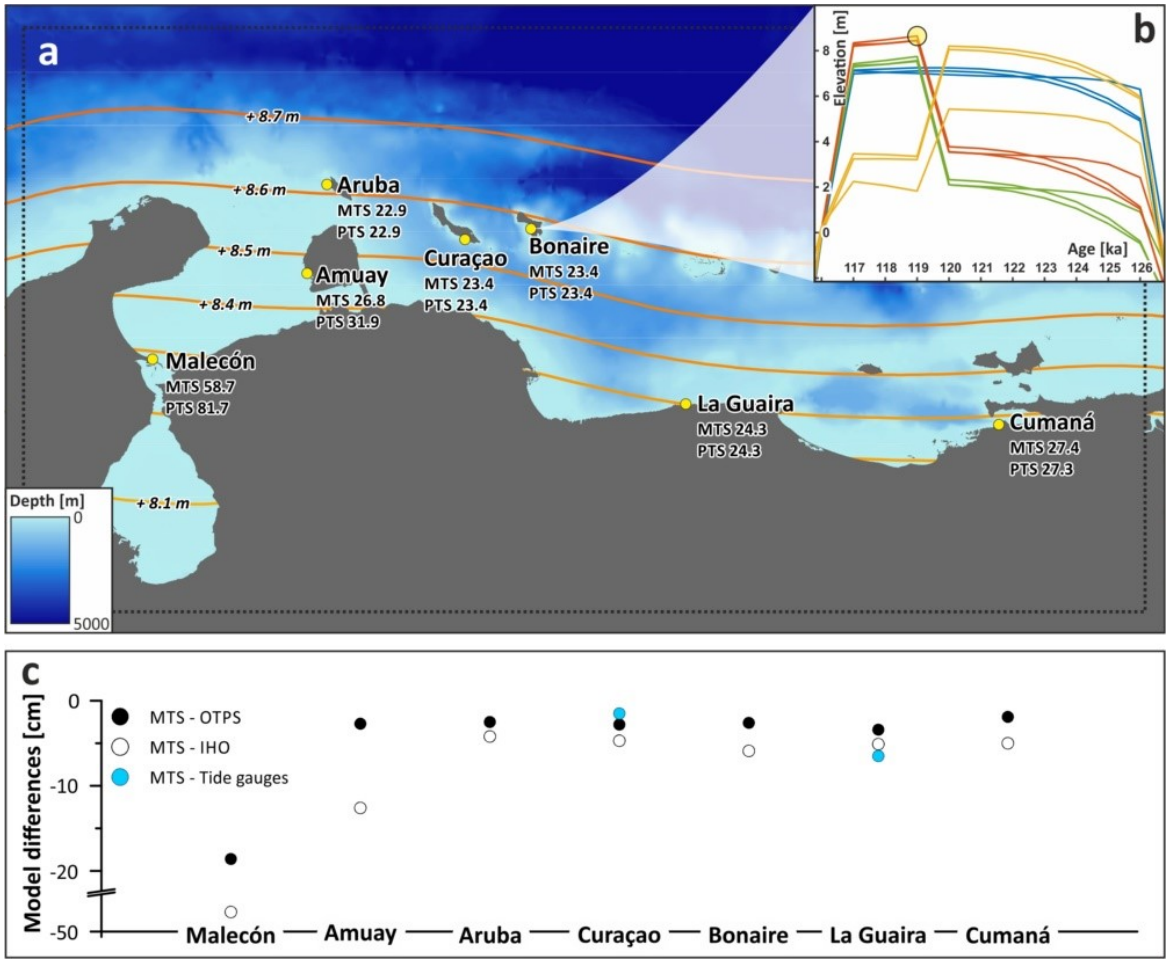

Fig. 6.3: Results of modern and palaeo tidal models. a) Boundary of modelled area (dotted line) and GEBCO_2014 bathymetry used in the MTS simulation. The yellow points indicate the sites where tidal predictions were extracted, with indication of the modelled Great Diurnal Range (in cm) from the modern (MTS) and the palaeo tidal simulations (PTS). Coloured contours represent the maximum palaeo RSL resulting predicted by the GIA model for 119 ka (corresponding to the yellow circle in b). b) Relative sea-level curves for Bonaire as predicted from the ANICE-SELEN GIA model (de Boer et al., 2014b) with the different mantle viscosity profiles and the four ESL scenarios described in Lorscheid et al. (2017). We chose the highest predicted sea level from this set of models (yellow circle, ca. 119 ka) and added the gridded RSL prediction to the initial bathymetry. c) Differences in the Great Diurnal Range between the model results and comparison datasets for all locations shown in a). Comparison data from tide gauges are only available for Curaçao and La Guaira (The map has been created with the software ESRI ArcMap 10.4.1 [http://www.arcgis.com] using data from the GEBCO_2014 grid for background bathymetry [http://www.gebco.net/]).

6.5. Discussion

6.5.1. Dating and elevation of tidal notches

Our results show that both coral subsamples taken from the deposit below the notches are diagenetically altered and biased towards older ages. Thus, they need to be regarded with caution. Nevertheless, these corals can be correlated with those found along the northeastern and eastern coast of Bonaire, that are constrained to MIS 5e through nine ^{230}Th/U-ages of Diploria strigosa coral colonies collected at elevations between ~1.5 and ~5.5 m (Felis et al., 2015; Brocas et al., 2016; Obert et al., 2016). The stratigraphy of the Lower Terrace is very similar between the western coast (investigated in this study) and the northeastern and eastern coasts, the only difference being the width of the fossil reef terrace, much larger on the eastern and northwestern, windward side of the island. Thus, it is reasonable to assume that the measured palaeo tidal notch was formed in MIS 5e, but it is not possible to pinpoint a specific time within MIS 5e (i.e., early or late in the interglacial) from our samples. However, most likely the formation took place at peak MIS 5e sea level, as no higher reef or deposits correlated with MIS 5e can be found in this area. According to the GIA models employed here (see Methods), the MIS 5e RSL reached its peak on Bonaire at 119 ka (Fig. 6.3b).

The elevation of the deepest point of the notch, which can also represent the palaeo RSL elevation, varies between +6.79 ± 0.18 in the Southeast and +7.37 ± 0.12 m in the Northwest (supplementary material S6.1). Applying a linear fit, we calculate a relative tilting of 192 mm/km to the Southeast. This is <1° of tilting and therefore at odds to the 20-30° tilting reported by Hippolyte and Mann (2011) for the larger region of the Leeward Antilles as the result of Pliocene to Quaternary compression on the island. This indicates that tectonic movements are present since the last interglacial, but can be neglected.

6.5.2. Notch geometry

As briefly summarized in the introduction, the width of a tidal notch is correlated with the GT. In general, empirical evidence shows that the notch is always wider than the GT at the location, where the notch is carved (Antonioli et al., 2015). This relationship is maintained also in Bonaire, where our MTS calculated a GT of 23.4 cm (consistent with other independent datasets and models, see next section) and the modern notch is 81 ± 13 cm wide. On average, the palaeo tidal notch is slightly narrower than the modern one (65 ± 19 cm), but, within their standard deviation, the modern and palaeo tidal notch in our study area have a very similar width, suggesting that also tidal range in MIS 5e was similar to today. This is supported by the results of our palaeo model simulation, which predicts a palaeo GT in Bonaire equal to the modern one.

The large variance that we measured between the width of palaeo and modern notches in Bonaire may reflect intra-site variability related, for example, to limestone dissolution processes at the palaeo notch as observed at many locations in Bonaire (Herweijer and Focke, 1977). Also, the biological rim that is present in the modern notch, and was most likely eroded with time in MIS 5e notches, might affect the discrepancy in width that we measured between modern and palaeo notches. As shown in Antonioli et al. (2015), also differences in lithology may cause the width of the notch to change, but

the MIS 5e limestone, the modern notch is carved into, and the older Pleistocene limestone, in which the MIS 5e notch is carved into, appear very similar in consistence. In addition, the larger width of the modern notch could be a result of a longer exposure to sea level at this elevation, as suggested by the slightly larger notch depth in the modern notch.

6.5.3. Tidal modelling

The basic assumption behind our palaeo tidal model is that the tidal constituents during MIS 5e are equal to today. This is in line with the fact that tidal range changes during the last glacial cycles are mostly related to the different geometric settings of coastal areas under different sea levels (Hill, 2016). Instead, changes in tidal constituents, that are influenced by the gravitational influence of the moon and sun, are considered of importance only at much longer timescales (Miocene and older) (Green et al., 2017).

The geometry of the notches measured in Bonaire supports the model result that indicates virtually no changes between modern and palaeo GT at this location (Fig. 6.2g,h). As our tidal model is forced by satellite altimetry data and a very coarse bathymetry, we explore the uncertainties in predicting the modern GT through comparison with other independent datasets (Fig. 6.3c). Within the modelled area, the only available tide gauge data are from Curaçao and La Guaira. Although data at these stations do not span an entire tidal cycle, our model compares well with both stations (blue circles in Fig. 6.3c), and differences between modelled and observed tides are -1.5 cm and -6.4 cm, respectively. A second-order comparison can be done against the GT as calculated from water level timeseries derived from tidal constituents available from the International Hydrographic Organization (IHO, Qi, 2000) and from the OSU Tidal Prediction Software (OTPS, Egbert and Erofeeva, 2002). The differences between our modelled GT and that obtained from these two sources (respectively white and black circles in Fig. 6.3c) are generally less than 6 cm, with our model always underestimating the GT. The only exception is represented by the Malecón and Amuay stations, for which some comparisons show departures from our modelled values up to 48 cm (in Malecón, Fig. 6.3c).

The comparison between daily water level extremes (Fig. 6.4b-e) confirms that the MTS fits the water levels calculated using the IHO tidal constituents generally well, with the exception of the Malecón site (Fig. 6.4e). In addition, at the Amuay site there is some scatter between MTS and IHO water levels. The same pattern is observed when we compare our MTS results with the OTPS dataset. In both comparisons the daily minima are better represented than the daily maxima. Besides the extreme values, the diurnal shape of the tidal curves also shows a good correlation (Fig. 6.4a). The same typical diurnal shape is represented in the MTS results, the IHO and OTPS datasets and the tide gauge measurements, although the amplitudes vary.

In summary, our modern tidal model underestimates the modern tidal range by 5-20% on the Leeward Antilles and along the open Venezuelan coastline. In the very shallow Gulf of Venezuela (less than 50 m depth for a distance of up to 100 km) the difference between GT derived from tidal constituents and our MTS raises up to 45% (Fig. 6.3c). In these areas, the larger discrepancy is probably due to the coarse bathymetry we used in our model: as already recognized by other studies addressing tidal range

changes (Hall et al., 2013), better predictions may be achieved using a higher-resolution bathymetry and a finer model grid size than the ones used here.

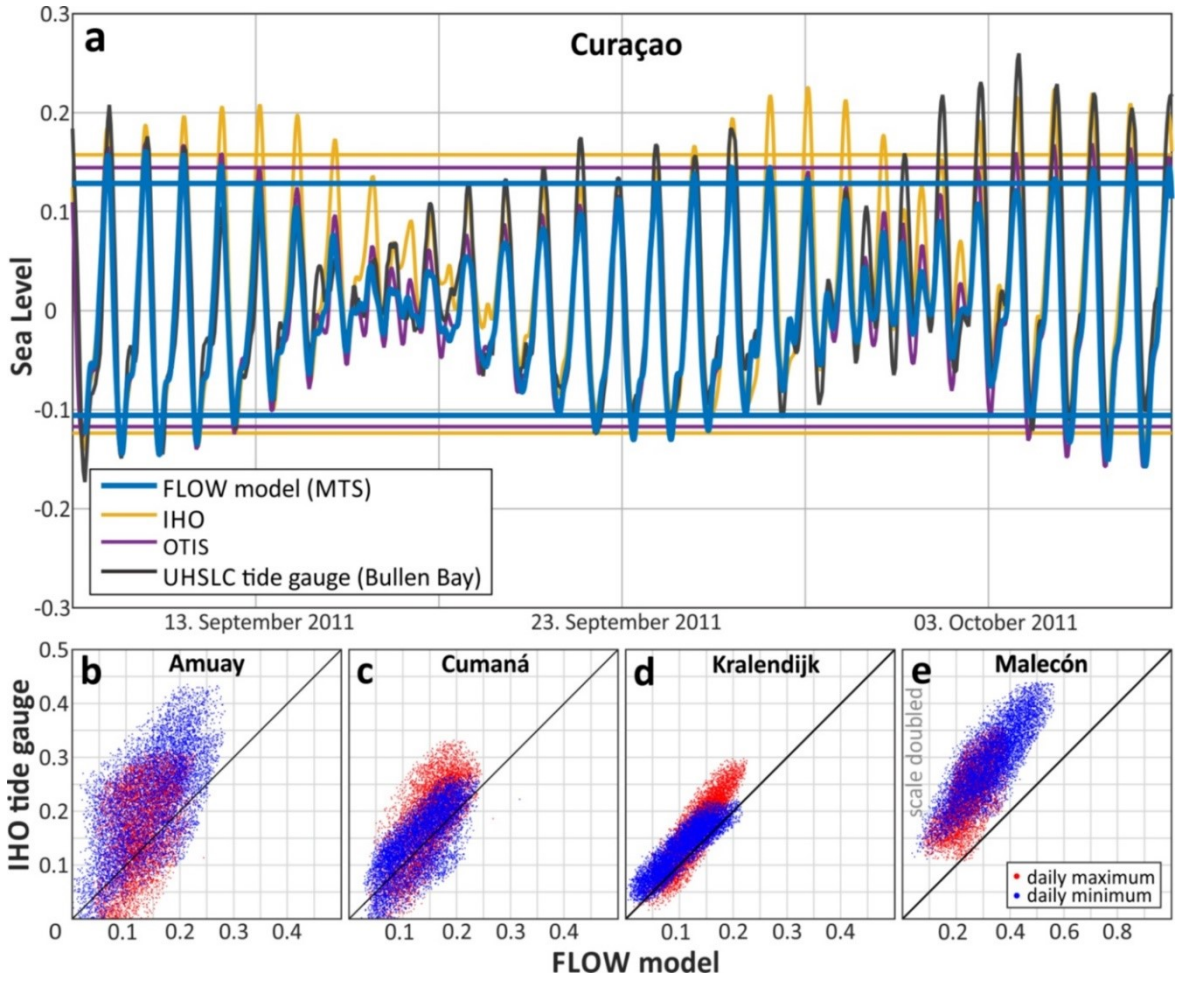

Fig. 6.4: Comparison of modern tidal simulation and independent tidal datasets. a) Tidal graph for Curaçao in September 2011. The graph shows the water level and the values for MHHW and MLLW for the MTS output as well as for the comparison datasets (tide gauge data is not referred to MSL). b-e) Correlation graph for the daily maxima and minima between the MTS output and the observational IHO data for the locations b) Amuay, c) Cumaná, d) Kralendijk and e) Malecón (notice different scales).

6.5.4. MIS 5e sea levels and palaeotides

The geometry of notches measured in Bonaire and our tidal models highlight some important points for which concerns the study of past sea levels and the importance of changes in palaeo tides in the Last Interglacial.

- For Bonaire, field data and models show that changes in palaeo tidal range are negligible, while at sites located along wide and shallow continental shelves such as Amuay and Malecón, changes in tidal range since MIS 5e might be instead relevant. At these two sites, our models are less accurate, but they show that the palaeo tidal range was 15-28% greater than modern one, as a result of the different bathymetry calculated by GIA models.

- Studies on Holocene RSL indicators show that changes in palaeo tidal range also affect the quantitative estimate of the indicative meaning, and hence the reconstruction of palaeo RSL (Hall et al., 2013). In MIS 5e this potential uncertainty is seldom, if ever, considered. Our results show that changes in the tidal range in MIS 5e might instead be significant, depending on the broader geographic setting of the study area considered. In absence of information or estimates of the palaeo tidal range, we therefore suggest that MIS 5e RSL indicators that have their indicative meaning tied to tidal datums (i.e. cheniers, coral reef terraces, lagoonal deposits, shore platforms and tidal notches Rovere et al., 2016a) must evaluate the possibility that tidal range changed since MIS 5e.
- There are two viable approaches that can be used when trying to estimate MIS 5e palaeo tides. If modern and palaeo tidal notches are available at the same location, measuring their geometric properties as described here might give a first-order estimate of GT changes in the palaeo record. If no tidal notches are preserved at the location of interest, a quantitative estimate of palaeo tidal range change can be given using a simple model such as the one described here, forced with global datasets and the best available bathymetry updated using GIA model outputs. This latter approach is not devoid of uncertainties that should be always evaluated comparing a model run simulating modern tidal ranges and comparing them with the best available tidal datasets.
- If it is not possible to use one of the two methods suggested here to evaluate palaeo tidal range changes, we suggest to consider an additional uncertainty of at least up to 15% of the modern tidal range (equal to the Amuay tidal range change shown in Fig. 6.3c). This value might be increased up to 30% in areas characterized by a large and shallow continental shelf.

6.6. Methods

6.6.1. Tidal notch geometry

We surveyed the geometry of the modern and a palaeo tidal notch at six sites along the southwestern coast of Bonaire (Fig. 6.1b), when possible, at a regular distance of ca. 300 m. At each site, we measured the geometry of three notch profiles located a few meters from each other for both the modern and the palaeo tidal notch, resulting in a total of 36 tidal notch profiles. Notch measures were undertaken with a metered rod. Recorded values describe the vertical and horizontal distance from the deepest eroded point of the notch to the foremost point of the notch roof (Wr and Dr in Fig. 6.2b) and to the foremost point of the notch floor (Wf and Df in Fig. 6.2b). For the geometric elements of the notch, we here adopt the definitions of Antonioli et al. (2015). We define Dr as the depth of the tidal notch, while the distance Wr+Wf is defined as the notch width. For the fossil tidal notches, the elevation of the notch floor was measured once per location with a differential GPS system receiving OmniSTAR G2 real-time corrections, and is presented above the EGM08 geoid. To avoid bad GPS signal reception in proximity of the cliff, we installed the GPS antenna on a tripod on the platform before the cliff and used a laser pointer to measure the remaining vertical difference to the notch floor (Fig. 6.2a).

6.6.2. ^{230}Th/U-dating

In order to determine the age of the notches, a 4x4x3 cm piece of a coral skeleton was separated with a hammer from a fossil *Montastraea* sp. colony (BON-39-A) located on the platform directly below the

palaeo notch (+2.65 ± 0.36 m, 12.210419°N, 68.321235°W) at site 4 (Fig. 6.1b). This *Montastraea* sp. coral forms an integral, cemented part of the Lower Terrace and, consequently, has been likely sampled in situ. Subsamples for dating were obtained from the most well-preserved skeletal parts of the coral in the laboratory using a diamond-coated micro-cutting disc. The average sample mass was ca. 0.15 g. After brief leaching in weak HNO3 in order to remove surface contamination, chemical separation of U and Th isotopes was performed as described by Yang et al. (2015). Uranium and Th isotopes were analysed using a MC-ICP-MS (Nu Plasma) at the Max Planck Institute for Chemistry, Mainz. Analytical details are described by Obert et al. (2016). Details about the calibration of the mixed U-Th spike are given by Gibert et al. (2016). To account for the potential effects of detrital contamination, all ages were corrected assuming an average upper continental crust $^{232}Th/^{238}U$ weight ratio of 3.8 for the detritus and ^{230}Th, ^{234}U and ^{238}U in secular equilibrium. All activity ratios were calculated using the half-lives from Cheng et al. (2000).

6.6.3. Tidal Modelling

To model the Great Diurnal Range in the wider Leeward Antilles - Venezuela region (Fig. 6.3a), we used the software Delft3D-FLOW. The simulation setup was done using the software Delft Dashboard v2.01 (supplementary material S6.1). The inputs of the model are a bathymetric-topographic raster and the astronomical forcing. The model extent is around 1080 x 560 km large and has a grid size of 0.03° (ca. 3.2 km). This area stretches from the Guajira Peninsula in the West to the Isla Margarita in the East and from the Venezuelan coastline to the abyssal plain of the Venezuelan Basin (Fig. 6.3a).

We ran two different simulations, the first using the present-day bathymetry and the second using a palaeo bathymetry. As modern bathymetry and topography we used the GEBCO_2014 dataset (GEBCO_2014_Grid, 2014) with a resolution of ca. 1 km. As palaeo bathymetry we used the GEBCO_2014 modified with results from the ANICE-SELEN coupled ice-earth model (de Boer et al., 2014b), representing the glacial isostatic adjustment (GIA) at 119 ka, which is the highest point sea level reached in our configurations (Fig. 6.3b). The GIA simulation uses an eustatic sea-level rise 2.5 m from the Greenland ice-sheets early and an additional 5.5 m from the Antarctic ice sheet later in the interglacial. The mantle is divided into three zones with different viscosities between 0.5x1021 and 5.0x1021 Pa s (see melting scenario 3 and mantle viscosity 2 in Lorscheid et al., 2017). This simulation only shows one example of the possible range of ice melting scenarios and mantle viscosities that can be used for modelling the isostatic respond during this interglacial.

As astronomical boundary conditions for both simulations we used the global tidal inverse solutions TPXO7.2 (Egbert et al., 1994; Egbert and Erofeeva, 2002). Both simulations were performed with a 5 minutes interval over 19 years (1998-2017), in order to include a full tidal cycle (Shennan, 2015). Monitoring stations were set at locations where tide gauge data from stations of the International Hydrographic Organization (IHO) were available.

We used these locations to evaluate the present-day bathymetry simulation against data from IHO tide gauge stations and the OSU Tidal Prediction Software (OTPS, Egbert and Erofeeva, 2002). Furthermore, we compared our results to observational data (Fig. 6.3c) from two tide gauges in Bullen Bay, Curaçao

(January 2011 to April 2012) and La Guaira, Venezuela (January 1985 to December 1994), both maintained by the University of Hawaii Sea-Level Center (UHSLC, data from *http://uhslc.soest.hawaii.edu/data/?rq#ned*). The data for the IHO tide stations for the entire modelled timeframe was extracted directly from Delft Dashboard. As input for the OTPS we used the global TPXO8-atlas data (downloadable on the website: *http://volkov.oce.orst.edu/tides/tpxo8_atlas.html*) and predicted the tidal curves between 1998 and 2017 for each of the observational stations.

The tidal datums of MHHW and MLLW were calculated by averaging the daily maximum and minimum values through a 19 years cycle (1998-2017), to consider changes in the lunar cycle of 18.6 years (Pugh, 1987; Shennan, 2015).

6.7. Supplementary Material

This manuscript is accompanied with supplementary data, which can be found with the corresponding paper online at *https://doi.org/10.1038/s41598-017-16285-6* and as part of a data collection of this thesis at *https://doi.pangaea.de/10.1594/PANGAEA.883825*.

This supplementary consists of:

- Supplementary Tables S6
  - S6.1 - Detailed measurements of the notch geometry
  - S6.2 - Details of the tidal model
  - S6.3 - Results of the Great Diurnal Range for all locations and datasets
  - S6.4 - Analytical details of the coral dating

7. A global compilation of Last Interglacial relative sea level indicators.

T. Lorscheid, A. Rovere
In preparation for submission to Quaternary Science Reviews

7.1. Abstract

The study of paleo sea levels relies largely on the interpretation of paleo relative sea-level (RSL) indicators. These are fossil coastal landforms or deposits that have a quantifiable relation to sea level (called the indicative meaning) and can be assigned an age. The majority of sea-level indicators preserved from past interglacials date to the Last Interglacial (MIS 5e, ~130-116 ka). Currently, three global MIS 5e RSL databases are available in literature, and include altogether more than 3500 data points. Here we use a series of simple hydro- and morphodynamic equations together with global wave and tide datasets to calculate the indicative meaning and the paleo RSL for the data points contained in these published databases. After screening, we accept 1441 points and we include them in a new synthesis. Our results show that, while to reconstruct precise sea level histories rigorous data on modern analogs are needed, at global scale it is possible to use global wave and tide datasets and simple hydrodynamic relations to calculate first-order indicative meanings for MIS 5e RSL indicators.

7.2. Introduction

Past interglacials are one of the main targets of paleoclimate science, as the climate patterns that characterized them can serve as possible analogs for future climates. Due to generally higher-than-today global and polar temperatures, past interglacials were characterized by smaller ice sheets and subsequently higher sea levels (Kopp et al., 2009; Dutton et al., 2015a; DeConto and Pollard, 2016; Hoffman et al., 2017). Constraining global mean sea level during such periods is therefore a central focus for the sea-level community, as it can provide insights on sea level patterns in a warming climate and can help improving models predicting the extent of future ice-sheet extent and consequently sea-level rise (DeConto and Pollard, 2016).

The most common proxies used to study paleo sea levels are paleo relative sea-level (RSL) indicators, i.e. fossil coastal landforms or deposits (e.g. a fossil coral reef terrace or a beach deposit) that have a quantifiable relation to a paleo sea level (called the indicative meaning) and for which an age can be established (Van De Plassche, 1986; Shennan, 2015). The vast majority of known sea-level indicators older than Holocene dates back to the Last Interglacial (MIS 5e, ~130-116 ka). For this period, several studies attempted to collect RSL indicators in organized databases at both regional (Koike and Machida, 2001; Muhs et al., 2003; Ferranti et al., 2008; Muhs et al., 2011; O'Leary et al., 2013) and global scale (Kopp et al., 2009; Pedoja et al., 2011a; Pedoja et al., 2014; Hibbert et al., 2016). The latter are often used to either estimate global mean sea level patterns in MIS 5e (Kopp et al., 2013) or to quantify non-eustatic processes that might affect the paleo RSL elevation (Austermann et al., 2017). While Holocene sea-level studies are reaching a critical mass and a global standardized database is now under construction (Shennan, 1982; Shennan, 1989; Woodroffe and Horton, 2005; Engelhart and Horton, 2012; Khan et al., 2015; Vacchi et al., 2016), the standardization of MIS 5e sea-level data is lagging behind and lacks common approaches to standardize uncertainties (Düsterhus et al., 2016).

One key point in the study of MIS 5e RSL is that the elevation and uncertainty of sea-level reconstructions rely largely on the interpretation of RSL indicators. For example, different interpretations of the paleo RSL associated with a fossil coral reef can be given by either choosing to interpret a reef terrace as paleo-landform (Rovere et al., 2016a) or by assessing the modern living depths of paleo corals found on the same terrace (Hibbert et al., 2016). A second key point is to distinguish between the elevation measurement of a RSL indicator and the related paleo RSL.

Currently, there are three major global RSL databases that collected MIS 5e RSL indicators examining original geological studies. The first has been compiled by (Kopp et al., 2009), hereafter K09, who reviewed studies reporting RSL indicators at 42 globally selected sites. The authors reviewed each study and they assigned to each RSL indicator an indicative meaning on the basis of the original author's description. While this ensures a good quality of the data points reported in K09, its limitation resides mostly on the limited amount of data points. A different approach, attempted by Pedoja et al. (2014), hereafter P14, presented a relevant simplification of the database fields, but it allowed to review a larger number of sites (935) than K09. P14 reports the elevation of each site and the related uncertainty, but does not include considerations on the indicative meaning and on radiometric ages. The

authors also chose to combine long stretches of coastline (up to at least 730 km) by averaging the elevation of several sites (up to 40). The third available database is the one recently compiled by Hibbert et al. (2016), hereafter H16, who concentrated on screening 2496 coral U-series ages from 88 studies and established the paleo RSL using the depth of modern analog living corals.

In this study, we merge the three databases cited above and we use the location information contained in each one to calculate the indicative meaning of MIS 5e paleo RSL indicators at each site. At the basis of our methodology is the assumption that hydro- and morphodynamics dictate the elevation range of the most common MIS 5e paleo RSL indicators and that present physical processes did not change over time. We therefore use a combination of global wave and tide datasets as input to a series of simple hydro- and morphodynamic equations to calculate the indicative meaning for each data point in K09 / P14 / H16 and hence the paleo RSL at each location in these databases, including the associated uncertainty.

7.3. Methods

7.3.1. Database compilation

The data contained in K09, P14 and H16 were first concatenated in a single spreadsheet and assigned a unique ID. The column with the original ID has been maintained for future reference. The columns reporting original references and site name were also preserved unaltered in our database. For K09 and H16, we assigned latitude and longitude coordinates as reported by each database. P14 reports boundaries for many sites rather than site coordinates, we averaged each latitude and longitude at these points. We also maintained from the original databases the columns reporting the description of the RSL indicator and those reporting elevation and associated error. The reported elevations of P14 are used as the original measurement, although we highlight that the elevations reported in that study may incorporate some variability as they sometimes represent averages of different sites. The age columns were also kept from the original databases. Where available, we also conserved information on the method and measurement amount of datings, as well as on the RSL interpretation by the original database compiler are stored in our database unchanged from K09, P14 and H16. The combined database can be found in the supplementary material S7.1. Each column is described in supplementary material S7.2.

In order to standardize the RSL data under a unique framework, we associated each entry in our database to one of the 10 RSL indicators identified by Rovere et al. (2016a, their Fig. 4) and reported in Table 7.1. All points were then checked for reasons to be rejected, identified as follows: (i) if no elevation or age was reported; (ii) if the RSL indicator was not sufficiently described to be assigned to one category; (iii) if the facies reported represents a marine or terrestrial limiting; (iv) if wave data for this location are not available from global atlases; (v) if the reported age is outside the broader MIS 5e range (110-130 ka). One point, which was already rejected in P14, was also rejected here as its reported elevation is 900 m and therefore too high to be explained by any tectonic forcing.

We attributed to each point a possible tectonic influence from active plate boundaries and hotspots by using the PB2002 plate model (Bird, 2003) and a hotspots compilation study of Anderson and

Schramm (2005). Any point located within 200 km from a hotspot or a plate boundary was considered as potentially affected by tectonics and is hereafter considered as being near active margins.

7.3.2. Tide and wave datasets

For each point in the database, we modelled the development of water levels for a period of 19-years using the OSU Tidal Prediction Software (OTPS, Egbert et al., 1994; Egbert and Erofeeva, 2002) and the Tidal Model Driver toolbox. We calculated the tidal level representing the highest (HAT) and lowest (LAT) astronomical tide as well as the mean higher high (MHHW) and lower low (MLLW) water using the mathematical definitions of these tidal datums (Pugh, 1987; Shennan, 2015). As not all the sites in our database are located close to the coast (where the OTPS can calculate predictions), we repeated the same procedure described above, calculating the same tidal datums on a global 1 arc-degree grid (~110 km latitudinal distance). From this grid, we used a bilinear interpolation to extract tidal datums at those points where values could not be calculated directly.

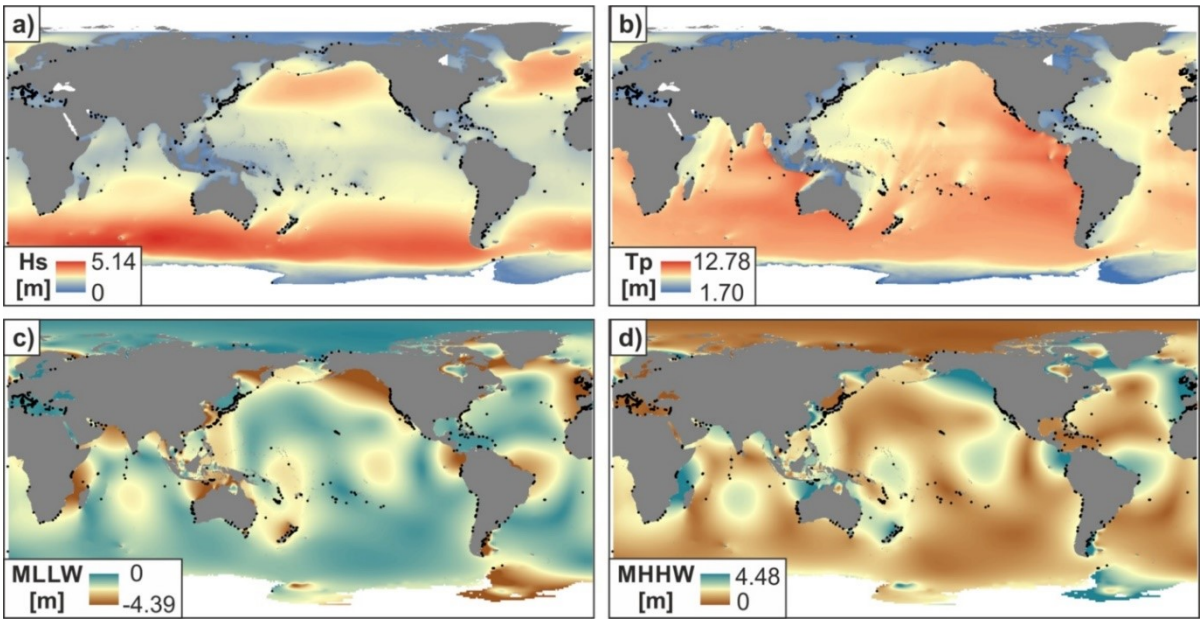

Fig. 7.1: Global grids of the wave conditions and tidal datums. a) Significant wave height; b) Mean wave period; c) Mean lower low water; d) Mean higher high water. Black points indicate all accepted data points in the database.

For which concerns wave characteristics, we extracted significant wave height (Hs) and wave period (Tp), from the CAWCR (Centre for Australian Weather and Climate Research) wave hindcast (Durrant et al., 2013). This dataset is based on the WaveWatch III wave model (Tolman, 1997, 2009) and the NCEP CFSR surface winds and sea ice data (Saha et al., 2010). Compared to the more often used WaveWatch III dataset, the CAWCR hindcast has a finer grid size, a longer record of data (January 1979 to June 2016) and includes also the Mediterranean and the Persian Gulf. The hourly data for Hs and Tp were downloaded for the entire available period (except for January 1979, which is used as a spin-up month) on a global grid. We then calculated 8 raster datasets corresponding to the mean, standard deviation, maximum and minimum values of both Hs and Tp. From the resulting grids, we extracted these values at the locations contained in our database. More details on these steps for calculation

can be found in the database description (supplementary material S7.2), MATLAB-scripts for calculating tidal and wave values in supplementary material S7.3.

7.3.3. Calculation of limits for the indicative range

The indicative meaning of a paleo RSL indicator can be calculated, if the upper and lower limit (with respect to mean sea level) of its formation can be quantified. Depending on the RSL indicator, these limits can be calculated from tidal or wave values and different morpho- and hydrodynamic equations. The limits are shown in Table 7.1 and detailed hereafter.

Table 7.1: Sea-level indicators used in this study with their limits and occurrence.

Indicator	Upper limit	Lower limit	Number of data points	Accepted data points	Points at passive margins	Points at active margins
Abrasion Notch	SWSH	d_b	1	0	0	0
Beach Deposit	O_b	d_b	267	163	128	35
Beach-Ridge	SWSH	O_b	6	6	5	1
Beachrock	Sz	d_b	17	17	5	12
Chenier	ec	MHHW	8	8	7	1
Coral Reef Terrace	MLLW	d_b	1433	588	379	209
Lagoonal Deposit	MLLW	ld	5	5	5	0
Marine Terrace	SWSH	d_b	687	635	244	391
Shore Platform	MHHW	(d_b +MLLW)/2	5	5	2	3
Tidal Notch	MHHW	MLLW	14	14	7	7
Indicator not given	-	-	*1104*	-	-	-
Sum			**3547**	**1441**	**782**	**659**

db: Breaking depth; ec: Elevation of chenier; ld: Lagoonal depth; MHHW: Mean higher high water; MLLW: Mean lower low water; Ob: Ordinary berm; SWSH: Storm wave swash height; Sz: Spray zone.

Breaking depth. The breaking depth of waves d_b, i.e. the lowest point of interaction between sediment and water, was calculated with the formula from Rattanapitikon et al. (2003), as reported in Lee and Mizutani (2010):

$$\frac{d_b}{L_0} = (3.86s^2 - 1.98s + 0.88)\left(\frac{HS}{L_0}\right)^{0.84} \quad \text{(Eq. 7.1)}$$

In this equation, *s* is the general beach slope, *Hs* the mean deepwater significant wave height (that we calculated from the CAWACR data) and L_0 is the mean deepwater wave length. For this database, the general slope of beaches *s* (0.08) was derived by averaging all reported data of beaches from a global compilation by Liu et al. (2011) and is uniformly used for all points in the database. This is possible as the resulting values for both limits, where this value is used, do not change significantly with a slope smaller than 0.5. The deepwater wave length L_0 was calculated using the formula proposed by Stockdon et al. (2006)

$$L_0 = \frac{g*Tp^2}{2*\pi}, \quad \text{(Eq. 7.2)}$$

with the gravity constant *g* (9.81 m/s²) and the mean deepwater wave period *Tp* (that we calculated from the CAWACR data).

Ordinary berm. The ordinary berm O_b can be approximated by the maximum run-up of waves, that can be in turn calculated using the Stockdon et al. (2006) formulation for the 2% run-up (R_2) and adding it to the *MHHW*

$$O_b = 1.1\left(0.35 * s * (Hs * L0)^{0.5} + \frac{\left[H_s L_0 (0.563 * s^2 + 0.004)\right]^{0.5}}{2}\right) + MHHW \quad \text{(Eq. 7.3)}$$

with the mean higher high water *MHHW* calculated by the OTPS model as described above, the general beach slope *s*, the mean deepwater significant wave height Hs and the mean deepwater wave length L_0.

We consider the **spray zone** *Sz* as the highest possible elevation that the wave spray can reach. As suggested by Rovere et al. (2016a) it is calculated by doubling the elevation of O_b.

To calculate the **storm waves swash height** *SWSH*, i.e. the highest point storm waves can reach, we used Eq. 7.3, but using the maximal instead of the mean values for the *Hs*, *Tp* and L_0.

For the highest point of **cheniers** *ec* a uniform, typical value of +3 m (Otvos, 2005) was assigned to all points in the database. As **deepest point of lagoons** *ld* also a uniform value of -2 m was used. This value is the mean value of several lagoonal depth reported in Rovere et al. (2016a).

7.3.4. Indicative meaning and paleo RSL

Once upper and lower limits were calculated as described above for each RSL indicator in our database, we proceeded to the calculation of the indicative range IR and the relative water level RWL using the formulas from Rovere et al. (2016a):

$$IR = upper\ limit - lower\ limit \quad \text{(Eq. 7.4)}$$

$$RWL = \frac{upper\ limit + lower\ limit}{2} \quad \text{(Eq. 7.5)}$$

Then, we calculated the paleo relative sea level PRSL and the associated uncertainty PRSLerr at each site:

$$PRSL = E - RWL \quad \text{(Eq. 7.6)}$$

$$PRSLerr = \sqrt{\left(\frac{Eerr}{2}\right)^2 + \left(\frac{IR}{2}\right)^2} \quad \text{(Eq. 7.7)}$$

with the indicative range IR and relative water level RWL as well as the measured elevation of the RSL indicator E and its associated total uncertainty Eerr.

The PRSL and PRSLerr were used for calculating a stacked probability density function (PDF). This method assigns a normal distribution to each point using the respective PRSL and PRSLerr and sums them into a stacked and normalized PDF (see also Lorscheid et al., 2017 for more information on this method). This approach ensures that the uncertainty of PRSL at each site is propagated to the overall results. We calculate two PDFs, one for sites located at active margins and one at passive margins. From the resulting curves we extracted the median values, representing half of the integrated areas, and the 1σ, 2σ and 3σ uncertainties.

7.4. Results

Our MIS 5e RSL compilation includes 3547 data points, 70% from H16, 27% from P14 and 3% from K09. Overall, we rejected 2010 data points, mainly from H16, because no stratigraphic context was given, the site was missing a reported elevation or had an age outside MIS 5e. Rejection of points from K09 and P14 was mainly based on RSL indicators describing a marine/terrestrial limiting (see definition in Rovere et al., 2016a) and missing wave conditions for the specific site. The RSL indicators for the remaining 1441 data points (Fig. 7.2) are mainly marine terraces (44%), coral reef terraces (41%) and beach deposits (11%). The largest part of marine terrace entries comes from P14, as well as most beach deposits. Coral reef terraces are mainly derived from H16, as they only used corals as paleo RSL indicators. Out of the accepted data points, 659 are at active margins, while 782 are near or at passive margins, and therefore can be considered devoid of major tectonic influences, although these points might be still significantly affected by glacial isostasy (Dutton and Lambeck, 2012; Creveling et al., 2015; Rovere et al., 2016b) and dynamic topography (Moucha et al., 2008; Austermann et al., 2017). The distribution of the different types of RSL indicators at active and passive margins is shown in Fig. 7.2.

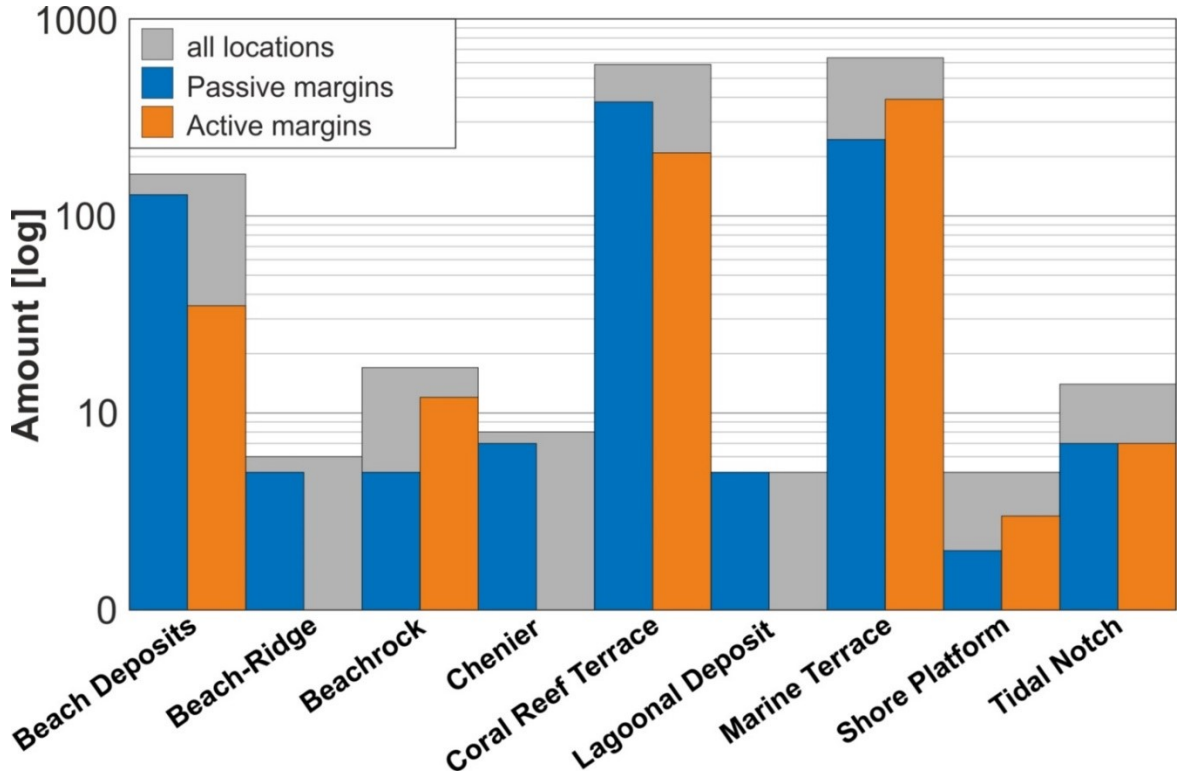

Fig. 7.2: Distribution of RSL indicators within the database. Grey bar shows overall amount, orange and blue bars show passive and active margins, respectively.

Sorting the upper and lower limits calculated at each site and calculating their relative frequency (Fig. 7.3), it is possible to compare how different indicators perform in indicating paleo RSL. The upper limits of beach-ridges and marine terraces (SWSH) have the highest value and are characterized by significant variations between sites. In contrast, the upper limits of tidal notches and coral reef terraces (represented by MHHW and MLLW, respectively) are characterized by low uncertainties. The spread of the lower limit is very similar for all indicators, although at different elevations, and is only narrower for

tidal notches and cheniers. In general, the tide-related limits show a smaller variance through all sites, whereas the wave-related values have a much larger spreading. The values of each limit for all indicators can be found in supplementary material S7.1.

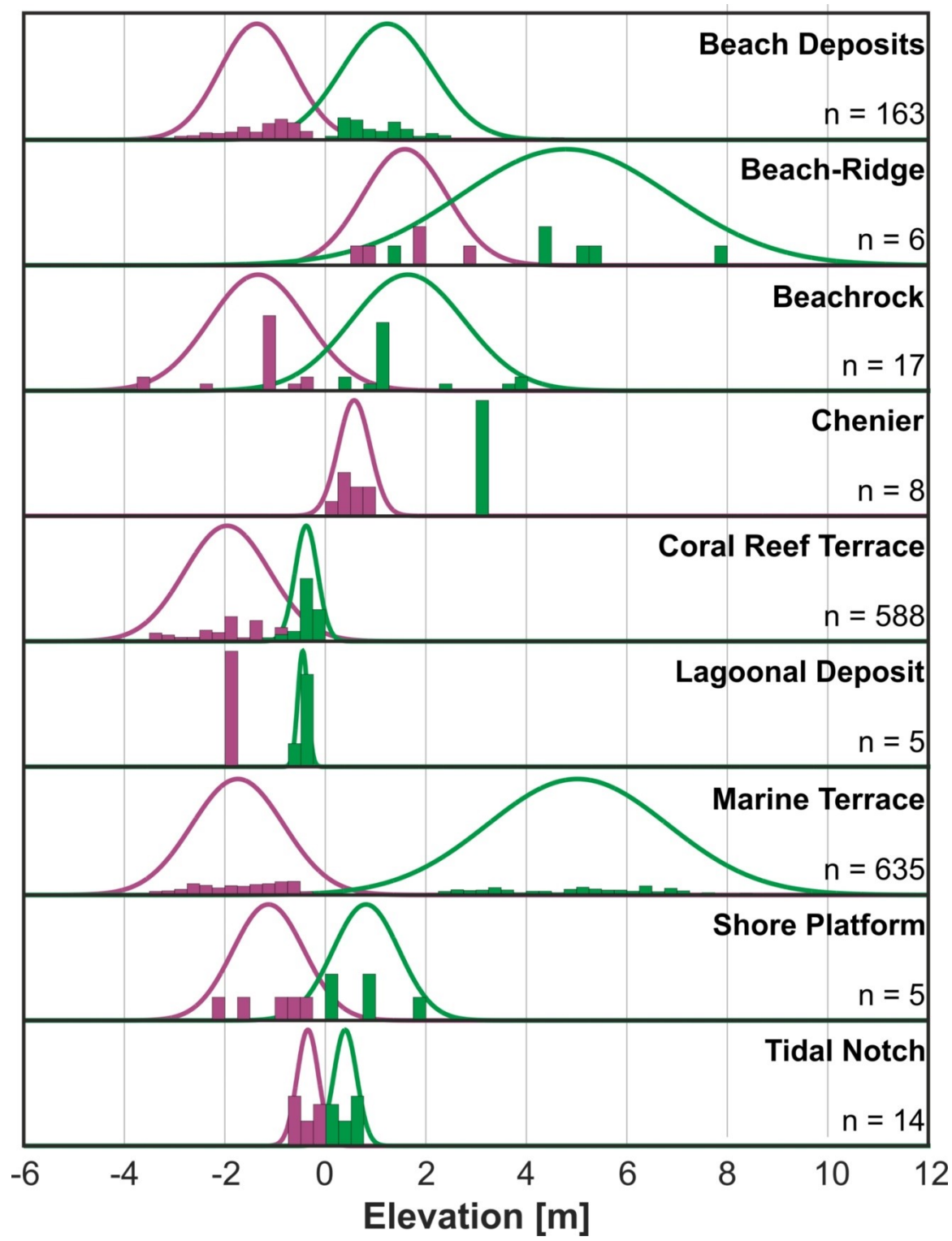

Fig. 7.3: Distribution of upper and lower limits per indicator. For each indicator a histogram and probability density function is shown (purple = lower limit; green = upper limit). For the upper limit of cheniers and the lower limit of lagoons only one bar is shown, as these limits are uniformly the same throughout the entire database.

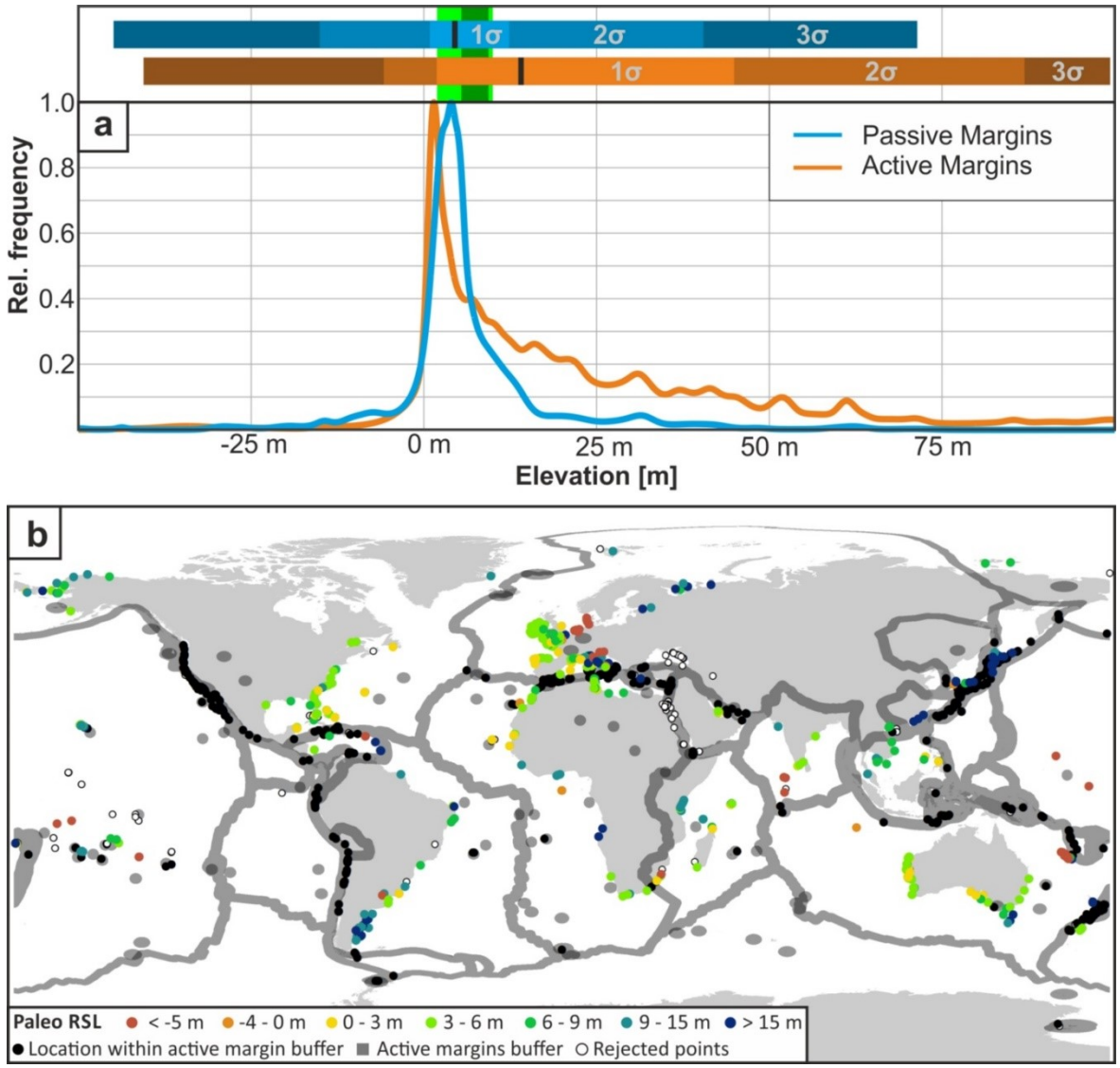

Fig. 7.4: a) Global stacked PDF for the paleo RSL for passive (blue) and active (orange) margins. Black bar represents the median and colored bars show the 1σ, 2σ, 3σ uncertainty. Green bars show published paleo RSL estimates without (light) and with (dark) GIA corrections as reported in (Dutton et al., 2015). b) Global distribution of the database points. Colored points indicated the accepted points at passive margins, colored according to their paleo RSL. Grey shaded areas represent active margins buffer and black points are locations within these buffers. White points represent rejected data points.

Plotting the frequency of our paleo RSL indicators (using a PDF, Fig. 7.4a) at passive and active margins shows that, at passive margins, the median paleo RSL is at +4.5 m +7.8/-3.6 m (1σ). At active margins, both the median paleo RSL and its uncertainties increase to +14.11 m +30.8/-12.2 m (1σ). We remark that the plot in Fig. 7.4a is illustrative of the fact that the tectonic signal can be already detected in the paleo RSL record. The paleo RSL for passive margins (blue line) represents most likely the sum of eustatic sea level, GIA and dynamic topography (Peltier, 1998; Moucha et al., 2008), while the one for active margins (orange line) includes additionally to these processes tectonic uplift and subsidence as well as volcanic isostasy. Further post-depositional movements, as illustrated by Rovere et al. (2016b), can still apply to both. The spatial distribution of all datapoints (Fig. 7.4b) shows a concentration mainly

in the Caribbean, the pacific islands, Western Australia and the US west- and eastcoast, as well as the Western Mediterranean, the British Islands and the Seychelles.

7.5. Discussion

In this study, we standardized under a unique framework three formerly published databases to derive a global overview of MIS 5e RSL indicators. We show that it is possible to quantify the indicative meaning of RSL indicators at global scale using a systematic and site-specific approach that uses known relations between wave and tide conditions with morpho- and hydrodynamic boundaries of landforms and deposits. Basically, we apply the assumption that processes in the past were regulated by the same physical laws of today (principle of uniformitarianism). For the most part of our compilation, we make use of global wave and tide data as input to equations that are then used to calculate the limits of the indicative meaning. We remark that such an approach only approximates the indicative range, but can be used if no data on specific modern analogs are available, as it is often the case for global sea level compilations.

Comparing our modeled limits with studies where modern analog landforms or deposits have been investigated provides some sensitivity to our method. Comparing the lower limit of beach deposits for two sites on the island of Mallorca (Cala Pudent and Cala Millor) we calculate with Eq. 7.1 (-0.8 m and -1.2 m, respectively). This compares relatively well with the lower limit measured in the field (-1.9 m at Cala Millor; Rovere et al., 2016a) and modeled using more accurate local wave data and a hydrodynamic model (respectively, -1.7 m and -4.9 m; Lorscheid et al., 2017). The same is true for the upper limit of beach deposits at these two sites that we calculate to be +0.6 m and +0.5 m. That is respectively at the same elevation or 0.2 m lower than calculated by the local hydrodynamic models (Lorscheid et al., 2017). The direct measurements of the modern ordinary berm at Cala Millor (Rovere et al., 2016a) are 0.3 m higher than those calculated using Eq. 7.3. Here we used the breaking depth also for estimating the depth of coral reef terraces. Based on 24 modern reefs reported by Rovere et al. (2016a), the average depth of reef flats calculated with our approach (-2.1 m) matches well with the average of the reported depth values (-1.8 m). More comparisons with local studies, such as the one presented above, will be ultimately needed to test the reliability of our approach in approximating the indicative range of RSL indicators.

Published estimates of global paleo RSL, reported by (Dutton et al., 2015a), ranging between +2 and +10 m, or just taking studies corrected for GIA between +5.5 and +9.4 m. Only regarding passive margins, we calculated an elevation of +4.5 m, which is lower than the narrower range of GIA corrected studies, but as we do not apply GIA here, our results fit in with the broader range of studies without GIA correction. The estimated range (1σ) in this study is between +0.9 and +12.3 m and therefore slightly larger than the range of previous studies. The range of our paleo RSL at active margins is with +14.11 m +30.8/-12.2 m (1σ) much larger and also the median is above the range of reported studies. This is a direct indication of the tectonic influence on the elevation of paleo RSL. Overall we show that, according to the type of indicator, paleo RSL indicators of MIS 5e sea levels are characterized by multimetric uncertainties (Fig. 7.3). Overall, these are probably well estimated by the database of Kopp et

al. (2009), underestimated by Pedoja et al. (2014), as only the indicator elevation and variability is taken into account at each site, and overestimated by Hibbert et al. (2016).

The spatial distribution of MIS 5e RSL indicators shows hotspots (Japanese Islands, Mediterranean, Northern Europe, North America and Caribbean), where several studies have investigated MIS 5e RSL indicators (Fig. 7.4b). On the other side, several regions show relevant gaps. There are no or only poorly described sites along the western and eastern coast of Central Africa, around India, several parts from the Gulf of Bengal along the Sunda Shelf and in the Arctic and Antarctic regions (Pedoja et al., 2014). Especially at passive margins, where at least post-depositional tectonics are not affecting the record more detailed studies are needed to improve the global coverage of information.

Besides the indicative meaning and the geographic coverage of data addressed above, we remark that there are at least two additional aspects that need to be addressed both when reporting MIS 5e RSL indicators and when compiling global databases. First, age attribution and dating remains one of the main problems when attempting to reconstruct MIS 5e RSLs. Exception made for the U-series dates reported in Hibbert et al. (2016) and for the points reporting U-series ages in Kopp et al. (2009), which largely coincide, large parts of our compilation is characterized by age attributions that span the entire duration of MIS 5e, dated with biostratigraphy, Amino Acid Racemization or Electro Spin Resonance (Hearty et al., 1986; Schellmann and Radtke, 2000; Wehmiller, 2013; Ávila et al., 2015). Overall, only 37% of the database records represent absolute ages. It is also not uncommon that older studies rely to the assumption that marine terraces or deposits close to the elevation of 7 meters (Lambeck et al., 2004) are considered as MIS 5e with no strict age constraints. The information contained in these studies needs to be carefully evaluated before being inserted in MIS 5e sea level compilations.

A second aspect, started to be considered only in recent studies, is related to how the elevation of a RSL indicator is measured. Accurate elevation measurements of MIS 5e and older shorelines (e.g. taken with differential GPS and referred to tidal benchmarks or local geoids) were not collected until very recently (Muhs et al., 2011; O'Leary et al., 2013; Rovere et al., 2014b; Dutton et al., 2015b; Ramalho et al., 2017). The errors related to the reported elevation of RSL indicators from older studies need therefore to be reconsidered in light of the technique used and the reference of every measurement reported in literature needs to be evaluated against the sea-level datum used. This could ideally be done by comparing the differences of elevations (and related uncertainty) that are obtained measuring the same RSL indicator with different measurement techniques. The offsets obtained could then be tentatively applied to global compilations such as the one presented here. In order to reevaluate previous studies, a comparison of the sites with new satellite data (e.g. from the TanDEM-X missions) may help improving the record.

7.6. Conclusions

In this paper, we present a standardized and globally applicable approach to calculate the indicative meaning of MIS 5e RSL indicators. This method is especially helpful when no data is available for the modern analog, or when a site-specific approach is not possible. Our discussion points to open research

lines on databases of MIS 5e RSL indicators that will need to be addressed to improve the information that we can derive from them in terms of Last Interglacial sea levels:

- It is necessary to re-evaluate original papers reporting on MIS 5e shorelines using a standard database structure, and rigorous reporting formats. A new database must necessarily consider RSL indicator as the basic element. One site may contain several RSL indicators, e.g. it may contain a fossil reef and a beach deposit covering it (e.g. Hearty et al., 1998). In addition, one RSL indicator might contain several samples with radiometric dating. Above all, averaging RSL indicators within several sites should be avoided (Hibbert et al., 2016).
- When no data on modern analogs are available, the limits of the indicative meaning for a MIS 5e RSL indicator can be derived from the equations and datasets presented in this paper. The proposed approach might still be improved by further research on this topic and needs to be validated with local studies, but it can give a first quantitative estimate on the indicative meaning at a specific site.
- The elevations extracted from older studies need to be carefully assessed, for which concerns both the survey method and the datum to which the measurement is referred to.
- Details on radiometric ages need to be always reported. In areas where no radiometric (U-series) methods are available, it is necessary to define the uncertainties related to ages obtained with other dating methods, and those obtained with chronostratigraphic and biostratigraphic approaches. If more than one RSL indicator is reported within one site or a section, attention must be given to the definition of temporal relationship between the indicators.

7.7. Supplementary Material

This manuscript is accompanied with supplementary data, which can be found as part of a data collection of this thesis at *https://doi.pangaea.de/10.1594/PANGAEA.883825*.

This supplementary consists of:

- Supplementary Tables S7
  - S7.1 - Concatenated database of MIS 5e RSL indicators with paleo RSL calculated for each site
  - S7.2 - Statistic information about the database
  - S7.3 - Data for building Fig. 7.3
  - S7.4 - Results for paleo RSL calculated with probability density functions used to build Fig. 7.4
  - S7.5 - Detailed information about the comparison of field data to the equation results
- Supplementary Text S7.6
  - Detailed description of each column in the database
- Supplementary Material S7.7
  - MATLAB-scripts for downloading and calculating wave and tidal datasets

8. Extended discussion and conclusions

The study of MIS 5e paleo sea levels has a long tradition, resulting in putting a large number of sites on the global map. Despite this long-lasting history of research, with respect to the global high-resolution sea-level reconstructions in the Holocene and the Common Era (e.g.Woodroffe and Horton, 2005; Khan et al., 2015; Kopp et al., 2016; Vacchi et al., 2016), the analysis and reporting of MIS 5e RSL indicators is seldom done in a structured and comprehensive way. Starting from their elevation and the determination of the indicative meaning, together with an age attribution and data about the post-depositional movements, these information are essential in order to estimate the MIS 5e eustatic sea level. In the introduction, I presented four research questions that were the main subject of the four chapters of this thesis. In the following chapter, I summarize and discuss my work, outlining possible future research directions.

8.1. How can RSL indicators be described from a geomorphological perspective?

RSL indicators represent the only direct evidence of past sea levels. For MIS 5e, several geological features can serve as potential RSL indicators, including sedimentological, biological and morphological elements of the landscape (Shennan, 2015). The elevation of a RSL indicator is a fundamental property, and in the work presented in chapter 4, guidelines on how it should be properly measured are given. The measurement must be done with the highest possible accuracy (e.g. by differential GPS) and needs to be referred to a known geodetic or tidal datum (e.g. EGM08; Pavlis et al., 2012). Each measurement needs to be associated with a measurement error, which depends on the technique used. In general, the elevation of a RSL indicator is an objective datum that can be updated only if better measurement techniques or datums become available. Survey method, elevation errors and datums should always be clearly reported, as shown for the studies in Mallorca (chapter 5) and Bonaire (Chapter 6).

The second main characteristic of a RSL indicator is the interpretation of its origin and formation, which is essential for calculating the paleo RSL. In the chapter 4, I show 10 different indicators, which summarize the most reported RSL indicators in MIS 5e. This classification may serve as a guideline for characterization of RSL indicators in future studies. Once the elevation and its associated error are known, each measured RSL indicator should be accompanied by an estimate of the indicative meaning. The indicative meaning is composed by the indicative range (IR), describing the possible vertical occurrence of this indicator, and the reference water level (RWL), representing the distance between the midpoint of the IR and mean sea level. These two values are usually derived by surveying a modern analog, i.e. the same feature used as RSL indicator in its modern environment of formation. Establishing the indicative meaning is a way to make more objective the interpretation of a RSL indicator, but it can be updated, if new information of the formation processes or a modern analog better representing the paleo feature become available.

Once type of indicator, elevation and indicative meaning are known, I suggest a simple set of formulas to calculate the paleo RSL (chapter 4), also suggesting how upper and lower limits can be calculated using hydrodynamic relationships and simple formulas. This is the base for chapter 7, where I reanalyze the given indicators and propose more advanced formulas for calculating their limits. For chapter 5,

the fundamental idea behind the use of a more complex morphodynamic model is also the correlation between limits for beach deposition and morphodynamics. A correct paleo RSL, with realistic uncertainties, is the basis to calculate past eustatic sea levels or can be used in GIA or tectonic inversion to disentangle the best performing models predicting such effects.

8.2. Is it possible to use modern morphodynamic models to determine the indicative meaning of beach deposits?

As described above, quantifying the indicative meaning of a MIS 5e RSL indicator is essential to calculate paleo RSL. The definition of the indicative meaning stems from Holocene sea-level studies (Shennan, 1982; Van De Plassche, 1986; Woodroffe and Horton, 2005; Engelhart and Horton, 2012). The standard approach to quantify the indicative meaning is the investigation of the vertical distribution of a RSL indicator in its modern environment. In the best case, this is done by coupling the survey of a paleo RSL indicator with that of a similar modern feature (Engelhart and Horton, 2012). For example, the formation of beach deposits is limited underwater by the deepest point of wave-sediment interaction (Chrzastowski, 2005), that can be quantified using the breaking depth of waves, often creating a submerged bar. The subaerial limit of a beach deposit is driven by wave-runup, that at most beaches forms an ordinary berm during fairweather conditions. While the berm can be easily surveyed along the beach, understanding the average elevation and depth at which beach bars and berms occur on a given beach would require the long-term observation of wave regime. Facing the problem of establishing indicative meaning for deposits in Mallorca (chapter 5), I decided to try a novel approach by using a morphodynamic model simulating several storm events to get a quantitative estimate of the upper and lower limits of the indicative meaning.

Using the 1D morphodynamic model CSHORE (Kobayashi, 1999, 2009), I simulated wave runup and sediment deposition in the submerged part of a beach during several swell events. Comparing the model results to data from a working example contained in the chapter 4 (derived by field measurements and bathymetric data) a first assessment of the methodology I used is possible. For the area of Cala Millor, I modelled the breaking depth and ordinary berm to, respectively, -4.87 m and +0.73 m. The survey data shows values of -1.9 m and +0.8 m, respectively. Another measurement of the ordinary berm in the Bay of Palma shows an elevation of +0.7 m, whereas the modelled value there is +0.55 m. At this location, the modelled breaking depth (based on more storm events than in Cala Millor) is -1.67 m, which is more similar to the one, measured in Cala Millor. Although the breaking depth in Cala Millor is modelled much deeper than the measurement, this short comparison shows that the employment of such a model is a good and easy usable method in quantifying the indicative meaning. Nevertheless, it also shows that on-site measurements are still important and should be used, at least for comparison, wherever possible.

The advantage of the modeling approach I propose is that it needs only two datasets as inputs that are not too difficult to obtain globally: a general beach profile and wave conditions (significant wave height, wave period and wave direction) for as many storm events as possible. For many locations, these information are available in a high resolution from local providers, or from global datasets (e.g.

the satellite dataset AVISO+ (McGregor et al., 2012) or the global wave model WaveWatch III (Moon et al., 2003)).

8.3. Can particular RSL indicators give an insights on further environmental information, e.g. changes in the tidal range?

The use of a modern analog to quantify the indicative meaning is based on the assumption that the environmental conditions under which a paleo RSL indicator formed are the same as today. In most cases, this is a reasonable assumption and one of the fundamental principles in geology. Nevertheless, it is known that the tidal range is sensible to changes in the geometry of the seafloor, which might be relevant under different sea levels (Hill, 2016). In the quantification of RSL indicators constrained by the tidal datums, it is important to investigate if changes in the tidal range between MIS 5e and today occurred.

There are two possibilities to assess changes in tidal range. The first is to measure the geometric properties of tidal notches. These morphological features are carved in the bedrock at mean sea level and the shaping processes are related to the tidal range. In Bonaire (chapter 6), modern and paleo tidal notches were measured at the same location, in order to compare their geometry. The notch width, i.e. the vertical distance between roof and floor (Antonioli et al., 2015), is consistent between modern and paleo notches. Therefore, I conclude that the tidal range in the past was similar to the modern. Nevertheless, as the notch geometry is also influenced by other processes (especially erosion acting on the paleo notch since its formation), I remark that this method can just give a first estimate on tidal changes.

Another possibility of assessing the tidal range changes is the hydrodynamic simulation of tidal ranges for an entire lunar cycle. To compare the results of the geometric survey from Bonaire, I set up the program Delft3D-FLOW with two tidal simulations. In the first simulation, I modeled modern tides using present day conditions and bathymetry and compared the resulting tides to real-time measurements in order to validate the model results. In a second simulation, I used the same set-up, but with a paleo bathymetry derived modifying the present-day one with the outputs of a GIA model.

The results of these simulations clearly show that, while for areas with a steeper continental shelf, tidal range changes between MIS 5e and modern can be neglected, they might be instead relevant in areas with very shallow shelves (e.g. the Venezuelan Gulf, the Adriatic Sea or the Gulf of Mexico). In these regions, the change in water depth between the MIS 5e and today can have a strong influence to the tidal range. Accordingly, it is important to quantify the tidal range change in these shallow areas for the determination of the indicative meaning. I conclude remarking that, if no tidal model can be employed, an additional uncertainty of at least 15 % of the modern tidal range should be added to the indicative range.

8.4. How could the indicative meaning be derived without site-specific data and reanalyze a global database in a more standardized way?

Global databases of MIS 5e RSL indicators are often lacking site-specific information on the indicative meaning (e.g. Pedoja et al., 2011a; Pedoja et al., 2014), mostly due to missing information from the

original authors. For some RSL indicators the indicative meaning can be determined with different approaches. As example, the indicative meaning of a fossil coral reef terrace can be quantified by estimating the ecological depth distribution of the associated corals, or it can be estimated using geomorphological elements. In the chapter 7, I attempt to find a unique framework to quantify the indicative meaning for the RSL indicators that are described in chapter 4.

Similar to the modeling approaches developed in the chapters 5 and 6, I attempt to apply a simplified set of equations to calculate the indicative meaning from modern hydro- and morphodynamic relationships. I use global wave and tide datasets to quantify the indicative meaning of the different RSL indicators, and I apply them to calculate paleo RSL from their elevation as reported in three MIS 5e RSL databases. Similarly to the results of the morphodynamic modelling (chapter 5), the results from these equations compare well to site-specific survey data.

Using this methodology, I calculate an average paleo RSL at +4.5 m at passive margins and +14.11 m at active margins, but both values carrying large uncertainties. These values are not corrected for GIA or DT, and therefore cannot be used as a direct eustatic estimate, but they can be used to test GIA, DT and tectonic models. The attribution of the indicative meaning to these limits, shows a large, multimetric uncertainty for most of the limits. In general, tide related limits have a narrower uncertainty, whereas wave-related boundaries have larger errors. Therefore, the attribution of the indicative meaning in a systematical structure is essential and should also employed for MIS 5e studies. If no site-specific data is available, the use of these simple equations and datasets is a valid method.

9. Outlook and future work

The attribution of the indicative meaning is, as shown above, a critical point in assessing the global sea level signal during MIS 5e. I showed in my thesis that the indicative meaning can be determined from field surveys and modelling, or it can be estimated using global datasets, but it needs to be reported. Many literature studies do not report the indicative meaning, or they do not define enough elements to estimate it. This leads to large uncertainties in the paleo RSL calculated from MIS 5e RSL indicators, which need to be necessarily added to those obtained by GIA and DT models (Austermann et al., 2017). In order to minimize these uncertainties, previously published studies have to be reanalyzed using a standardized methodologies and rigorous quantifications of the indicative meaning.

In addition to the indicative meaning, this reanalysis will necessarily have to cover the aspects of dating and measurement. The dating of many sites reporting MIS 5e RSL indicators is based on (bio)stratigraphy, Amino Acid Racemization or Electro Spin Resonance (Hearty et al., 1986; Schellmann and Radtke, 2000; Wehmiller, 2013; Ávila et al., 2015). These relative dating approaches can correctly estimate the MIS 5e age of a fossil-bearing deposit, but they can hardly differentiate within MIS 5e in absolute timing. Wherever corals are available, absolute dating methods (e.g. U-series) should be given preference, but previously published U-series ages might need to be recalculated from the original reports to obtain comparable dates (Hibbert et al., 2016). The elevation measurement of previous studies also needs to be addressed more precisely than in the original. If possible, high-accuracy elevation measurements should replace older measurements at key sites. New-generation satellite data (e.g. from the TanDEM-X-mission), might help achieving more accurate elevations for a number of MIS 5e features globally, such as marine and coral reef terraces. If remeasuring the elevation of important sites is not possible (as they might have been lost to urban development), the original measurements need to be attributed with a relevant uncertainty.

Nevertheless, even a global database with indicative meaning, age attribution and measurement can only show the global distribution of paleo RSL, which is by definition not corrected for post-depositional movements. In order to be useful in assessing the global ESL, this database would need to be corrected for these movements. Besides the tectonic influence, which has to be assessed site by site, especially the processes of GIA and DT have to be taken into account and attributed to each location.

Finally, the global distribution of reported MIS 5e RSL indicators shows some spatial gaps. This includes the western and eastern coast of Central Africa, around India, several parts from the Gulf of Bengal along the Sunda Shelf and in the Arctic and Antarctic regions (Pedoja et al., 2014). In these areas, new research on possible landforms has to be undertaken to fill the gaps in the global coverage.

10. References

Anderson, D.L., Schramm, K.A., 2005. Global Hotspot Maps, Plates, plumes, and paradigms: Geological Society of America Special Papers 388, pp. 19-29.

Antevs, E.V., 1929. Quaternary marine terraces in nonglaciated regions and changes of level of sea and land. American Journal of Science s5-17, pp. 35-49.

Anthony, E.J., 2005. Beach Erosion, in: Schwartz, M.L. (Ed.), Encyclopedia of Coastal Science. Springer Netherlands, Dordrecht, pp. 140-145.

Anthony, E.J., 2008. Shore Processes and their Palaeoenvironmental Applications. Developments in Marine Geology 4, pp. 325-367.

Antonioli, F., Bard, E., Potter, E.-K., Silenzi, S., Improta, S., 2004. 215-ka History of sea-level oscillations from marine and continental layers in Argentarola Cave speleothems (Italy). Global and Planetary Change 43, pp. 57-78.

Antonioli, F., Chemello, R., Improta, S., Riggio, S., 1999. Dendropoma lower intertidal reef formations and their palaeoclimatological significance, NW Sicily. Mar Geol 161, pp. 155-170.

Antonioli, F., Ferranti, L., Kershaw, S., 2006. A glacial isostatic adjustment origin for double MIS 5.5 and Holocene marine notches in the coastline of Italy. Quaternary International 145-146, pp. 19-29.

Antonioli, F., Lo Presti, V., Rovere, A., Ferranti, L., Anzidei, M., Furlani, S., Mastronuzzi, G., Orru, P.E., Scicchitano, G., Sannino, G., Spampinato, C.R., Pagliarulo, R., Deiana, G., de Sabata, E., Sansò, P., Vacchi, M., Vecchio, A., 2015. Tidal notches in Mediterranean Sea: a comprehensive analysis. Quaternary Science Reviews 119, pp. 66-84.

Antonioli, F., Oliverio, M., 1996. Holocene Sea-Level Rise Recorded by a Radiocarbon-Dated Mussel in a Submerged Speleothem beneath the Mediterranean Sea. Quaternary Research 45, pp. 241-244.

Antonioli, F., Presti, V.L., Rovere, A., Ferranti, L., Anzidei, M., Furlani, S., Mastronuzzi, G., Orrù, P.E., Scicchitano, G., Sannino, G., Spampinato, C.R., Pagliarulo, R., Deiana, G., de Sabata, E., Sansò, P., Vacchi, M., Vecchio, A., 2016. Reply to comment by Evelpidu N., and Pirazzoli P. on "Tidal notches in the Mediterranean sea: A comprehensive analysis". Quaternary Science Reviews 131, pp. 238-241.

Antonioli, F., Silenzi, S., Frisia, S., 2001. Tyrrhenian Holocene palaeoclimate trends from spelean serpulids. Quaternary Science Reviews 20, pp. 1661-1670.

Austermann, J., Mitrovica, J.X., 2015. Calculating gravitationally self-consistent sea level changes driven by dynamic topography. Geophysical Journal International 203, pp. 1909-1922.

Austermann, J., Mitrovica, J.X., Huybers, P., Rovere, A., 2017. Detection of a dynamic topography signal in last interglacial sea-level records. Science Advances 3, pp. e1700457.

Ávila, S.P., Melo, C., Silva, L., Ramalho, R.S., Quartau, R., Hipólito, A., Cordeiro, R., Rebelo, A.C., Madeira, P., Rovere, A., Hearty, P.J., Henriques, D., Silva, C.M.d., Martins, A.M.d.F., Zazo, C., 2015. A review of the MIS 5e highstand deposits from Santa Maria Island (Azores, NE Atlantic): palaeobiodiversity, palaeoecology and palaeobiogeography. Quaternary Science Reviews 114, pp. 126-148.

Bard, E., Antonioli, F., Silenzi, S., 2002. Sea-level during the penultimate interglacial period based on a submerged stalagmite from Argentarola Cave (Italy). Earth and Planetary Science Letters 196, pp. 135-146.

Bard, E., Hamelin, B., Fairbanks, R.G., 1990. U/Th ages obtained by mass spectrometry in corals from Barbados. Chemical Geology 84, pp. 157-158.

Bardají, T., Goy, J.L., Zazo, C., Hillaire-Marcel, C., Dabrio, C.J., Cabero, A., Ghaleb, B., Silva, P.G., Lario, J., 2009. Sea level and climate changes during OIS 5e in the Western Mediterranean. Geomorphology 104, pp. 22-37.

Barlow, N.L.M., Shennan, I., Long, A.J., Gehrels, W.R., Saher, M.H., Woodroffe, S.A., Hillier, C., 2013. Salt marshes as late holocene tide gauges. Global and Planetary Change 106, pp. 90-110.

Barnett, R.L., Gehrels, W.R., Charman, D.J., Saher, M.H., Marshall, W.A., 2015. Late Holocene sea-level change in Arctic Norway. Quaternary Science Reviews 107, pp. 214-230.

Beckley, B.D., Zelensky, N.P., Holmes, S.A., Lemoine, F.G., Ray, R.D., Mitchum, G.T., Desai, S.D., Brown, S.T., 2010. Assessment of the Jason-2 Extension to the TOPEX/Poseidon, Jason-1 Sea-Surface Height Time Series for Global Mean Sea Level Monitoring. Marine Geodesy 33, pp. 447-471.

Beets, D., 1977. Guide to the field excursions on Curaçao, Bonaire and Aruba, Netherlands Antilles. GUA Pap. Geol. Ser. 10, pp. 7-17.

Bellucci, L.G., Frignani, M., Paolucci, D., Ravanelli, M., 2002. Distribution of heavy metals in sediments of the Venice Lagoon: the role of the industrial area. The Science of the total environment 295, pp. 35-49.

Bianchi, C.N., Aliani, S., Morri, C., 1995. Present-day serpulid reefs, with reference to an on-going research project on Ficopomatus enigmaticus. Publications du Service géologique du Luxembourg 29, pp. 61-65.

Bintanja, R., van de Wal, R.S.W., 2008. North American ice-sheet dynamics and the onset of 100,000-year glacial cycles. Nature 454, pp. 869-872.

Bird, E.C.F., 2008. Coastal Geomorphology: An Introduction. John Wiley & Sons Ltd.

Bird, M.I., Fifield, L.K., Teh, T.S., Chang, C.H., Shirlaw, N., Lambeck, K., 2007. An inflection in the rate of early mid-Holocene eustatic sea-level rise: A new sea-level curve from Singapore. Estuarine, Coastal and Shelf Science 71, pp. 523-536.

Bird, P., 2003. An updated digital model of plate boundaries. Geochemistry, Geophysics, Geosystems 4.

Blanchon, P., 2011. Geomorphic Zonation, in: Hopley, D. (Ed.), Encyclopedia of Modern Coral Reefs: Structure, Form and Process. Springer Netherlands, Dordrecht, pp. 469-486.

Blanchon, P., Eisenhauer, A., Fietzke, J., Liebetrau, V., 2009. Rapid sea-level rise and reef back-stepping at the close of the last interglacial highstand. Nature 458, pp. 881-884.

Bonnet, D., Molinero, J.C., Schohn, T., Yahia, M.N.D., 2012. Seasonal changes in the population dynamics of Aurelia aurita in Thau lagoon. Cahiers De Biologie Marine 53, pp. 343-347.

Braithwaite, C.J.R., Taylor, J.D., Kennedy, W.J., 1973. The Evolution of an Atoll: The Depositional and Erosional History of Aldabra. Philosophical Transactions of the Royal Society B: Biological Sciences 266, pp. 307-340.

Brocas, W.M., Felis, T., Obert, J.C., Gierz, P., Lohmann, G., Scholz, D., Kölling, M., Scheffers, S.R., 2016. Last interglacial temperature seasonality reconstructed from tropical Atlantic corals. Earth and Planetary Science Letters 449, pp. 418-429.

Broecker, W.S., Thurber, D.L., 1965. Uranium-Series Dating of Corals and Oolites from Bahaman and Florida Key Limestones. Science 149, pp. 58-60.

Bruneau, N., Fortunato, A.B., Dodet, G., Freire, P., Oliveira, A., Bertin, X., 2011. Future evolution of a tidal inlet due to changes in wave climate, Sea level and lagoon morphology (Óbidos lagoon, Portugal). Continental Shelf Research 31, pp. 1915-1930.

Buddemeier, R.W., Smith, S.V., Kinzie, R.A., 1975. Holocene windward reef-flat history, Enewetak Atoll. Geological Society of America Bulletin 86, pp. 1581.

Butzer, K.W., 1975. Pleistocene littoral-sedimentary cycles of the Mediterranean basin: a Mallorquin view, in: Butzer, K.W., Isaac, G.L. (Eds.), After the Australopithecines, pp. 25-71.

Butzer, K.W., Cuerda, J., 1962. Coastal stratigraphy of southern Mallorca and its implications for the Pleistocene chronology of the Mediterranean Sea. The Journal of Geology 70, pp. 398-416.

Carlston, C.W., 1950. Pleistocene History of Coastal Alabama. Geological Society of America Bulletin 61, pp. 1119.

Carobene, L., 2015. Marine Notches and Sea-Cave Bioerosional Grooves in Microtidal Areas: Examples from the Tyrrhenian and Ligurian Coasts—Italy. Journal of Coastal Research 313, pp. 536-556.

Carr, A.S., Bateman, M.D., Roberts, D.L., Murray-Wallace, C.V., Jacobs, Z., Holmes, P.J., 2010. The last interglacial sea-level high stand on the southern Cape coastline of South Africa. Quaternary Research 73, pp. 351-363.

Casella, E., Rovere, A., Pedroncini, A., Mucerino, L., Casella, M., Cusati, L.A., Vacchi, M., Ferrari, M., Firpo, M., 2014. Study of wave runup using numerical models and low-altitude aerial photogrammetry: A tool for coastal management. Estuarine, Coastal and Shelf Science 149, pp. 160-167.

Casella, E., Rovere, A., Pedroncini, A., Stark, C.P., Casella, M., Ferrari, M., Firpo, M., 2016. Drones as tools for monitoring beach topography changes in the Ligurian Sea (NW Mediterranean). Geo-Marine Letters 36, pp. 151-163.

Chandana, E.P.S., De S. Amarasinghe, N.J., Samayawardhena, L.A., 2008. Factors affecting the avi-faunal distribution in the three lagoons (Malala, Embillakala and Bundala Lewaya) of Bundala National Park (A Ramsar Wetland) in Sri Lanka. Ruhana Journal of Science 3, pp. 34-43.

Chappell, J., Omura, A., Esat, T., McCulloch, M., Pandolfi, J., Ota, Y., Pillans, B., 1996. Reconciliation of late Quaternary sea levels derived from coral terraces at Huon Peninsula with deep sea oxygen isotope records. Earth and Planetary Science Letters 141, pp. 227-236.

Chappell, J., Shackleton, N.J., 1986. Oxygen isotopes and sea level. Nature 324, pp. 137-140.

Chen, J.H., Curran, H.A., White, B., Wasserburg, G.J., 1991. Precise chronology and the last interglacial period: 234U- 230Th data from fossil coral reefs in the Bahamas. Geological Society of America Bulletin 103, pp. 82-97.

Cheng, H., Edwards, R.L., Hoff, J., Gallup, C.D., Richards, D.A., Asmerom, Y., 2000. The half-lives of uranium-234 and thorium-230. Chemical Geology 169, pp. 17-33.

Choi, S.J., Merritts, D.J., Ota, Y., 2008. Elevations and ages of marine terraces and late Quaternary rock uplift in southeastern Korea. Journal of Geophysical Research: Solid Earth 113.

Chrzastowski, M.J., 2005. Beach Features, in: Schwartz, M.L. (Ed.), Encyclopedia of Coastal Science. Springer Netherlands, Dordrecht, pp. 145-147.
Cicogna, F., Bianchi, C.N., Ferrari, G., Forti, P., 2003. Le Grotte Marine: cinquant'anni di Ricerca in Italia. Ministero dell'Ambiente e della Tutela del Territorio, Rome.
Colantoni, P., 1976. Aspetti geomorfologici e genesi delle grotte sottomarine. Pubbl. Stn. Zool. Napoli 40, pp. 460-472.
Contreras Ruiz Esparza, A., Douillet, P., Zavala-Hidalgo, J., 2014. Tidal dynamics of the Terminos Lagoon, Mexico: Observations and 3D numerical modelling. Ocean Dynamics 64, pp. 1349-1371.
Cooke, C.W., 1930. Correlation of Coastal Terraces. The Journal of Geology 38, pp. 577-589.
Creveling, J.R., Mitrovica, J.X., Hay, C.C., Austermann, J., Kopp, R.E., 2015. Revisiting tectonic corrections applied to Pleistocene sea-level highstands. Quaternary Science Reviews 111, pp. 72-80.
Cuerda, J., 1975. Los Tiempos Cuaternarios en Baleares. Diputación Provincial de Baleares.
Cuerda, J., 1979. Formaciones cuaternarias de la Bahía de Palma., Guía a la excursión n° 4 del VI. Coloquio de Geografía, Palma de Mallorca.
Cuerda, J., Soler, A., Antich, S., 1983. Nuevos yacimientos del Pleistoceno marino de Mallorca. Bol. Soc. Hist. Nat. Baleares 27, pp. 117-125.
Dalca, A.V., Ferrier, K.L., Mitrovica, J.X., Perron, J.T., Milne, G.A., Creveling, J.R., 2013. On postglacial sea level-III. Incorporating sediment redistribution. Geophysical Journal International 194, pp. 45-60.
Dangendorf, S., Marcos, M., Wöppelmann, G., Conrad, C.P., Frederikse, T., Riva, R., 2017. Reassessment of 20th century global mean sea level rise. Proceedings of the National Academy of Sciences 114, pp. 5946-5951.
Darwin, C., 1846. Geological Observations on South America: Being the Third Part of the Geology of the Voyage of the Beagle. Smith, Elder and Company.
de Boer, B., Lourens, L.J., van de Wal, R.S.W., 2014a. Persistent 400,000-year variability of Antarctic ice volume and the carbon cycle is revealed throughout the Plio-Pleistocene. Nature Communications 5, pp. 2999.
de Boer, B., Stocchi, P., Van De Wal, R.S.W., 2014b. A fully coupled 3-D ice-sheet-sea-level model: Algorithm and applications. Geoscientific Model Development 7, pp. 2141-2156.
de Boer, B., van de Wal, R.S.W., Lourens, L.J., Bintanja, R., Reerink, T.J., 2013. A continuous simulation of global ice volume over the past 1 million years with 3-D ice-sheet models. Climate Dynamics 41, pp. 1365-1384.
De Francesco, C.G., Isla, F.I., 2003. Distribution and abundance of hydrobiid snails in a mixed estuary and a coastal lagoon, Argentina. Estuaries 26, pp. 790-797.
Dean, A.J., Steneck, R.S., Tager, D., Pandolfi, J.M., 2015. Distribution, abundance and diversity of crustose coralline algae on the Great Barrier Reef. Coral Reefs 34, pp. 581-594.
Debenay, J.-P., Guillou, J.-J., Redois, F., Geslin, E., 2000. Distribution Trends of Foraminiferal Assemblages in Paralic Environments, in: Martin, R.E. (Ed.), Environmental Micropaleontology: The Application of Microfossils to Environmental Geology. Springer US, Boston, MA, pp. 39-67.
DeConto, R.M., Pollard, D., 2016. Contribution of Antarctica to past and future sea-level rise. Nature 531, pp. 591-597.
Desruelles, S., Fouache, É., Ciner, A., Dalongeville, R., Pavlopoulos, K., Kosun, E., Coquinot, Y., Potdevin, J.-L., 2009. Beachrocks and sea level changes since Middle Holocene: Comparison between the insular group of Mykonos–Delos–Rhenia (Cyclades, Greece) and the southern coast of Turkey. Global and Planetary Change 66, pp. 19-33.
Dias, J.M., Lopes, J.F., Dekeyser, I., 2001. Lagrangian transport of particles in Ria de Aveiro lagoon, Portugal. Physics and Chemistry of the Earth, Part B: Hydrology, Oceans and Atmosphere 26, pp. 721-727.
Dorale, J.A., Onac, B.P., Fornos, J.J., Gines, J., Gines, A., Tuccimei, P., Peate, D.W., 2010. Sea-Level Highstand 81,000 Years Ago in Mallorca. Science 327, pp. 860-863.
Dunham, R.J., 1970. Keystone Vugs in Carbonate Beach Deposits. Am. Assoc. Pet. Geol. Bull. 54, pp. 845.
Durrant, T., Hemer, M., Trenham, C., Greenslade, D., 2013. CAWCR Wave Hindcast 1979-2010.
Düsterhus, A., Rovere, A., Carlson, A.E., Horton, B.P., Klemann, V., Tarasov, L., Barlow, N.L.M., Bradwell, T., Clark, J., Dutton, A., Roland Gehrels, W., Hibbert, F.D., Hijma, M.P., Khan, N., Kopp, R.E., Sivan, D., Törnqvist, T.E., 2016. Palaeo-sea-level and palaeo-ice-sheet databases: Problems, strategies, and perspectives. Climate of the Past 12, pp. 911-921.
Dutton, A., Bard, E., Antonioli, F., Esat, T.M., Lambeck, K., McCulloch, M.T., 2009a. Phasing and amplitude of sea-level and climate change during the penultimate interglacial. Nature Geoscience 2, pp. 355-359.
Dutton, A., Carlson, A.E., Long, A.J., Milne, G.A., Clark, P.U., DeConto, R., Horton, B.P., Rahmstorf, S., Raymo, M.E., 2015a. Sea-level rise due to polar ice-sheet mass loss during past warm periods. Science 349, pp. aaa4019-aaa4019.
Dutton, A., Lambeck, K., 2012. Ice Volume and Sea Level During the Last Interglacial. Science 337, pp. 216-219.

Dutton, A., Scicchitano, G., Monaco, C., Desmarchelier, J.M., Antonioli, F., Lambeck, K., Esat, T.M., Fifield, L.K., McCulloch, M.T., Mortimer, G., 2009b. Uplift rates defined by U-series and 14C ages of serpulid-encrusted speleothems from submerged caves near Siracusa, Sicily (Italy). Quaternary Geochronology 4, pp. 2-10.

Dutton, A., Webster, J.M., Zwartz, D., Lambeck, K., Wohlfarth, B., 2015b. Tropical tales of polar ice: Evidence of Last Interglacial polar ice sheet retreat recorded by fossil reefs of the granitic Seychelles islands. Quaternary Science Reviews 107, pp. 182e196.

Egbert, G.D., Bennett, A.F., Foreman, M.G.G., 1994. TOPEX/POSEIDON tides estimated using a global inverse model. Journal of Geophysical Research 99, pp. 24821.

Egbert, G.D., Erofeeva, S.Y., 2002. Efficient inverse modeling of barotropic ocean tides. Journal of Atmospheric and Oceanic Technology 19, pp. 183-204.

Eisenhauer, A., Zhu, Z.R., Collins, L.B., Wyrwoll, K.H., Eichstätter, R., 1996. The Last Interglacial sea level change: new evidence from the Abrolhos islands, West Australia. Geologische Rundschau 85, pp. 606-614.

Engel, M., Brückner, H., Scheffers, A.M., May, S.M., Kelletat, D.H., 2014. Holocene sea levels of Bonaire (Leeward Antilles) and tectonic implications. Zeitschrift für Geomorphologie, Supplementary Issues 58, pp. 159-178.

Engelhart, S.E., Horton, B.P., 2012. Holocene sea level database for the Atlantic coast of the United States. Quaternary Science Reviews 54, pp. 12-25.

Engelhart, S.E., Horton, B.P., Douglas, B.C., Peltier, W.R., Törnqvist, T.E., 2009. Spatial variability of late Holocene and 20th century sea-level rise along the Atlantic coast of the United States. Geology 37, pp. 1115-1118.

Engelhart, S.E., Peltier, W.R., Horton, B.P., 2011. Holocene relative sea-level changes and glacial isostatic adjustment of the U.S. Atlantic coast. Geology 39, pp. 751-754.

Engineers, U.A.C.O., 1984. Shore Protection Manual. MS. 2v, Vicksburg, pp. 37-53.

Evelpidou, N., Kampolis, I., Pirazzoli, P.A., Vassilopoulos, A., 2012. Global sea-level rise and the disappearance of tidal notches. Global and Planetary Change 92-93, pp. 248-256.

Falter, J.L., Lowe, R.J., Zhang, Z., McCulloch, M., 2013. Physical and Biological Controls on the Carbonate Chemistry of Coral Reef Waters: Effects of Metabolism, Wave Forcing, Sea Level, and Geomorphology. PLoS ONE 8.

Felis, T., Giry, C., Scholz, D., Lohmann, G., Pfeiffer, M., Pätzold, J., Kölling, M., Scheffers, S.R., 2015. Tropical Atlantic temperature seasonality at the end of the last interglacial. Nature Communications 6, pp. 6159.

Ferranti, L., 1998. Underwater cave systems in carbonate rocks as semi-proxy indicators of paleo-sea-levels. Il Quaternario Ital. J. Quat. Sci. 11, pp. 41-52.

Ferranti, L., Antonioli, F., Mauz, B., Amorosi, A., Dai Pra, G., Mastronuzzi, G., Monaco, C., Orr??, P., Pappalardo, M., Radtke, U., Renda, P., Romano, P., Sans??, P., Verrubbi, V., 2006. Markers of the last interglacial sea-level high stand along the coast of Italy: Tectonic implications. Quaternary International 145-146, pp. 30-54.

Ferranti, L., Monaco, C., Morelli, D., Antonioli, F., Maschio, L., 2008. Holocene activity of the Scilla Fault, Southern Calabria: Insights from coastal morphological and structural investigations. Tectonophysics 453, pp. 74-93.

Fornos, J.J., Balaguer, P., Gelabert, B., Gomez-Pujol, L., 2005. Pleistocene formation, evolution and retreat rates of a carbonate coastal cliff (Mallorca Island, Western Mediterranean). Journal of Coastal Research 49, pp. 15-21.

Fornós, J.J., Forteza, V., Martínez-Taberner, A., 1997. Modern polychaete reefs in Western Mediterranean lagoons: Ficopomatus enigmaticus (Fauvel) in the Albufera of Menorca, Balearic Islands. Palaeogeography, Palaeoclimatology, Palaeoecology 128, pp. 175-186.

Fornós, J.J., Gelabert, B., Ginés, A., Ginés, J., Tuccimei, P., Vesica, P., 2002. Phreatic overgrowths on speleothems: A useful tool in structural geology in littoral karstic landscapes. The example of eastern Mallorca (Balearic Islands). Geodinamica Acta 15, pp. 113-125.

Foster, J., 2015. GPS and surveying, Handbook of Sea-Level Research, pp. 157-170.

Fruergaard, M., Andersen, T.J., Nielsen, L.H., Johannessen, P.N., Aagaard, T., Pejrup, M., 2015. High-resolution reconstruction of a coastal barrier system: impact of Holocene sea-level change. Sedimentology 62, pp. 928-969.

Gaki-Papanastassiou, K., Karymbalis, E., Papanastassiou, D., Maroukian, H., 2009. Quaternary marine terraces as indicators of neotectonic activity of the Ierapetra normal fault SE Crete (Greece). Geomorphology 104, pp. 38-46.

GEBCO_2014_Grid, 2014. The GEBCO_2014 Grid.

Gehrels, W.R., Belknap, D.F., Pearce, B.R., Gong, B., 1995. Modeling the contribution of M2 tidal amplification to the Holocene rise of mean high water in the Gulf of Maine and the Bay of Fundy. Mar Geol 124, pp. 71-85.

Gehrels, W.R., Long, A.J., 2007. Quaternary land–ocean interactions: Sea-level change, sediments and tsunami. Mar Geol 242, pp. 1-4.

Gelabert, B., Fornós, J.J., Gómez-Pujol, L., 2003. Geomorphological characteristics and slope processes associated with different basins: Mallorca (Western Mediterranean). Geomorphology 52, pp. 253-267.

Gibert, L., Scott, G.R., Scholz, D., Budsky, A., Ferràndez, C., Ribot, F., Martin, R.A., Lería, M., 2016. Chronology for the Cueva Victoria fossil site (SE Spain): Evidence for Early Pleistocene Afro-Iberian dispersals. Journal of Human Evolution 90, pp. 183-197.

Ginés, A., Ginés, J., Fornos, J.J., Bover, P., Gómez-Pujol, L., Gràcia, F., Merino, A., Vicens, D., 2012. An introduction to the Quaternary of Mallorca, in: Ginés, A., Gómez-Pujol, L., Onac, B.P., Fornos, J.J. (Eds.), Mallorca: A Mediterranean Benchmark for Quaternary Studies. Monografies de la Societat d'Història Natural de les Balears, p. 220.

Goatley, C.H.R., Bellwood, D.R., 2012. Sediment suppresses herbivory across a coral reef depth gradient. Biology letters 8, pp. 24-27.

Gómez-Pujol, L., Cruslock, E.M., Fornós, J.J., Swantesson, J.O.H., 2006. Unravelling factors that control shore platforms and cliffs in microtidal coasts: The case of Mallorcan, Catalonian and Swedish coasts. Zeitschrift fur Geomorphologie, Supplementband 144, pp. 117-135.

Gómez-Pujol, L., Orfila, A., Álvarez-Ellacuría, A., Tintoré, J., 2011. Controls on sediment dynamics and medium-term morphological change in a barred microtidal beach (Cala Millor, Mallorca, Western Mediterranean). Geomorphology 132, pp. 87-98.

Gomez-Pujol, L., Perez-Alberti, A., Blanco-Chao, R., Costa, S., Neves, M., Del Rio, L., 2014. Chapter 6 The rock coast of continental Europe in the Atlantic. Geological Society, London, Memoirs 40, pp. 77-88.

Graciotti, R., Foresi, L.M., Pantaloni, M., 2002. Caratteristiche Geomorfologiche dell'Isola di Pianosa (Arcipelago Toscano). Atti Soc. Toscana Di Sci. Nat. Mem. 108, pp. 95-111.

Green, J.A.M., Huber, M., Waltham, D., Buzan, J., Wells, M., 2017. Explicitly modelled deep-time tidal dissipation and its implication for Lunar history. Earth and Planetary Science Letters 461, pp. 46-53.

Grün, R., 1989. Electron spin resonance (ESR) dating. Quaternary International 1, pp. 65-109.

Guillaume, M.M.M., Reyss, J.L., Pirazzoli, P.A., Bruggemann, J.H., 2013. Tectonic stability since the last interglacial offsets the Glorieuses Islands from the nearby Comoros archipelago. Coral Reefs 32, pp. 719-726.

Hall, G.F., Hill, D.F., Horton, B.P., Engelhart, S.E., Peltier, W.R., 2013. A high-resolution study of tides in the Delaware Bay: Past conditions and future scenarios. Geophysical Research Letters 40, pp. 338-342.

Hallermeier, R.J., 1980. A profile zonation for seasonal sand beaches from wave climate. Coastal Engineering 4, pp. 253-277.

Hanna, A.J.M., Allison, M.A., Bianchi, T.S., Marcantonio, F., Goff, J.A., 2014. Late Holocene sedimentation in a high Arctic coastal setting: Simpson Lagoon and Colville Delta, Alaska. Continental Shelf Research 74, pp. 11-24.

Hansen, J., Sato, M., Hearty, P., Ruedy, R., Kelley, M., Masson-Delmotte, V., Russell, G., Tselioudis, G., Cao, J., Rignot, E., Velicogna, I., Tormey, B., Donovan, B., Kandiano, E., Von Schuckmann, K., Kharecha, P., Legrande, A.N., Bauer, M., 2016. Ice melt, sea level rise and superstorms: Evidence from paleoclimate data, climate modeling, and modern observations that 2 °c global warming could be dangerous. Atmospheric Chemistry and Physics 16, pp. 3761-3812.

Haq, B.U., Hardenbol, J., Vail, P.R., 1987. Chronology of Fluctuating Sea Levels Since the Triassic. Science 235, pp. 1156-1167.

Harmon, R.S.R., Land, L.S.L., Mitterer, R.R.M., Garrett, P., Schwartz, H., Larson, G.G.J., Schwarcz, H.P., Larson, G.G.J., 1981. Bermuda sea level during the last interglacial. Nature 289, pp. 481-483.

Harris, D.L., Vila-Concejo, A., Webster, J.M., Power, H.E., 2015. Spatial variations in wave transformation and sediment entrainment on a coral reef sand apron. Mar Geol 363, pp. 220-229.

Hawkes, A.D., Kemp, A.C., Donnelly, J.P., Horton, B.P., Peltier, W.R., Cahill, N., Hill, D.F., Ashe, E., Alexander, C.R., 2016. Relative sea-level change in northeastern Florida (USA) during the last ~8.0 ka. Quaternary Science Reviews 142, pp. 90-101.

Hay, C.C., Morrow, E., Kopp, R.E., Mitrovica, J.X., 2015. Probabilistic reanalysis of twentieth-century sea-level rise. Nature 517, pp. 481-484.

Hearty, P.J., 1987. New data on the pleistocene of Mallorca. Quaternary Science Reviews 6, pp. 245-257.

Hearty, P.J., 2002. Revision of the late Pleistocene stratigraphy of Bermuda. Sedimentary Geology 153, pp. 1-21.

Hearty, P.J., Hollin, J.T., Neumann, A.C., O'Leary, M.J., McCulloch, M., 2007. Global sea-level fluctuations during the Last Interglaciation (MIS 5e). Quaternary Science Reviews 26, pp. 2090-2112.
Hearty, P.J., Kaufman, D.S., 2000. Whole-Rock Aminostratigraphy and Quaternary Sea-Level History of the Bahamas. Quaternary Research 54, pp. 163-173.
Hearty, P.J., Kindler, P., Cheng, H., Edwards, R.L., 1999. A +20 m middle Pleistocene sea-level highstand (Bermuda and the Bahamas) due to partial collapse of Antarctic ice. Geology 27, pp. 375.
Hearty, P.J., Miller, G.H., Stearns, C.E., Szabo, B.J., 1986. Aminostratigraphy of Quaternary shorelines in the Mediterranean basin. Geological Society of America Bulletin 97, pp. 850-858.
Hearty, P.J., Neumann, A.C., 2001. Rapid sea level and climate change at the close of the Last Interglaciation (MIS 5e): Evidence from the Bahama Islands. Quaternary Science Reviews 20, pp. 1881-1895.
Hearty, P.J., Neumann, A.C., Kaufman, D.S., 1998. Chevron Ridges and Runup Deposits in the Bahamas from Storms Late in Oxygen-Isotope Substage 5e. Quaternary Research 50, pp. 309-322.
Hearty, P.J., Vacher, H.L., Mitterer, R.M., 1992. Aminostratigraphy and ages of Pleistocene limestones of Bermuda. Geological Society of America Bulletin 104, pp. 471-480.
Herweijer, J.P., Focke, J.W., 1977. Late Pleistocene Depositonal and Denudational History of Aruba, Bonaire and Curacao (Netherlands Antilles). Geologie en Mijnbouw 57, pp. 177-187.
Hesp, P.A., 1984. Foredune Formation in Southeast Australia, Coastal Geomorphology in Australia, pp. 69-97.
Hibbert, F.D., Rohling, E.J., Dutton, A., Williams, F.H., Chutcharavan, P.M., Zhao, C., Tamisiea, M.E., 2016. Coral indicators of past sea-level change: A global repository of U-series dated benchmarks. Quaternary Science Reviews 145, pp. 1-56.
Hijma, M.P., Engelhart, S.E., Törnqvist, T.E., Horton, B.P., Hu, P., Hill, D.F., 2015. A protocol for a geological sea-level database, Handbook of Sea-Level Research. John Wiley & Sons, Ltd, Chichester, UK, pp. 536-553.
Hill, D.F., 2016. Spatial and Temporal Variability in Tidal Range: Evidence, Causes, and Effects. Current Climate Change Reports 2, pp. 232-241.
Hillaire-Marcel, C., Gariépy, C., Ghaleb, B., Goy, J.L., Zazo, C., Barcelo, J.C., 1996. U-series measurements in Tyrrhenian deposits from mallorca - Further evidence for two last-interglacial high sea levels in the Balearic Islands. Quaternary Science Reviews 15, pp. 53-62.
Hippolyte, J.C., Mann, P., 2011. Neogene-Quaternary tectonic evolution of the Leeward Antilles islands (Aruba, Bonaire, Curaçao) from fault kinematic analysis. Marine and Petroleum Geology 28, pp. 259-277.
Hoang, C.T., Hearty, P.J., 1989. A comparison of U-series disequilibrium dates and amino acid epimerization ratios between corals and marine molluscs of Pleistocene age. Chemical Geology: Isotope Geoscience Section 79, pp. 317-323.
Hoffman, J.S., Clark, P.U., Parnell, A.C., He, F., 2017. Regional and global sea-surface temperatures during the last interglaciation. Science 355, pp. 276-279.
Hutton, F.W., 1885. Sketch of the Geology of New Zealand. Quarterly Journal of the Geological Society 41, pp. 191-220.
IGN, 2009. El nuevo modelo de geoide para Espana EGM08 - REDNAP.
IPCC, 2014. Climate Change 2013 - The Physical Science Basis. Climate Change 2014: Synthesis Report, pp. 151.
Jokiel, P.L., Rodgers, K.S., Storlazzi, C.D., Field, M.E., Lager, C.V., Lager, D., 2014. Response of reef corals on a fringing reef flat to elevated suspended-sediment concentrations: Moloka'i, Hawai'i. PeerJ 2, pp. e699.
Joughin, I., Smith, B.E., Medley, B., 2014. Marine Ice Sheet Collapse Potentially Underway for the Thwaites Glacier Basin, West Antarctica. Science (New York, N.Y.) 344, pp. 735-738.
Juggins, S., Birks, H.J.B., 2012. Quantitative environmental reconstructions from biological data, Tracking Environmental Change Using Lake Sediments, Data Handling and Numerical Tehcnqiues, pp. 431-494.
Kanyaya, J.I., Trenhaile, A.S., 2005. Tidal wetting and drying on shore platforms: An experimental assessment. Geomorphology 70, pp. 129-146.
Kattsov, V.M., Källén, E., Cattle, H.P., Christensen, J., Drange, H., Hanssen-Bauer, I., Jóhannesen, T., Karol, I., Räisänen, J., Svensson, G., 2005. Future Climate Change: Modeling and Scenarios for the Arctic, Arctic Climate Impact Assessment - Scientific Report. Cambridge University Press, pp. 99-150.
Kaufman, A., Broecker, W.S., Ku, T.L., Thurber, D.L., 1971. The status of U-series methods of mollusk dating. Geochimica et Cosmochimica Acta 35, pp. 1155-1183.
Kelletat, D., 2007. Reply to: KNIGHT, J., 2007. Beachrock Reconsidered. Discussion of: KELLETAT, D., 2006. Beachrock as Sea-Level Indicator? Remarks from a Geomorphological Point of View, Journal of Coastal Research, 22(6), 1558–1564; Journal of Coastal Research, 23(4), 1074. Journal of Coastal Research, pp. 1605-1606.
Kelsey, H.M., 2015. Geomorphological indicators of past sea levels, Handbook of Sea-Level Research. John Wiley & Sons, Ltd, Chichester, UK, pp. 66-82.

Kemp, A.C., Hawkes, A.D., Donnelly, J.P., Vane, C.H., Horton, B.P., Hill, T.D., Anisfeld, S.C., Parnell, A.C., Cahill, N., 2015. Relative sea-level change in Connecticut (USA) during the last 2200 yrs. Earth and Planetary Science Letters 428, pp. 217-229.

Kemp, A.C., Telford, R.J., 2015. Transfer functions, Handbook of Sea-Level Research. John Wiley & Sons, Ltd, Chichester, UK, pp. 470-499.

Kench, P.S., Brander, R.W., 2006. Wave Processes on Coral Reef Flats: Implications for Reef Geomorphology Using Australian Wave Processes on Coral Reef Flats: Implications for Reef Geomorphology Using Australian Case Studies. Journal of Coastal Research 22, pp. 209-223.

Kennedy, D.M., 2015. Where is the seaward edge? A review and definition of shore platform morphology. Earth-Science Reviews 147, pp. 99-108.

Kennedy, D.M., Dickson, M.E., 2006. Lithological control on the elevation of shore platforms in a microtidal setting. Earth Surface Processes and Landforms 31, pp. 1575-1584.

Kern, J.P., 1977. Origin and history of upper Pleistocene marine terraces, San Diego, California. Geological Society of America Bulletin 88, pp. 1553-1566.

Khan, N.S., Ashe, E., Shaw, T.A., Vacchi, M., Walker, J., Peltier, W.R., Kopp, R.E., Horton, B.P., 2015. Holocene Relative Sea-Level Changes from Near-, Intermediate-, and Far-Field Locations. Current Climate Change Reports 1, pp. 247-262.

Kharroubi, A., Gargouri, D., Baati, H., Azri, C., 2012. Assessment of sediment quality in the Mediterranean Sea-Boughrara lagoon exchange areas (southeastern Tunisia): GIS approach-based chemometric methods. Environmental Monitoring and Assessment 184, pp. 4001-4014.

Kim, K.H., Lee, D.-J., 1999. Distribution and depositional environments of coralline lithofacies in uplifted Pleistocene coral reefs of Bonaire, Netherlands Antilles. J. Paleontol. Soc. Korea 15, pp. 115-133.

Kjerfve, B., 1994. Coastal Lagoons, pp. 1-8.

Knight, J., 2007. Beachrock Reconsidered. Discussion of: . Beachrock as Sea-Level Indicator? Remarks from a Geomorphological Point of View. Journal of Coastal Research, 22(6), 1558–1564. Journal of Coastal Research, pp. 1074-1078.

Kobayashi, N., 1999. Numerical Modeling of Wave Runup on Coastal Structures and Beaches. Marine Technology Society Journal 33, pp. 33-37.

Kobayashi, N., 2009. Documentation of Cross-shore Numerical Model CSHORE 2009, Newark, Delaware.

Koike, K., Machida, H., 2001. Atlas of Quaternary marine terraces in the Japanese islands. University of Tokyo Press, Tokyo.

Kopp, R.E., Kemp, A.C., Bittermann, K., Horton, B.P., Donnelly, J.P., Gehrels, W.R., Hay, C.C., Mitrovica, J.X., Morrow, E.D., Rahmstorf, S., 2016. Temperature-driven global sea-level variability in the Common Era. Proceedings of the National Academy of Sciences, pp. 1-8.

Kopp, R.E., Simons, F.J., Mitrovica, J.X., Maloof, A.C., Oppenheimer, M., 2009. Probabilistic assessment of sea level during the last interglacial stage. Nature 462, pp. 863-867.

Kopp, R.E., Simons, F.J., Mitrovica, J.X., Maloof, a.C., Oppenheimer, M., 2013. A probabilistic assessment of sea level variations within the last interglacial stage. Geophysical Journal International 193, pp. 711-716.

Ku, T.-L., Kern, J.P., 1974. Uranium-Series Age of the Upper Pleistocene Nestor Terrace, San Diego, California. Geological Society of America Bulletin 85, pp. 1713.

Kummu, M., de Moel, H., Salvucci, G., Viviroli, D., Ward, P.J., Varis, O., 2016. Over the hills and further away from coast: global geospatial patterns of human and environment over the 20th–21st centuries. Environmental Research Letters 11, pp. 034010.

Laborel, J., Laborel-Deguen, F., 1994. Biological Indicators of Relative Sea-Level Variations and of Coseismic Displacements in the Mediterranean Region. Journal of Coastal Research 10, pp. 395-415.

Laborel, J., Laborel-Deguen, F., 1996. Biological indicators of Holocene sea-level and climatic variations on rocky coasts of tropical and subtropical regions. Quaternary International 31, pp. 53-60.

Lambeck, K., Antonioli, F., Purcell, A., Silenzi, S., 2004. Sea-level change along the Italian coast for the past 10,000 yr. Quaternary Science Reviews 23, pp. 1567-1598.

Lambeck, K., Bard, E., 2000. Sea-level change along the French Mediterranean coast for the past 30000 years. Earth and Planetary Science Letters 175, pp. 203-222.

Lambeck, K., Nakada, M., 1990. Late Pleistocene and Holocene sea-level change along the Australian coast. Global and Planetary Change 3, pp. 143-176.

Lambeck, K., Nakada, M., 1992. Constraints on the age and duration of the last interglacial period and on sea-level variations. Nature 357, pp. 125-128.

Lambeck, K., Rouby, H., Purcell, A., Sun, Y., Sambridge, M., 2014. Sea level and global ice volumes from the Last Glacial Maximum to the Holocene. Proceedings of the National Academy of Sciences 111, pp. 15296-15303.

Lamothe, M., 2016. Luminescence dating of interglacial coastal depositional systems: Recent developments and future avenues of research. Quaternary Science Reviews 146, pp. 1-27.

Lamptey, A.M., Ofori-Danson, P.K., Abbenney-Mickson, S., Breuning-Madsen, H., Abekoe, M.K., 2013. The Influence of Land-Use on Water Quality in a Tropical Coastal Area: Case Study of the Keta Lagoon Complex, Ghana, West Africa. Open Journal of Modern Hydrology 3, pp. 188-195.

Larson, M., Kraus, N.C., 1994. Temporal and spatial scales of beach profile change, Duck, North Carolina. Mar Geol 117, pp. 75-94.

Lasagna, R., Albertelli, G., Colantoni, P., Morri, C., Bianchi, C.N., 2010. Ecological stages of Maldivian reefs after the coral mass mortality of 1998. Facies 56, pp. 1-11.

Lee, G.h., Nicholls, R.J., Birkemeier, W.A., 1998. Storm-driven variability of the beach-nearshore profile at Duck, North Carolina, USA, 1981-1991. Mar Geol 148, pp. 163-177.

Lee, K.-H., Mizutani, N., 2010. Experimental Study of Wave Breaking of Periodic Waves on a Gravel Beach. Journal of Coastal Research 265, pp. 967-975.

Liu, Y., Niu, X., Yu, X., 2011. A new predictive formula for inception of regular wave breaking. Coastal Engineering 58, pp. 877-889.

Long, A.J., Barlow, N.L.M., Busschers, F.S., Cohen, K.M., Gehrels, W.R., Wake, L.M., 2015. Near-field sea-level variability in northwest Europe and ice sheet stability during the last interglacial. Quaternary Science Reviews 126, pp. 26-40.

Lorscheid, T., Stocchi, P., Casella, E., Gómez-Pujol, L., Vacchi, M., Mann, T., Rovere, A., 2017. Paleo sea-level changes and relative sea-level indicators: Precise measurements, indicative meaning and glacial isostatic adjustment perspectives from Mallorca (Western Mediterranean). Palaeogeography, Palaeoclimatology, Palaeoecology 473, pp. 94-107.

Lunt, D.J., Abe-Ouchi, A., Bakker, P., Berger, A., Braconnot, P., Charbit, S., Fischer, N., Herold, N., Jungclaus, J.H., Khon, V.C., Krebs-Kanzow, U., Langebroek, P.M., Lohmann, G., Nisancioglu, K.H., Otto-Bliesner, B.L., Park, W., Pfeiffer, M., Phipps, S.J., Prange, M., Rachmayani, R., Renssen, H., Rosenbloom, N., Schneider, B., Stone, E.J., Takahashi, K., Wei, W., Yin, Q., Zhang, Z.S., 2013. A multi-model assessment of last interglacial temperatures. Climate of the Past 9, pp. 699-717.

Lyell, C., 1837. Principles of Geology: Being an Inquiry how far the Former Changes of the earth's Surface are Referable to Causes now in Operation.

Macintyre, I.G., 1967. Submerged Coral Reefs, West Coast of Barbados, West Indies. Canadian Journal of Earth Sciences 4, pp. 461-474.

Mann, T., Rovere, A., Schöne, T., Klicpera, A., Stocchi, P., Lukman, M., Westphal, H., 2016. The magnitude of a mid-Holocene sea-level highstand in the Strait of Makassar. Geomorphology 257, pp. 155-163.

Mariath, R., Rodriguez, R.R., Figueiredo, M.A.O., 2013. Succession of crustose coralline red algae (Rhodophyta) on coralgal reefs exposed to physical disturbance in the southwest Atlantic. Helgoland Marine Research 67, pp. 687-696.

Mauz, B., Hassler, U., 2000. Luminescence chronology of late pleistocene raised beaches in southern Italy: New data of relative sea-level changes. Mar Geol 170, pp. 187-203.

Mauz, B., Hijma, M.P., Amorosi, A., Porat, N., Galili, E., Bloemendal, J., 2013. Aeolian beach ridges and their significance for climate and sea level: Concept and insight from the Levant coast (East Mediterranean). Earth-Science Reviews 121, pp. 31-54.

Mauz, B., Vacchi, M., Green, A., Hoffmann, G., Cooper, A., 2015. Beachrock: A tool for reconstructing relative sea level in the far-field. Mar Geol 362, pp. 1-16.

Mayer, R.H., Kriebel, D.L., 1994. Wave Runup on Composite-Slope and Concave Beaches. Coastal Engineering, pp. 2325-2339.

McGregor, S., Gupta, A.S., England, M.H., 2012. Constraining Wind Stress Products with Sea Surface Height Observations and Implications for Pacific Ocean Sea Level Trend Attribution. Journal of Climate 25, pp. 8164-8176.

Meco, J., Scaillet, S., Guillou, H., Lomoschitz, A., Carlos Carracedo, J., Ballester, J., Betancort, J.F., Cilleros, A., 2007. Evidence for long-term uplift on the Canary Islands from emergent Mio-Pliocene littoral deposits. Global and Planetary Change 57, pp. 222-234.

Medina-Elizalde, M., 2013. A global compilation of coral sea-level benchmarks: Implications and new challenges. Earth and Planetary Science Letters 362, pp. 310-318.

Meyers, J.H., 1987. Marine vadose beachrock cementation by cryptocrystalline magnesian calcite--Maui, Hawaii. Journal of Sedimentary Petrology v. 57, pp. p. 558-570.

Miller, K.G., 2005. The Phanerozoic Record of Global Sea-Level Change. Science 310, pp. 1293-1298.

Milne, G.A., Long, A.J., Bassett, S.E., 2005. Modelling Holocene relative sea-level observations from the Caribbean and South America. Quaternary Science Reviews 24, pp. 1183-1202.

Milne, G.A., Mitrovica, J.X., 2008. Searching for eustasy in deglacial sea-level histories. Quaternary Science Reviews 27, pp. 2292-2302.
Mitrovica, J.X., Forte, A.M., 1997. Radial profile of mantle viscosity: Results from the joint inversion of convection and postglacial rebound observables. Journal of Geophysical Research 102, pp. 2751.
Mongin, M., Baird, M., 2014. The interacting effects of photosynthesis, calcification and water circulation on carbon chemistry variability on a coral reef flat: A modelling study. Ecological Modelling 284, pp. 19-34.
Montaggioni, L.F., 2005. History of Indo-Pacific coral reef systems since the last glaciation: Development patterns and controlling factors. Earth-Science Reviews 71, pp. 1-75.
Moon, I.J., Ginis, I., Hara, T., Tolman, H.L., Wright, C.W., Walsh, E.J., 2003. Numerical simulation of sea surface directional wave spectra under hurricane wind forcing. Journal of Physical Oceanography 33, pp. 1680-1706.
Moucha, R., Forte, A.M., Mitrovica, J.X., Rowley, D.B., Quéré, S., Simmons, N.A., Grand, S.P., 2008. Dynamic topography and long-term sea-level variations: There is no such thing as a stable continental platform. Earth and Planetary Science Letters 271, pp. 101-108.
Muhs, D.R., Kennedy, G.L., Rockwell, T.K., 1994. Uranium-Series Ages of Marine Terrace Corals from the Pacific Coast of North America and Implications for Last-Interglacial Sea Level History. Quaternary Research 42, pp. 72-87.
Muhs, D.R., Meco, J., Simmons, K.R., 2014. Uranium-series ages of corals, sea level history, and palaeozoogeography, Canary Islands, Spain: An exploratory study for two Quaternary interglacial periods. Palaeogeography, Palaeoclimatology, Palaeoecology 394, pp. 99-118.
Muhs, D.R., Rockwell, T.K., Kennedy, G.L., 1992. Late quaternary uplift rates of marine terraces on the Pacific coast of North America, southern Oregon to Baja California sur. Quaternary International 15-16, pp. 121-133.
Muhs, D.R., Simmons, K.R., Meco, J., Porat, N., 2015. Uranium-series ages of fossil corals from Mallorca, Spain: The "Neotyrrhenian" high stand of the Mediterranean Sea revisited. Palaeogeography, Palaeoclimatology, Palaeoecology 438, pp. 408-424.
Muhs, D.R., Simmons, K.R., Schumann, R.R., Halley, R.B., 2011. Sea-level history of the past two interglacial periods: New evidence from U-series dating of reef corals from south Florida. Quaternary Science Reviews 30, pp. 570-590.
Muhs, D.R., Szabo, B.J., 1982. Uranium-series age of the Eel Point terrace San Clemente Island, California. Geology 10, pp. 23-26.
Muhs, D.R., Wehmiller, J.F., Simmons, K.R., York, L.L., 2003. Quaternary sea-level history of the United States, Developments in Quaternary Sciences, pp. 147-183.
Müller, R.D., Sdrolias, M., Gaina, C., Steinberger, B., Heine, C., 2008. Long-Term Sea-Level Fluctuations Driven by Ocean Basin Dynamics. Science 319, pp. 1357-1362.
Mulvaney, R., Abram, N.J., Hindmarsh, R.C.a., Arrowsmith, C., Fleet, L., Triest, J., Sime, L.C., Alemany, O., Foord, S., 2012. Recent Antarctic Peninsula warming relative to Holocene climate and ice-shelf history. Nature 489, pp. 141-144.
Murray-Wallace, C.V., Belperio, A.P., 1991. The last interglacial shoreline in Australia - A review. Quaternary Science Reviews 10, pp. 441-461.
Murray-Wallace, C.V., Belperio, A.P., Bourman, R.P., Cann, J.H., Price, D.M., 1999. Facies architecture of a last interglacial barrier: a model for Quaternary barrier development from the Coorong to Mount Gambier Coastal Plain, southeastern Australia. Mar Geol 158, pp. 177-195.
Murray-Wallace, C.V., Woodroffe, C.D., 2012. Quaternary sea-level changes: A global perspective. Quaternary Sea-Level Changes: A Global Perspective, pp. 1-484.
Mylroie, J.E., Carew, J.L., Moore, A.I., 1995. Blue holes: Definition and genesis. Carbonates and Evaporites 10, pp. 225-233.
Nagasaka, M., Takano, M., 2014. Spatial and Seasonal Variability of Turbidity in Lake Kahokugata, a Shallow Eutrophic Lagoon in Japan, Lakes : The Mirrors of the Earth, pp. 139-141.
Naylor, L.A., Stephenson, W.J., 2010. On the role of discontinuities in mediating shore platform erosion. Geomorphology 114, pp. 89-100.
Neumann, A.C., Hearty, P.J., 1996. Rapid sea-level changes at the close of the last interglacial (substage 5e) recorded in Bahamian island geology. Geology 24, pp. 775-778.
Neumann, A.C., Macintyre, I.G., 1985. Reef response to sea-level rise: keep-up, catch-up or give-up. Int. Coral Reef Symp. 3, pp. 105-110.
Neumeier, U., 1998. Tidal dunes and sand waves in deep outer-shelf environments, Bajocian, SE Jura, France. Journal of Sedimentary Research 68, pp. 507-514.

Nichol, S.L., 2002. Morphology, Stratigraphy and Origin of Last Interglacial Beach Ridges at Bream Bay, New Zealand. Journal of Coastal Research 18, pp. 149-159.

Nichols, M.M., 1989. Sediment accumulation rates and relative sea-level rise in lagoons. Mar Geol 88, pp. 201-219.

Nisi, M.F., Antonioli, F., Pra, G.D., Leoni, G., Silenzi, S., 2003. Coastal deformation between the Versilia and the Garigliano plains (Italy) since the last interglacial stage. Journal of Quaternary Science 18, pp. 709-721.

O'Leary, M.J., Hearty, P.J., McCulloch, M.T., 2008. U-series evidence for widespread reef development in Shark Bay during the last interglacial. Palaeogeography, Palaeoclimatology, Palaeoecology 259, pp. 424-435.

O'Neal, M.L., Dunn, R.K., 2003. GPR investigation of multiple stage-5 sea-level fluctuations on a siliciclastic estuarine shoreline, Delaware Bay, southern New Jersey, USA. Geological Society, London, Special Publications 211, pp. 67-77.

O'Leary, M.J., Hearty, P.J., Thompson, W.G., Raymo, M.E., Mitrovica, J.X., Webster, J.M., 2013. Ice sheet collapse following a prolonged period of stable sea level during the last interglacial. Nature Geoscience 6, pp. 796-800.

Obert, J.C., Scholz, D., Felis, T., Brocas, W.M., Jochum, K.P., Andreae, M.O., 2016. 230Th/U dating of Last Interglacial brain corals from Bonaire (southern Caribbean) using bulk and theca wall material. Geochimica et Cosmochimica Acta 178, pp. 20-40.

Ota, Y., Omura, A., 1991. Late Quaternary Shorelines in the Japanese Islands. The Quaternary Research (Daiyonki-Kenkyu) 30, pp. 175-186.

Otto-Bliesner, B.L., Marshall, S.J., Overpeck, J.T., Miller, G.H., Hu, A., 2006. Simulating Arctic climate warmth and icefield retreat in the last interglaciation. Science 311, pp. 1751-1753.

Otto-Bliesner, B.L., Rosenbloom, N., Stone, E.J., McKay, N.P., Lunt, D.J., Brady, E.C., Overpeck, J.T., 2013. How warm was the last interglacial? New model-data comparisons. Philos Trans A Math Phys Eng Sci 371, pp. 20130097.

Otvos, E.G., 2005. Cheniers, in: Schwartz, M.L. (Ed.), Encyclopedia of Coastal Science. Springer Netherlands, Dordrecht, pp. 233-235.

Ozturk, M.Z., Erginal, A.E., Kiyak, N.G., Ozturk, T., 2016. Cement fabrics and optical luminescence ages of beachrock, North Cyprus: Implications for Holocene sea-level changes. Quaternary International 401, pp. 132-140.

Pavlis, N.K., Holmes, S.A., Kenyon, S.C., Factor, J.K., 2012. The development and evaluation of the Earth Gravitational Model 2008 (EGM2008). Journal of Geophysical Research: Solid Earth 117, pp. n/a-n/a.

Pedoja, K., Husson, L., Johnson, M.E., Melnick, D., Witt, C., Pochat, S., Nexer, M., Delcaillau, B., Pinegina, T., Poprawski, Y., Authemayou, C., Elliot, M., Regard, V., Garestier, F., 2014. Coastal staircase sequences reflecting sea-level oscillations and tectonic uplift during the Quaternary and Neogene. Earth-Science Reviews 132, pp. 13-38.

Pedoja, K., Husson, L., Regard, V., Cobbold, P.R., Ostanciaux, E., Johnson, M.E., Kershaw, S., Saillard, M., Martinod, J., Furgerot, L., Weill, P., Delcaillau, B., 2011a. Relative sea-level fall since the last interglacial stage: Are coasts uplifting worldwide? Earth-Science Reviews 108, pp. 1-15.

Pedoja, K., Regard, V., Husson, L., Martinod, J., Guillaume, B., Fucks, E., Iglesias, M., Weill, P., 2011b. Uplift of quaternary shorelines in eastern Patagonia: Darwin revisited. Geomorphology 127, pp. 121-142.

Peltier, W.R., 1996. Mantle viscosity and ice-age ice sheet topography. Science v273, pp. p1359(1356).

Peltier, W.R., 1998. Postglacial variations in the level of the sea: Implications for climate dynamics and solid-Earth geophysics. Reviews of Geophysics 36, pp. 603-689.

Peltier, W.R., 2001. Chapter 4 Global glacial isostatic adjustment and modern instrumental records of relative sea level history. International Geophysics 75, pp. 65-95.

Petit, R.J., Raynaud, D., Basile, I., Chappellaz, J., Ritz, C., Delmotte, M., Legrand, M., Lorius, C., Pe, L., 1999. Climate and atmospheric history of the past 420,000 years from the Vostok ice core, Antarctica. Nature 399, pp. 429-413.

Pirazzoli, P.A., 1986. Marine notches, in: van de Plassche, O. (Ed.), Sea-Level Research: a manual for the collection and evaluation of data. Springer Netherlands, Dordrecht, pp. 361-400.

Pirazzoli, P.A., 1996. Sea-level changes: the last 20 000 years. Sea-level changes: the last 20 000 years.

Pirazzoli, P.A., 2005. Marine Terraces, in: Schwartz, M.L. (Ed.), Encyclopedia of Coastal Science. Springer Netherlands, Dordrecht, pp. 632-633.

Pirazzoli, P.A., Evelpidou, N., 2013. Tidal notches: A sea-level indicator of uncertain archival trustworthiness. Palaeogeography, Palaeoclimatology, Palaeoecology 369, pp. 377-384.

Pirazzoli, P.A., Radtke, U., Hantoro, W.S., Jouannic, C., Hoang, C.T., Causse, C., Best, M.B., 1991. Quaternary Raised Coral-Reef Terraces on Sumba Island, Indonesia. Science 252, pp. 1834-1836.

Potter, E.K., Lambeck, K., 2004. Reconciliation of sea-level observations in the Western North Atlantic during the last glacial cycle. Earth and Planetary Science Letters 217, pp. 171-181.

Pugh, D.T., 1987. Tides, Surges and mean sea-level. John Wiley & Sons Ltd., Chichester.

Qi, S., 2000. Use of International Hydrographic Organization Tidal Data for Improved Tidal Prediction, Portland, OR.

Ramalho, R.S., Helffrich, G., Madeira, J., Cosca, M., Thomas, C., Quartau, R., Hipólito, A., Rovere, A., Hearty, P.J., Ávila, S.P., 2017. Emergence and evolution of Santa Maria Island (azores)- The conundrum of uplifted islands revisited. Bulletin of the Geological Society of America 129, pp. 372-391.

Ramsay, P.J., Cooper, J.A.G., 2002. Late Quaternary Sea-Level Change in South Africa. Quaternary Research 57, pp. 82-90.

Ratsimandresy, A.W., Sotillo, M.G., Álvarez Fanjul, E., Carretero Albiach, J.C., Pérez Gómez, B., Hajji, H., 2008a. A 44-year (1958-2001) sea level residual hindcast over the Mediterranean Basin. Physics and Chemistry of the Earth 33, pp. 250-259.

Ratsimandresy, A.W., Sotillo, M.G., Carretero Albiach, J.C., Álvarez Fanjul, E., Hajji, H., 2008b. A 44-year high-resolution ocean and atmospheric hindcast for the Mediterranean Basin developed within the HIPOCAS Project. Coastal Engineering 55, pp. 827-842.

Rattanapitikon, W., Vivattanasirisak, T., Shibayama, T., 2003. A proposal of new breaker height formula. Coastal Engineering Journal 45, pp. 29-48.

Raymo, M.E., Mitrovica, J.X., 2012. Collapse of polar ice sheets during the stage 11 interglacial. Nature 483, pp. 453-456.

Raymo, M.E., Mitrovica, J.X., O'Leary, M.J., DeConto, R.M., Hearty, P.J., 2011. Departures from eustasy in Pliocene sea-level records. Nature Geoscience 4, pp. 328-332.

Ribolini, A., Aguirre, M., Baneschi, I., Consoloni, I., Fucks, E., Isola, I., Mazzarini, F., Pappalardo, M., Zanchetta, G., Bini, M., 2011. Holocene Beach Ridges and Coastal Evolution in the Cabo Raso Bay (Atlantic Patagonian Coast, Argentina). Journal of Coastal Research 276, pp. 973-983.

Rignot, E., Mouginot, J., Morlighem, M., Seroussi, H., Scheuchl, B., 2014. Widespread, rapid grounding line retreat of Pine Island, Thwaites, Smith, and Kohler glaciers, West Antarctica, from 1992 to 2011. Geophysical Research Letters 41, pp. 3502-3509.

Rohling, E.J., Grant, K., Hemleben, C., Siddall, M., Hoogakker, B.A.A., Bolshaw, M., Kucera, M., 2008. High rates of sea-level rise during the last interglacial period. Nature Geoscience 1, pp. 38-42.

Rose, J., Meng, X., Watson, C., 1999. Palaeoclimate and palaeoenvironmental responses in the western Mediterranean over the last 140 ka: evidence from Mallorca, Spain. Journal of the Geological Society 156, pp. 435-448.

Rovere, A., Antonioli, F., Bianchi, C.N., 2015a. Fixed biological indicators, Handbook of Sea-Level Research, pp. 268-280.

Rovere, A., Casella, E., Vacchi, M., Parravicini, V., Firpo, M., Ferrari, M., Morri, C., Bianchi, C.N., 2014a. Coastal and marine geomorphology between Albenga and Savona(NW Mediterranean Sea, Italy). Journal of Maps 11, pp. 278-286.

Rovere, A., Hearty, P.J., Austermann, J., Mitrovica, J.X., Gale, J., Moucha, R., Forte, A.M., Raymo, M.E., 2015b. Mid-Pliocene shorelines of the US Atlantic Coastal Plain — An improved elevation database with comparison to Earth model predictions. Earth-Science Reviews 145, pp. 117-131.

Rovere, A., Raymo, M.E., Mitrovica, J.X., Hearty, P.J., O'Leary, M.J., Inglis, J.D., 2014b. The Mid-Pliocene sea-level conundrum: Glacial isostasy, eustasy and dynamic topography. Earth and Planetary Science Letters 387, pp. 27-33.

Rovere, A., Raymo, M.E., O'Leary, M.J., Hearty, P.J., 2012. Crowdsourcing in the Quaternary sea level community: Insights from the Pliocene. Quaternary Science Reviews 56, pp. 164-166.

Rovere, A., Raymo, M.E., Vacchi, M., Lorscheid, T., Stocchi, P., Gómez-Pujol, L., Harris, D.L., Casella, E., O'Leary, M.J., Hearty, P.J., 2016a. The analysis of Last Interglacial (MIS 5e) relative sea-level indicators: Reconstructing sea-level in a warmer world. Earth-Science Reviews 159, pp. 404-427.

Rovere, A., Stocchi, P., Vacchi, M., 2016b. Eustatic and Relative Sea Level Changes. Current Climate Change Reports 2, pp. 221-231.

Rovere, A., Vacchi, M., Firpo, M., Carobene, L., 2011. Underwater geomorphology of the rocky coastal tracts between Finale Ligure and Vado Ligure (western Liguria, NW Mediterranean Sea). Quaternary International 232, pp. 187-200.

Rowley, D.B., Forte, A.M., Moucha, R., Mitrovica, J.X., Simmons, N.a., Grand, S.P., 2013. Dynamic topography change of the eastern United States since 3 million years ago. Science 340, pp. 1560-1563.

Rybak, O., Huybrechts, P., 2013. Modeling the configuration of the Greenland ice sheet during the Last Interglacial constrained by ice core data. EGU General Assembly Conference.

Sàbat, F., Gelabert, B., Rodríguez-Perea, A., Giménez, J., 2011. Geological structure and evolution of Majorca: Implications for the origin of the Western Mediterranean. Tectonophysics 510, pp. 217-238.

Saha, S., Moorthi, S., Pan, H.L., Wu, X., Wang, J., Nadiga, S., Tripp, P., Kistler, R., Woollen, J., Behringer, D., Liu, H., Stokes, D., Grumbine, R., Gayno, G., Wang, J., Hou, Y.T., Chuang, H.Y., Juang, H.M.H., Sela, J., Iredell, M., Treadon, R., Kleist, D., Van Delst, P., Keyser, D., Derber, J., Ek, M., Meng, J., Wei, H., Yang, R., Lord, S., Van Den Dool, H., Kumar, A., Wang, W., Long, C., Chelliah, M., Xue, Y., Huang, B., Schemm, J.K., Ebisuzaki, W., Lin, R., Xie, P., Chen, M., Zhou, S., Higgins, W., Zou, C.Z., Liu, Q., Chen, Y., Han, Y., Cucurull, L., Reynolds, R.W., Rutledge, G., Goldberg, M., 2010. The NCEP climate forecast system reanalysis. Bulletin of the American Meteorological Society 91, pp. 1015-1057.

Schellmann, G., Beerten, K., Radtke, U., 2008. Electron spin resonance (ESR) dating of Quaternary materials. Quaternary Science Journal 57, pp. 150-178.

Schellmann, G., Radtke, U., 2000. ESR dating stratigraphically well-constrained marine terraces along the Patagonian Atlantic coast (Argentina). Quaternary International 68-71, pp. 261-273.

Schellmann, G., Radtke, U., 2004. A revised morpho- and chronostratigraphy of the Late and Middle Pleistocene coral reef terraces on Southern Barbados (West Indies). Earth-Science Reviews 64, pp. 157-187.

Schellmann, G., Radtke, U., 2010. Timing and magnitude of Holocene sea-level changes along the middle and south Patagonian Atlantic coast derived from beach ridge systems, littoral terraces and valley-mouth terraces. Earth-Science Reviews 103, pp. 1-30.

Schellmann, G., Radtke, U., Potter, E.K., Esat, T.M., McCulloch, M.T., 2004. Comparison of ESR and TIMS U/Th dating of marine isotope stage (MIS) 5e, 5c, and 5a coral from Barbados-implications for palaeo sea-level changes in the Caribbean. Quaternary International 120, pp. 41-50.

Schwartz, 2005. Encyclopedia of Coastal Science. Encyclopedia of Earth Sciences Series, pp. 1-1213.

Schwindt, E., De Francesco, C.G., Iribarne, O.O., 2004. Individual and reef growth of the invasive reef-building polychaete Ficopomatus enigmaticus in a south-western Atlantic coastal lagoon. Journal of the Marine Biological Association of the UK 84, pp. 987-993.

Serrano, D., Ramírez-Félix, E., Valle-Levinson, A., 2013. Tidal hydrodynamics in a two-inlet coastal lagoon in the Gulf of California. Continental Shelf Research 63, pp. 1-12.

Seu-Anoï, N.M., Ouattara, A., Koné, Y.J.-M., Gourène, G., 2011. Seasonal distribution of phytoplankton in the Aby lagoon system, Ivory Coast, West Africa. African Journal of Aquatic Science 36, pp. 321-330.

Shennan, I., 1982. Interpretation of Flandrian sea-level data from the Fenland, England. Proceedings of the Geologists' Association 93, pp. 53-63.

Shennan, I., 1989. Holocene crustal movements and sea-level changes in Great Britain. Journal of Quaternary Science 4, pp. 77-89.

Shennan, I., 2015. Handbook of sea-level research: Framing research questions, Handbook of Sea-Level Research, pp. 3-25.

Shennan, I., Horton, B., 2002. Holocene land- and sea-level changes in Great Britain. Journal of Quaternary Science 17, pp. 511-526.

Shennan, I., Milne, G., Bradley, S., 2012. Late Holocene vertical land motion and relative sea-level changes: Lessons from the British Isles. Journal of Quaternary Science 27, pp. 64-70.

Sherman, C.E., Glenn, C.R., Jones, A.T., Burnett, W.C., Schwarcz, H.P., 1993. New evidence for two highstands of the sea during the Last Interglacial, oxygen isotope substage 5e. Geology 21, pp. 1079-1082.

Short, A.D., 1999. Handbook of Beach and Shoreface Morphodynamics. John Wiley & Sons Ltd.

Sivan, D., Gvirtzman, G., Sass, E., 1999. Quaternary Stratigraphy and Paleogeography of the Galilee Coastal Plain, Israel. Quaternary Research 51, pp. 280-294.

Sivan, D., Sisma-Ventura, G., Greenbaum, N., Bialik, O.M., Williams, F.H., Tamisiea, M.E., Rohling, E.J., Frumkin, A., Avnaim-Katav, S., Shtienberg, G., Stein, M., 2016. Eastern Mediterranean sea levels through the last interglacial from a coastal-marine sequence in northern Israel. Quaternary Science Reviews 145, pp. 204-225.

Smith, J.M., 2003. Surf Zone Hydrodynamics. Coastal Engineering Manual 1100, pp. 1-42.

Spada, G., Stocchi, P., 2007. SELEN: A Fortran 90 program for solving the "sea-level equation". Computers and Geosciences 33, pp. 538-562.

Stearns, C.E., 1976. Estimates of the position of sea level between 140,000 and 75,000 years ago. Quaternary Research 6, pp. 445-449.

Stearns, C.E., Thurber, D.L., 1965. Th230/U234 dates of late Pleistocene marine fossils from the Mediterranean and Moroccan littorals. Progress in Oceanography 4, pp. 293-305.

Stempfhuber, W., Buchholz, M., 2011. A Precise , Low-Cost Rtk Gnss System for Uav Applications. UAV-g 2011 XXXVIII, pp. 289-293.

Stephenson, W.J., 2000. Shore platforms: a neglected coastal feature? Progress in Physical Geography 24, pp. 311-327.

Stephenson, W.J., Kirk, R.M., 1996. Measuring erosion rates using the micro-erosion meter: 20 years of data from shore platforms, Kaikoura Peninsula, South Island, New Zealand. Mar Geol 131, pp. 209-218.

Stephenson, W.J., Kirk, R.M., 1998. Rates and patterns of erosion on inter-tidal shore platforms, Kaikoura Peninsula, South Island, New Zealand. Earth Surface Processes and Landforms 23, pp. 1071-1085.

Stephenson, W.J., Kirk, R.M., 2000. Development of shore platforms on Kaikoura Peninsula, South Island, New Zealand Part one: The role of waves. Geomorphology 32, pp. 21-41.

Stirling, C.H., Andersen, M.B., 2009. Uranium-series dating of fossil coral reefs: Extending the sea-level record beyond the last glacial cycle. Earth and Planetary Science Letters 284, pp. 269-283.

Stirling, C.H., Esat, T.M., Lambeck, K., McCulloch, M.T., 1998. Timing and duration of the Last Interglacial: Evidence for a restricted interval of widespread coral reef growth. Earth and Planetary Science Letters 160, pp. 745-762.

Stirling, C.H., Esat, T.M., McCulloch, M.T., Lambeck, K., 1995. High-precision U-series dating of corals from Western Australia and implications for the timing and duration of the Last Interglacial. Earth and Planetary Science Letters 135, pp. 115-130.

Stocchi, P., Spada, G., 2009. Influence of glacial isostatic adjustment upon current sea level variations in the Mediterranean. Tectonophysics 474, pp. 56-68.

Stockdon, H.F., Holman, R.A., Howd, P.A., Sallenger, A.H., 2006. Empirical parameterization of setup, swash, and runup. Coastal Engineering 53, pp. 573-588.

Storlazzi, C.D., Logan, J.B., Field, M.E., 2003. Quantitative morphology of a fringing reef tract from high-resolution laser bathymetry: Southern Molokai, Hawaii. Bulletin of the Geological Society of America 115, pp. 1344-1355.

Suga, N., Montani, S., 2012. The Effect of Microphytobenthic Resuspension on Suspended Particulate Matter Dynamics in a Shallow Lagoon in Hokkaido, Japan. Interdisciplinary Studies on Environmental Chemistry—Marine Environmental Pollution & Ecotoxicology, pp. 353-365.

Sunamura, T., 1992. Geomorphology of Rocky Coasts. Coll. Coastal morphology and research, pp. 302.

Surić, M., Lončarić, R., Lončar, N., 2010. Submerged caves of Croatia: Distribution, classification and origin. Environmental Earth Sciences 61, pp. 1473-1480.

Surić, M., Richards, D.A., Hoffmann, D.L., Tibljaš, D., Juračić, M., 2009. Sea-level change during MIS 5a based on submerged speleothems from the eastern Adriatic Sea (Croatia). Mar Geol 262, pp. 62-67.

Takasu, T., Yasuda, A., 2009. Development of the low-cost RTK-GPS receiver with an open source program package RTKLIB. International Symposium on GPS/GNSS, pp. 4-6.

Tamura, T., 2012. Beach ridges and prograded beach deposits as palaeoenvironment records. Earth-Science Reviews 114, pp. 279-297.

Ten Hove, H.A., 1979. Different causes of mass occurrence in serpulids. Biol. Syst. Colon. Org. 11, pp. 281--298.

Ten Hove, H.A., Weerdenburg, J.C.A., 1978. A Generic Revision of the Brackish-Water Serpulid Ficopomatus Southern 1921 (Polychaeta: Serpulinae), Including Mercierella Fauvel 1923, Sphaeropmatus Treadwell 1934, Mercierellopsis Rioja 1945 and Neopomatus Pillai 1960. The Biological Bulletin 154, pp. 96-120.

Thompson, W.G., Allen Curran, H., Wilson, M.a., White, B., 2011. Sea-level oscillations during the last interglacial highstand recorded by Bahamas corals - Supplement. Nature Geoscience 4, pp. 684-687.

Tintoré, J., Medina, R., Gómez-Pujol, L., Orfila, A., Vizoso, G., 2009. Integrated and interdisciplinary scientific approach to coastal management. Ocean and Coastal Management 52, pp. 493-505.

Tintoré, J., Vizoso, G., Casas, B., Heslop, E., Pascual, A., Orfila, A., Ruiz, S., Martínez-Ledesma, M., Torner, M., Cusí, S., Diedrich, A., Balaguer, P., Gómez-Pujol, L., Álvarez-Ellacuria, A., Gómara, S., Sebastian, K., Lora, S., Beltrán, J.P., Renault, L., Juzà, M., Álvarez, D., March, D., Garau, B., Castilla, C., Cañellas, T., Roque, D., Lizarán, I., Pitarch, S., Carrasco, M.A., Lana, A., Mason, E., Escudier, R., Conti, D., Sayol, J.M., Barceló, B., Alemany, F., Reglero, P., Massuti, E., Vélez-Belchí, P., Ruiz, J., Oguz, T., Gómez, M., Álvarez, E., Ansorena, L., Manriquez, M., 2013. SOCIB: The Balearic Islands Coastal Ocean Observing and Forecasting System Responding to Science, Technology and Society Needs. Marine Technology Society Journal 47, pp. 101-117.

Tojo, B., Ohno, T., Fujiwara, T., 1999. Late pleistocene changes of tidal amplitude and phase in Osaka Bay, Japan, reconstructed from fossil records and numerical model calculations. Mar Geol 157, pp. 241-248.

Tolman, H.L., 1997. User manual and system documentation of WAVEWATCH-III version 1.15. NOAA / NWS / NCEP / OMB Technical note 151, pp. 97.

Tolman, H.L., 2009. User manual and system documentation of WAVEWATCH-IIITM version 3.14. NOAA / NWS / NCEP / MMAB Technical note 276, pp. 194.

Tormey, B., Neumann, A.C., 2007. Rapid Sea-Level Change and Intensified Storms during the Last Interglacial: A High Resolution Record from the Bahamas, GSA Denver Annual Meeting.

Torres, T., Ortiz, J.E., Arribas, I., 2013. Variations in racemization/epimerization ratios and amino acid content of Glycymeris shells in raised marine deposits in the Mediterranean. Quaternary Geochronology 16, pp. 35-49.

Trenhaile, A.S., 1987. The Geomorphology of Rock Coasts. The Geomorphology of Rock Coasts., pp. x + 384 pp Price #335.300.

Trenhaile, A.S., 2008. Modeling the role of weathering in shore platform development. Geomorphology 94, pp. 24-39.

Trenhaile, A.S., 2014. Modelling tidal notch formation by wetting and drying and salt weathering. Geomorphology 224, pp. 139-151.

Trenhaile, A.S., 2015. Coastal notches: Their morphology, formation, and function. Earth-Science Reviews 150, pp. 285-304.

Trenhaile, A.S., Kanyaya, J.I., 2007. The Role of Wave Erosion on Sloping and Horizontal Shore Platforms in Macro- and Mesotidal Environments. Journal of Coastal Research 23, pp. 298-309.

Trenhaile, A.S., Pepper, D.A., Trenhaile, R.W., Dalimonte, M., 1998. Stacks and notches at Hopewell Rocks, New Brunswick, Canada. Earth Surface Processes and Landforms 23, pp. 975-988.

Trenhaile, A.S., Porter, N.J., 2007. Can shore platforms be produced solely by weathering processes? Mar Geol 241, pp. 79-92.

Trowbridge, A.C., 1954. Mississippi River and Gulf Coast Terraces and Sediments as Relaed to Pleistocene History-A Problem. Geological Society of America Bulletin 65, pp. 793.

Tuccimei, P., Fornós, J.J., Ginés, A., Ginés, J., Gràcia, F., Mucedda, M., 2007. Sea level change at Capo Caccia (NW Sardinia) and Mallorca (Balearic Islands) during oxygen isotope substage 5e, based on Th/U datings of phreatic overgrowths on speleothems. Geomorfologia Litoral i Quaternari. Homenatge a Joan Cuerda Barcelo. Monografies de la Societat d'Historia Natural de les Balears 14, pp. 121-136.

Tuccimei, P., Gines, J., Delitala, M.C., Gracia, F., Fornos, J.J., Taddeucci, A., 2006. Last interglacial sea level changes in Mallorca island (Western Mediterranian). High precision U-series data from phreatic overgrowths on speleotherms. Z. Geomorph. N. E. 50, pp. 1-21.

Tuccimei, P., Onac, B.P., Dorale, J.A., Ginés, J., Fornós, J.J., Ginés, A., Spada, G., Ruggieri, G., Mucedda, M., 2012. Decoding last interglacial sea-level variations in the western Mediterranean using speleothem encrustations from coastal caves in Mallorca and Sardinia: A field data -- model comparison. Quaternary International 262, pp. 56-64.

Tulipani, S., Grice, K., Krull, E., Greenwood, P., Revill, A.T., 2014. Salinity variations in the northern Coorong Lagoon, South Australia: Significant changes in the ecosystem following human alteration to the natural water regime. Organic Geochemistry 75, pp. 74-86.

Turney, C.S.M., Jones, R.T., 2010. Does the Agulhas Current amplify global temperatures during super-interglacials? Journal of Quaternary Science 25, pp. 839-843.

Vacchi, M., Marriner, N., Morhange, C., Spada, G., Fontana, A., Rovere, A., 2016. Multiproxy assessment of Holocene relative sea-level changes in the western Mediterranean: Sea-level variability and improvements in the definition of the isostatic signal. Earth-Science Reviews 155, pp. 172-197.

Vacchi, M., Montefalcone, M., Schiaffino, C.F., Parravicini, V., Bianchi, C.N., Morri, C., Ferrari, M., 2014. Towards a predictive model to assess the natural position of the Posidonia oceanica seagrass meadows upper limit. Marine Pollution Bulletin 83, pp. 458-466.

Vacchi, M., Rovere, A., Zouros, N., Desruelles, S., Caron, V., Firpo, M., 2012. Spatial distribution of sea-level markers on Lesvos Island (NE Aegean Sea): Evidence of differential relative sea-level changes and the neotectonic implications. Geomorphology 159-160, pp. 50-62.

Van De Plassche, O., 1986. Introduction, in: van de Plassche, O. (Ed.), Sea-Level Research: a manual for the collection and evaluation of data. Springer Netherlands, Dordrecht, pp. 1-26.

Van Hengstum, P.J., Richards, D.A., Onac, B.P., Dorale, J.A., 2015. Coastal caves and sinkholes, Handbook of Sea-Level Research, pp. 83-103.

Vesica, P.L., Tuccimei, P., Turi, B., Fornós, J.J., Ginés, A., Ginés, J., 2000. Late Pleistocene Paleoclimates and sea-level change in the Mediterranean as inferred from stable isotope and U-series studies of overgrowths on speleothems, Mallorca, Spain. Quaternary Science Reviews 19, pp. 865-879.

Vicens, D., 2010. El registre paleontològic dels dipòsits litorals quaternaris a la zona Nord-oriental de Mallorca (Badia de Pollença i Badia d'Alcúdia), Memòria d'investigació, p. 337.

Vicens, D., Gracia, F., Gines, A., 2012. Quaternary beach deposits in Mallorca: paleontological and geomorphological data, in: Gines, A., Ginés, J., Gomez-Pujol, L., Onac, B.P., Fornós, J.J. (Eds.), Mallorca: A

Mediterranean Benchmark for Quaternary Studies. Monografies de la Societat d'Història Natural de les Balears.

Vousdoukas, M.I., Velegrakis, A.F., Karambas, T.V., 2009. Morphology and sedimentology of a microtidal beach with beachrocks: Vatera, Lesbos, NE Mediterranean. Continental Shelf Research 29, pp. 1937-1947.

Wehmiller, J.F., 2013. United States Quaternary coastal sequences and molluscan racemization geochronology - What have they meant for each other over the past 45 years? Quaternary Geochronology 16, pp. 3-20.

Woodroffe, C.D., McGregor, H.V., Lambeck, K., Smithers, S.G., Fink, D., 2012. Mid-Pacific microatolls record sea-level stability over the past 5000 yr. Geology 40, pp. 951-954.

Woodroffe, C.D., Murray-Wallace, C.V., Bryant, E.A., Brooke, B., Heijnis, H., Price, D.M., 1995. Late Quaternary sea-level highstands in the Tasman Sea: evidence from Lord Howe Island. Mar Geol 125, pp. 61-72.

Woodroffe, S.A., Barlow, N.L.M., 2015. Reference water level and tidal datum, Handbook of Sea-Level Research. John Wiley & Sons, Ltd, Chichester, UK, pp. 171-180.

Woodroffe, S.A., Horton, B.P., 2005. Holocene sea-level changes in the Indo-Pacific. Journal of Asian Earth Sciences 25, pp. 29-43.

Yang, Q., Scholz, D., Jochum, K.P., Hoffmann, D.L., Stoll, B., Weis, U., Schwager, B., Andreae, M.O., 2015. Lead isotope variability in speleothems-A promising new proxy for hydrological change? First results from a stalagmite from western Germany. Chemical Geology 396, pp. 143-151.

Zazo, C., Goy, J.L., Dabrio, C.J., Bardají, T., Hillaire-Marcel, C., Ghaleb, B., González-Delgado, J.Á., Soler, V., 2003. Pleistocene raised marine terraces of the Spanish Mediterranean and Atlantic Coasts: Records of coastal uplift, sea-level highstands and climate changes. Mar Geol 194, pp. 103-133.

Zazo, C., Goy, J.L., Dabrio, C.J., Soler, V., Hillaire-Marcel, C., Ghaleb, B., González-Delgado, J.A., Bardají, T., Cabero, A., 2007. Quaternary marine terraces on Sal Island (Cape Verde archipelago). Quaternary Science Reviews 26, pp. 876-893.

Zazo, C., Silva, P.G., Goy, J.L., Hillaire-Marcel, C., Ghaleb, B., Lario, J., Bardají, T., González, A., 1999. Coastal uplift in continental collision plate boundaries: Data from the Last Interglacial marine terraces of the Gibraltar Strait area (south Spain). Tectonophysics 301, pp. 95-109.

Zecchin, M., Nalin, R., Roda, C., 2004. Raised Pleistocene marine terraces of the Crotone peninsula (Calabria, southern Italy): Facies analysis and organization of their deposits. Sedimentary Geology 172, pp. 165-185.

11. Appendix

During my PhD, I was involved as geologist expert on land surveys and paleo sea levels in a number of projects that have been communicated to conferences and will result in additional manuscripts that are at the moment in preparation. In this appendix, the both contributions are listed together with a corresponding abstract.

11.1. Conference contributions

11.1.1. EGU General Assembly 2015, Vienna, Austria

New sea-level data of the MIS 5e interglacial of Mallorca Island, Spain

T. Lorscheid, P. Stocchi, B. de Boer, T. Mann, H. Westphal, A. Rovere

The island of Mallorca (Balearic Islands, Spain) is one of the key locations in the Western Mediterranean for the study of Last Interglacial sea levels. Although MIS 5e deposits and landforms have been investigated by several authors since CUERDA 1979, most former studies concentrate on few outcrops. Although description of fossils, facies and age attribution for these outcrops are known in detail, these sites have never been the object of differential GPS measurements and glacial isostatic adjustment effects have never been taken into consideration. In this study, we present the results of fieldwork at several outcrops around the Island of Mallorca. We measured the elevation of deposits and landforms associated with the Last Interglacial with a high-precision GPS-system, and we calculated for each the reference water level and indicative range using modern analogs along the same shorelines. Moreover, we took samples of some outcrops for radiometric dating. The outcrops consist mainly of beach deposits at 1-3 m apsl and one elevated deposit in the Southeast of the island at 8 m apsl. We use an earth-ice coupled GIA-model for the Mediterranean to compare the elevation of our deposits to expected GIA signal in this region and discuss our results in terms of tectonics and eustasy.

11.1.2. Global and Regional Sea Level Variability and Change Workshop 2015, Palma de Mallorca, Spain

Sea-level highstands in Mallorca during the last interglacial

T. Lorscheid, P. Stocchi, A. Rovere, L. Gómez-Pujol, B. de Boer, T. Mann, H. Westphal, J.J. Fornós

Deposits of the last interglacial, analysed in light of glacio-hydro-isostatic adjustment models, can provide us with information on the sea-level history and the response of polar ice-sheets in slightly warmer climates. Mallorca is one of the key areas in the Western Mediterranean for such deposits. The outcrops representing this period were intensely investigated by several authors since CUERDA 1979. According to their observations, the sedimentological and fossil content is well known and the age was determined by the presence of the Senegalese fauna and, more recently, by dating with U/Th and AAR. Three aspects of Mallorcan deposits were still underinvestigated. i) precise elevation measurements with differential GPS. ii) estimates of reference water level and indicative range of the deposits and landforms at each site. iii) estimates of glacial isostatic adjustment (GIA) effects since MIS 5e. In this study we present the results of two field trips aimed at measuring last interglacial deposits in Mallorca with high-accuracy GPS and establishing, using modern shorelines as analogs, indicative ranges and

reference water level values for paleo deposits. We then used an earth-ice coupled GIA-model to investigate isostatic adjustment since MIS 5e in the island, and compared the elevation of our deposits to the expected GIA signal in this region. We discuss our results in terms of tectonics and eustasy.

11.1.3. MEDFLOOD meeting 2015, Trieste, Italy

Sea-level highstands during the last interglacial in Mallorca.

T. Lorscheid, P. Stocchi, A. Rovere, L. Gómez-Pujol, B. de Boer, T. Mann, H. Westphal, J.J. Fornós

- No abstract -

11.1.4. AGU Fall meeting 2015, San Francisco, CA, USA

Sea-level highstands during the Last interglacial (MIS 5e) in Mallorca

T. Lorscheid, P. Stocchi, A. Rovere, L. Gómez-Pujol, T. Mann, J.J. Fornos

Last Intergalcial in the island of Mallorca (NW Mediterranean) have been the subject of research since the early 60's (Butzer & Cuerda 1960). Despite both the location and stratigraphy of MIS 5e outcrops in the island are well known, the elevation of relative sea level (RSL) markers around the island has never been measured with high-accuracy topographic techniques (e.g. DGPS) and the interpretation of the paleo RSL has never been carried out using standardized definition of the indicative meaning of each RSL marker. In this study we present the results of two field trips aimed at measuring last interglacial deposits in Mallorca with high-accuracy GPS and at establishing, surveying modern shorelines as analogs, indicative ranges and reference water level values for RSL markers across the island. Using an earth-ice coupled GIA-model we performed several model-runs for investigating isostatic adjustment since MIS 5e in the island. These results are compared with the elevation of our deposits in the field and discussed in terms of tectonics and eustasy.

11.1.5. Bremen PhD days 2016, Etelsen, Germany

Sea-level highstand during Marine Isotopic Stage 5e – The Mallorca example

T. Lorscheid, P. Stocchi, A. Rovere, L. Gómez-Pujol, T. Mann, J.J. Fornós

Last Interglacial deposits in the island of Mallorca (NW Mediterranean) have been the subject of research since the early 60's (Butzer & Cuerda 1960). Despite both the location and stratigraphy of MIS 5e outcrops in the island are well known, the elevation of relative sea level (RSL) markers around the island has never been measured with high-accuracy topographic techniques (e.g. DGPS) and the interpretation of the paleo RSL has never been carried out using standardized definition of the indicative meaning of each RSL marker. We will present the results of two field trips aimed at measuring Last Interglacial deposits in Mallorca with high-accuracy GPS and at establishing, surveying modern shorelines as analogs, indicative ranges and reference water level values for RSL markers across the island. Using an earth-ice coupled GIA-model for investigating isostatic adjustment since MIS 5e in the island we performed several model-runs, which are compared with the elevation of our deposits in the field.

11.1.6. MEDFLOOD-MOPP meeting 2016, Bremen, Germany

MIS 5e sea-level changes, relative sea-level indicators and their modern analogs in Mallorca

T. Lorscheid, P. Stocchi, E. Casella, L. Gómez-Pujol, M. Vacchi, T. Mann, A. Rovere

- No abstract –

11.1.7. PALSEA2 meeting 2016, Mount Hood, OR, USA

MIS 5e sea-level database for the northern Atlantic and the Mediterranean

T. Lorscheid, A. Rovere, P. Stocchi

The Marine Isotopic Stage (MIS) 5e is a major topic of recent sea-level studies, as it is representative of a period with smaller polar ice sheets and higher sea levels coupled with slightly higher temperatures than today. Several sea level indicators representing MIS 5e relative sea level, were reported on the coastlines of the Northern Atlantic and the Western Mediterranean. Elevation of the sea level indicators, interpretations on the paleo sea level (trough modern analog and indicative meaning) and age attributions have a large span in accuracy and detail. In addition, the effect of Glacial Isostatic Adjustment (GIA) on these shorelines has been seldom considered. We present here a quality-controlled sea level database containing data from the Northern Atlantic and the Western Mediterranean. For each site, we collected elevation of relative sea level markers with topographic-grade instruments (e.g. DGPS) and we provide a description of the indicative meaning of MIS 5e sea level indicators. Coupling our research with considerations on modern processes, we calculated values for the modern analog, which represents the vertical occurrence of a sea-level marker in the modern environment. Together with the measured elevations, this will lead to elevations of the paleo relative sea-level and associated uncertainties. We compared our results with the ANICE-SELEN ice-earth coupled GIA model and conclude that our dataset, which crosses a gradient in the forebulges of the Fennoscandian and Laurentide ice sheets, can be used as a ground truth to GIA models and inferences on post-depositional displacements of MIS 5e shorelines in the Atlantic-Mediterranean Region.

11.1.8. Bremen PhD days 2017, Etelsen, Germany

The role of sea-level indictors for paleo sea-level studies

T. Lorscheid, P. Stocchi & A. Rovere

The interpretation of sea-level indicators is essential for the study of sea-level changes during past interglacial periods. Sea-level indicators can be of different origins, for example biological, sedimentological or morphological. In order to be used in reconstructing paleo sea-level histories, it is necessary to attribute an indicative meaning to each paleo sea-level indicator. This property describes the possible vertical variation in the relation between the indicator and sea level, which can be caused by different local conditions (e.g. wave exposure, tide range). The values for the indicative meaning are usually derived by using a modern analog, which represents the vertical range, where a certain indicator can be surveyed in the modern environment. Here we present a set of novel methodologies, in order to model the indicative meaning for some indicators using hydro- or morphodynamic models. We apply these methods to establish the indicative meaning of MIS 5e beach deposits on the island of Mallorca (Western Mediterranean) and of tidal notches on the island of Bonaire (Caribbean Netherlands). The described methodologies can be used in global datasets to assign values of the indicative meaning systematically and on a local basis to the available database of MIS 5e sea-level studies.

11.1.9. Regional Sea Level Changes and Coastal Impacts 2017, New York, USA

Numerical modelling of the indicative meaning of sea-level indicators in Pleistocene sea-level studies

T. Lorscheid, P. Stocchi, T. Felis, E. Casella, L. Gómez-Pujol, J. C. Obert, D. Scholz, M. Vacchi, T. Mann & A. Rovere

The interpretation of sea-level indicators is essential for the study of sea-level changes during past interglacial periods. Sea-level indicators can be of different origin, for example biological, sedimentological or morphological. In order to be used in reconstructing paleo sea-level histories, it is necessary to attribute an indicative meaning to each paleo sea-level indicator. This property describes the possible vertical variation in the formation of the indicator that can be caused by different local conditions (e.g. wave exposure, tide range). For example, a beach deposit can form between the highest and lowest point of wave-sediment interaction, i.e. the ordinary berm and the breaking depth of waves. In this case, the elevation of these elements represents the limits of the indicative meaning. Especially in Holocene sea-level studies, the values for the indicative meaning are usually derived by observing a modern analog, which represents the elevational range of a certain indicator surveyed in the modern environment. In this study, we present a set of novel methodologies to model the indicative meaning for some indicators using hydro- or morphodynamic models. We apply these methods to establish the indicative meaning of MIS 5e beach deposits on the island of Mallorca (Western Mediterranean) and of tidal notches with data from the island of Bonaire (Caribbean Netherlands). In Mallorca, we used a 1D morphodynamic model (CSHORE) in order to model the elevation of the beach berm and of the breaking depth of waves during typical storms between 2002 and 2013. Our results shows that beach deposits can have a large indicative meaning of up to 5.6 m. In Bonaire, we used a 3D hydrological model (Delft3D-FLOW) to calculate water levels during a complete tidal cycle (19 years). We repeated our calculations using a present-day topography and bathymetry and a MIS 5e one, derived adding to the present-day bathymetry the results of the ANICE-SELEN ice-earth coupled GIA-model. Both, field data and models, suggest that the tidal ranges did not change in Bonaire between MIS 5e and today, and that the indicative meaning of tidal notches can be constrained as a function of the tidal range. In the investigation of paleo sea-level changes a site-based study of the indicative meaning is important. While the necessary data might not be available for known sites of MIS 5e sea-level study, the described methodologies can be used in many more places, because global datasets can be used as inputs. In an ongoing study we will use these methods in order to assign values of the indicative meaning systematically and on a local basis to the available database of MIS 5e sea-level studies.

11.2. Further publications in preparation

11.2.1. MIS 5e relative sea-level changes in the Mediterranean Sea: contribution of isostatic disequilibrium

P. Stocchi, M. Vacchi, T. Lorscheid, B. de Boer, A.R. Simms, R. van de Wal, B. Vermeersen, M. Pappalardo & A. Rovere

Pending revisions, Quaternary Science Reviews

The Last Interglacial, or Marine Isotope Stage (MIS) 5e, is often considered as an analog for future scenarios of global warming. Constraining the contribution of the Greenland and Antarctic Ice Sheets to the MIS 5e sea-level highstand is crucial for validating models that predict the response of present-day polar ice sheets to climate change scenarios. It is important that geological relative sea-level (RSL) observations must come either from tectonically stable sites, or from areas where tectonics and their evolution through time are well known. On the other hand, MIS 5e sea level is a reference frame for quantifying local and regional vertical tectonic movements. In this paper, we re-assess paleo RSL indicators at 11 Mediterranean sites, which have been generally considered tectonically stable or affected by mild tectonics based on the geodynamic setting. The MIS 5e RSL indicators are found at these sites at an elevation of 2-10 m above modern mean sea level. Four sites are characterized by two separate sea-level stands, which suggest a two-step sea-level highstand or a fluctuation during MIS 5e. Numerical glacio- and hydro-isostatic adjustment (GIA) predictions show that GIA is an important contributor to the spatial and temporal variability of the sea-level highstand during MIS 5e. Therefore, we highlight that assumptions of tectonic stability on the basis of the MIS 5e record carry intrinsically large uncertainties, stemming either from uncertainties in field data or GIA models. The latter are propagated to either Holocene or Pleistocene sea-level reconstructions if tectonic rates are considered linear through time.

11.2.2. North Atlantic "Superstorms" during the Last Interglacial? Modeling paleo waves and the transport of giant boulders.

A. Rovere, E. Casella, D.L. Harris, T. Lorscheid, N.A.K. Nandasena, B. Dyer, M.R. Sandstrom, P. Stocchi, W.J. D'Andrea & M.E. Raymo

Pending revisions, Proceedings of the National Academy of Sciences
(Published on 14th November 2017 in *Proceedings of the National Academy of Sciences, 146 (46), 12144-12149, https://doi.org/10.1073/pnas.1712433114*)

As global climate warms and sea level rises, coastal areas will be subject to more frequent extreme flooding and hurricanes. Geologic evidence for extreme coastal storms in past warm periods has the potential to provide fundamental insights into their future intensity. Recent studies argue that, during the Last Interglacial (MIS 5e, ~128 to 116 ka), tropical and extra-tropical North Atlantic cyclones may have been more intense than at present, and may have produced swell waves larger than those observed historically. Such strong swells have been inferred to have created a number of geologic features that can be observed today along the coastlines of Bermuda and the Bahamas. In this paper, we investigate the most iconic among these features: massive boulders atop a cliff in North Eleuthera, Bahamas. We combine geologic field surveys, wave models, and boulder transport equations to test the hypothesis that such boulders were emplaced by storms of greater than-historical intensity. Our results refute this hypothesis: we calculate that, with the higher relative sea level (RSL) estimated for the Bahamas during MIS 5e, boulders of this size could have been transported by waves generated by storms of historical intensity. Our results indicate that the mega-boulders of Eleuthera cannot be used as geologic proof for past "superstorms", but also show that, with rising sea levels, cliffs and coastal barriers will be subject to greater forces even without changes in storm intensity.